The Consolidation and Strength Behavior of Mechanically Compressed Fine-Grained Sediments

by

Brendan Casey

B. Eng. in Civil and Environmental Engineering, University College Cork, 2009
S.M. in Civil and Environmental Engineering, Massachusetts Institute of Technology, 2011

Submitted to the Department of Civil and Environmental Engineering
in partial fulfillment of the requirements for the degree of

Doctor of Philosophy in the field of Geotechnical and Geoenvironmental Engineering
at the
Massachusetts Institute of Technology

June 2014

Signature of Author.. Signature redacted ..
Department of Civil and Environmental Engineering
May 2nd, 2014

Certified by.............. Signature redacted ....
John T. Germaine
Senior Research Associate of Civil and Environmental Engineering
Thesis Supervisor

Accepted by.. Signature redacted .
Heidi M. Nepf
Chair, Departmental Committee for Graduate Students

The Consolidation and Strength Behavior of Mechanically Compressed Fine-Grained Sediments

by

Brendan Casey

Submitted to the Department of Civil and Environmental Engineering on
May 2nd, 2014 in partial fulfillment of the requirements for the degree of
Doctor of Philosophy in the field of Geotechnical and Geoenvironmental Engineering

ABSTRACT

This thesis investigates the consolidation and shear strength behavior of saturated fine-grained sediments over the effective stress range of 0.1 to 100 MPa. The research makes use of samples which are resedimented in the laboratory from natural soils. In addition to practical benefits, resedimentation allows for isolation and quantification of individual factors influencing behavior such as composition, consolidation stress and overconsolidation ratio (OCR).

K_O-consolidated triaxial compression tests were performed on eight resedimented soils at room temperature. The results demonstrate conclusively that the conventional assumption of these soils exhibiting constant normalized properties is not valid when behavior is evaluated over a significant stress range. The direction and rate at which a soil's strength properties vary depend on its composition, with high plasticity soils showing a much more rapid reduction in both normalized undrained strength and critical state friction angle with increasing stress compared to low plasticity soils. For all soils, increasing consolidation stress results in a more ductile stress–strain response during undrained shearing as strain to failure increases and the amount of post-peak strain softening reduces at each OCR. Variations in strength properties as a function of stress level and soil type are closely linked to K_O, with higher values of K_O associated with both lower friction angles and lower undrained strengths. During virgin compression, high plasticity soils display a rapid increase in K_O and values in excess of 0.80 have been measured at high stresses.

The permeability behavior of a large number of resedimented soils has been investigated over a permeability range of 10^{-14} m^2 to 10^{-20} m^2 and a porosity range of about 0.75 to 0.20. The permeability-porosity relationship for a soil can be correlated to its liquid limit, which provides a robust indicator of the combined effects of pore size distribution and clay minealogy on behavior. Virgin compression behavior is strongly influenced by composition at low stresses, although at high stresses all fine-grained soils display a similar compression behavior regardless of their composition. The conventional 'Terzaghi' definition of effective stress is shown to be applicable to fine-grained sediments at pore pressures up to at least 10 MPa.

Thesis Supervisor: John T. Germaine
Title: Senior Research Associate of Civil and Environmental Engineering

ACKNOWLEDGEMENTS

Without question my greatest thanks goes to my research supervisor, teacher and friend Dr. Jack Germaine. The utmost respect and admiration is given to his knowledge of laboratory testing, and indeed engineering as a whole. Almost as important for a person committing to life as an MIT graduate student, Dr. Germaine's personality and sense of humor makes working with him a pleasure. I am also extremely grateful to Prof. Peter Flemings for teaching a poor communicator how to effectively present technical data to an audience, this is an invaluable skill in any field for which I have Peter to thank.

I would like to thank my committee members for their invaluable contributions and insights into the work: Prof. Chuck Ladd, Dr. Dick Plumb, Prof. Brian Evans and Prof. Herbert Einstein. I would also like to acknowledge my other teachers of geotechnical engineering; Prof. Andrew Whittle and Dr. Lucy Jen. I recognize that I have been advised and educated by some of the best in the world.

I am sincerely thankful for all my friends with whom I began my career at MIT and share almost every day with, in particular Amy, Amer, Steve, and Jana. The daily banter has made demanding times seem less daunting, and indeed often a lot of fun. Lastly, to Erin, who has given me unconditional support, happiness and clothing throughout my last few years at MIT.

TABLE OF CONTENTS

LIST OF TABLES

LIST OF FIGURES

LIST OF SYMBOLS

QBASIC	Quick Beginner's All-purpose Symbolic Instruction Code
BBC	Boston Blue Clay
CIUC	Isotropically Consolidated Undrained Triaxial Compression Test
CK$_O$U	K$_O$-Consolidated Undrained Triaxial Test
CK$_O$UC	K$_O$-Consolidated Undrained Triaxial Compression Test
CK$_O$UDSS	K$_O$-Consolidated Undrained Direct Simple Shear Test
CK$_O$UE	K$_O$-Consolidated Undrained Triaxial Extension Test
CH	High Plasticity Clay
CL	Low Plasticity Clay
CL-ML	Silty clay
CR	Virgin Compression Ratio
CRS	Constant Rate of Strain
CSL	Critical State Line
DSS	Direct Simple Shear
GOM	Gulf of Mexico
LVDT	Linear Variable Differential Transformer
MH	Elastic silt
MIT	Massachusetts Institute of Technology
NC	Normally Consolidated
OC	Overconsolidated
OCR	Overconsolidation Ratio
PSC	Plane Strain Compression
PSE	Plane Strain Extension
PVA	Pressure-Volume Actuator
R	Resedimented

RBBC	Resedimented Boston Blue Clay
RGoM EI	Resedimented Gulf of Mexico Eugene Island Clay
RGoM Ursa	Resedimented Gulf of Mexico Ursa Clay
RLC	Resedimented London Clay
RPC	Resedimented Presumpscot Clay
RSFBM	Resedimented San Francisco Bay Mud
RUC	Resedimented Ugnu Clay
SHANSEP	Stress History and Normalized Soil Engineering Properties
SR	Swelling Ratio
SS	Skibbereen Silt
TC	Triaxial Compression
TE	Triaxial Extension
TX	Triaxial
USCS	Unified Soil Classification System
VCL	Virgin Compression Line

$A_{cylindrical}$	Right cylinder area correction for a specimen
A_f	Skempton's pore pressure parameter A at failure
A_o	Initial specimen area
$A_{parabolic}$	Parabolic area correction for a specimen
B	Skempton's pore pressure parameter B
B_{meas}	Measurable/observable B-value in a triaxial test
B_{true}	True B-value of a soil specimen
C	Compressibility of a soil specimen with respect to a change in consolidation stress
C_c	Compression index

C_L	Compressibility of the drainage lines and valves in a triaxial cell
C_M	Compressibility of a pore pressure transducer
C_s	Compressibility of the solid material(s) forming soil particles
C_w	Compressibility of the pore fluid within a specimen
c_v	Vertical coefficient of consolidation
c’	Apparent cohesion intercept
E	Young’s modulus
E_u, E_{uMAX}	Undrained secant Young’s modulus, maximum undrained secant Young’s modulus
e	Void ratio
G_s	Specific gravity
I_p	Plasticity index
K	Lateral stress ratio
K_O	Coefficient of lateral earth pressure at rest
K_{ONC}	Coefficient of lateral earth pressure at rest for NC soil
K_{OS}	Coefficient of lateral earth pressure at rest for a soil undergoing swelling
K_{OR}	Coefficient of lateral earth pressure at rest for a soil undergoing recompression
k	Vertical (bedding perpendicular) permeability
$k_{0.5}$	Vertical (bedding perpendicular) permeability at a porosity of 0.5
m	Exponent in the SHANSEP equation describing the change in normalized strength with OCR
n	porosity, or exponent describing the change in K_O with OCR
p’	Average effective stress, $\frac{1}{2}(\sigma'_a + \sigma'_r)$
p'_m	Mean effective stress, $\frac{1}{3}(\sigma'_1 + 2\sigma'_3)$
q	Shear stress, $\frac{1}{2}(\sigma_v - \sigma_h)$
r^2	Regression coefficient
S	Normalized undrained strength for NC soil in SHANSEP equation

s_u	Undrained shear strength
t	Time
u	Pore pressure
u_b	Back-pressure
u_e	Excess pore pressure
u_s	Shear induced pore pressure
V_L	Volume of fluid in the drainage lines, valves and porous stones of a triaxial cell
V	volume of a soil specimen
v	specific volume
w_c	Water content
w_L	Liquid limit
w_p	Plastic limit
ΔV_{app}	The volume of pore fluid which flows from a specimen into the drainage lines at the point of undrained failure
ΔV_{shear}	The volume of pore fluid which must drain from a soil specimen in order to fully develop its drained strength

ε	Strain
ε_a	Axial strain
ε_f	Axial strain at shear failure
ε_v	Volume strain
γ	Slope of [log] permeability-porosity relationship
φ'_{cs}	Secant critical state friction angle
φ'_p	Secant friction angle at peak shear strength
σ'_p	Preconsolidation pressure
σ'_v	Vertical effective stress

σ'_{vy}	Vertical effective yield stress
σ_1, σ_2, σ_3	Major, intermediate and minor principal stresses
σ_{oct}	Octahedral stress, $\frac{1}{3}(\sigma_1 + 2\sigma_3)$ (same as total mean stress)
τ	Shear stress

1 INTRODUCTION

1.1 PROBLEM STATEMENT

The mechanical behaviour of fine-grained soils is now relatively well understood for the range of stresses conventionally encountered in geotechnical engineering practice. Traditionally, the geotechnical engineering discipline has been focused on applications involving stresses less than about 1 MPa, with behavior at higher stresses being of much less concern. On the other hand, the field of rock mechanics has traditionally been associated with the study of lithified materials, often at pressures in excess of 100 MPa. As a result, the mechanical behavior of intermediatory materials, which include hard clays and unlithified or weakly lithified soft clay-shales, is far less well understood. Such materials are the most abundant in the uppermost 5 km of the Earth's crust (Petley 1999). In recent years a desire to gain a deeper understanding of the behavior of these materials has been driven primarily by the petroleum industry for applications in hydrocarbon reservoir development.

This thesis involves an extensive experimental investigation of the compressibility, permeability and shear strength behavior of fine-grained sediments over the stress range of 0.1 – 100 MPa. The work focuses particularly on strength behavior, and examines the friction angle and undrained strength properties of a variety of fine-grained materials from a wide range of geologic backgrounds. The work also examines the systematic variation of these properties with effective stress level, and demonstrates that the degree to which these strength properties vary as a function of stress is closely related to a soil's composition.

The overall goal of this work is to increase understanding of the consolidation and shearing behavior of fine-grained sediments at stresses traditionally encountered in geotechnical engineering practice but also at much higher stresses. The research aims to make a consistent link between the mechanical behavior of soft soils and unlithified soft rock.

1.2 THESIS SCOPE AND OBJECTIVES

The research presented in this thesis has three main objectives. The first and primary objective is to examine the shear strength behavior of a variety of fine-grained sediments over the stress range of 0.1 – 100 MPa and to determine the effects of soil composition, effective stress level and overconsolidation ratio (OCR) on this behavior. This is achieved through a program of K_O-consolidated undrained triaxial tests on fully saturated specimens possessing varying degrees of mechanical consolidation. The vast majority of tests are performed in triaxial compression mode of shear and all are performed at room temperature. Test specimens are produced by resedimenting the natural source materials in the laboratory. Resedimentation allows one to produce saturated samples of identical composition from source material with any desired preconsolidation stress or porosity, something which would be impossible with the use of intact samples.

A secondary objective of the research is to examine the principle of effective stress in relation to the shear strength of fine-grained soils. In particular, to investigate whether there is any effect of interparticle contact area on how effective stress should be defined at the pressures relevant to the research. The conventional Terzaghi definition of effective stress, i.e. total stress minus pore water pressure, assumes that there is no effect of interparticle contact area on effective stress, or at least that any such effect is negligible. While this assumption has long been shown to be valid at pressures typically encountered in geotechnical engineering practice, validation of its applicability for fine-grained soils at the pressures encountered in this research has not previously been demonstrated. It was therefore necessary to investigate if the conventional definition of effective stress would be appropriate to apply in the analysis of high pressure triaxial tests such as performed in this research.

The third objective of the research is to develop the necessary equipment for testing conventional sized specimens (3.5 cm diameter and 8.1 cm height) at effective stresses up to 100 MPa. Existing low and medium pressure triaxial systems in the MIT Geotechnical Engineering Laboratory only enable triaxial testing at effective stresses up to 2 MPa and 10 MPa respectively. A new high pressure triaxial system is custom designed and built to achieve this objective. The new system consists of a high pressure triaxial cell with internal deviator load measurement, pressure volume actuators to generate the necessary cell, pore and load frame pressures, as well as a new control system to allow for continuous automated test control. The system has the ability to perform both K_O or stress path consolidation prior to shearing.

The work presented in this thesis represents one element of the wider research objectives of the UT GeoFluids Consortium, a joint venture between the Massachusetts Institute of Technology and the University of Texas at Austin. The high level objective of the GeoFluids group is "*to study the state and evolution of pressure, stress, deformation and fluid migration through experiments, theoretical analysis, and field study*". The author's research focuses solely on mechanical behavior determined through experimentation, and provides a baseline behavior for use in analytical geomechanical models.

1.3 ORGANIZATION OF THE THESIS

This thesis is organized into seven chapters, each of which has a separate and distinct function, as given below.

Chapter 2 provides a literature review of important background information relevant to the research. The aim is to establish an overall picture of the current level of knowledge regarding the shear strength behaviour of unlithified fine-grained sediments at stresses higher than those typically encountered in geotechnical engineering, i.e. > 1 MPa. The effects of natural micro-structure, particularly cementation due to diagenesis, on strength properties are discussed. The concept of normalized soil behavior is then introduced, including the SHANSEP normalization procedure. Chapter 2 also provides a review of the principle of effective stress, including previous studies which have examined the applicability of the standard Terzaghi definition of effective stress at high pressures. Finally, Chapter 2 discusses the issue of specimen saturation and introduces the concept of a B-value.

Chapter 3 discusses the origin and index properties of soils tested as part of this work, including Presumpscot Clay, Boston Blue Clay, Ursa Clay, Ugnu Clay, San Francisco Bay Mud, London Clay, Skibbereen Silt and Eugene Island Clay. These fine-grained soils cover a very wide range in terms of composition, geologic origin and mechanical properties. Chapter 3 also provides a detailed description of the resedimentation process, including the processing method used for the various source materials, a brief background of resedimentation at MIT, the procedure and equipment used as part of this work, and an evaluation of sample uniformity.

Chapter 4 describes the equipment and procedures used in the triaxial testing program carried out during the course of the research. A description is given of the three different automated triaxial systems designed for low, medium, and high stresses that were used throughout the testing program. A more detailed discussion is provided of the high pressure triaxial system which was developed as part of this work, including a description of the high pressure cell, pressure volume actuators, automated control system and data acquisition. The issue of apparatus compressibility in relation to the pore fluid drainage system and its impact on measurements of pore pressure is also addressed. In addition, an evaluation is given of the reproducibility and reliability of test results obtained using the three types of triaxial system.

Chapter 5 presents the consolidation properties of soils as determined from the results of resedimentation, CRS tests and the K_O-consolidation phase of triaxial tests. The chapter begins by presenting the one dimensional virgin compression behavior of the soils tested, and describes how this behavior changes as a function of soil type and stress level. The permeability behavior of the soils is then presented and it is shown that the permeability-porosity relationships of wide range of different soils can be successfully correlated to liquid limit, liquid limit being used as a convenient indicator of soil composition. Comparisons made between the measured permeabilities of intact samples of Boston Blue Clay and Gulf of Mexico Ursa Clay against those predicted using the liquid limit correlations are used to demonstrate the value of the correlations for predicting in situ permeability. Data on the coefficient of consolidation for the different soils is also presented, together with a discussion of how this value changes over a very wide range of effective stresses. Finally, Chapter 5 presents data on the K_O value of soils as determined from triaxial tests and discusses the dependence of K_O on soil type, stress level and OCR.

Chapter 6 presents results obtained during the shearing phase of triaxial tests. First, the results of tests carried out specifically to investigate the principal of effective stress are presented. Following this, the shear stress – strain and effective stress behavior observed for each soil during undrained shearing is discussed separately. The effect of overconsolidation on undrained shear response is presented for one soil, RBBC. When viewed over a significant stress range, is it shown that the critical state friction angle and undrained strength ratio of most soils vary consistently as a function of effective stress level. Comparisons are then made between the different soils, where it is shown that variations in strength properties are closely related to soil composition. Correlations are presented which allow a reasonable estimate of the drained or undrained strength of a fine-grained soil in triaxial compression to obtained from liquid limit together with a knowledge of the in situ effective stress and OCR. Finally, the important link between undrained strength ratio and the pre-shear value of K_O for normally consolidated soil is discussed.

Chapter 7 summarizes the main conclusions which can be drawn from the results of the research. A hypothesis is proposed to explain the strength behavior of soils as presented in Chapter 6. Recommendations for future work are also given.

2 BACKGROUND

2.1 INTRODUCTION

The mechanical behaviour of fine-grained soils at effective stresses typically encountered in geotechnical engineering applications, below about 2 MPa, is relatively well understood and documented throughout the literature. However, considerably less is known about the behaviour of these soils at much higher stresses. Recent work by Abdulhadi (2009) involved an extensive experimental program to examine systematically the strength properties of resedimented clay as a function of both stress level and OCR for vertical consolidation stresses (σ'_{vc}) up to 10 MPa. Above this stress level, however, there has been no similar experimental program previously carried out to examine systematically the behaviour of clay as a function of both stress level and OCR.

This chapter begins with a review of previous experimental studies carried out to examine the behaviour of both intact and resedimented hard clays in triaxial compression at high stresses. Particular attention is paid to the findings of Abdulhadi (2009).

In Section 2.3 emphasis is placed on the effects of natural micro-structure, particularly cementation due to diagenesis, on the behaviour of intact fine-grained soils at high stresses. These materials are often regarded as clay shales. The brittle-ductile transition in stress-strain response often experienced by these materials is discussed along with some basic models that have been proposed to define their behaviour.

Section 2.4 reviews our current understanding of the normalized behaviour of fine-grained soils at high stresses. The SHANSEP normalization procedure and its applicability at high stresses are discussed. Previous attempts to relate normalized strengths to soil index properties such as the Atterberg limits are also mentioned.

Section 2.5 presents a discussion on the concept of effective stress as well as on assumptions regarding its definition for stresses much higher than those commonly encountered in soil mechanics.

The research presented in this thesis only considers materials which are fully saturated with a single pore fluid. Section 2.6 discusses saturation together with the issue of pore pressure generation in response to an increase in applied boundary stresses. These are important concerns for laboratory testing of any type of porous material, particularly at the stress range encountered in this research.

2.2 PREVIOUS STUDIES OF HARD CLAYS IN TRIAXIAL COMPRESSION

One of the earliest programs of triaxial testing at relatively high stresses is that of Bishop et al. (1965) on London Clay from Ashford Common for σ'_{vc} up to approximately 7.5 MPa. Boom clay has been investigated by both Horseman et al. (1993) and Taylor and Coop (1993) for σ'_{vc} up to 5.4 MPa. Petley et al. (1993) tested Kimmeridge Clay up to 10.6 MPa and Eocene North Sea Shale up to 16 MPa, and compared their undrained shear deformation behaviour with that of chalk. Petley (1999) tested London Clay up to 30.1 MPa in an effort to define the form of the peak strength envelope. Marsden et al. (1992) conducted tests on Weald Shale and Fullers Earth up to 23 MPa and on London Clay up to 8 MPa with the objective of making correlations between petrophysical and mineralogical properties and the measured mechanical behaviour. More recently, Gutierrez et al. (2008) tested Kimmeridge Clay up to 30 MPa and Barents Sea Shale up to 63 MPa as part of an investigation into normalized behaviour.

All of the studies mentioned above involved isotropically consolidated undrained triaxial compression (CIUC) tests on unweathered intact samples. Obtaining intact samples generally involves some sampling disturbance, even with the use of careful sampling procedures, and ideally large diameter or block samples should be used. However, this is generally too expensive or infeasible, particularly in the case of deep samples or samples from the deep ocean. Even more important, the use of intact samples rather than resedimented ones does not allow one to control the stress history, i.e. preconsolidation pressure (σ'_p), of the sample. As a result, intact samples with a high σ'_p require a large consolidation stress to reach the normally consolidated range while samples with a low σ'_p require the development of large strains in order to test at high stresses. Combined, these factors make a systematic investigation of the mechanical behaviour of any soil as a function of both stress level and OCR practically impossible. It is important to note that the above studies also involved isotropic consolidation of test specimens prior to shearing. Unlike one-dimensional (i.e. K_O) consolidation which best mimics in situ conditions, isotropic consolidation is a very rare occurrence in nature and can produce a significantly misleading behaviour in laboratory shear testing. A compilation of a large variety soft clays in both intact and resedimented states by Belviso et al. (2001) illustrates the large difference in undrained strength which some clays exhibit depending on the laboratory consolidation procedure used. For consolidation to the same σ'_{vc}, isotropically consolidated specimens will generally have a higher undrained strength (Resedimented Boston Blue Clay is a notable exception). This is due to the fact that, assuming $K_O < 1$, the mean effective stress prior to shearing will be larger, thereby producing a lower water content/void ratio and a higher undrained strength. On the other hand, due to the anisotropic micro-structure possessed by soil in a K_O condition, K_O consolidated specimens will generally exhibit a higher undrained strength than isotropically consolidated specimens when consolidated to the same mean effective stress. Isotropic consolidation can also produce a very misleading stress-strain response during shearing (Ladd and Varallyay 1965). For samples of resedimented clay and low OCR intact clay in particular, isotropic consolidation can result in a much larger strain to failure (ε_f) and a less distinct peak shear strength compared to samples subjected to K_O consolidation.

Amorosi and Rampello (2007) investigated the behaviour of Vallericca Clay, a structured stiff clay of marine origin from Italy, using a series isotropically and anisotropically consolidated triaxial compression tests for σ'_{vc} up to 11 MPa and 6.75 MPa respectively. These tests were performed on intact samples, though some isotropically consolidated tests were also performed on resedimented samples for σ'_{vc} up to approximately 1.2 MPa. Specimens were sheared under both drained and undrained conditions. Figure 2-1 shows some typical effective stress paths in Cambridge stress space[1] for anisotropically consolidated intact specimens sheared undrained in both the normally consolidated (NC) and overconsolidated (OC) range. Amorosi and Rampello reported that, under both isotropic and anisotropic consolidation to stresses greater than σ'_p, major and irreversible damage to the soil's initial interparticle bonding (likely weak cementation) was produced. While significant changes to the initial soil fabric (where fabric refers to the arrangement of soil particles) also occurred during isotropic consolidation to stresses beyond σ'_p, only minor changes to the soil's fabric were induced by anisotropic consolidation to stresses

---

[1] Cambridge stress space plots deviatoric stress ($\sigma_1 - \sigma_3$) versus mean effective stress $p'_m = ⅓(\sigma'_1 + 2\sigma'_3)$

beyond σ'_p under nearly K_O conditions. It was proposed that, unlike for purely cemented soils, the natural fabric of the Vallericca Clay gave the intact specimens an undrained strength much higher than the resedimented counterparts and this difference was not eliminated by consolidation to high stresses nor by shearing. This can be seen in Figure 2-2, where stress paths for both drained and undrained shearing of intact and resedimented specimens are plotted in specific volume ($v = 1+e$) versus mean stress space. The end points of the tests where a constant shear stress was observed with continued straining produce a critical state line (CSL). A single CSL can be defined for the intact specimens irrespective of their isotropic or anisotropic consolidation histories. The critical states observed for resedimented specimens define a CSL significantly below the one associated with the intact specimens, though characterized by the same slope $\lambda = 0.148$. Since the intact and resedimented CSLs were found to be parallel it was concluded, that over the stress range investigated, the natural Vallericca Clay does not tend to the reference state defined by the corresponding resedimented material. Amorosi and Rampello attributed the variation in behavior between the intact and resedimented samples to a difference in soil fabric. Images taken of the fabric of the natural clay showed a prevalence of edge-to-face contacts with average intra-aggregate pore spaces of 1 – 3 μm and inter-aggregate pores of 3 – 6 μm. In contrast, the resedimented material displayed mostly face-to-face contacts with more closely spaced aggregates. However, Vallericca Clay also contains an unusually large proportion of microfossils, giving the clay a calcium carbonate content of about 30%. It is possible that these microfossils provide the intact material with additional strength which is destroyed by the resedimentation process, though not by shearing in the triaxial device.

One of the most comprehensive and systematic investigations of the mechanical behaviour of a clay for σ'_{vc} up to 10 MPa was carried out by Abdulhadi (2009). Abdulhadi tested Resedimented Boston Blue Clay (RBBC) through a series of CK_OUC tests. Some of the main findings of this investigation are summarized in Table 2-1, which shows the separate effects of varying OCR and stress level on the behaviour of RBBC. Regarding the effect of increasing OCR, the findings are in agreement with previous well established knowledge of behaviour of clays, e.g. Burland (1990) and Amorosi and Rampello (2007), as well as with previous work carried out on RBBC, e.g. Sheahan (1991), Santagata (1994) and Santagata (1998). The increase in normalized undrained strength (s_u/σ'_{vc}, a.k.a. undrained strength ratio) associated with increasing OCR is due to the dilative response of OC clay during shearing. As a result of dilation, OC samples tend to generate lower excess pore pressures and fail at an effective stress higher than the consolidation stress. On the other hand, NC samples exhibit entirely contractive behaviour during shearing as positive excess pore pressures are produced and tend to fail at an effective stress much lower than the consolidation stress. Figure 2-3 shows effective stress paths for specimens of RBBC at OCRs 1, 2 and 4 in MIT stress space[2] normalized to the same σ'_p of 10 MPa. As shown in Figure 2-4, increasing OCR also leads to a more ductile response as the strain to failure increases and post-peak strain softening decreases. An increase in the value of K_O and normalized undrained secant Young's Modulus (E_u/σ'_{vc}) with increasing OCR, as well as a decreasing A parameter (Skempton 1954) at failure (A_f) with increasing OCR, are also results that are to be expected for clay.

Unlike the effect of OCR, the effect of stress level on the mechanical properties of clay is less well established. Significantly, Abdulhadi (2009) found that increasing consolidation stress causes a reduction in normalized undrained strength. Figure 2-5 clearly illustrates the consistent trend of decreasing normalized strength with increasing stress level for each OCR tested. Most of the decrease occurs at low stresses < 1 MPa. This reduction in normalized strength with stress corresponds with an increase in the normally consolidated value of K_O (K_{ONC}) at the end of virgin consolidation as stress level increases, as shown in Figure 2-6. Abdulhadi suggested that the link between normalized undrained strength and K_O is more pronounced in the NC clay than the OC clay, since for the NC clay a relatively small shear stress increment is required to attain the peak stress state from the pre-shear stress state. At a given stress level, the stress paths for each OCR approach a common failure envelope at large strains, as shown in Figure 2-3 for σ'_p = 10 MPa. However, while the failure envelope at 10 MPa has a critical state friction angle φ'_{cs} = 26.8° and normalized cohesion intercept $c'/\sigma'_p = 0.032$, the failure envelope at 0.2 MPa has φ'_{cs} = 33.7° and $c'/\sigma'_p = 0.018$. This implies a failure envelope having significant curvature. The secant friction angle at peak shear strength (φ'_p) decreases with increasing stress level for the OC clay, which is expected given that φ'_p coincides with φ'_{cs}. However, for the NC clay φ'_p is unrelated φ'_{cs} and the value of φ'_p is found to be unaffected by stress level. Increasing consolidation stress also produces a more ductile response during shearing as strain to failure increases and post-peak strain softening decreases for a given OCR, a behaviour illustrated in

---

[2] MIT stress space plots shear stress $q = ½(\sigma_v - \sigma_h)$ versus effective stress $p' = ½(\sigma'_v + \sigma'_h)$

Figure 2-4. The normalized Young's Modulus also displays stress level dependence, decreasing in magnitude with increasing consolidation stress for each OCR tested. This is illustrated in Figure 2-7, where it can also be seen that the high pressure tests show a larger strain range of linear behaviour than the low pressure tests. The reduction in normalized undrained strength with increasing stress level found by Abdulhadi (2009) is discussed further in Section 2.4.2.

One might suspect that the decrease in normalized strength with increasing stress level found by Abdulhadi (2009) would be associated with an increase in excess pore pressure (u_e) at failure. Significantly, however, Abdulhadi (2009) found that as consolidation stress increases, the normalized excess pore pressures generated during undrained shearing decreased for each OCR tested. To isolate the pore pressure response due to changes in shear stress alone, the shear induced pore pressure ($u_s = \Delta u - \Delta\sigma_{oct}$)[3] provides a better understanding of pore pressure generation during undrained shearing as it essentially removes the effect of total stress path. Note that unlike u_e, u_s is a soil property. Figure 2-8 shows the normalized shear induced pore pressure (u_s/σ'_{vc}) generation with strain for RBBC at OCRs 1, 2, and 4 at low and high stress levels (σ'_p = 0.2 and 10 MPa). In all cases the shear induced pore pressures initially increase, indicating contractive behaviour. The NC clay remains contractive throughout shearing, while the OCR = 2 clay changes to slightly dilative behaviour before contracting again with increasing strain. The shear induced pore pressures decrease beyond 0.5% strain for the OCR = 4 clay which ultimately displays dilative behaviour with continued shearing. As the stress level increases, the shear induced pore pressures decrease for the NC and OCR = 2 clay while for the OCR = 4 clay the pore pressures instead increase, i.e. become less negative.

Some of the very limited triaxial compression testing carried out on resedimented clays for σ'_{vc} higher than the 10 MPa achieved by Abdulhadi (2009) includes William (2007), Yassir (1989), Berre (1992) and Bishop et al. (1975)[4]. William (2007) tested both resedimented and intact Bringelly Shale from Sydney for σ'_{vc} up to 60 MPa. However, these tests involved incremental isotropic consolidation of test specimens prior to drained shearing. Only a limited number of tests were performed on the resedimented material and the results are of little

---

[3] Octahedral stress (σ_{oct}) is the same as total mean stress (p_m). For conventional triaxial compression testing where there is no change in cell pressure during shearing, i.e. $\Delta\sigma_3 = 0$, u_s is simply equal to $\Delta u - ⅓\Delta\sigma_v$

[4] Some of the findings of Bishop et al. (1975) are discussed in Section 2.4.2

relevance to the author's research. Berre (1992) attempted to mimic the behaviour of intact natural clay shale using artificial shale produced in the laboratory by resedimentation. Mixtures of remolded Moum Clay and kaolinite were created so that their composition would be as close as possible to that of the natural clay shale. The mixture had a clay fraction of approximately 58%, liquid limit (w_L) of 60% and plasticity index (I_p) of 37%, resulting in a Unified Soil Classification System (USCS) classification of CH. Samples were consolidated in an oedometer to $\sigma'_p = 32$ MPa before being unloaded and dismounted. Triaxial specimens were then cut from the oedometer sample and reconsolidated anisotropically in the triaxial cell to $\sigma'_{vc} = 20$ MPa (corresponding to an OCR = 1.6) before being sheared undrained. A comparison of very limited results from triaxial tests performed on the resedimented material and on the natural clay shale shows that while the undrained strengths were somewhat similar for the two materials when compared at the same porosity, the stress-strain responses were very different. The resedimented material behaved in a purely ductile manner with ε_f of almost 5%, while the intact natural clay shale behaved in a brittle manner with ε_f varying from 0.4% to 2.4% and increasing with stress level. It should be noted that ε_f of 5% is extremely large even for resedimented clay at an OCR of 1.6. In addition to the differences in stress-strain response, the resedimented specimens displayed a pronounced barrel shape when dismounted from the triaxial cell after shearing, with little sliding along a slip surface. This is in contrast to the intact specimens where most of the displacements after the small strain failure took place along one or two very distinct slip surfaces. This type of shear deformation reported by Berre has also been found to occur in many other natural clay shales (e.g. Petley (1999) and Petley et al. (1993)). Berre concluded that the artificial clay shale may be considered as an uncemented version of the natural clay shale.

Yassir (1989) carried out an investigation into the undrained shear behaviour of several resedimented soils from mud volcanoes. A clay obtained from a mud volcano in Taiwan was tested for σ'_{vc} up to 68 MPa. This clay had a clay fraction of approximately 29%, $w_L = 32\%$ and $I_p = 13\%$, resulting in a USCS classification of CL (low plasticity clay). Since it was obtained in a completely remolded state from nature, it contained little or no cementation bonding. The samples tested were prepared by consolidating a vacuumed slurry in an oedometer to $\sigma'_p = 2.45$ MPa. Triaxial specimens were then trimmed from the oedometer sample and reconsolidated in the triaxial cell to a stress higher than the oedometer σ'_p using either isotropic or anisotropic consolidation. All specimens were normally consolidated prior to undrained shearing. A peak shear strength was not observed in any of the anisotropically consolidated tests and the clay behaved in a completely ductile fashion, maintaining maximum deviatoric stress without significant strain weakening for axial strains up to 16%. This is shown in Figure 2-9, where one can also see a large difference in stress-strain response for tests TA and TF which involved isotropic consolidation to $\sigma'_{vc} = 50$ and 5 MPa respectively, compared to tests TC, TD and TE which were anisotropically consolidated (with $K = 0.6$) to $\sigma'_{vc} = 68$, 20 and 34 MPa ($p'_m = 50$, 15 and 25 MPa) respectively. Figure 2-10 shows the corresponding undrained effective stress paths for the tests in Cambridge stress space. It can be seen that the shape of the stress paths followed by the anisotropically consolidated specimens is somewhat different from that typically expected for NC clay, e.g. by comparison with Figure 2-1 for tests carried out by Amorosi and Rampello (2007). Similar to the findings of Abdulhadi (2009), Yassir reported a failure envelope having significant curvature, with φ'_{cs} (assuming $c' = 0$) decreasing from 26.1° for test TF ($\sigma'_{vc} = 5$ MPa) to 22.6° for test TC ($\sigma'_{vc} = 68$ MPa). A line drawn through the end points of the tests at lower stresses in Figure 2-10 is used to demonstrate the curvature of the failure envelope. Pore pressures increased initially during undrained shearing after which they remained approximately constant, indicating that critical state had been achieved.

The normalized undrained shear strengths found by Yassir (1989) vary very little over the entire stress range investigated, ranging between just 0.24 to 0.25 for the anisotropically consolidated tests, with no clear trend with stress level. This is in contrast to the findings of Abdulhadi (2009) and may be related to the fact that Yassir used a constant $K = 0.6$ for all anisotropically consolidated tests. Abdulhadi employed K_O consolidation and found K_{ONC} to increase with increasing consolidation stress as normalized undrained strength decreased. However, similar to Abdulhadi, Yassir did find a clear decrease in normalized excess pore pressures with increasing consolidation stress. Figure 2-11 illustrates this trend for both the isotropically and anisotropically consolidated tests (keep in mind that Figure 2-11 plots excess pore pressure u_e normalized with respect to the pre-shear mean consolidation stress p'_o, while Figure 2-8 by Abdulhadi (2009) plots shear induced pore pressure u_s normalized with respect to the pre-shear vertical consolidation stress σ'_{vc}). The decrease in normalized excess pore pressures indicates an increasingly dilative shear response with increasing stress level. Yassir concluded that there is strong evidence to suggest that the normalized behaviour of a sediment changes with increasing stress level.

Nüesch (1991) pioneered work on laboratory testing of reconstituted clay shale. Nüesch tested partially saturated samples of Opalinus Shale from the Jura Mountains in both triaxial and simple shear configurations. Tests were performed at temperatures of 20 – 350 °C, strain rates of 10^{-4} – 10^{-6} s^{-1}, and confining pressures of 0.1 - 400 MPa. It was found that water content and confining pressure were the most important factors controlling the strength of the partially saturated samples, with temperature and strain rate having much smaller influences by comparison. Experiments performed at room temperature and at a confining pressure of 50 MPa showed that a water content corresponding to a single layer of absorbed water had little effect on strength when compared to a dry sample, but that a second layer of absorbed water reduced strength by 20 % and a third layer by 50 %. The partially saturated nature of samples, however, reduces the relevance of the study to the author's work.

2.3 EFFECTS OF DIAGENETIC CEMENATATION ON BEHAVIOUR

2.3.1 Introduction

Diagenesis refers to chemical and physical processes that affect the mechanical properties, fabric and mineralogical composition of sediments from the time of their deposition but prior to the onset of metamorphism. A common diagenetic process in clays involves the gradual breakdown of smectite to illite and is a well known occurrence in sedimentary basins. One of the most significant diagenetic processes which occurs in both clayey and granular soils involves the cementation of soil particles by the precipitation from the pore fluid of calcium carbonates, aluminum and iron hydroxides, silicates as well as other organic or inorganic compounds at interparticle contacts. Cementation is regarded as a form of natural micro-structure and can have a major effect on soil properties including void ratio, stiffness, apparent preconsolidation and shear strength (Gutierrez et al. 2008). It is also a possible cause of 'true' cohesion for soils. Cementation is a particularly important phenomenon influencing the behaviour of natural fine-grained soils which exist at high in situ effective stresses. As a result of their diagenetic history, these materials are more difficult to characterize and their behaviour much more difficult to predict than soft clays.

2.3.2 Classification of Fine-grained Materials

Before proceeding any further it is important to clarify the terminology used to describe and classify fine-grained materials in general. The materials referred to in this section lie in a transitional regime between hard clay and soft ductile argillaceous rock. This transitional nature has lead to great confusion and researchers neither in soil mechanics, rock mechanics nor geology have succeeded in adopting a consistent classification scheme for these materials. For example, while one author may refer to a material simply as shale, others may refer to the same material as clay, clay shale or mudstone. For clarification, the following descriptions are given based on definitions suggested by Stokes and Varnes (1955):

Shale: A general term for lithified clays and silts which are *fissile* and break along planes parallel to the original bedding.

Clay shale: A shale that consists primarily of clay minerals.

Claystone: Now used mainly to designate clay which has become indurated by some means, e.g. due to cementation. It is the same as *clay rock* and is sometimes used to designate concretionary masses found in clay deposits. Unlike shale, claystone does not necessarily possess significant fissility.

Mudstone: Mudstone (sometimes mudrock) is a generic term for all fine-grained sediments and includes clay, silt, siltstone, claystone, shale and argillite. It should be used when there is doubt as to a precise identification or when a deposit consists of a mixture of clay, silt and sand sized particles.

While the above descriptions are helpful, they are by no means definitions that all in the geology and engineering professions follow. A good review of the various geological and engineering classification schemes which have been proposed for fine-grained materials over the years is given in William (2007). To add to complication, the terms clay and silt also have more than one definition:

Clay:

Definition 1: Under the USCS classification system, a fine-grained soil whose Atterberg Limits (ASTM D4318) cause it to be plotted above the 'A' Line in the Casagrande Plasticity chart (Lambe and Whitman 1969).

Definition 2: A soil which, by weight, more than 50 % of its particles are smaller than 0.002 mm.

Definition 3: A soil consisting primarily of clay minerals, e.g. smectite, illite, kaolinite.

Silt:

Definition 1: A soil which, by weight, more than 50 % of its particles are smaller than 0.075 mm and whose Atterberg Limits cause it to be plotted below the 'A' Line in the Casagrande Plasticity chart

Definition 2: A soil which, by weight, consists primarily of particles in the size range 0.075 - 0.002 mm

It is therefore necessary for the author to adopt some reasonable terminology which can be used consistency throughout this literature review. Since the research presented in this thesis focuses on the mechanical behaviour of resedimented fine-grained soils at relatively high stresses, this material will be regarded by the author as 'hard clay' (with clay being defined using Definition 1 above). This is in accordance with the classification scheme proposed by Terzaghi et al. (1996) for clays exhibiting an undrained strength $s_u > 0.2$ MPa. The same designation will be used for intact clay subjected to high stresses but not possessing significant cementation, such as London Clay for example. Uncemented clay subjected to densification under high stresses may also be referred to as a 'compaction shale' (H.H. Einstein, personal communication). However, to avoid confusion, when referring to materials tested by other researchers in this literature review, the author will use the names adopted by those researchers.

As mentioned previously, many studies on the mechanical behaviour of fine-grained materials at relatively high stress levels have been carried out using intact samples. These intact samples often possess varying degrees of cementation due to diagenesis and are usually referred to by the authors simply as shale or clay shale. While it is possible that many of these materials do possess significant fissility, it seems likely that some do not and would therefore be better classified generally as a mudstone. However, for the purpose of consistency and simplicity, the author will use the term 'clay shale' throughout this literature review when referring to these materials.

2.3.3 Apparent Preconsolidation

Cementation is often attributed to causing an increase in the preconsolidation stress of sediments significantly above that caused by mechanical compression. In fact, for older sediments that have been subjected to high stresses as a result of burial at a great depth, diagenetic processes such as cementation can be a much more important cause of overconsolidation than mechanical processes, e.g. due to increased overburden pressure. This increase in overconsolidation due to non-mechanical processes such as cementation is often referred to as 'apparent' or 'quasi' preconsolidation (Gutierrez et al. 2008). The ratio of the apparent preconsolidation stress to the current in situ effective stress is sometimes referred to as the yield stress ratio (YSR) rather than overconsolidation ratio (OCR). It should be noted that, apart from cementation, many other natural phenomenon may cause an apparent preconsolidation to develop in a soil. These phenomena include ageing (often referred to as creep or secondary compression) or desiccation caused by evaporation or freezing (Ladd 1985).

2.3.4 Stress-Strain Response during Shearing

Diagenetic cementation also has a major effect on the stress-strain and strength behaviour of fine-grained materials by imparting a considerable stiffness and brittleness that would not otherwise exist. In comparison to the behaviour of OC resedimented clay discussed earlier, OC clay shales at a similar stress level exhibit an extremely brittle behaviour characterized by a well defined peak strength and large amounts of post-peak strain softening (Berre 1992, Horseman et al. (1993), Taylor and Coop (1993), Petley et al. 1993, Marsden et al. 1992). On the other hand, NC clay shales (i.e. produced by consolidating a clay shale well beyond its apparent preconsolidation stress) show a ductile response with a less well defined peak strength, much less post-peak strain softening and contractive behaviour similar to that exhibited by NC resedimented clay. Figure 2-12 shows normalized shear stress-strain responses for intact samples of Kimmeridge Shale and Barents Sea Shale subjected to CIUC tests by Gutierrez et al. (2008).

The apparent preconsolidation stresses for the Kimmeridge Shale and Barents Sea Shale were estimated to be 22 MPa and 40 MPa respectively. The general trend observed in each case is that, as the consolidation stress increases (i.e. OCR decreases), brittleness decreases as post-peak strain softening and stiffness are reduced.

The behaviour of clay shales as described in the preceding paragraph can be attributed to a brittle-ductile transition in the stress strain response. This is a well known phenomenon in the field of rock mechanics (e.g. Paterson and Wong 2005). Though less well understood for clay shales, work has been carried in this area as well as on the deformation and fabric changes induced in these materials due to high pressure consolidation and shear by Petley et al. (1993) and Petley (1999). Figure 2-13 illustrates conceptually the different types of stress-strain response observed in clay shales. At relatively low consolidation stresses the response is brittle, with a distinct peak strength followed by strain softening to a post-rupture strength. Brittle failure occurs rapidly once the stresses at certain inter-particle contacts reach the bond strength and a de-bonding process is initiated. Failure of a triaxial specimen occurs along one or two very distinct slip surfaces, or failure planes, with large deformations occurring along these slip surfaces. Micrographs of sheared triaxial specimens illustrate that these slip surfaces are at the centre of a shear zone in which the original bonded structure is progressively re-oriented, causing the platy clay particles to become increasingly aligned parallel to the surface (Petley et al. 1993). This realignment of clay particles increases with increasing shear strain. On the other hand, at higher stresses where the yield strength of the bonded structure has been exceeded during consolidation, the response is ductile with peak strength being maintained for the accumulation of large strains. The specimen deforms pervasively in a pronounced barrel shape with no slip surface generally being present. At intermediate stresses a transitional regime exists in which the response is a combination of ductile behaviour, during which a peak strength is maintained up to a certain strain, followed by brittle behaviour, during which failure and strain weakening occur. During the maintenance of peak strength, Petley (1999) postulated that "*the sample is undergoing pervasive micro-cracking, such that on the micro-scale the deformation is brittle. However, on the macro-scale (whole sample) the deformation is uniformly distributed and is effectively ductile*". Brittle failure "*occurs as a result of the formation of a single fracture caused by the coalescence of micro-cracks formed during the ductile deformation phase*". Once this occurs the shear strength along the slip surface quickly drops to the post-rupture value. After increasing initially as deviatoric stress increases, pore pressures remain approximately constant during the ductile phase. An excellent example of the brittle-ductile transition experienced by two clay shales is given in Figure 2-12 (keep in mind that Figure 2-12 plots *normalized* shear stress versus axial strain).

2.3.5 Failure Envelopes

Factors such as natural micro-structure, OCR and stress level result in several failure envelopes being defined for a fine-grained soil. Burland (1990) reviewed the behaviour of different intact and resedimented clays and demonstrated that the peak undrained strength of undisturbed clays is often significantly greater than that of the corresponding resedimented material at the same void ratio due to the effects of natural micro-structure. Burland concluded that four fundamental failure envelopes may be defined for clays: 1) a peak strength envelope defining brittle failure of undisturbed OC clays; 2) a post-rupture strength envelope representing the end of rapid post-peak strain softening of undisturbed OC clays; 3) an 'intrinsic' critical strength envelope defined by the failure of resedimented samples; and 4) a residual strength envelope reached only after very large strains as particles become aligned parallel to the failure surface. The four failure envelopes defined by Burland (1990) are shown in Figure 2-14. The peak strength envelope is curved, shows a cohesive intercept and lies above the intrinsic critical state envelope due to the influence of natural micro-structure possessed by undisturbed OC clay. On the other hand, undisturbed NC clay (i.e. intact clay which possesses no mechanical or apparent preconsolidation) will tend to fail on the intrinsic critical state envelope and then travel down this envelope. The intrinsic critical state envelope may be interpreted as a basic property independent of the undisturbed state of the material and can be viewed as providing a good basis for comparison of the properties of different clays. The post-rupture envelope can be seen to lie very close to the intrinsic critical state envelope. After very large shear strains, such as can be attained in a ring shear device, both undisturbed and resedimented clay will reach a common residual strength envelope as the platy clay particles become aligned parallel to a shear surface.

Petley (1999) reviewed the undrained shear behaviour of some resedimented and intact hard clays and clay shales and proposed an extension to the work of Burland (1990) to include the behaviour of these materials for consolidation stresses up to 50 MPa. The conceptual form of the failure envelopes proposed by Petley (1999) is shown in Figure 2-15 (it should be noted that what Petley (1999) refers to as the 'residual' strength envelope in Figure 2-15 is in fact the intrinsic critical state envelope under Burland's (1990) definition; a true residual strength envelope is not considered by Petley). The brittle failure envelope (i.e. the 'peak strength' envelope under Burland's terminology) is initially approximately linear with a cohesive intercept but reduces in gradient with increasing consolidation stress as the material undergoes a transition to a more ductile stress-strain response. The gradient of the brittle failure envelope decreases such that it ultimately intersects the intrinsic critical state envelope, at which point behavior is purely ductile. The stress level at which these envelopes intersect will likely depend on the amount and strength of natural micro-structure which the material possesses, as indicated by the magnitude of the [apparent] preconsolidation stress, with strongly structured soils showing a distinct peak strength up to relatively high stresses. After brittle failure, the undisturbed material will strain weaken to the post-rupture envelope. The shape of the post-rupture envelope is poorly understood and difficult to define, but evidence suggests that it has a curved form at high stresses. For relatively low consolidation stresses, undisturbed natural OC clays and clay shales do not reach the intrinsic critical state envelope except at large strains. On the other hand, at relatively high consolidation stresses the peak strength envelope coincides with the intrinsic critical state envelope. However, the form of the failure envelope in the ductile regime is not well understood. Based on the work of Yassir (1989), Petley concluded that the intrinsic critical state envelope is linear for mean consolidation stresses up to at least 50 MPa. However, as mentioned previously, Yassir (1989) actually found that slope of this envelope decreases slightly with stress level. Moreover, the findings of Abdulhadi (2009) give strong indication that the intrinsic critical state envelope is in fact also non-linear.

2.4 NORMALIZED BEHAVIOUR

2.4.1 Introduction

The Normalized Soil Parameter concept is based on the empirical observation that clay samples having a similar OCR but different consolidation stresses, and therefore different preconsolidation pressures, exhibit similar properties (e.g. undrained strength, shear induced pore pressures) when normalized with respect to the consolidation stress. This has led to the SHANSEP (Stress History and Normalized Soil Engineering Properties) design procedure developed by Ladd and Foott (1974). The Normalized Soil Parameter concept is also the basis for other frameworks which describe soil behaviour such as Critical State Soil Mechanics (Schofield and Wroth, 1968), or analytical models such as Modified Cam Clay (Roscoe and Burland 1968) and MIT-E3 (Whittle and Kavvadas 1994).

The SHANSEP normalization procedure is generally applied to undrained shear in triaxial compression (TC) and extension (TE), plain strain compression (PSC) and extension (PSE) and direct simple shear (DSS). Figure 2-16 shows typical results of a SHANSEP test program performed on AGS Plastic Marine Clay in TC, TE and DSS. The results can be represented using an expression commonly referred to as the SHANSEP equation:

$$s_u/\sigma'_{vc} = S(OCR)^m \tag{2-1}$$

where S is the undrained strength ratio for NC clay and m is the power coefficient. The difference in behaviour for the three modes of shearing is a reflection of the anisotropic nature of soil. The procedure should ideally only be applied to tests involving K_O consolidation. While the use instead of isotropic consolidation is generally believed to have a small impact on the measured undrained strength of intact OC specimens, for resedimented specimens or for intact specimens consolidated into the NC range where the yield surface changes, K_O consolidation prior to shearing is especially important (Belviso et al. 2001, Ladd and Varallyay 1965).

2.4.2 Effect of Stress Level on Normalized Strength

The underlying assumption of SHANSEP is that normalized behaviour is only dependent on OCR. Thus, while the pre-shear stresses used in the laboratory testing program may be different from the in situ stresses, the method predicts identical behaviour for a given OCR. However, the work of Abdulhadi (2009) shows clearly that normalized properties can vary as a function of stress level. Figure 2-17 by Abdulhadi illustrates the effect of stress level on the SHANSEP S and m parameters for RBBC in triaxial compression. Although the regression line for each stress level only contains three data points, excellent conformity of the data is illustrated by regression coefficient (r^2) values greater than 0.998 in each case. It can be seen that the S parameter decreases consistently with increasing consolidation stress from 0.314 at σ'_p = 0.2 MPa to 0.281 at σ'_p = 10 MPa. On the other hand, the m parameter varies only slightly, ranging from 0.770 to 0.738, and does not appear to be a function of stress level. This observation would seem to indicate that the effect of increasing stress level on undrained strength ratio is the same for all OCRs. A value of 0.314 for the S parameter is consistent with results obtained previously by other researchers who investigated RBBC in triaxial compression at low stresses, e.g. Sheahan (1991) and Santagata (1994). However, the m parameter reported by Abdulhadi (2009) is slightly higher than previously quoted values. This is believed to be due the fact that values of m in the past were determined by matching data points from tests at different stress levels (i.e. higher OCR tests were consolidated to higher values of σ'_p). It could be said that while the effect of stress level on the SHANSEP S parameter of RBBC is relatively small compared to the effects of soil type or mode of shear (see Figure 2-20 for perspective on how S changes due to plasticity and mode of shear), most of the variation occurs within the range of stresses commonly encountered in geotechnical engineering, i.e. < 1 MPa. Recall from Section 2.2 that increasing stress level also affects normalized stiffness and normalized shear induced pore pressures.

One of the earliest programs of triaxial testing at relatively high stresses is that of Bishop et al. (1965) who conducted CIUC tests on London Clay for σ'_{vc} up to approximately 7.5 MPa. While the vast majority of these tests involved the use of intact block samples, a limited number of tests were also carried out on resedimented samples for comparative purposes. The tests on the resedimented clay were carried out in the NC range and it was found that while the undrained strength ratio for the low pressure tests varied from 0.22 to 0.24, it reduced to 0.20 at σ'_{vc} = 6 MPa. It should be kept in mind that these numbers should not be regarded as SHANSEP S parameters due to the use of isotropic consolidation. The failure envelope for the resedimented clay (i.e. the intrinsic critical state envelope under Burland's (1990) definition) was also found to possess significant curvature, with φ'_{cs} decreasing from 21° in the low pressure range to 16.1° at σ'_{vc} = 6 MPa (assuming c' = 0).

Bishop et al. (1975) conducted a series of high pressure CIUC tests on NC resedimented London Clay for σ'_{vc} up to 62.1 MPa. The tests were carried out to determine the effect of negative pore pressure on the strength of clay. This was done by comparing the results of conventional CIUC tests (referred to as confined tests by Bishop et al.) with tests where the cell pressure was removed under undrained conditions prior to shearing, thereby producing negative pore pressure but keeping the same consolidation stress (referred to as unconfined tests by Bishop et al.).

Figure 2-18 shows a graph of undrained strength plotted against consolidation stress where the slope of the graph is equal to the undrained strength ratio. Disregarding the results for the unconfined tests, a definite reduction in the slope of the graph at high consolidation stresses for the confined tests indicates a decreasing normalized undrained strength. Once again, however, due to the isotropic consolidation of specimens, the slope of the graph at a given point should not be regarded as the SHANSEP S parameter. It should also be pointed out that these tests were conducted without back-pressure and as a result full saturation of the specimens prior to shearing is not certain. Pore pressure measurements were not taken during the tests and so the effective stress behaviour of the clay is unknown. In addition, the specimens were sheared very quickly at an axial strain rate of 2% per minute. Combined, these factors reduce the relevance of the tests to the research presented in this thesis.

Jones (2010) performed a series of CK_OUC triaxial tests on Resedimented Ugnu Clay from Northern Alaska for σ'_p up to 10 MPa. Figure 2-19 shows the variation in the undrained strength ratio of the soil with stress level at OCR = 1. It can be seen that there is a relatively consistent trend of decreasing strength ratio with increasing stress level (the results of the test at $\sigma'_p = 0.69$ MPa would appear to be anomalous). Similar to Abdulhadi (2009), Jones reported that the decrease in normalized strength of the soil corresponds to an increase in the pre-shear K_{ONC} with increasing consolidation stress. In addition, the intrinsic failure envelope of the clay was found to have significant curvature, with φ'_{cs} decreasing from 35.1° at $\sigma'_p = 0.2$ MPa to 23.6° at $\sigma'_p = 9.8$ MPa (assuming $c' = 0$).

It is important to keep in mind that the results mentioned above from Bishop et al. (1965), Bishop et al. (1975) and Jones (2010) were all limited to the NC range of the soils tested. Only Abdulhadi (2009) examined the effect of stress level on normalized strength in the OC range.

2.4.3 Correlations with Atterberg Limits

The Atterberg limits (Atterberg 1911) were adopted in geotechnical engineering as a formal way of classifying clayey and silty soils according to the USCS. Due to their widespread use and ease of measurement, it is not surprising that attempts have previously been made to relate the Atterberg limits of a soil to its normalized properties. With regard to undrained strength, Skempton (1957) proposed a correlation between the field vane strength of NC clays and I_p. More recently, Ladd (1991) compiled undrained strength data on a wide variety of NC clays and silts in different modes of shear. Ladd's results are shown in Figure 2-20 which plots values of undrained strength ratio measured at various low stresses (less than about 1 MPa) versus I_p. The undrained strength ratios can be seen to vary from about 0.13 to 0.37 depending on soil type and mode of shearing (values as low as 0.07 have been observed for sodium montmorillonite in CIUC tests by Mesri and Olson (1970)). With regard to friction angle, Figure 2-21 adapted from Terzaghi et al. (1996) shows φ'_{cs} data for a wide variety of clay soils measured at various low stresses plotted against I_p. While there appears to be a general trend for φ'_{cs} to decrease with increasing I_p, there is an enormous amount of scatter, with φ'_{cs} varying between about 20° to 36°. The correlations of both Ladd (1991) and Terzaghi et al. (1996) highlight the difficulty in choosing reasonable strength parameters for fine-grained soils without resorting to field or laboratory testing.

The results presented in Section 2.4.2 give a good indication as to why previous correlations between undrained strength ratios and Atterberg limits and between friction angles and Atterberg limits show a great deal of scatter. Such correlations assumed constant normalized properties (for a given mode of shear) and were based on results from laboratory shear tests performed at various stress levels, typically less than 1 MPa. As discussed, undrained strength ratios and friction angles can change significantly with stress level, particularly at these low stresses. It is therefore not surprising that any attempt to correlate these strength properties to Atterberg limits without accounting for the effect of stress level would be limited in its predictive capability.

2.4.4 SHANSEP versus Recompression

It is important to distinguish between using SHANSEP as a *normalization* procedure, i.e. demonstrating that clays at the same OCR display similar normalized properties, and the SHANSEP *reconsolidation* technique used in the laboratory to create a desired stress history prior to shearing. The SHANSEP reconsolidation technique is illustrated in Figure 2-22. The desired stress history is achieved by K_O consolidation well past the in situ σ'_p into the virgin compression range to a new maximum stress 1.5 - 2 greater than σ'_p (points A and B in Figure 2-22). This is done to remove effects of sampling disturbance. For OCRs greater than unity, the specimen is mechanically overconsolidated by K_O swelling (points C and D in Figure 2-22). The SHANSEP reconsolidation technique is applicable to clays that are close to being normally consolidated or have been mechanically overconsolidated (i.e. possess a true preconsolidation as opposed to an apparent preconsolidation) and maintain the same basic structure once consolidated beyond the in situ σ'_p. The method is therefore ideal for resedimented samples. However, the method is not applicable to sensitive clays or clay shales possessing significant cementation, since laboratory consolidation past the in situ σ'_p will result in irreversible destruction to natural micro-structure. For these materials, the undrained strength measured using the SHANSEP technique can be much lower than the in situ value (Ladd 1991).

Another common reconsolidation procedure used to determine soil shear strengths from laboratory testing is the Recompression technique (Bjerrum 1973). As illustrated in Figure 2-22, this technique involves laboratory K_O reconsolidation of an intact specimen back to the in situ vertical effective stress (σ'_{vo}) before shearing. However, because of sampling disturbance, the water content of the intact specimen reconsolidated to σ'_{vo} will invariably be somewhat lower than the in situ value, thereby resulting in an overestimation of the in situ strength. The validity of the technique therefore depends on the degree of sampling disturbance which the sample was subjected to and the associated water content reduction during laboratory reconsolidation. As such, the technique is favoured more if large diameter or block samples are available. Recompression should never be used for samples close to being normally consolidated since the significant reduction in water content at $\sigma'_{vo} \sim \sigma'_p$ would give unrealistic strength results. The technique is more appropriate for sensitive and cemented materials whose structure would be destroyed if the SHANSEP reconsolidation procedure were used. The Recompression technique is also more appropriate for highly overconsolidated samples since the larger pressures required by the SHANSEP technique in the laboratory may make it impractical to employ.

2.4.5 Normalized Behaviour of Clay Shales

Gutierrez et al. (2008) attempted to apply the SHANSEP normalization procedure to clay shales. Data on 25 different intact clay shales, having varying degrees of cementation, were compiled and it was concluded that SHANSEP may be applicable to these materials. Figure 2-23 shows the SHANSEP normalization procedure applied to four individual clay shales. All of the shales included in the study have a clay content greater than 50% based on mineralogy and the values of porosity range from 62.5% for Fuller's Earth to about 15% for Barent's Sea Shale. Due to the highly anisotropic mechanical behaviour of clay shales caused by their distinct lamination and fissility, Gutierrez et al. highlighted that the results were strictly limited to the case of triaxial compression with the axial stress normal to the direction of bedding.

It is important to point out that Gutierrez et al. (2008) only applied the normalization aspect of SHANSEP. Since the SHANSEP reconsolidation technique would be entirely inappropriate to apply to intact clay shale specimens possessing significant diagenetic cementation, Recompression was used to reconsolidate the test specimens prior to shearing in all cases. However, as previously mentioned, Recompression will result in an overestimation of undrained shear strength for NC and low OCR samples due to a reduction in water content caused by sampling disturbance. In addition, unlike true Recompression which requires K_O consolidation, the majority of tests compiled in the study by Gutierrez et al. (2008) likely involved isotropic consolidation with only limited testing involving K_O or even anisotropic consolidation. As well as a reduction in water content due to sampling disturbance, isotropic consolidation into the NC range involves a rotation of the yield surface, thereby producing unusually high and misleading undrained strengths. Although Gutierrez et al. claim a good correlation between normalized undrained strength and OCR, thereby confirming the applicability of SHANSEP, the quoted R^2 values would seem to indicate that the correlation is by no means as good as for uncemented clays. The SHANSEP S parameters quoted for various clay shales, e.g. in Figure 2-23, are very much larger, and the m parameters vary over a much wider range, than values typically quoted for soft clays, e.g. by Ladd and Foott (1974). The effects of both isotropic consolidation and sampling disturbance are more pronounced in the NC range, thereby reducing the validity of both the measured SHANSEP S parameter as well as the m parameter.

A significant conclusion of Gutierrez et al. (2008) is that the normalization of undrained strength is valid regardless of the cause of the preconsolidation of the material. Thus, the normalized behaviour predicted by SHANSEP could be used without the need to determine the separate contributions of mechanical overconsolidation and diagenetic cementation on the apparent preconsolidation stress. The term preconsolidation stress could therefore be used without regard to the underlying mechanism causing overconsolidation and it is this definition of preconsolidation stress which Gutierrez et al. used to define all quoted values of OCR. This is in contrast to Burland (1990) who recommended that the term yield stress, or more precisely vertical yield stress σ'_{vy}, be used while the term preconsolidation stress should be reserved for situations where the magnitude of such a stress can be established by geologic means.

2.5 THE CONCEPT OF EFFECTIVE STRESS

2.5.1 Introduction

All of the previous studies on the mechanical behaviour of fine-grained soils at high stresses reviewed so far, including those carried out on clay shales, have relied on the underlying assumption of the Terzaghi definition of effective stress to be true. At high stresses, however, deviation from this assumption may need to be considered. Effective stress (σ') can be defined as the partial stress which controls changes in deformation and shear resistance of porous materials and was defined by Terzaghi (1923) for saturated soil as simply being the difference between the total stress (σ) and the pressure of the pore fluid (u), i.e.:

$$\sigma' = \sigma - u \qquad 2\text{-}2$$

The applicability of this expression has been verified experimentally for practically all soil types in the range of stresses typically encountered in geotechnical engineering. It is worth noting that this definition of effective stress does not involve any material properties. Since the expression was first put forward by Terzaghi (1923), several researchers have proposed modifications to produce a more general expression which can be used over a wide range of stresses to include materials from soft soils to lithified rock. This will be discussed in the following section.

2.5.2 Proposed Modifications to Terzaghi's Definition of Effective Stress

(i) *Intergranular Stress*

Some researchers have claimed that effective stress is technically the stress transmitted through the mineral skeleton, often referred to as the intergranular stress, which for a saturated soil can be shown to be:

$$\sigma' = (\sigma - u) + au + (R - A) \quad \text{2-3}$$

where a is the contact area between particles per unit surface area and (R – A) is the net physico-chemical inter-particle stress (Lambe and Whitman 1969). Most investigators have agreed, however, that *a* is small in cohesionless soils, and probably in clay, at stress levels commonly encountered in engineering practice (Bishop and Skinner 1977). In addition, although the effect of the (R – A) term is difficult to quantify experimentally, it is invariably taken to be insignificant even for clay. For higher stresses, however, the contact area between particles becomes non-negligible and, as the spacing between individual clay particles reduces, physico-chemical inter-particle stresses may also become more important. As such, it is only for soil at relatively high stresses that effective stress as predicted by Equation 2-3 may deviate noticeably from that predicted by Terzaghi's expression.

(ii) *Effective stress for changes in volume*

When a porous material is subjected to a change in all-round total stress with no variation in pore pressure, its volume will change. By definition, this volume change is controlled by the change in effective stress. The Terzaghi definition of effective stress assumes that the compressibility of the soil particles is negligibly small compared to the bulk compressibility of the soil skeleton. Biot (1941) proposed an expression to account for the compressibility of soil particles when defining effective stress with respect to a change in volume:

$$\sigma' = \sigma - \left(1 - \frac{C_s}{C}\right)u \quad \text{2-4}$$

where: C_s = compressibility of the soil particles

C = compressibility of the soil skeleton with respect to a change in consolidation stress. C is the inverse of bulk modulus and is defined as $3(1 - 2v)/E$, where E is Young's Modulus and v is Poisson's ratio

The above expression for effective stress in relation to volume change is supported by results from tests carried out on lead shot (Skempton 1960). Lead shot was used as it can produce a high C_s/C ratio at relatively low stresses. For consolidation stresses up to 20 MPa, Skempton (1960) suggested that the ratio C_s/C is unlikely to exceed 0.01 for clays.

More recently, Lade and de Boer (1997) carried out a series of tests on porous cubical specimens of basswood and balsawood which were used to replicate porous media such as soil and rock. They concluded that Biot's Equation 2-4 is more applicable in the case of solid rock with interconnected pores. For soil consisting of separate particles with small contact points, effective stress for volume change is better defined using an equation originally proposed by Suklje (1969):

$$\sigma' = \sigma - \left(1 - (1 - n)\frac{C_s}{C}\right)u \qquad 2\text{-}5$$

where n is porosity. In the case of clay, C_s is approximately 2×10^{-5} MPa^{-1} (Skempton 1960). For the relatively low effective stresses typically encountered in geotechnical engineering practice, the value of C is generally larger by several orders of orders of magnitude, being equal to 3000×10^{-5} MPa^{-1} for a typical sample of heavily overconsolidated London Clay, for example (Bishop et al. 1975). As such, similar to the case for intergranular stress, it is only for soil at relatively high stresses that Equation 2-5 predicts a noticeable deviation from effective stress as defined by Terzaghi's equation. Lade and de Boer (1997) concluded that in practice it is likely not possible to recognize or even measure the difference in effective stress predicted by these two equations for consolidation stresses up to and possibly beyond 100 MPa. It should also be noted that while effective stress as defined in Equation 2-5 (or Equation 2-4 for that matter) determines the overall volume change, it is the component (σ - u), i.e. the consolidation stress, that determines the change in compressibility C (Bishop and Skinner 1977). The value of C depends not only on the current consolidation stress which the soil is subjected to but is also strongly dependent on its stress history, that is OC clay will have a much lower compressibility than NC clay at the same consolidation stress. Other factors such as strain rate, temperature and pore fluid chemistry can also affect the value of C.

(iii) *Effective stress for changes in shear strength*

Of more relevance to the research presented in this thesis is the definition of effective stress that applies to changes in the shear strength of soil. In addition to the assumption that C_s can be considered negligibly small compared to C, the Terzaghi definition of effective stress also assumes that the yield stress of the solid material forming the soil particles, which controls the contact area and intergranular shearing resistance, is independent of confining pressure. If an analogy can be drawn between interparticle friction and conventional metallic friction, then friction would be controlled by the contact area and this area, like the deformation of soil particles, would in turn be controlled by the component (σ - u). It could therefore be inferred that the Terzaghi definition of effective stress would be valid for shear strength irrespective of contact area (Bishop and Skinner 1977). Skempton (1960) extended this theory to include the more general case of soil particle materials whose strength is a function of confining pressure. For these materials, Skempton derived an expression for effective stress that is applicable to changes in shear strength:

$$\sigma' = \sigma - \left(1 - a\frac{\tan\psi}{\tan\varphi'}\right)u \qquad 2\text{-}6$$

where: a = the contact area between soil particles per unit surface area, as before

ψ = the [tangent] angle of intrinsic friction of the material forming the soil particles

φ' = the angle of internal friction of the soil mass

Skempton presented evidence from tests on marble and Solnhofen Limestone which broadly supports the above equation for defining effective stress with respect to changes in the shear strength of rock and concrete. While there was a complete lack of evidence for soils, Skempton concluded that in the range of stresses generally encountered in engineering practice, where soils typically have a small contact area ratio, Terzaghi's equation would be a valid approximation. Once again, it would only be at relatively high stresses when the contact area between particles becomes non-negligible that deviation from Terzaghi's definition of effective stress may need to be considered.

The intrinsic friction angle (not to be confused with Burland's (1990) *intrinsic critical state* friction angle, φ'_{cs}) in the Equation 2-6 was defined by Skempton (1960) as the friction angle of the solid material forming the soil or rock particles. For example, ψ of a silt composed entirely of quartz would be the friction angle of a solid block of quartz. Most materials possess a non-zero value of ψ, even those typically assumed to possess an entirely cohesive strength, such as metals. By analyzing the results of extremely high pressure (> 1 GPa) triaxial tests performed by other researchers on various porous materials, Skempton (1960) proposed the idea that "*at a pressure sufficiently high to cause complete yield of the particles, when the voids are eliminated, the failure envelope becomes coincidental with the intrinsic line*". For rock minerals, Skempton (1960) quoted [tangent] ψ values of 3.5°, 8° and 13.25° for rock salt, calcite and quartz respectively. Based on a re-assessment of published data at the time, Bishop and Skinner (1977) proposed a higher ψ of 16.25° for quartz. No experimental data was available for clay minerals, though Skempton (1960) predicted that ψ would have quite low values for these materials. Since fine-grained soils often contain significant quantities of silt, Skempton hypothesized average values of ψ for these soils to be roughly in the range of 5° to 10°. It is important to keep in mind that while ψ is expressed as a tangent value of friction angle, the internal friction angles measured in the author's research are generally expressed in terms of a secant value.

2.5.3 Experimental Investigation of the Definition of Effective Stress

One of the few, and most significant, attempts to examine the validity of the various definitions of effective stress in relation to the shear strength of particulate materials was carried out by Bishop and Skinner (1977). Constant rate of strain drained triaxial compression tests were carried out on sand, silt, crushed marble and lead shot over a wide range of stresses. The testing program consisted of the observation of strength changes resulting from large changes in cell pressure (σ_3) and back-pressure (u_b) but with the difference between the two pressures kept constant to a high degree of accuracy. Due to the difficulty in reproducing identical specimens of granular materials in the laboratory, which could mask small strength changes, multistage tests were carried out whereby the cell pressure and back pressure were varied during individual tests. If the *au* term predicted by the intergranular stress equation (Equation 2-3) has an effect on strength, this could be detected with an accuracy of about ±0.5% from discontinuities in the stress-strain curve, as illustrated diagrammatically in Figure 2-24. The results of a typical test carried out on Ham River sand are shown in Figure 2-25. It was found over the full range of stresses tested, for u_b up to approximately 40 MPa, that the basic Terzaghi definition of effective stress, i.e. $\sigma' = \sigma - u$, controlled the behaviour of each material to a very high degree of accuracy. Bishop and Skinner concluded that the proposition of intergranular stress controlling shear strength is invalid. In the case of the lead shot in particular, the assumption that intergranular stress controls shear strength would have led to very large overestimates of effective stress. Equation 2-6 derived by Skempton (1960) to take account of the intrinsic angle of friction of the material forming the soil particles also gave less favourable agreement with the experimental results than the Terzaghi equation. This was attributed to Skempton's incorrect assumption in the derivation of Equation 2-6 that a relationship exists between the internal friction angle of the soil mass and the intrinsic friction angle of the soil particle material.

Unfortunately, because the time required for pore pressure equalization during drained tests on clay is very much longer and it could have taken weeks to run a single test, no such tests were carried out by Bishop and Skinner (1977). Although the physical nature of inter-particle contacts may be significantly different for clayey and granular materials, it is generally assumed that Terzaghi's equation is applicable to clayey materials at high stresses (as was assumed by all experimental studies previously mentioned in this chapter). However, experimental verification that the Terzaghi definition of effective stress holds rigorously for clayey materials at high stresses is lacking.

2.6 SATURATION AND B-VALUE

2.6.1 Introduction

An important underlying assumption of the Terzaghi definition of effective stress, as well as all proposed variations for the definition of effective stress described in the previous section, is that the soil is fully saturated, i.e. S = 100 %. Values of saturation which deviate only slightly below 100% can result in dramatic changes in soil behaviour. These changes in behaviour include, for example, reductions in hydraulic conductivity, the development of pore water tension (i.e. soil suction) as well a different undrained shear response as excess pore pressures are reduced. It is therefore of paramount importance for the research described in this thesis that full saturation of clay specimens be achieved during triaxial testing. This is done by a process known as back-pressure saturation which is carried out prior to consolidation in a convention triaxial test. Laboratory techniques to determine whether a triaxial specimen is fully saturated include:

1. Measure the volume of pore fluid entering the specimen as u_b is increased. The amount of pore fluid entering should initially increase as the back-pressure (u_b) is raised, indicating increasing saturation of the specimen and the drainage system. The volume of pore fluid should then level off and remain almost constant with increasing u_b (demonstrating that saturation of the specimen and drainage system has been achieved), though a slight increase in volume may be observed due to the finite compressibility of the drainage system, i.e. valves, drainage lines and the pore fluid itself.
2. Measure the B-value (Skempton 1954) as u_b is increased. The measured B-value should initially increase as u_b is raised, indicating increasing saturation of the specimen and the drainage system. Once saturation is complete the B-value should remain approximately constant with increasing u_b.
3. Measure the B-value over time, say 2 minutes. If the soil is fully saturated then the measured B-value should increase relatively quickly before reaching a constant value. If the soil is not fully saturated then the B-value will initially increase before decreasing again. On the other hand, a slowly increasing B-value which asymptotically approaches a constant value may indicate a pore fluid system which is not fully saturated. These different responses are illustrated in Figure 2-26.

2.6.2 Skempton's Pore Pressure Parameter B

The B-value, mentioned above, is not a soil property but an experimentally useful parameter defined (along with the pore pressure parameter A) by Skempton (1954) as being the ratio of the observed change in pore pressure to an applied change in total octahedral stress[5] ($\Delta u/\Delta\sigma_{oct}$) in an undrained system. A theoretical derivation for the ratio $\Delta u/\Delta\sigma_{oct}$ was first put forward by Bishop and Eldin (1950):

---

[5] Octahedral stress is the same as mean stress used in Cambridge stress space, i.e. $\sigma_{oct} = p_m = \frac{1}{3}(\sigma_1 + \sigma_2 + \sigma_3)$

$$\frac{\Delta u}{\Delta\sigma_{oct}} = \frac{1}{1 + n(\frac{C_w}{C})} \quad \text{2-7}$$

where: n = porosity

C_w = compressibility of the pore fluid

C = compressibility of the soil skeleton, as in Section 2.5.2

The derivation of the above equation by Bishop and Eldin (1950) involves the following assumptions:

- the soil pores are interconnected
- the solid material(s) forming the soil particles is elastic and isotropic
- the bulk behaviour of an element of the soil when subjected to a change in effective stress is that of an elastic isotropic material
- the distribution of pore space within the soil skeleton is statistically random
- the pore fluid is linearly compressible

In the derivation of Equation 2-7 it is also assumed that the compressibility of the solid material(s) forming the soil particles (C_s) can be neglected. A more general expression which takes account of C_s (but still involves all of the aforementioned assumptions) is given by Bishop (1973):

$$\frac{\Delta u}{\Delta\sigma_{oct}} = \frac{1}{1 + n\frac{(C_w - C_s)}{(C - C_s)}} \quad \text{2-8}$$

If the pore fluid is water then C_w can be assumed to be approximately constant and equal to 48.9 x 10^{-5} MPa^{-1}. As mentioned previously, C_s for clay is approximately 2 x 10^{-5} MPa^{-1} (Skempton 1960) while C is generally larger by several orders of magnitude in the range of stresses typically encountered in engineering practice. Under these circumstances Equation 2-8 is dominated by the ratio of C_w to C, and since C is very large compared to C_w, the ratio $\Delta u/\Delta\sigma_{oct}$ (i.e. the B-value) is close to 1. However, for soils subjected to high effective stresses the value of C reduces enormously and can even drop to below that of water, leading to B-values significantly below 1. The C_s term also becomes more significant at lower values of C. For example, in the series of tests carried out by Bishop et al. (1975) on resedimented London Clay, the B-value calculated from Equation 2-8 would be 0.97 and 0.80 at consolidation stresses of 20.7 MPa and 62.1 MPa respectively.

Lade and de Boer (1997) presented a technically more correct theoretical derivation for the B-value by making a distinction between the compressibilities of the soil particles and skeleton due to total pressures and pore pressures. However, given the fact that the error associated with apparatus compressibility (as discussed below) is likely to be a far more significant issue to address, Lade and de Boer's complication is probably unjustified and of little practical benefit. As such, it will not be considered here.

2.6.3 Apparatus Compressibility

When the undrained pore pressure response to a change in total stress is measured in the triaxial apparatus, the measured Δu is also affected by the compressibility of the pore pressure measuring system. Wissa (1969) derived an expression for $\Delta u/\Delta\sigma_{oct}$ including terms representing system compressibility but, similar Bishop and Eldin (1950), did not account for compressibility of the soil particles. Bishop (1976) presented a modification to Equation 2-8 to include terms associated with system compressibility:

$$\frac{\Delta u}{\Delta\sigma_{oct}} = \frac{1}{1 + n\frac{(C_w - C_s)}{(C - C_s)} + \frac{V_L}{V}\frac{C_w}{(C - C_s)} + \frac{C_L + C_M}{V(C - C_s)}} \qquad 2\text{-}9$$

where: n, C, C_s and C_w are as before

C_L = compressibility of the drainage lines and valves

C_M = compressibility of the pore pressure transducer

V_L = volume of fluid in the drainage lines, valves and porous stones

V = volume of the soil specimen

If the system compressibility were zero, the measured B-value would theoretically be equal to $\Delta u/\Delta\sigma_{oct}$ as defined in Equation 2-8. One can therefore re-arrange Equation 2-9 to provide an expression for B in the case of a system of finite compressibility:

$$B = B_{true} = \frac{1}{\frac{1}{(B_{meas})} - \frac{V_L}{V}\frac{C_W}{(C - C_s)} - \frac{C_L + C_M}{V(C - C_s)}} \qquad \text{2-10}$$

where: B_{true} = true B-value of the soil specimen corrected for system compressibility

B_{meas} = $(\Delta u/\Delta\sigma_{oct})_{meas}$ = measurable/observable B-value in a triaxial test

The terms involving system compressibility in Equation 2-10 are defined as Ω and can be re-arranged in the form (Bellwald 1990):

$$\Omega = \underbrace{\left\{\frac{-C_W}{(C - C_s)}\frac{1}{V}\right\}}_{term\ 1} x \underbrace{\left\{V_L + \frac{C_L + C_M}{C_w}\right\}}_{term\ 2} \qquad \text{2-11}$$

This allows one to make the following conclusions:

- *Term 1* depends only on the characteristics of the soil specimen. The larger and more compressible the specimen, the lower the value of Ω, and therefore the smaller the effect of system compressibility on the observed B-value.
- *Term 2* depends on the characteristics of the pore pressure measuring system. To keep the effect of system compressibility as small as possible, the volume of pore fluid in the system should be kept to a minimum and the system should be built as stiff as possible.

While a correction exists to account for system compressibility when computing a B-value, i.e. Equation 2-10, Bishop (1976) suggested that testing should ideally involve $B_{meas}/B_{true} > 90$ % in order to obtain the most accurate picture of the undrained behavior of the soil. It should also be kept in mind that, even corrected, the theoretically computed B-value is subject to the set of assumptions involved in its derivation and therefore may never exactly equal the measured $\Delta u/\Delta\sigma_{oct}$.

Yassir (1989) and Berre (1992), whose work was discussed previously in Section 2.2, both reported problems with unsatisfactory observed B-values which cannot be explained solely by consideration of system compressibility. Berre (1992) concluded that, in the case of very stiff specimens, the observation of B-value alone is not sufficient to judge whether the specimen and the pore pressure measuring system are fully saturated. Yassir (1989) reported B-values greater than 1 which should be an impossibility. However, this may be due to the effects of undrained creep as Yassir conducted B-value measurements at intervals during the isotropic consolidation of specimens.

Table 2-1: Summary of the main findings of Abdulhadi (2009) for CK_OUC test program on RBBC

Parameter	**Effect of Increasing OCR at a given σ'_{vc}**	**Effect of increasing σ'_{vc} at a given OCR**
s_u/σ'_{vc}	increases	decreases (more pronounced at low stresses)
K_O	increases	increases
ε_f	increases	increases
φ'_p	increases	decreases for OC, ~ no change for NC
φ'_{cs}	~ no change	decreases
u_e and u_s	decreases	decreases for OCR=1 & 2, increases for OCR=4
A_f	decreases	increases
E_u/σ'_{vc}	increases	decreases

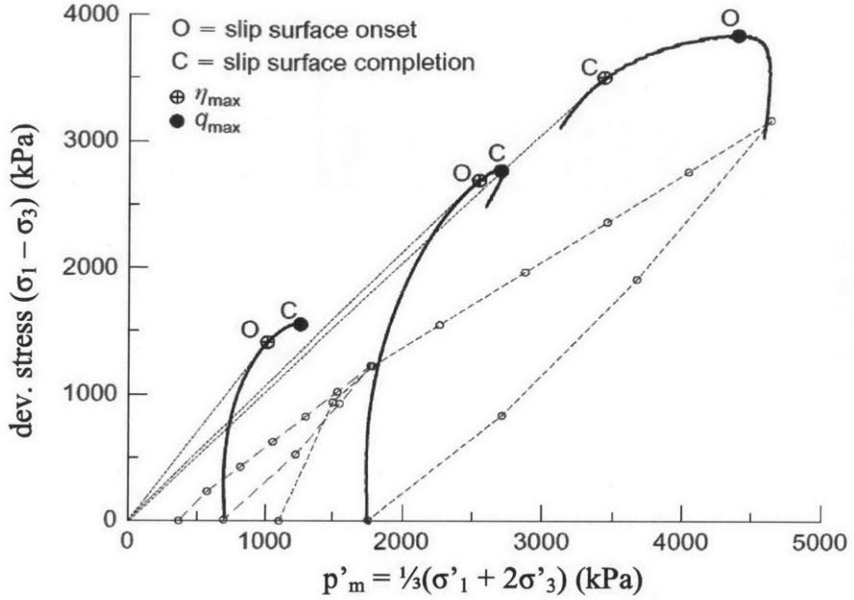

Figure 2-1: Effective stress paths (Cambridge stress space) in undrained triaxial compression for Vallericca Clay. The onset and development of slip surfaces in specimens is also shown (Amorosi and Rampello 2007)

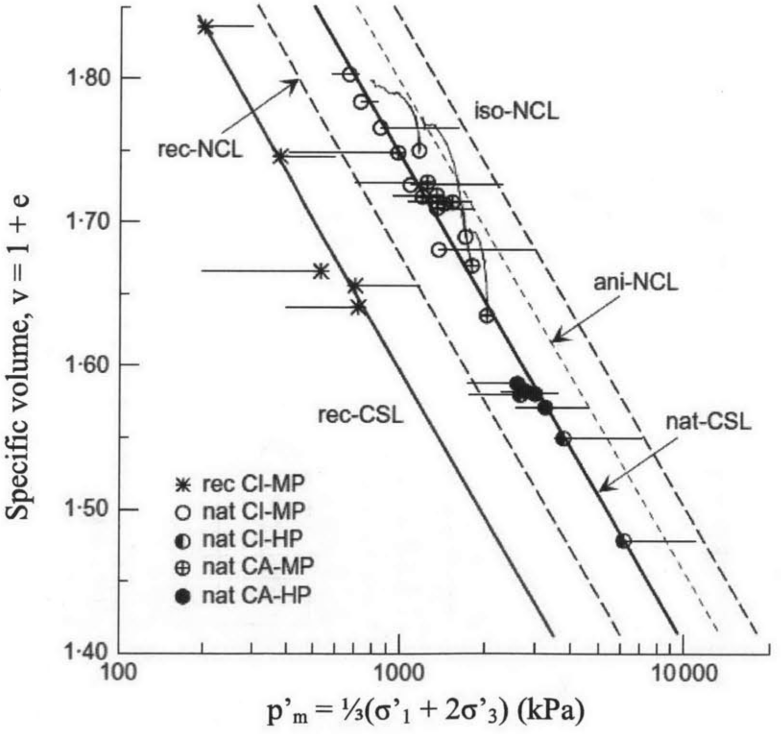

Figure 2-2: Virgin compression and critical state conditions for intact and resedimented specimens of Vallericca Clay (Amorosi and Rampello 2007)

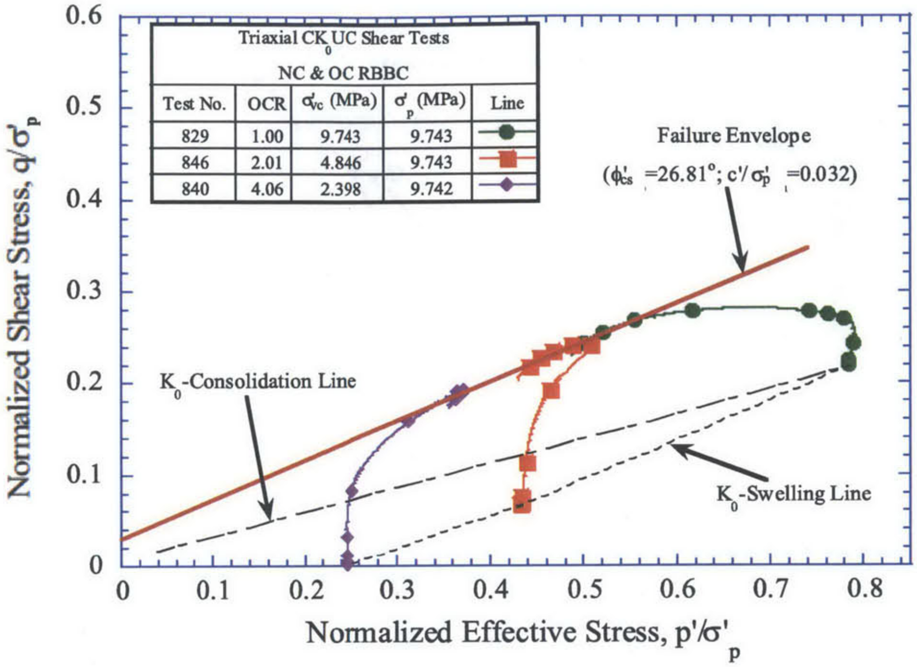

Figure 2-3: Normalized effective stress paths (MIT stress space) for RBBC at OCRs 1, 2 and 4 from CK_OUC triaxial tests with $\sigma'_p = 10$ MPa (Abdulhadi 2009)

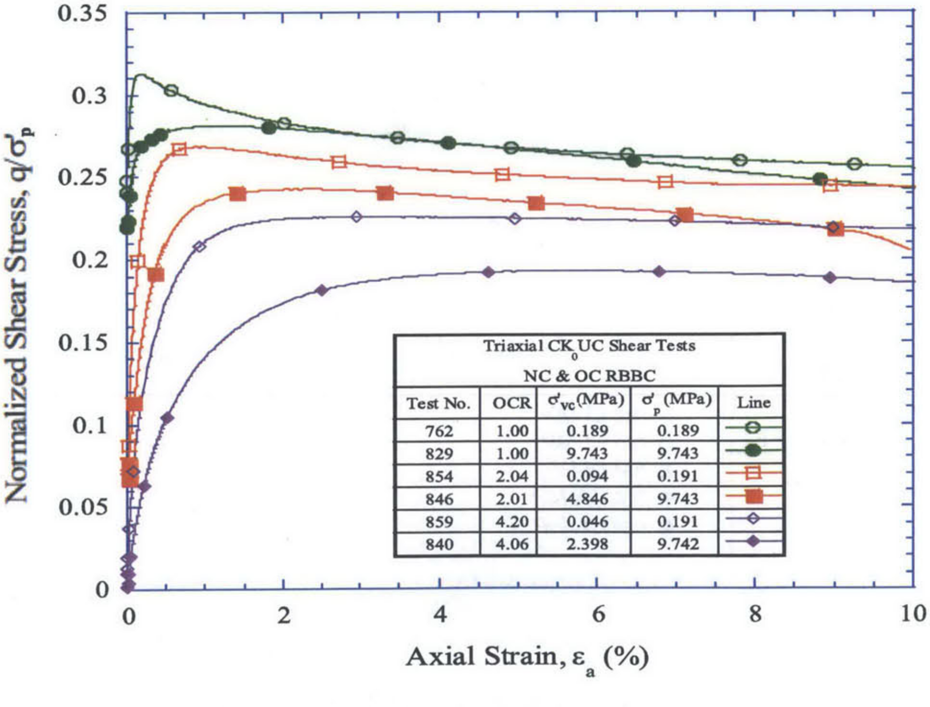

Figure 2-4: Normalized shear stress-strain responses for RBBC at OCRs 1, 2 and 4 from CK_OUC triaxial tests with $\sigma'_p = 0.2$ and 10 MPa (Abdulhadi 2009)

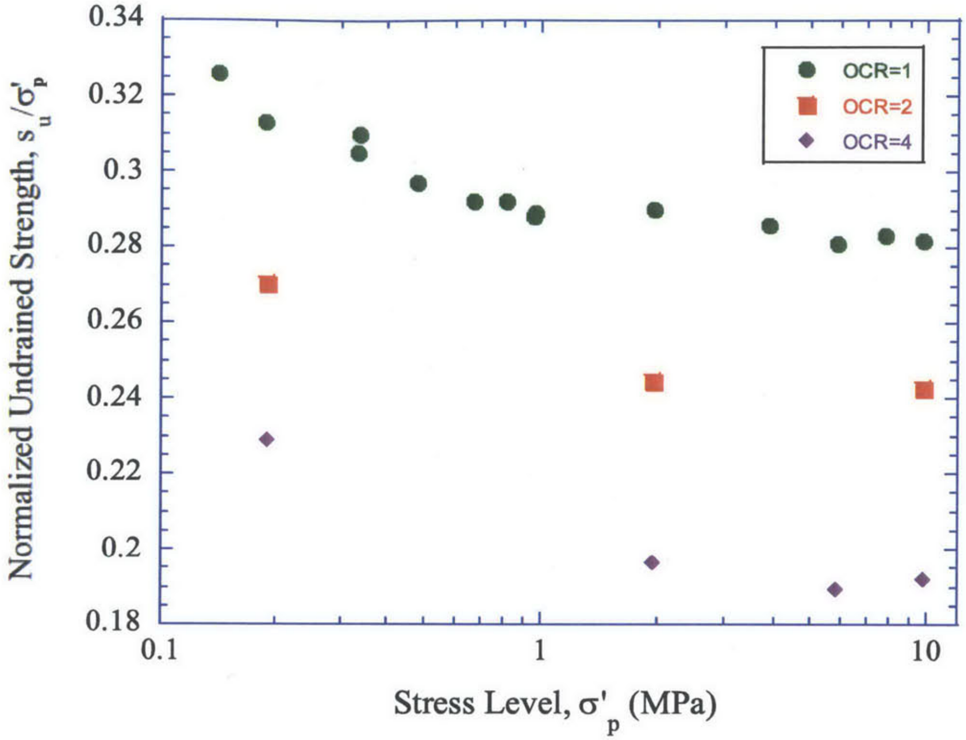

Figure 2-5: Variation in normalized undrained strength with stress level for RBBC at OCRs = 1, 2 and 4 from CK_OUC triaxial tests (Abdulhadi 2009)

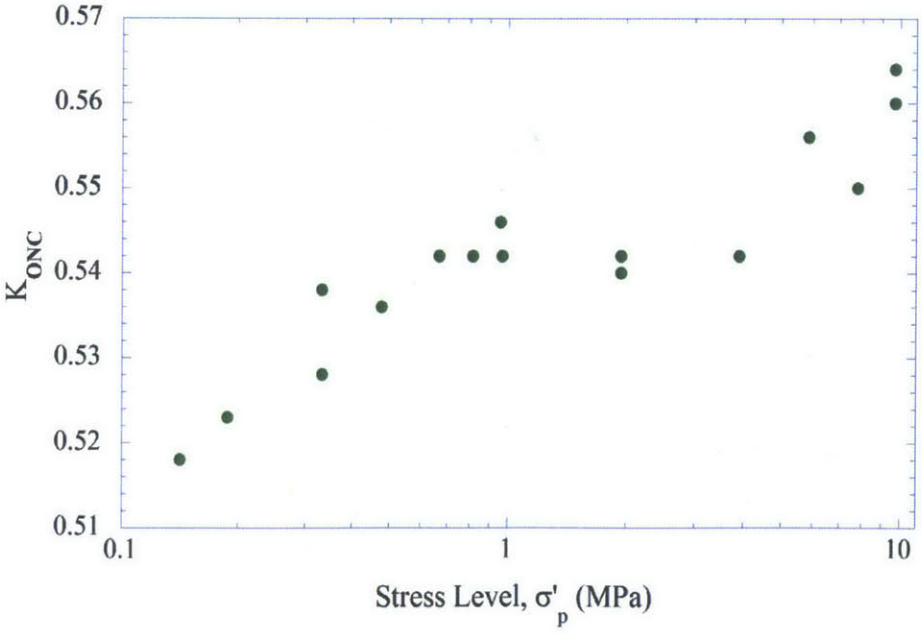

Figure 2-6: Value of K_{ONC} at the end of virgin consolidation versus stress level for RBBC from CK_OUC triaxial tests (Abdulhadi 2009)

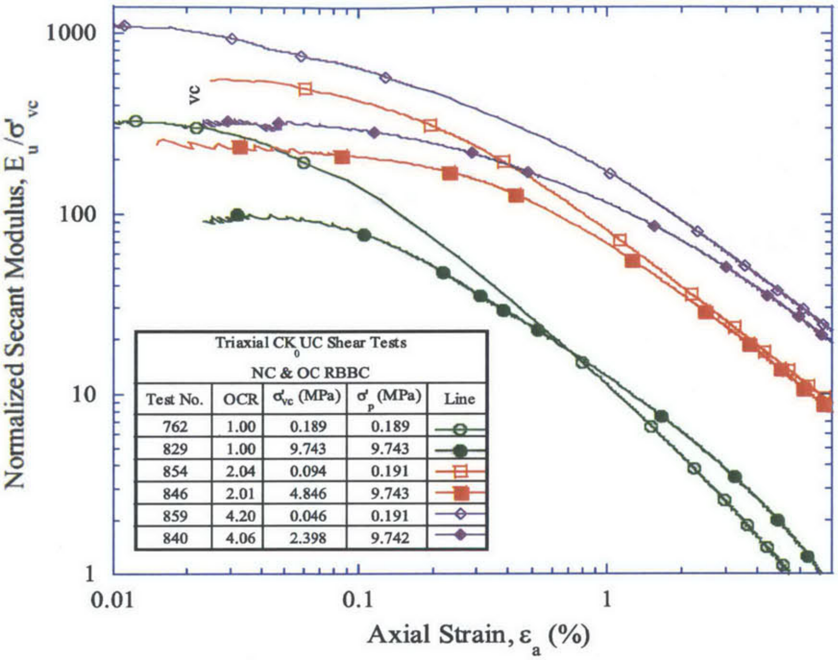

Figure 2-7: Normalized undrained secant Young's modulus versus axial strain for RBBC at OCRs 1, 2 and 4 from CK_OUC triaxial tests at $\sigma'_p = 0.2$ and 10 MPa (Abdulhadi 2009)

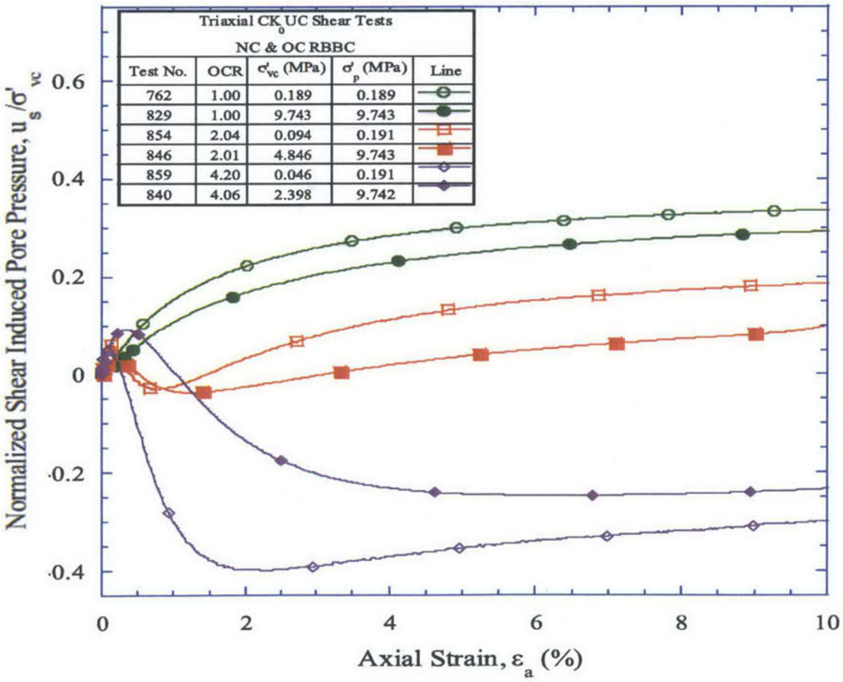

Figure 2-8: Normalized shear induced pore pressure versus axial strain for RBBC at OCRs 1, 2 and 4 from CK_OUC triaxial tests at $\sigma'_p = 0.2$ and 10 MPa (Abdulhadi 2009)

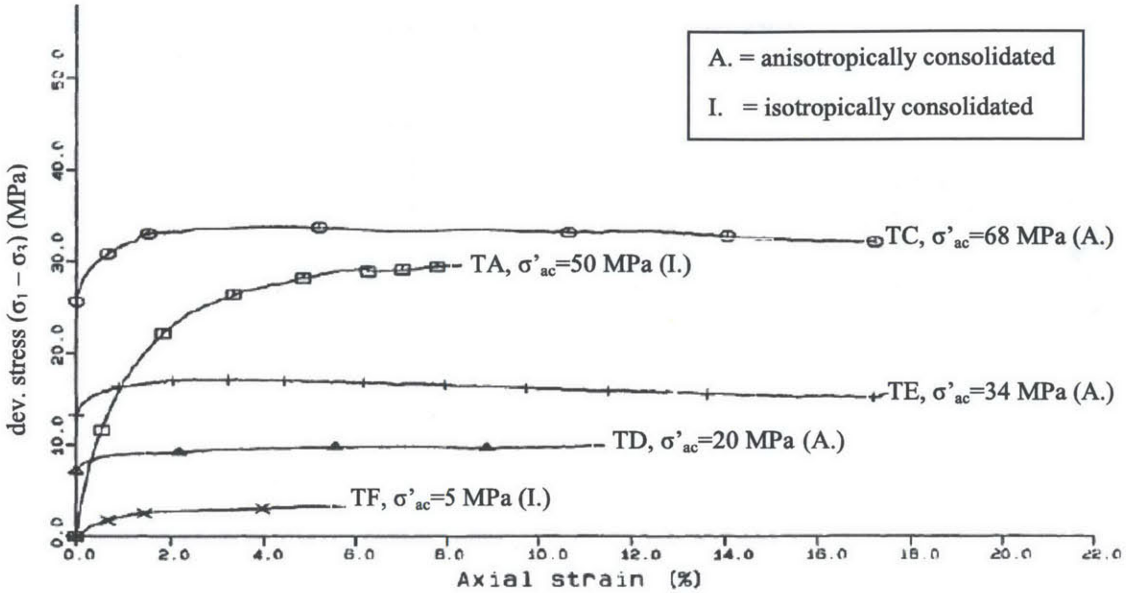

Figure 2-9: Deviatoric stress-strain response during undrained triaxial compression for a NC mud volcano clay (Yassir 1989)

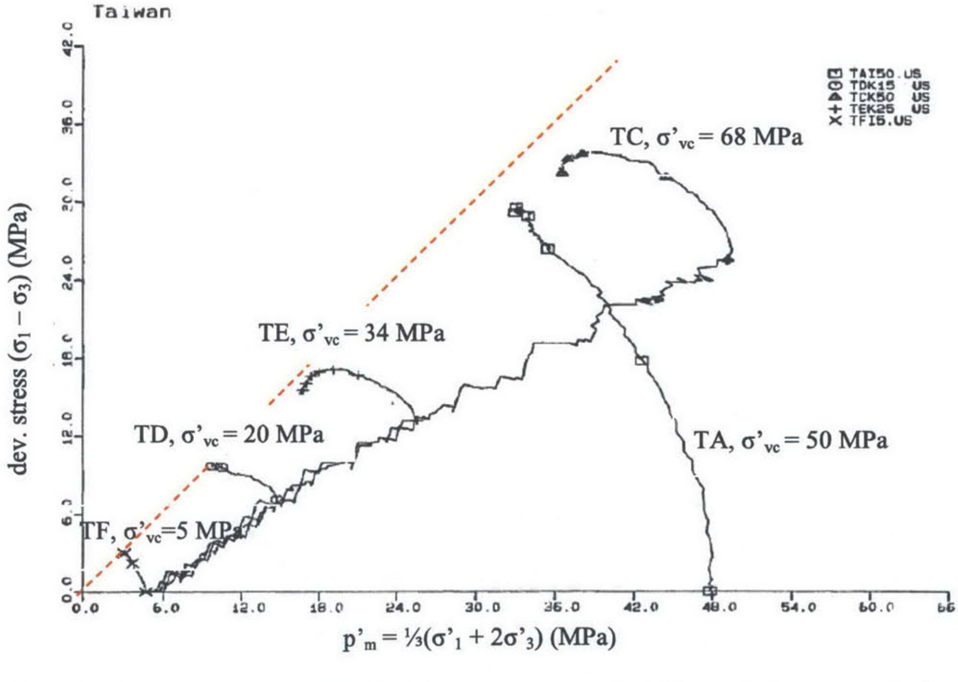

Figure 2-10: Effective stress paths (Cambridge stress space) followed during undrained triaxial compression of a NC mud volcano clay (Yassir 1989). The dashed red line is added to illustrate curvature of the failure envelope

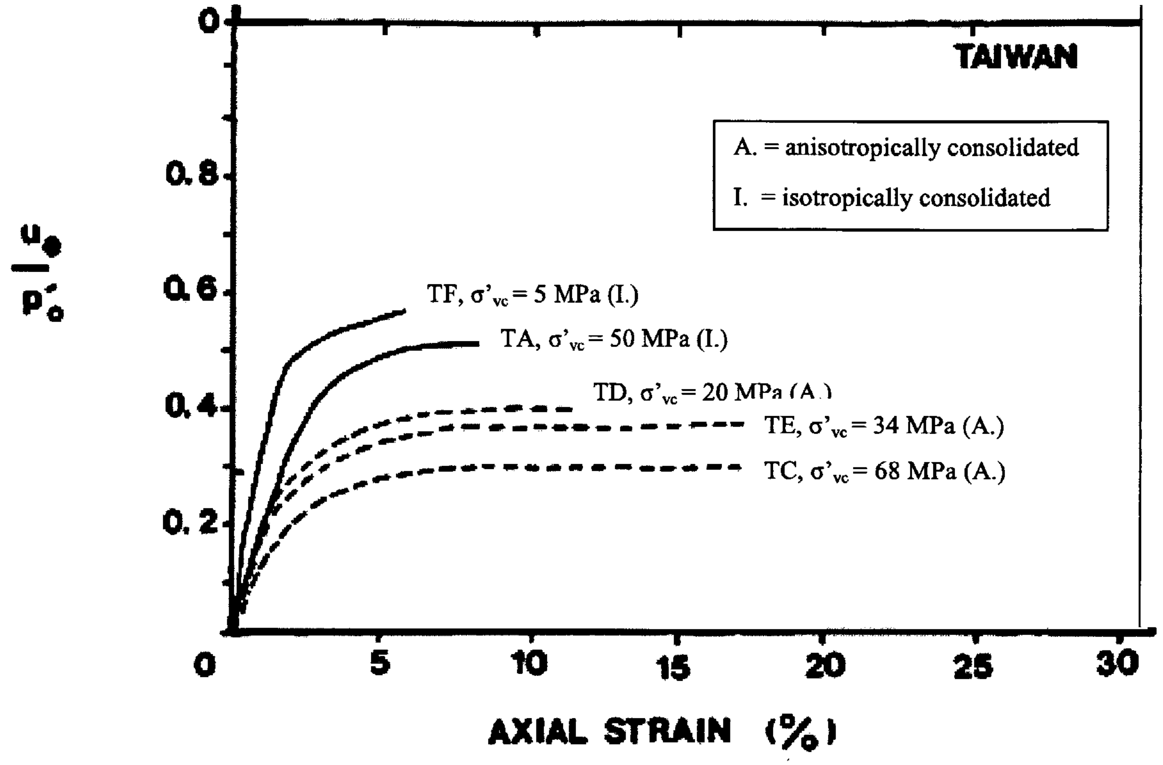

Figure 2-11: Normalized excess pore pressure (u_e/p'_o) versus axial strain during undrained triaxial compression of a NC mud volcano clay (Yassir 1989)

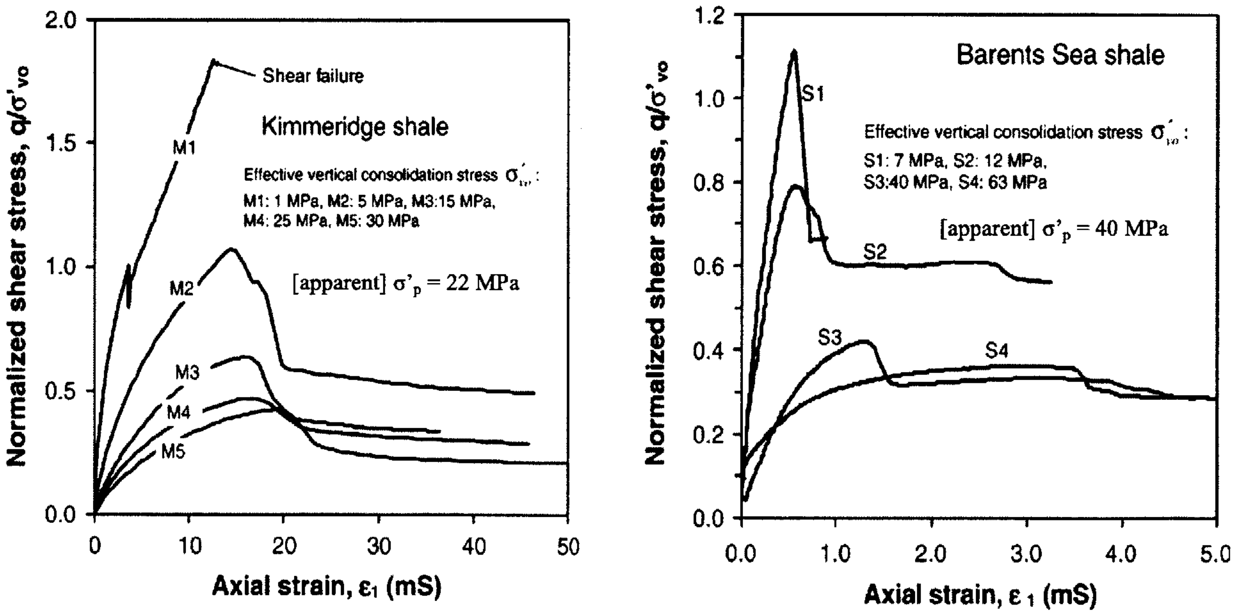

Figure 2-12: Normalized shear stress versus axial strain for CIUC tests on Kimmeridge Shale and Barents Sea Shale. Note that strain is given millistrain, mS (Gutierrez et al. 2008)

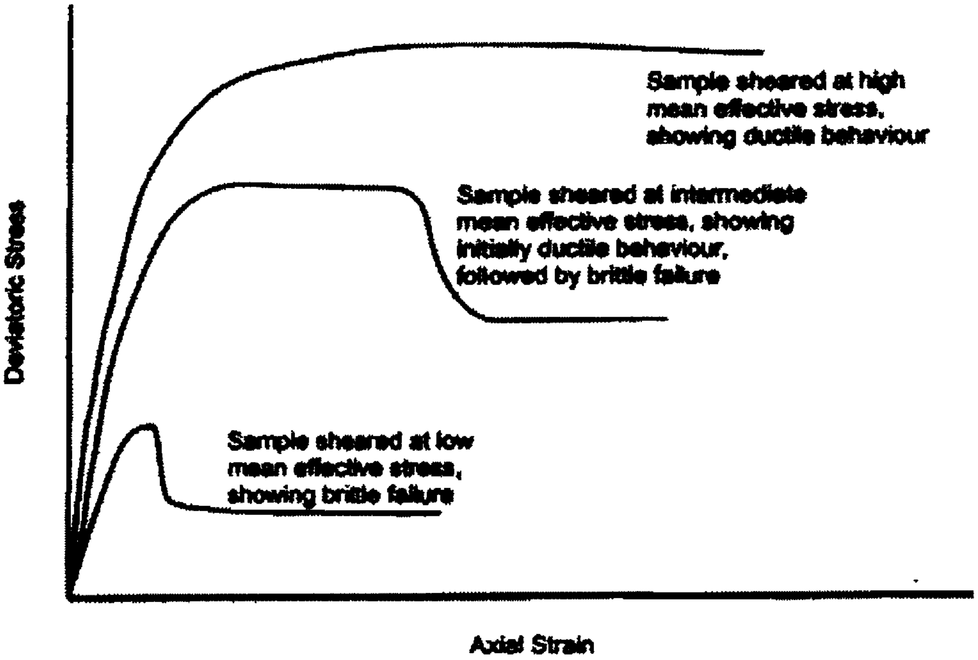

Figure 2-13: General forms of stress-strain response for clay shales (Petley 1999)

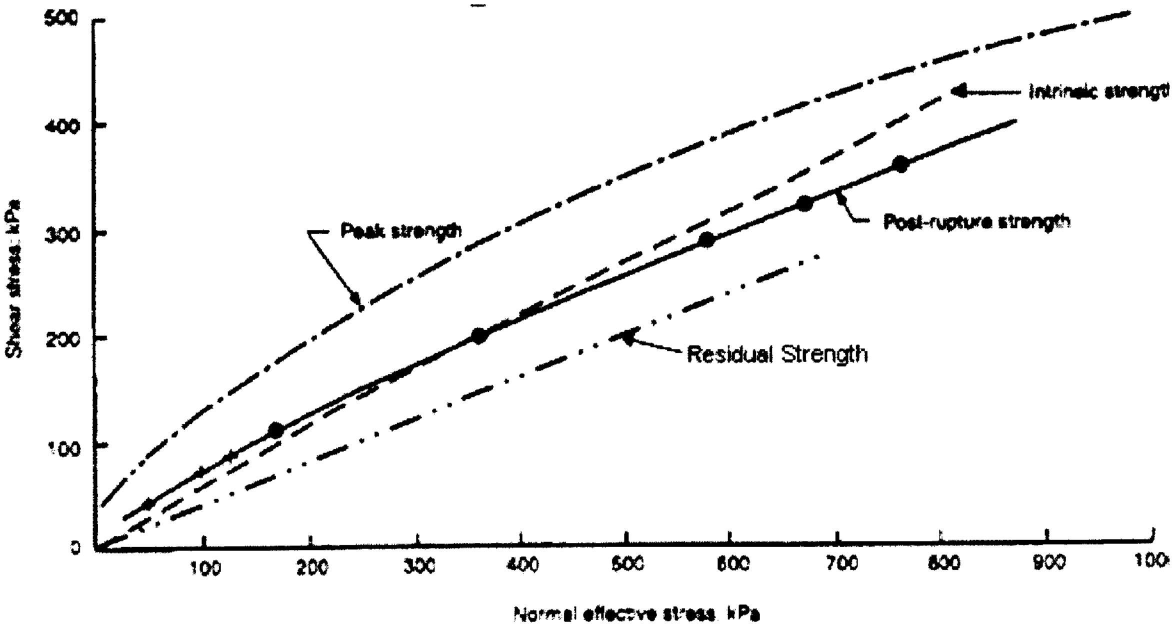

Figure 2-14: Conceptual form of failure envelopes for clays by Burland (1990) (from Abdulhadi 2009)

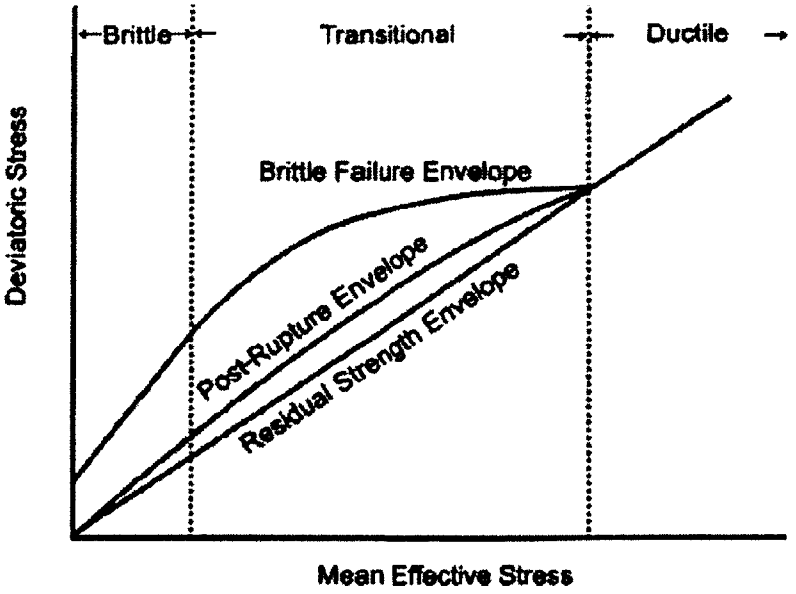

Figure 2-15: Conceptual form of failure envelopes for hard clays and clay shales (Petley 1999). Note that the residual strength envelope would be better designated as the intrinsic critical state envelope

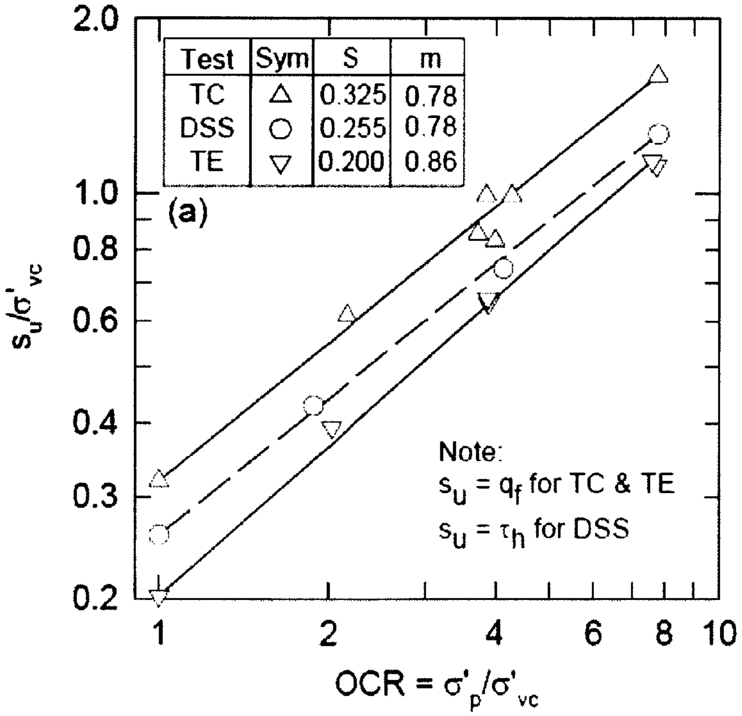

Figure 2-16: Normalized undrained shear strength versus OCR for a SHANSEP test program on AGS Plastic Marine Clay (Koutsoftas and Ladd 1985)

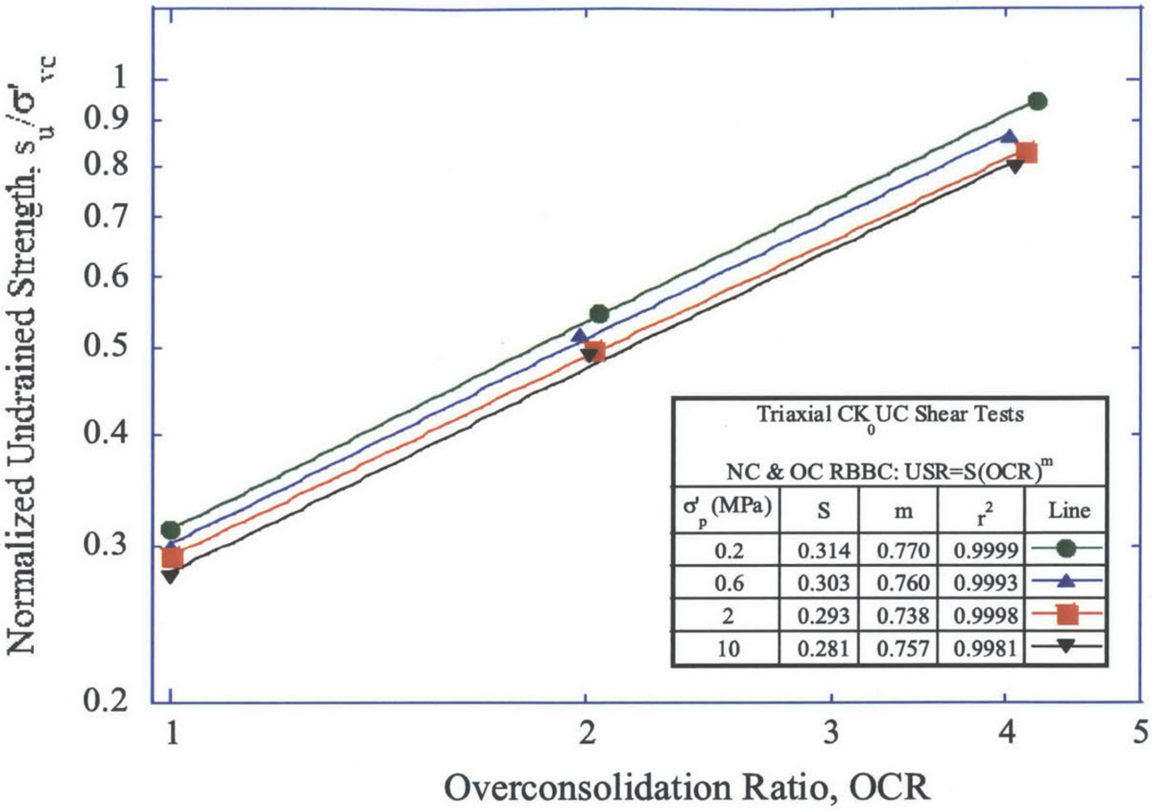

Figure 2-17: Effect of stress level on the SHANSEP S and m parameters for RBBC in triaxial compression (Abdulhadi 2009)

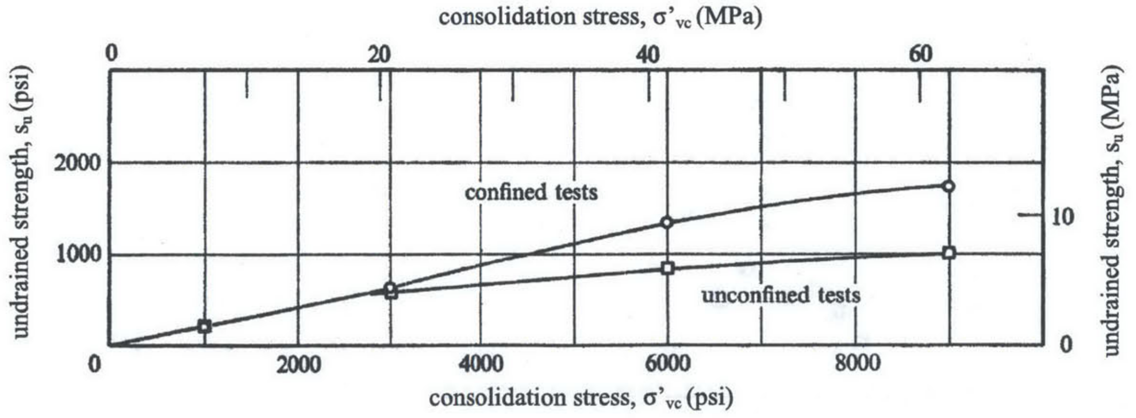

Figure 2-18: Relationship between undrained strength and consolidation stress for CIUC tests performed on resedimented London Clay. Where multiple tests were performed at a particular stress, the average value is plotted (Bishop et al. 1975)

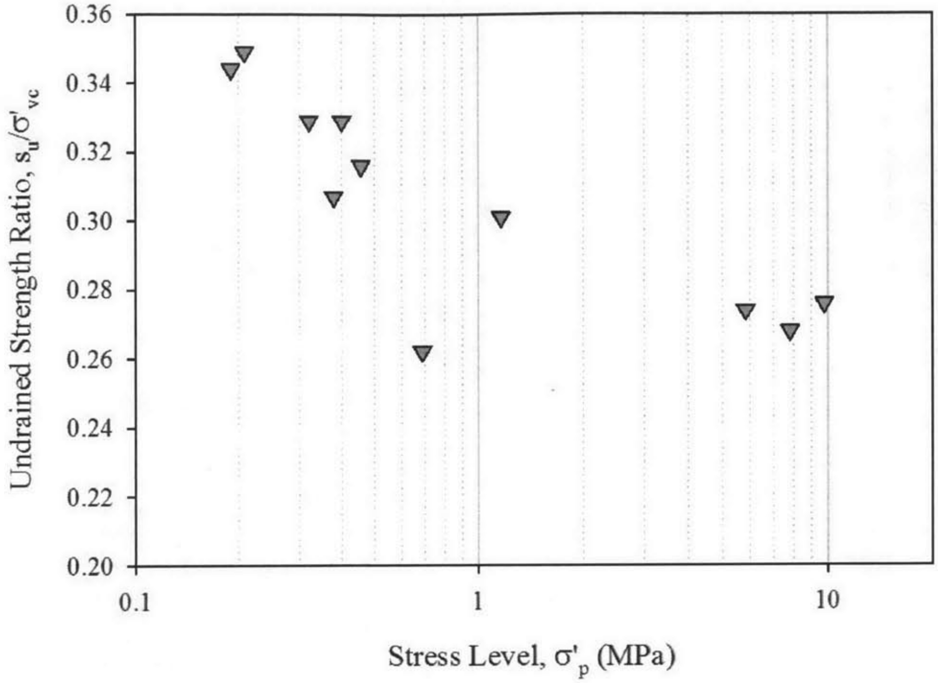

Figure 2-19: Variation in normalized undrained strength with stress level for Resedimented Ugnu Clay at OCR = 1 from CK_0UC triaxial tests (from Jones 2010)

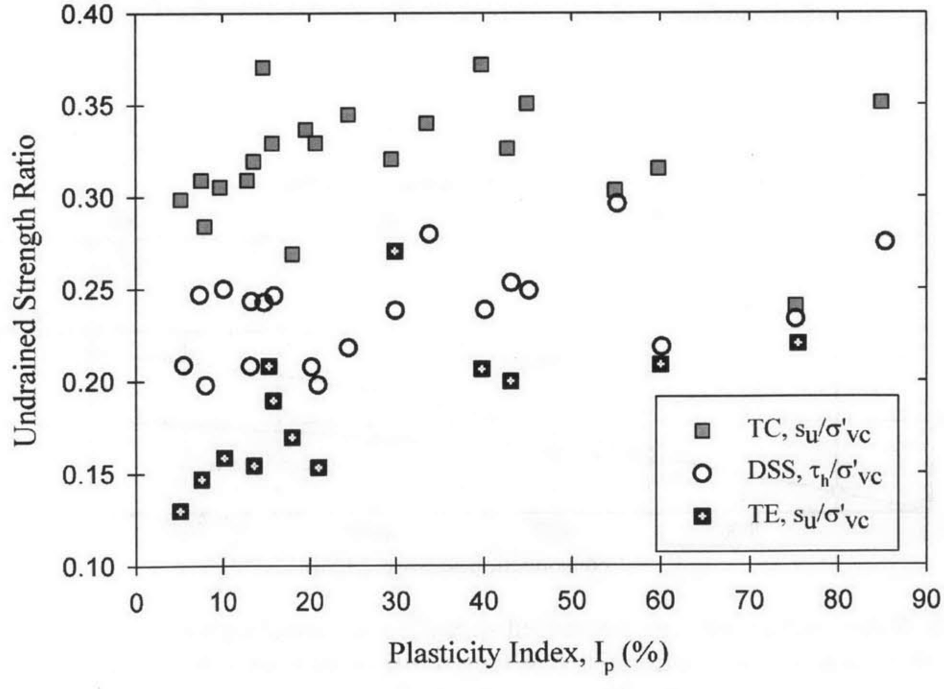

Figure 2-20: Undrained strength ratios of various NC clays and silts plotted against plasticity index (adapted from Ladd 1991)

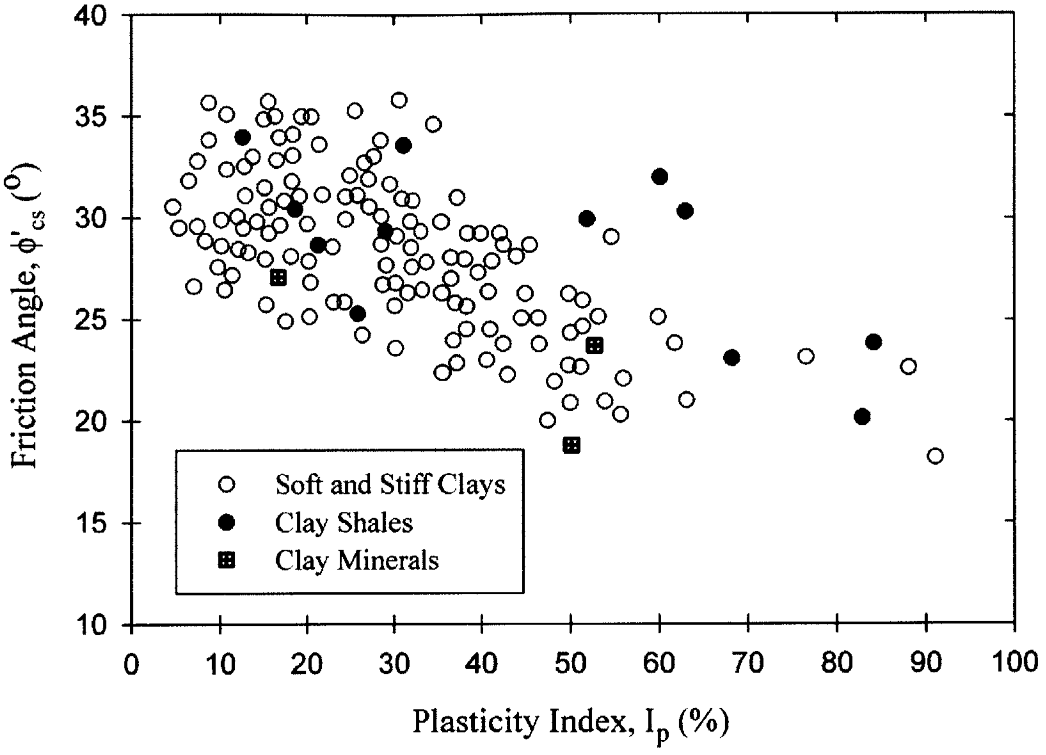

Figure 2-21: Friction angles of various clays plotted against plasticity index (adapted from Terzaghi et al. 1996)

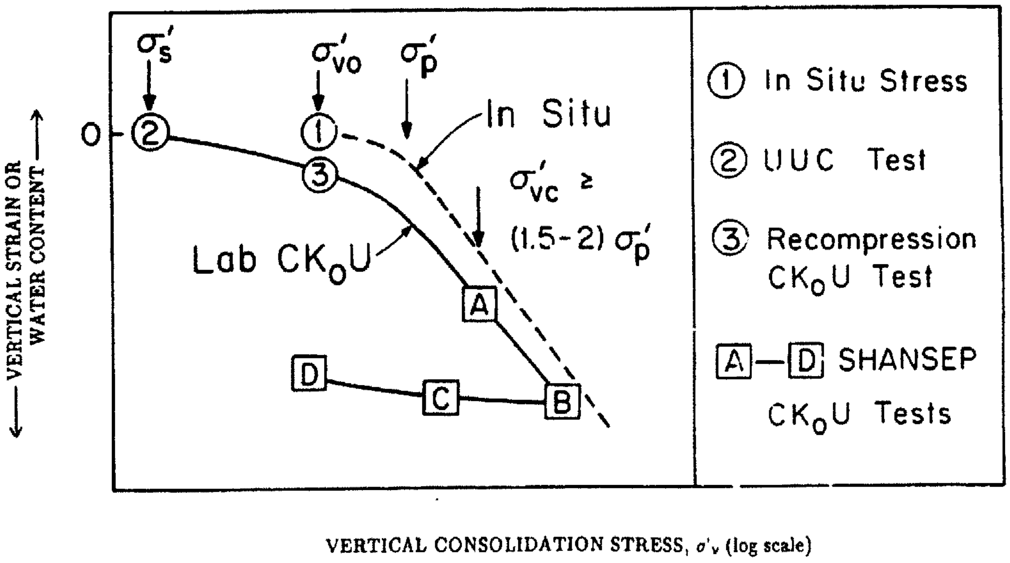

Figure 2-22: Reconsolidation procedures for laboratory CK_0U testing (Ladd 1991)

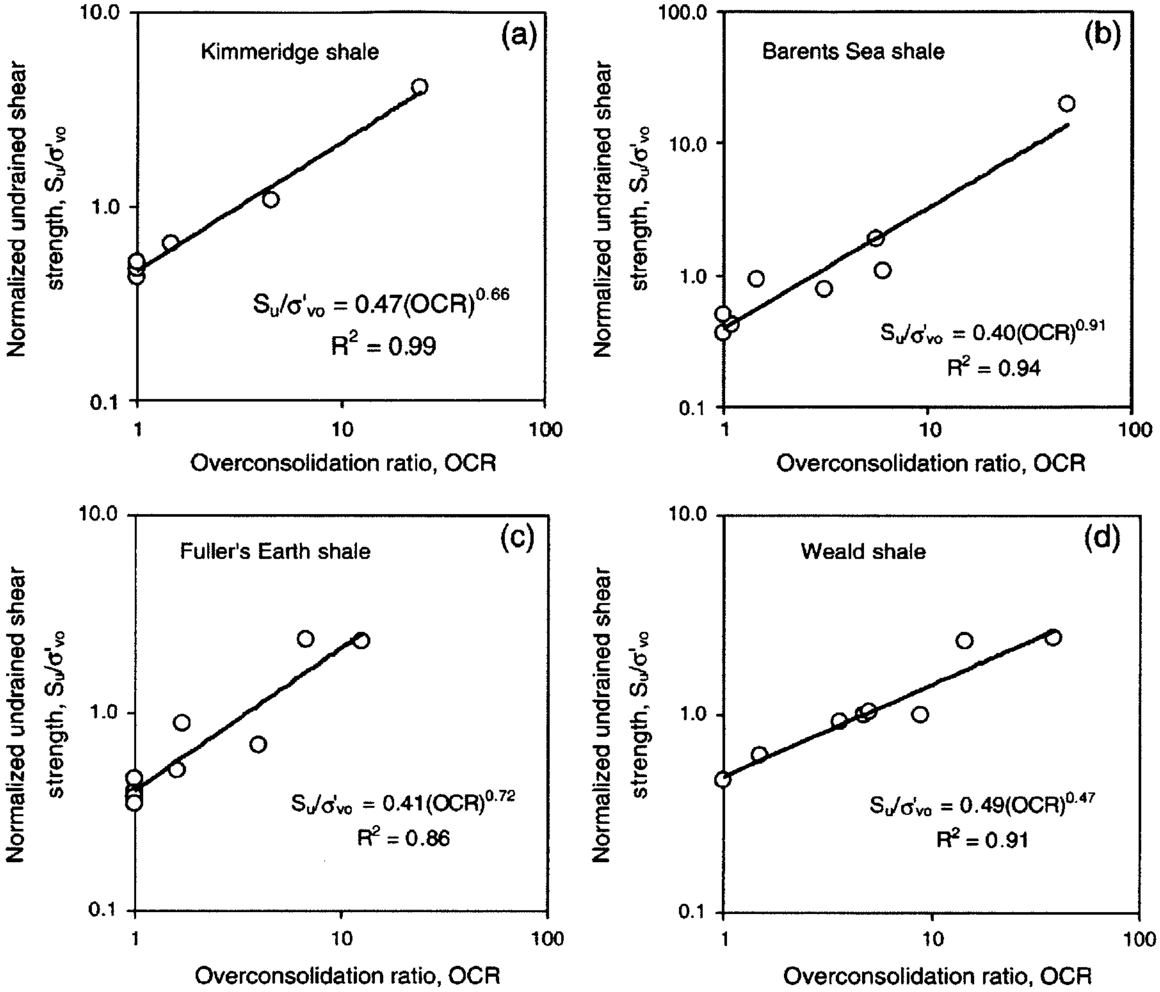

Figure 2-23: Normalized undrained shear strength versus OCR for four clay shales (Gutierrez et al. 2008)

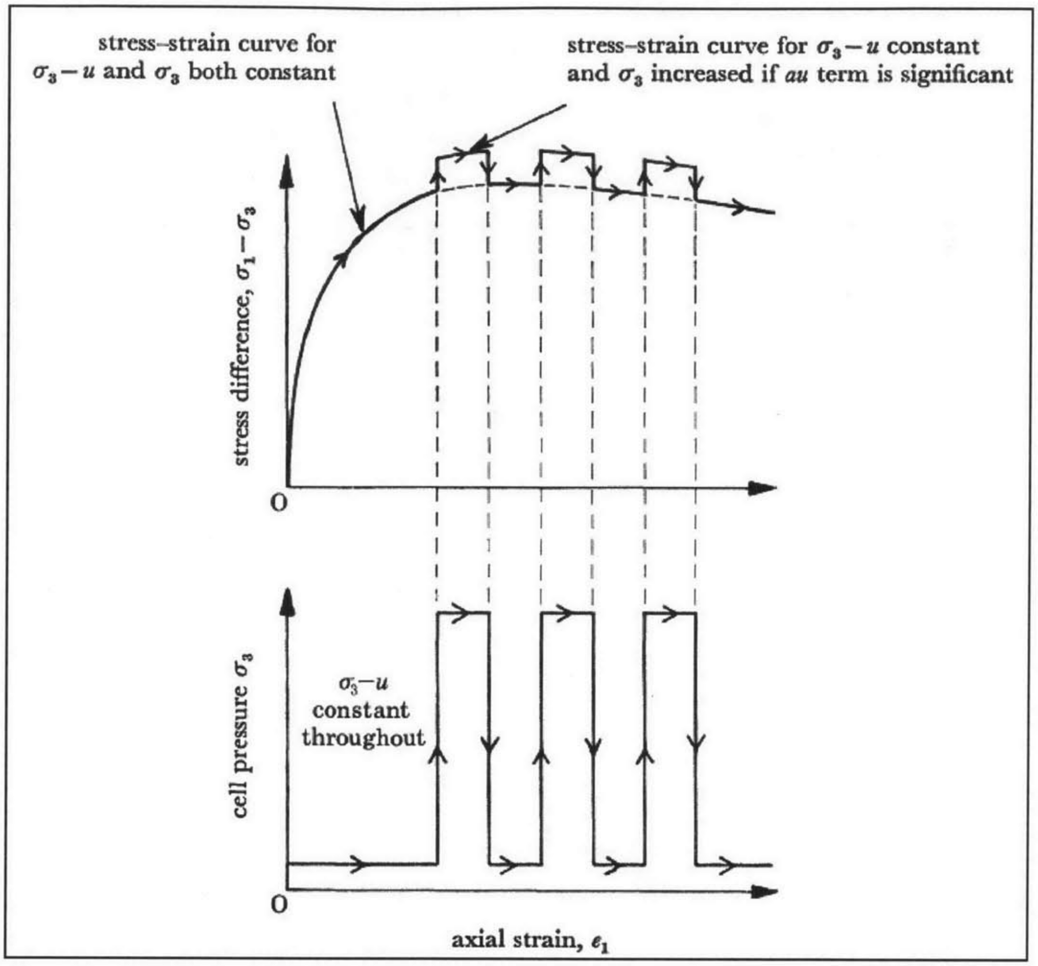

Figure 2-24: Testing procedure for a multistage drained triaxial compression test to determine the significance of the *au* term in defining effective stress (Bishop and Skinner 1977)

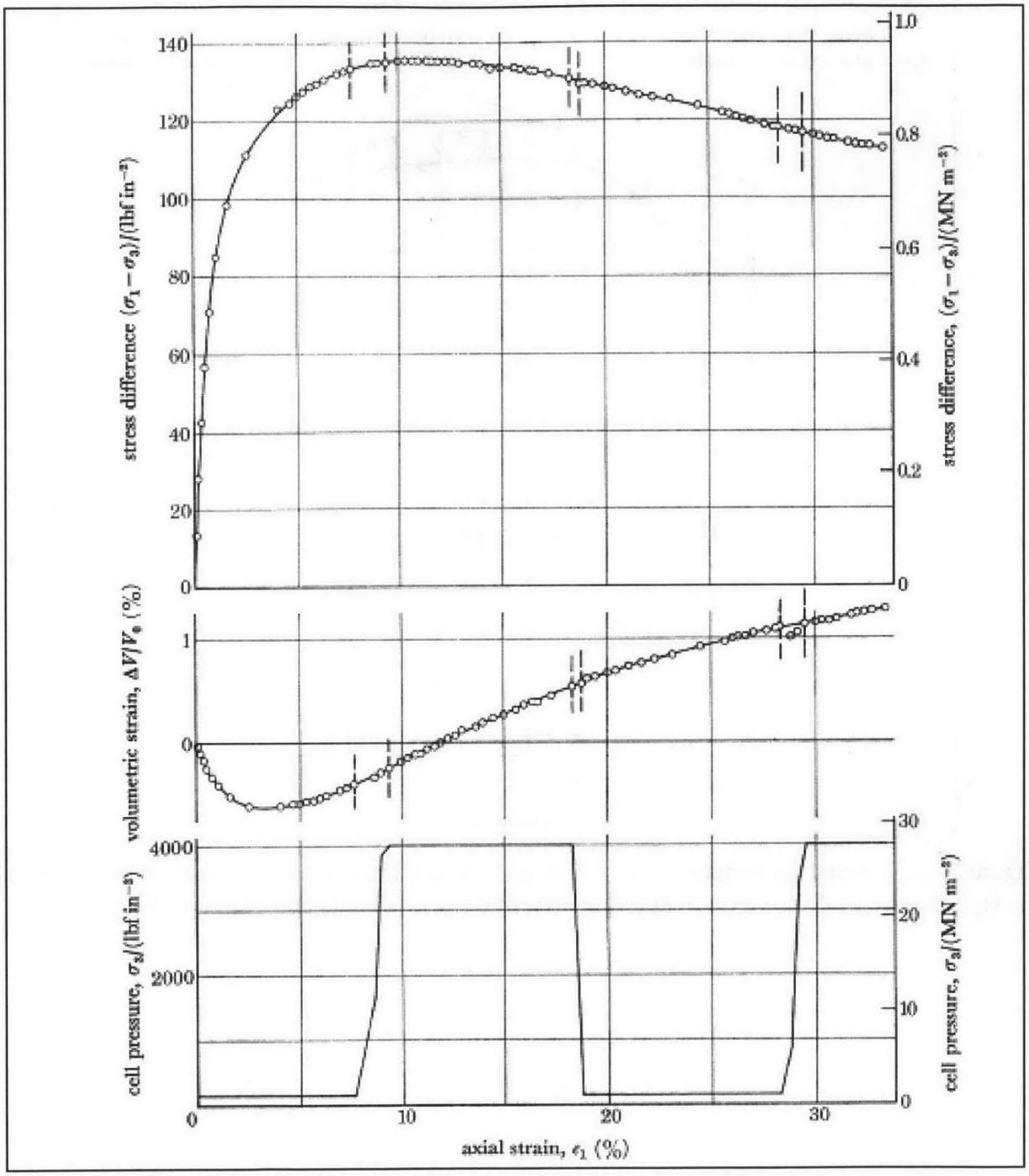

Figure 2-25: Typical multistage drained triaxial compression test carried out on Ham River sand with $(\sigma_3 - u) = 363$ kPa throughout (Bishop and Skinner 1977)

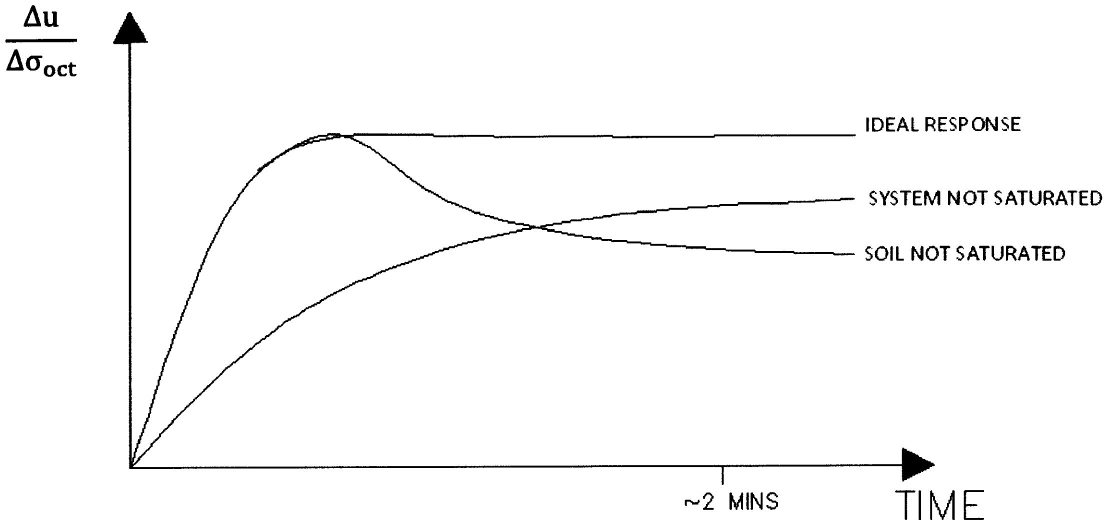

Figure 2-26: Various B-value responses over time as a function of saturation

3 RESEDIMENTATION AND TEST MATERIALS

3.1 INTRODUCTION

This chapter describes the origin and index properties of soils tested as part of this work as well as the process used to produce samples of these soils for laboratory testing, i.e. resedimentation. Section 3.2 provides background information on Presumpscot Clay, Boston Blue Clay, Ursa Clay, Ugnu Clay, San Francisco Bay Mud, London Clay, Skibbereen Silt and Eugene Island Clay. These fine-grained soils cover a very wide range in terms of composition, geologic origin and mechanical properties. In addition to being tested as part of this work, some of these soils have previously been investigated to a greater extent by individual researchers. The dissertations of these researchers provide additional information on the geologic origin and processing of these soils, as well as on the particular aspects of mechanical behavior which were examined during the course of these investigations. In the case of Skibbereen Silt and Eugene Island Clay, no tests have been performed on these soils as part of this work, but the results of laboratory tests conducted by other researchers are included in Chapters 5 and 6 of this thesis.

Resedimentation allows one to produce samples of identical composition from source material with any desired preconsolidation stress, porosity or pore fluid salt concentration. This enables the effect of each of these important variables to be separated and subjected to systematic laboratory investigations, a process which would be not be possible with the use of intact samples. Resedimenting soil samples for laboratory testing also overcomes enormous practical problems of sampling disturbance and cost associated with intact samples (particularly for deep or offshore samples). The resedimentation technique eliminates variability among samples and produces uniform specimens with K_O-consolidation histories and complete saturation. Because of its capability to produce a large number of identical samples, resedimentation is also an essential asset in the development and proofing of new laboratory testing equipment as well as the modification of existing equipment. Section 3.3 describes the process of resedimentation, including a brief background of resedimentation at MIT, the procedure and equipment used as part of this work, and an evaluation of sample uniformity.

3.2 TEST MATERIALS

3.2.1 Introduction

For each soil included in this thesis, Table 3-1 provides its origin, liquid limit, plasticity index, specific gravity, and clay fraction, where clay fraction is defined as the percentage of particles with an equivalent diameter < 2 μm as determined by sedimentation (ASTM D422). Liquid limits were determined by either the Casagrande cup method (ASTM D4318) or the fall cone method (BS 1377). The classification of each soil according to the Unified Soil Classification System (USCS) (ASTM D2487) is also provided. In addition, relevant citations for previous investigations by other researchers are included in Table 3-1. Figure 3-1 shows the location of the soils on a plasticity chart. The particle size distributions of the soils as determined from hydrometer tests (ASTM D422) are shown in Figure 3-2. It can be seen from Figure 3-2 that the lowest plasticity soil, the Skibbereen Silt, is comprised of the largest sized particles and possesses the smallest fraction of clay sized particles. This result is consistent with the notion that the Atterberg limits of soils decrease with decreasing clay fraction. However, for the other soils in the data set this trend breaks down, an indication of the fact that the Atterberg limits (and therefore engineering properties) are heavily influenced by clay mineralogy as well as clay fraction (Seed et al. 1964).

The clay mineralogical compositions of soils included in this research are given in Table 3-2. The mineralogy analyses (except for that of Bisaccia clay from Di Maio et al. (2004)) were carried out by Macaulay Scientific Consulting Ltd. of Aberdeen, U.K. The samples primarily contain quartz, plagioclase, K-feldspar and clay minerals in varying proportions, as well as several other minerals in minor proportions. Table 3-2 shows the percentages of clay minerals determined for the bulk (whole) samples, as well as the relative proportions of these minerals in the < 2 μm fraction of each sample. The bulk samples were wet ground in ethanol and spray dried to produce random powders (Hillier 1999). X-ray powder diffraction (XRPD) patterns were recorded from 2-75° 2θ using Cobalt Kα radiation and quantitative analysis was done by a normalized full pattern reference intensity ratio method. Uncertainty in the concentration of an individual mineral is given within 95 % by $\pm X^{0.35}$, where X = concentration in percent, e.g. 20±2.9 % (Hillier 2003). The < 2 μm fractions were separated from the bulk samples by timed sedimentation. They were then prepared as oriented mounts and scanned from 2-45° 2θ in the air-dried state, after glycolation and after heating to 300°C for one hour. Clay minerals identified were quantified using a mineral intensity factor approach based on calculated XRPD patterns. For clay minerals present in relative amounts > 10 %, uncertainty is estimated as better than ± 5 % at the 95% confidence level (Hillier 2003).

Table 3-1 and Table 3-2 provide information on several soils which have not been experimentally tested by the author but are included in correlations for permeability presented in Chapter 5. These include Nankai Clay, Cornwall Kaolin, Villanova Tulo White Kaolin, Edgar Plastic Kaolin, Bisaccia Clay, and two clays from a proprietary location in the Gulf of Mexico.

3.2.2 Boston Blue Clay

Natural Boston Blue Clay is a glacio-marine clay of low sensitivity and a USCS classification of CL (low plasticity clay). It consists of glacial outwash deposited in a marine environment about 12,000 to 14,000 years ago in the period immediately following deglaciation of the Boston basin (Kenney 1964). The clay is present throughout the Boston area varying in thickness from 20 to 40 m. A stiff overconsolidated crust (OCR of 2 – 5) forms the upper 12 to 20 m of the deposit while underneath the clay is close to normally consolidated (Santagata, 1998). Although the depositional and general characteristics of BBC are fairly similar throughout most of the Boston area, some variability can be expected in clay retrieved from different locations. The index properties of the clay can vary slightly depending on several factors including particle size distribution, pore fluid chemistry and mineralogy. These properties can also change at a given location as a function of depth.

Resedimented Boston Blue Clay has been studied extensively at MIT since 1961 (Bailey 1961) and a large database exists on its properties. Its engineering behavior is very similar to many natural uncemented clays, including low to medium sensitivity, stress-strain behavior, strength anisotropy, significant strain rate dependency and typical consolidation characteristics. Along with its virtually infinite local supply, these key characteristics have made the soil an ideal research material to investigate fundamental aspects of soil behaviour without having to take into account the wide variability of natural soils.

Over the past five decades several different sources have been used to produce RBBC, with these sources defining different RBBC series. The RBBC used in this research is from Series IV which was obtained in 1992 from the base of an excavation for MIT's Biology Building. Approximately 2500 kg of BBC was excavated at a depth of about 12 m where the OCR of the clay varied from 1.3 to 4.3 (Berman 1993). The natural material obtained from the ground was first softened with tap water and mixed into a thick slurry. The slurry was then passed through a #10 sieve (nominal diameter of 2 mm) to remove all non-natural material, gravel, coarse sand and large shell fragments before being oven-dried at 60°C. This oven-dried material was then ground to 95% passing a #100 sieve (nominal diameter of 0.15 mm) by the Sturtevant Company using a roller mill. Finally, the material was manually blended to produce a homogenous powder before being stored in 40 gallon drums (Cauble 1996).

The pore fluid of natural BBC contains salt which varies in concentration as a function of both location and depth. The salt content of BBC Series IV powder used for resedimentation was measured using the conductivity method and calibrated against a KCL standard. The salt content was found to be 2.68±0.05 g per kg of dry powder. At an in situ water content of 40 %, this would correspond to 6.70±0.12 g per litre of pore fluid. Cauble (1996) determined the organic content of Series IV powder to be 4.4% by the loss on ignition method (ASTM D2974), though Horan (2012) later measured a much lower value of just 1.4 %.

A limited number of researchers who have studied RBBC previously and whose results are included in this thesis are listed in Table 3-1. Comparisons between the behaviors of intact and resedimented Boston Blue Clay have been made by Berman (1993), Casey (2011), House (2012) and Horan (2012). The results of these investigations will not be repeated here.

3.2.3 Presumpscot Clay

This is a glacio-marine clay of low plasticity from central Maine. The clay is blue-grey in color and has a similar geologic origin to Boston Blue Clay. A study of the in situ shearing behavior of the clay during a staged construction project is described in Reynolds and Germaine (2007). Resedimented Presumpscot Clay (RPC) is derived from a large number of individual shallow cores. These cores were first broken up and air-dried, after which they were combined and mixed together to create a uniform composition for resedimentation. The mixed and broken-up core was then ground into a fine powder using a commercial disc-style grinder. RPC has a low plasticity ($w_L = 33.1$ %) and a clay fraction of 37 % as determined by sedimentation. The mineralogical clay fraction was found to be 22.8 %, the dominant clay minerals being illite and chlorite.

3.2.4 Ursa Clay

This clay is from the Ursa Basin in the Gulf of Mexico, located 210 km south-southeast of New Orleans (Figure 3-3). The region is at the center of rapid deposition for late Pleistocene sediments from the Mississippi River. Between May and July of 2005, Integrated Ocean Drilling Project (IODP) Expedition Leg 308 drilled at six sites in the Gulf of Mexico, three of which were in the Ursa Basin. The purpose of Expedition 308 was to study fluid-flow and overpressure in the Gulf of Mexico continental slope (Expedition 308 Scientists 2006a). The Resedimented Gulf of Mexico Ursa Clay (RGoM Ursa) included in this research is derived from core taken at site U1322, specifically borehole U1322D (Mazzei 2008). At this borehole the seafloor was encountered at a depth of 1330 m and the hole was drilled in five steps to a total depth of 175 m below seafloor (mbsf). Three piston cores were obtained from seafloor to 9.5 mbsf, 70.0 - 79.5 mbsf and 100.0 - 107.8 mbsf (Expedition 308 Scientists 2006b). Tubes from the expedition were X-rayed in the MIT Geotechnical Engineering Laboratory and triaxial tests were carried out on the intact material. Tube material which was not tested in the triaxial device was air-dried and then pulverized using a mortar and pestle to the point that it would pass through a #100 sieve (nominal diameter of 0.150 mm) (Mazzei 2008). It is this material which was subsequently used for resedimentation.

3.2.5 Ugnu Clay

This clay comes from the North Slope of Alaska near the shore of the Beaufort Sea. The clay has dark grey/black color and a strong smell of hydrocarbon. Resedimented Ugnu Clay (RUC) is derived from two tube samples taken at depths > 1 km from a boring in the Schrader Bluff Formation in the Ugnu Region of the Alaskan North Slope (exact location is proprietary). The two tube samples are shown in Figure 3-4. A slake test performed on the intact material showed that it disintegrates in water, demonstrating the absence of significant cementation. The tube samples were air-dried, broken down into smaller pieces, and then ground into a powder using a custom built ball-mill grinder to achieve 100 % passing a #200 sieve (nominal diameter of 0.075 mm) (Jones 2010). RUC has a medium plasticity (w_L = 56.4 %) and a clay fraction of 45 % as determined by sedimentation. The mineralogical clay fraction was found to be 37.3 %, the dominant clay minerals being illite and smectite. A detailed description of the geologic origin of the clay, its processing for resedimentation as well as some consolidation and shear strength properties are given in Jones (2010).

3.2.6 San Francisco Bay Mud

This is a soft marine deposit from the Bay Area of San Francisco in California. Deposition in the San Francisco Bay Area has been repeatedly interrupted over time by sea-level changes, and the sediment originates from three general sources (Kontopoulos 2012):

- Alluvial deposits (clay, silt and sand) from streams and unconsolidated interglacial deposits from marshlands
- Silts and organic or inorganic detritus that formed a distinct layer in periods of high glaciation (Quaternary period, up to 2.5 million years ago)
- Human activities, i.e. mining and filling

The sediment is broadly categorized by geologists as Young Bay Mud or Older Bay Mud. Resedimented San Francisco Bay Mud (RSFBM) is derived from sixteen tube samples obtained from relatively shallow depths < 50 m. These sixteen tubes were selected based on their quality as judged by X-ray images and CRS tests performed on each tube. The tube material was then extruded and broken down into smaller cylindrical pieces before being air-dried. The air-dried material was ground into a powder using a ball-mill grinder developed by Jones (2010) to achieve 100 % passing a #200 sieve (nominal diameter of 0.075 mm) (Kontopoulos 2012). RSFBM possesses a dark grey color, a relatively high plasticity (w_L = 60.2 %) and a USCS classification of MH. It has a clay fraction of 52 % as determined by sedimentation and a mineralogical clay fraction of 51.2 %, the dominate clay minerals being illite and smectite. The organic content of the clay was determined to be 5.0 % using the loss on ignition method. A more complete description of the processing and shear strength properties of RSFBM are given in Kontopoulos (2012).

3.2.7 London Clay

This is a stiff, heavily overconsolidated and high plasticity marine clay deposited across the London and Hampshire Basins of South-East England. It was deposited during the Eocene period around 30 million years ago. The soil is the principal geological formation in the London district and is therefore of considerable engineering importance. In some locations, the clay deposit is between 100 and 145 m thick, though under London itself the formation has undergone considerable erosion and is now only between 28 - 43 m thick. The clay is fissured and slightly laminated. Normally it has a dark bluish-grey color, though oxidation near the surface changes its color from blue to brown. In some regions, this zone of oxidation has been found to occur to a depth of 13 m (Cooling and Skempton 1942, Horan 2012).

Resedimented London Clay (RLC) has been tested by many researchers in the past, including Bishop et al. (1965), Bishop et al. (1975), Marsden et al. (1992) and Petley (1999), to name but a few. The particular version of RLC tested as part of this work was obtained from a tunnel excavated in the Hendon area of London. The clay is of the aforementioned oxidized type and possesses a light brown color. Approximately 300 kg of the clay was excavated from the site by Ward and Burke Construction Ltd. during the Summer of 2011 and then shipped to the MIT Geotechnical Engineering Laboratory. The bulk material was first broken down into smaller pieces by hand and air-dried, after which it was mixed together to create a uniform composition for resedimentation. It was found to be necessary to further oven-dry the clay at 105 °C before it could be successfully ground into a powder using a commercial disc-style grinder. The organic content of the clay was determined to be 4.1 % using the loss on ignition method (Horan 2012). RLC has a high plasticity (w_L = 73.8 %) and a clay fraction of 63 % as determined by sedimentation. The mineralogical clay fraction was found to be 54.6 %, the dominant clay mineral being smectite. A detailed description of the geologic origin, index testing and the consolidation behavior of RLC is given in Horan (2012).

3.2.8 Skibbereen Silt

This is a soft silt from the town of Skibbereen in Southern Ireland. It was originally deposited in a marine environment, though most the salt has since been leached out of the soil by fresh groundwater flow and it now possesses a salt concentration < 1 g/l. The silt has a light grey color and a low plasticity. The Skibbereen Silt (SS) tested in the MIT Geotechnical Engineering laboratory was obtained from shallow cores taken by Ward & Burke Construction Ltd. in 2008 as part of an upgrade to the town's wastewater infrastructure. Following shipment to MIT these cores were broken up and air-dried, after which they were combined and mixed together to create a uniform composition. The mixed and broken-up core was then ground into a fine powder to achieve 100 % passing a #40 sieve (nominal diameter of 0.425 mm) (Grennan 2010).

Overall, Skibbereen Silt is a difficult soil to test in both the field and the laboratory. The silt cannot be successfully resedimented due to a lack of cohesiveness and is instead prepared for laboratory testing using the undercompaction method (Ladd 1978). It displays atypical mechanical behavior, such as an increase in critical state friction angle with increasing confining pressure. The silt has a low plasticity ($w_L = 25.8$ %), a USCS classification of CL-ML, and a clay fraction of 10 % as determined by sedimentation. The mineralogical clay fraction was found to be 7.5 %, the dominant clay mineral being illite. The organic content of the clay was determined to be just 0.4 % using the loss on ignition method. A complete description of the processing and mechanical properties of the soil are given in Grennan (2010).

3.2.9 Eugene Island Clay

This high plasticity clay comes from the Eugene Island region located off the coast of Louisiana in the Gulf of Mexico (Figure 3-5). Resedimented Gulf of Mexico Eugene Island Clay (RGoM EI) is derived from two 10.2 cm cores drilled in the 1990's, specifically from boreholes A-20 in Block 330 and A-12 in Block 316. In this area, the basin consists of over 4 km of Pliocene and Pleistocene sedimentary fill deposited over a salt-weld. A large quantity of core material was collected from each borehole at depths ranging from approximately 2200 m to 2500 m. The in situ salinity of the clay at this depth is approximately 80 g/l (Betts 2014). Core was later removed from the tubes at the University of Texas at Austin using hand tools and sandy intervals were discarded. Although the A-20 core had been sealed in wax, most of the core was in a damp to dry condition when it was finally opened. The clayey material was broken down into fist-sized pieces, spread on plastic sheeting, and allowed to air-dry for 18 days. It was then roller ground into a powder by an external company to the specification that 99 % should pass through a #100 sieve (nominal diameter of 0.15 mm) and homogenized. RGoM EI has a high plasticity (w_L = 85.8 %) and a clay fraction of 63 % as determined by sedimentation. The mineralogical clay fraction was found to be 53.9 %, the dominant clay mineral being smectite. A detailed description of the geologic origin, processing and consolidation behavior of RGOM-EI is given in Betts (2014). The results of a large number of triaxial tests performed on RGoM EI are provided in Fahy (2014).

3.3 RESEDIMENTATION

3.3.1 Introduction

Samples of resedimented clay are prepared by one-dimensionally consolidating a dilute slurry of the clay in a rigid-walled cylindrical container referred to as a consolidometer. The early method of resedimentation carried out at MIT was performed almost exclusively on BBC (e.g. Ladd and Varallyay 1965) and involved the production of large diameter soil cakes which were subsequently divided into smaller samples for testing. This method produced partially saturated clay which could only be subsequently saturated using a 200 kPa back-pressure. This became a critical issue when RBBC was used in the directional shear cell by Germaine (1982) since the clay specimens could not be back-pressure saturated in this device. Germaine therefore substantially revised the resedimentation technique to produce fully saturated and uniform samples with a salt concentration of approximately 16 g/l. Further modifications were later introduced by Seah (1990) who improved the layout of the system to increase productivity, modified the technique for extrusion of the soil cake from the consolidometer and implemented remote data acquisition to provide continuous monitoring of the consolidation process. Abdulhadi (2009) introduced a substantially different approach by preparing individual resedimented samples for each test specimen. This dramatically reduces the load which must be applied to achieve a particular preconsolidation stress, a critical issue for samples which need to be consolidated to high stresses.

3.3.2 Resedimentation Procedure

For this work the approach of preparing individual resedimented samples for each test specimen was used. Regardless of the type of clay to be resedimented, the basic procedure remains the same and can be divided into four main stages: powdering, deposition, consolidation, and sample extrusion and preparation. These stages are described below.

(i) Powdering

After the natural material has been obtained from the field it is broken down, dried, and ground into a powder. This powder is then blended to produce a homogenous composition. As described in Sections 3.2, however, the specific procedure differed slightly for the various soils, and this is due to the fact that the soils were processed by several different researchers at different time periods. RBBC, RUC, RSFBM, SS and RGoM EI were processed by Cauble (1996), Jones (2010), Kontopoulos (2012), Grennan (2010) and Betts (2014) respectively, while the remainder of the soils were processed as part of this work. After processing, each clay powder was stored in buckets or drums to be used intermittently for resedimenting samples.

(ii) Deposition

After retrieving the desired mass of clay powder from storage, it is mixed thoroughly with water using an electric blender to produce a homogenous slurry without lumps (Figure 3-6). The water used is distilled, often with some amount of seasalt added to achieve a desired pore fluid salt concentration in the resedimented sample. The salt added at this point is in addition to any already naturally existing in the clay powder. The salt concentrations and water contents at which the various soils are mixed are summarized in Table 3-3. The mixing water content is approximately twice the liquid limit of the soil, and results in a workable yet stable slurry with no free water present. The slurry is then vacuumed (under > 20 inches Hg) to remove any entrapped air using the setup shown in Figure 3-7. The flask used to vacuum the slurry has two lines, with one connected to the vacuum pump while the second line is used to pull the slurry from the adjacent container. The slurry is effectively de-aired as it drops into the vacuum flask. Following vacuuming, the de-aired slurry is carefully placed in a consolidometer using a funnel in such a manner as to minimize entrapment of air bubbles.

(iii) Consolidation

The slurry is loaded incrementally in a consolidometer using a load increment ratio of one. Porous stones placed at the top and bottom of the sample allow for double drainage. Each load increment is maintained at least until the end of primary consolidation as determined by the root time method. Once the desired maximum vertical stress, i.e. σ'_p, has been achieved, the resedimented sample is allowed additional time for secondary compression before being rebounded to OCR = 5 using a single load increment. At OCR = 5 the clay is close to isotropic effective stress conditions ($K_O \sim 1$) and the shear strains due to sample extrusion from the consolidometer are minimized, as confirmed by the work of Santagata (1994).

(iv) Extrusion and Preparation

After resedimentation in the consolidometer is completed, the sample is removed and prepared for triaxial testing. Samples resedimented to below approximately 1 MPa can be extruded manually. These samples are subsequently trimmed to the required diameter for testing using a wire saw and mitre box, with the last portion of trimming being performed using a razor blade. Trimmed material is taken for water content measurements. Samples resedimented to above 1 MPa require a hydraulic jack for extrusion. In addition, these samples are typically not soft enough to be manually trimmed to a smaller diameter using a wire saw. To overcome this issue the samples are resedimented using a consolidometer of the same inside diameter as a triaxial specimen. Once a resedimented sample possesses the required diameter for testing, it is placed in a sleeve and the ends are cut off to achieve the required height and to ensure that the two ends of the specimen are parallel. The pieces trimmed off the ends are also taken for water content measurements. Finally, the ends of the specimen are smoothed down using a razor blade.

3.3.3 Equipment

The consolidometers used to resediment samples consist of a smooth acrylic tube in which the clay consolidates between top and bottom porous stones. Nylon filter fabric is placed between the porous stones and the clay. A thin film of silicon oil is used to lubricate the inside of the tubes in order to reduce friction acting between the tube walls and the sample. The basic setup of a consolidometer is illustrated in Figure 3-8. A PVC spacer, topped with a porous stone and filter fabric, is placed at the bottom of the acrylic tube. The bottom portion of the tube is submerged in a bath filled with water of the same salt concentration as the pore fluid of the clay. Load is applied to the sample through a top spacer which rests on the top porous stone. Clamps are used to ensure that the entire setup is maintained vertical during the consolidation process. During each consolidation increment, axial deformation can be measured using a linear variable differential transducer (LVDT) to establish the end of primary consolidation as well as to gain information on the consolidation properties of the soil. For the first series of load increments, up to about 30 kPa, the load is applied by simply stacking weights on the top piston. For higher loads, the weights are placed on a hanger which in turn transfers load to the top piston, as shown in Figure 3-8. When the consolidometer is initially set up, the acrylic tube rests on the base of the water bath. However, at the point at which the method of load application is changed to the hanger system, the bottom spacer is replaced with a taller one and the acrylic tube no longer makes contact with the base of the water bath. This allows the sample to strain from both ends (i.e. as is achieved in a floating ring oedometer), thereby halving the amount of side wall friction which the sample is subjected to. Once a sample has been consolidated to 0.25 MPa, and if further consolidation is necessary, the consolidometer is removed from the hanger system and transferred to a pneumatic actuator. This pneumatic actuator, shown in Figure 3-9, has a maximum capacity of 8.9 kN. For a 9.35 cm^2 sample, this corresponds to a maximum consolidation stress of about 10 MPa. The transfer from the hanger system to the pneumatic actuator is performed rapidly to prevent significant swelling of the sample.

The time required to produce a resedimented sample for testing depends very strongly on the particular soil in question. For example, while a sample of RBBC may require approximately four weeks to reach to 2 MPa, a sample of RLC may take approximately 10 weeks to reach the same stress level. This is one of the major reasons why RBBC is favored in laboratory investigations of soil behavior over higher plasticity materials such as RLC.

3.3.4 Evaluation of Specimen Uniformity

In addition to reducing the actual stress imposed on the soil, side wall friction encourages sample non-uniformity during resedimentation in both the axial and radial directions and may create a slightly smeared outer layer. The uniformity and quality of resedimented samples produced by the large diameter (30 cm) consolidometers used in the past was evaluated by Germaine (1982) and Seah (1990). Uniformity of individual soil cakes was examined by measuring the variation of water content throughout the sample, utilizing X-ray diffraction pattern methods, as well as air-drying vertical and radial slices to check for stratification. Results from all these procedures verified that the batches were indeed uniform. However, as mentioned previously in Section 3.3.2., many of the samples resedimented as part of this research have been done so in consolidometers of the same inside diameter as a triaxial specimen, i.e. 3.45 cm.

These samples have a height to diameter ratio (H/D) of approximately 3 at the end of resedimentation (in contrast to a H/D of about 0.4 for the large diameter soil cakes of the past) with the result that side wall friction acting between the consolidometer tube and the soil has a much larger impact on samples prepared for this research. The impact of side wall friction is limited to some extent, however, by allowing the samples to consolidate from both ends, as described in Section 3.3.3.

Figure 3-10 compares the virgin compression curve of RBBC measured in a typical CRS test against the compression curves exhibited by two RBBC samples undergoing resedimentation in consolidometers to [applied] preconsolidation stresses of 2 and 10 MPa. The void ratios for the resedimented samples are calculated based on the final heights and water contents of the extruded samples together with LVDT readings at the end of each load increment. At a given applied stress, the void ratios of the samples in the consolidometers are significantly higher than in the CRS test. This is due to the fact that the stress applied to a sample in a consolidometer only acts fully at the top and bottom of the sample, as side wall friction reduces the applied stress to a lower value away from the ends. As a result, the void ratio of a resedimented sample is lowest at the ends and highest in the middle, with an average void ratio displayed in Figure 3-10. The two samples, RS137 and RS324, were consolidated to 2 and 10 MPa respectively, and had initial H/D ratios at the beginning of resedimentation of approximately 6.1 and 6.4 respectively. However, the samples underwent large axial strains > 50 % during consolidation, and at 0.1 MPa these values had reduced to 4.1 and 4.2 respectively. By the time the samples had reached their preconsolidation stresses of 2 and 10 MPa, the H/D ratios had decreased to about 3.1 and 2.8 respectively. While these H/D ratios are much higher than those of the large diameter soil cakes used in the past, it can be seen from Figure 3-10 that the void ratios of the resedimented samples at their respective σ'_p are reasonably close to the those observed in the CRS test, where H/D < 0.35 and the effects of side wall friction are believed to be insignificant.

Figure 3-11 plots the ratio of vertical stresses within sample RS324 normalized with respect to the applied vertical stress as the sample undergoes resedimentation to $\sigma'_p = 10$ MPa. As the sample height reduces dramatically during resedimentation, the height for each load increment is normalized by the distance to the bottom porous stone. The actual stresses within the sample are calculated by dividing the sample into multiple layers and assigning a coefficient of friction (f) which acts between the soil and the wall of the consolidometer. The void ratio of each layer is then calculated by assuming a virgin compression line (VCL) for RBBC based on the results of CRS testing (as $\sigma'_p = 0.1$ MPa in the CRS test, this VCL is extrapolated for stresses < 0.1 MPa). The value of f is adjusted for each load increment such that the calculated average void ratio of the layers is equal to the measured average void ratio of the sample. Figure 3-12 shows the variation in the calculated coefficients of friction as a function of applied stress level for samples RS324, RS137 and RS128. The value of f for each sample increases from less than 0.1 at very low stresses, when is soil is still essentially a viscous slurry, to about 0.15 at 0.035 MPa. During these initial load increments the sample undergoes loading from the top piston only, and side wall friction reduces the stress at the bottom of the sample to about 20 % of the applied stress at the top. While the H/D ratio of the sample is reducing during this time, this effect of offset by an increasing value of f with decreasing void ratio, the overall result being that the ratio of stress to applied stress remains fairly constant. At higher stresses the sample undergoes equal loading from both ends, though a higher coefficient of friction results in stresses still being reduced to as low as 20 % of the applied stress in the middle of sample RS324. As can be seen in Figure 3-12, however, the calculated values of f for each resedimented sample vary quite significantly at stresses > 0.1 MPa, reaching a value as high as 0.33 for sample RS324 before decreasing again.

Following the SHANSEP reconsolidation procedure (described previously in Chapter 2), the effects of side wall friction, or indeed any other disturbance effects caused by extrusion from the consolidometer, should be effectively eliminated following K_O-consolidation in the triaxial device to stresses much higher than the preconsolidation stress imposed during resedimentation. This ensures that any specimen non-uniformity is eliminated prior to the shearing phase of a triaxial test. Confirmation of this has been demonstrated by Abdulhadi (2009) who compared the consolidation and shear results of two CK_OUC tests on RBBC where one specimen was prepared in a 3.45 cm diameter consolidometer while the other was prepared in a consolidometer of 6.35 cm inside diameter (actually a modified oedometer) and was trimmed prior to triaxial testing. The results of the two tests are presented in Figure 3-13 and Figure 3-14 (Abdulhadi refers to the small diameter consolidometer as 'Plexi.' and the larger consolidometer as 'Stnd.'). Both specimens were consolidated to the same target stress in the consolidometers ($\sigma'_p = 0.1$ MPa) and in the triaxial apparatus ($\sigma'_p = 0.35$ MPa). Figure 3-13 shows the compression curves obtained during the K_O-consolidation phase of the triaxial tests. At the pre-shear consolidation stress of 0.35 MPa the two specimens have an almost identical void ratio, but slightly different values of K_O and axial strain. The compression curve exhibited by the specimen prepared in the small diameter consolidometer has a yield stress which would appear to be significantly less than the preconsolidation stress of 0.1 MPa which was supposedly applied during resedimentation. The yield stress is also quite poorly defined. In addition, the initial void ratio of the specimen is significantly higher than that possessed by the specimen prepared in the larger diameter consolidometer. These observations could reasonably be attributed to an increased impact of side wall friction occurring in the small diameter consolidometer. However, as can be seen in Figure 3-14, the stress-strain responses during undrained shearing are almost identical for the two tests, with both tests having the same strain to peak, undrained strength and shear resistance at large strains. Since the consolidation and shear behavior measured by Abdulhadi (2009) for RBBC at low stresses agrees very well with that measured by previous researchers who tested specimens trimmed from large diameter soil cakes, it is concluded that the impact of side wall friction on specimens prepared in small diameter consolidometers has a negligible effect on undrained shear behaviour, provided that the SHANSEP reconsolidation procedure is adopted.

Table 3-1: Origin, index properties and USCS classification of soils included in this thesis

Soil	Origin	Contributing researchers	Liquid Limit, w_L (%)	Plasticity Index, I_p (%)	Clay fraction (%)	Specific Gravity	USCS classif-ication
Boston Blue Clay	Boston, Massachusetts	author, Walbaum (1988), Ahmed (1990), Seah (1990), Sheahan (1991), Santagata (1994), Santagata (1998) Abdulhadi (2009), Moniz (2009), Horan (2012)	46.5^{C}	22.7	56	2.779	CL
Ugnu Clay	Alaskan North Slope	author, Jones (2010)	56.4	30.0	45	2.699	CH
Ursa Clay	Ursa Basin, Gulf of Mexico	author, Mazzei (2008)	51.7	28.0	54	2.667	CH
San Francisco Bay Mud	San Francisco, California	author, Kontopoulos (2012)	60.2	28.6	52	2.690	MH
London Clay	West Hendon, London	author, Horan (2012)	73.8	48.4	63	2.80	CH
Presumpscot Clay	Central Maine	author	33.1	13.7	37	2.772	CL
Skibbereen Silt	Skibbereen, Ireland	Grennan (2010)	25.8	7.5	10	2.724	CL-ML
Eugene Island Clay	Eugene Island, Gulf of Mexico	Betts (2014), Fahy (2014)	85.8^{C}	62.9	63	2.775	CH
Nankai Clay	Nankai Trough, offshore Japan	Schneider (2011)	68^{C}	39	56	N/A	CH
Cornwall Kaolin	Cornwall, U.K.	Ms. Baiyuan Gao	48^{C}	19	65	N/A	ML
Villanova Tulo White Kaolin	Sardinia, Italy	Gao (2013)	49.0^{C}	15.0	50	N/A	ML
Edgar Plastic Kaolin	Florida	Ms. Baiyuan Gao	68^{C}	31	73	N/A	MH
Bisaccia Clay	Bisaccia, Italy	Di Maio et al. (2004)	66	34	59	2.78	CH
G.O.M. Clay A	Proprietary location	Fahy (2014)	70.4^{C}	41.9	52	2.704	CH
G.O.M. Clay B	Proprietary location	Fahy (2014)	90.2^{C}	60.3	59	2.760	CH
G.O.M. Lower Clay	Proprietary location	Fahy (2014)	62.7	36.7	54	2.710	CH
G.O.M. Upper Clay	Proprietary location	Fahy (2014)	64.7	39.2	70	2.804	CH

^{C} determined using the Casagrande cup method, all other liquid limits were determined using the fall cone method

Table 3-2: Mineralogy of soils included in this thesis. Mineral quantities are quoted as both absolute percentages of the bulk (whole) sample by mass, as well as the relative percentages of these minerals in the < 2 μm fraction of each sample. Expandables in the < 2 μm fraction are given as a relative percentage of the mixed-layer illite-smectite

Soil		**Chlorite (%)**	**Kaolinite (%)**	**Illite (%)**	**Illite-Smectite (%)**	**Expand-ables (%)**	**Total clay (%)**
Boston Blue Clay	Whole sample	6.2	2.9		7.3*	N/A	16.4
	< 2 μm fraction	5	2	65	28	5-10	
Ugnu Clay	Whole sample	7.0	1.5	16.0	12.8	12.8	37.3
	< 2 μm fraction	5	3	21	71	40-50	
GoM Ursa Clay	Whole sample	2.8	3.3	14.3	17.0	17.0	37.4
	< 2 μm fraction	7	2	30	61	80-90	
San Francisco Bay Mud	Whole sample	15.8	0.0	0.0	35.4	35.4	51.2
	< 2 μm fraction	6	2	11	81	50-60	
London Clay	Whole sample	1.6	9.4		43.6*	N/A	54.6
	< 2 μm fraction	1	5	7	87	70-80	
Presumpscot Clay	Whole sample	13.0	0.0	9.8	0.0	0	22.8
	< 2 μm fraction	20	2	66	12	< 10	
Skibbereen Silt	Whole sample	7.5	0.0	0.0	0.0	N/A	7.5
	< 2 μm fraction	13	1	76	10	N/A	
GoM Eugene Island Clay	Whole sample	0.4	9.1	0.0	44.4	N/A	53.9
	< 2 μm fraction	1	4	8	87	70-80	
Nankai Clay	Whole sample	3.8	1.2	5.8	44.7 (smectite)		55.5
	< 2 μm fraction	3	1	11	85	80	
Bisaccia Clay^	Whole sample	10	10	20	30 (Ca-smectite)		70
GoM Clay A	Whole sample	1.7	0.9		38.2*	N/A	40.8
	< 2 μm fraction	2	1	13	84	50-60	
GoM Clay B	Whole sample	2.3	0.9		45.1	N/A	48.3
	< 2 μm fraction	2	1	11	86	50-60	
GoM Lower Clay	Whole sample	1.3	8.9		37.8*	N/A	48.0
	< 2 μm fraction	1	6	6	87	40-50	
GoM Upper Clay	Whole sample	0.4	6.1		44.4*	N/A	50.9
	< 2 μm fraction	1	3	8	88	70-80	

*includes both illite and mixed layer illite-smectite

^ from Di Maio et al. (2004)

Table 3-3: Water contents and salt concentrations at which resedimented samples are mixed to form a slurry

Soil	**Mixing water content (%)**	**Salt content of mixing fluid (g/L)**	**Natural salt content of powder (g/kg)**
Boston Blue Clay	100	16	2.7
Ugnu Clay	90	10	1.5
GoM Ursa Clay	100	0	N/A
San Francisco Bay Mud	100	0	N/A
London Clay	120	16	3.7
Presumpscot Clay	65	0	N/A
Skibbereen Silt	N/A	0	< 1
GoM Eugene Island Clay	~ 118	varies	~ 14

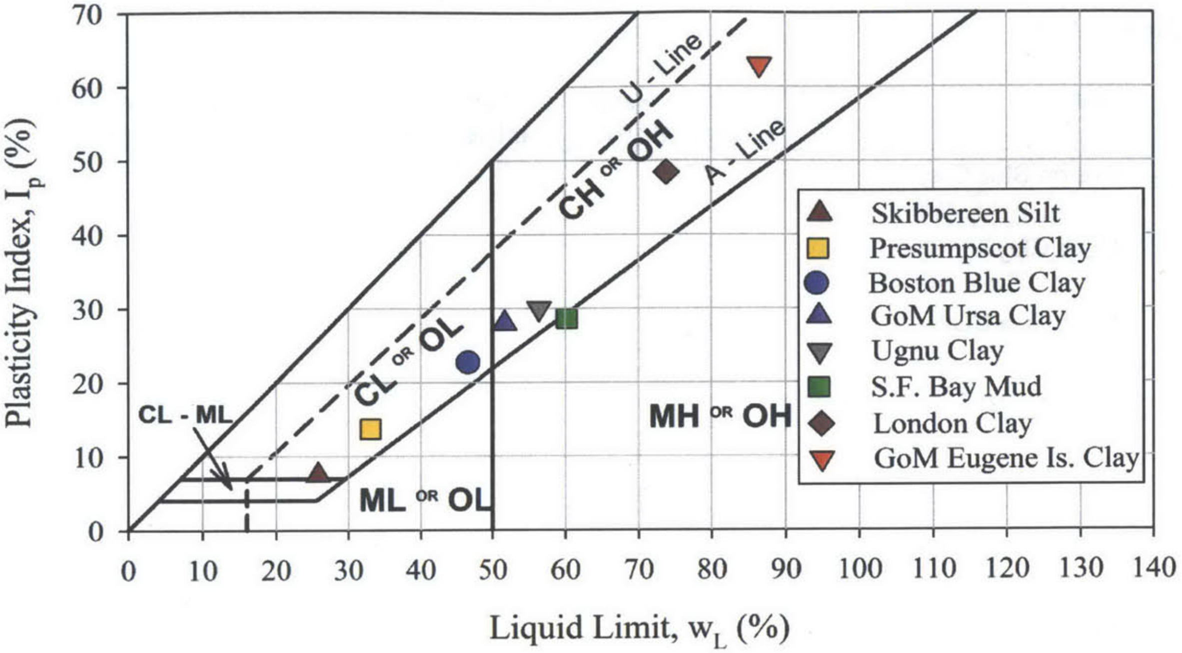

Figure 3-1: Plasticity chart showing the location of soils tested as part of this work

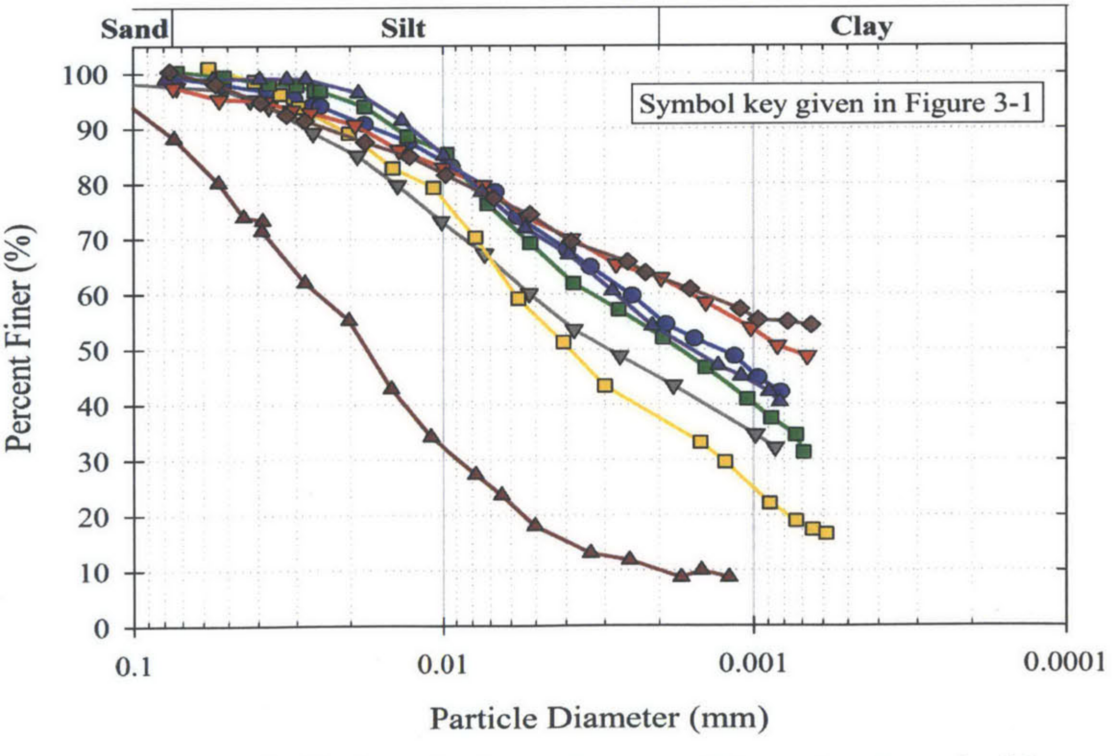

Figure 3-2: Particle size distributions of soils tested as part of this work as determined from hydrometer tests

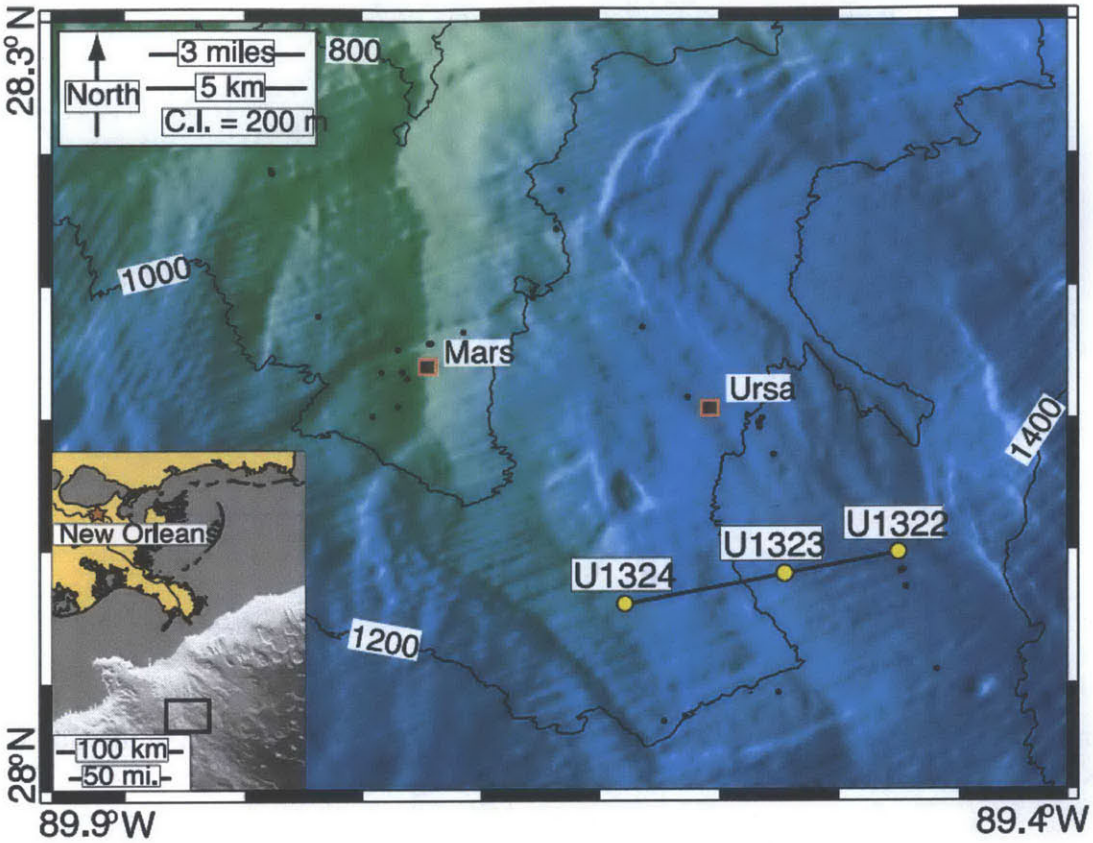

Figure 3-3: Location of site U1322 in the Ursa Basin of the Gulf of Mexico (Reece et al. 2012)

Figure 3-4: Tube samples of Ugnu Clay used for resedimentation (Jones 2010)

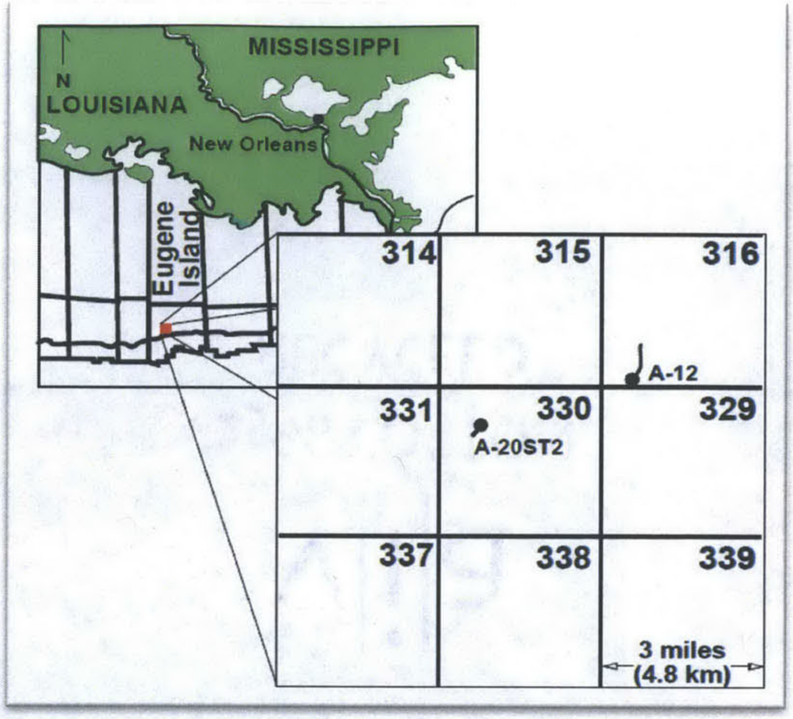

Figure 3-5: Location of boreholes A-12 and A-20 in the Eugene Island region of the Gulf of Mexico (Betts 2014)

Figure 3-6: Mixing of clay powder and water into a slurry

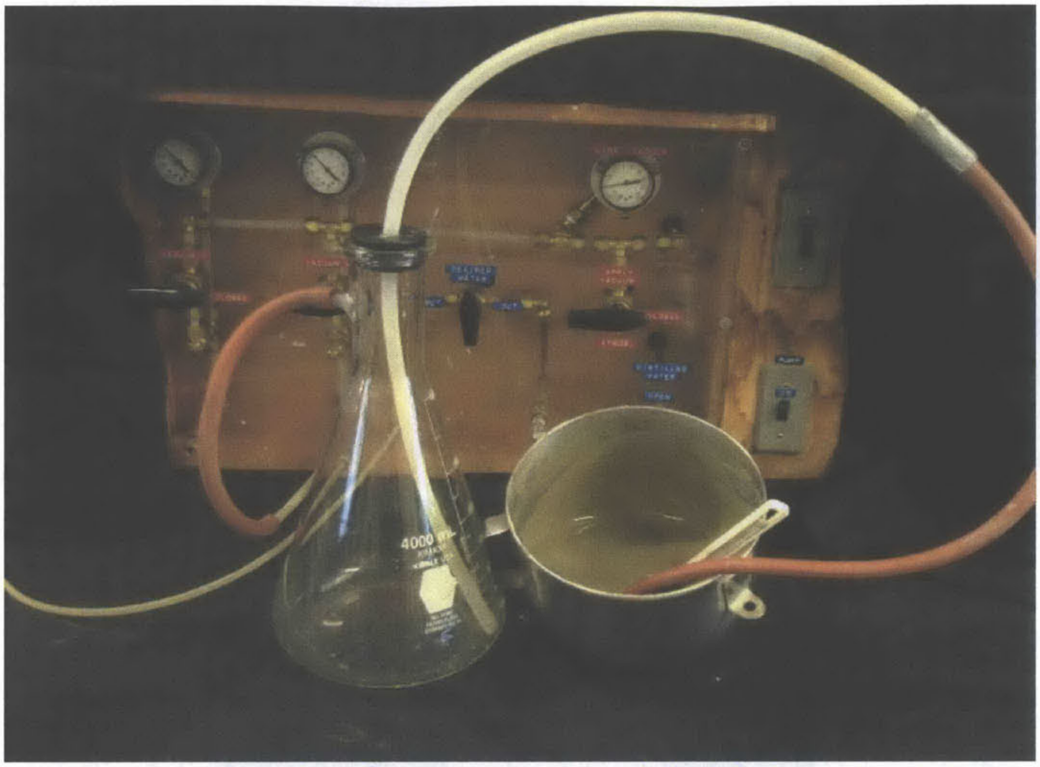

Figure 3-7: Vacuuming of clay slurry to remove any entrapped air

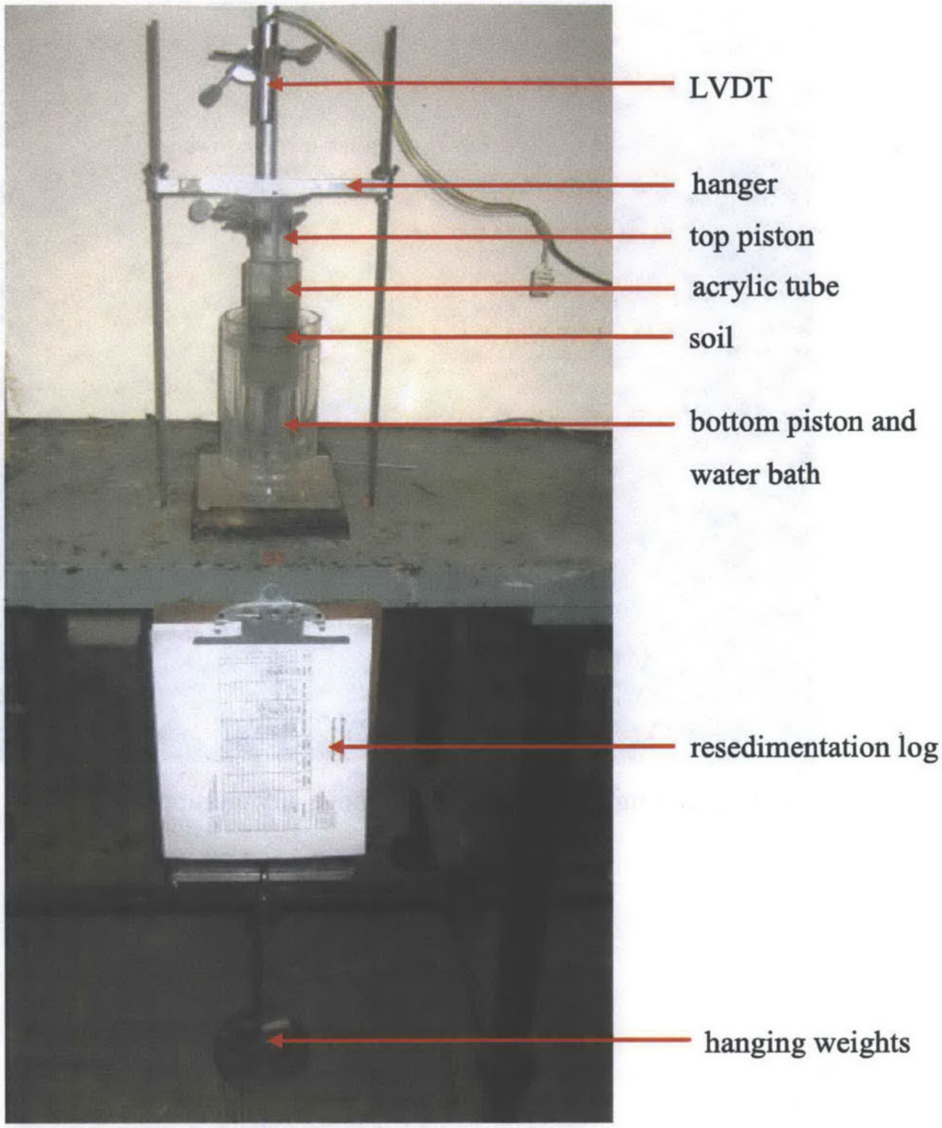

Figure 3-8: Setup of consolidometer with hanger system

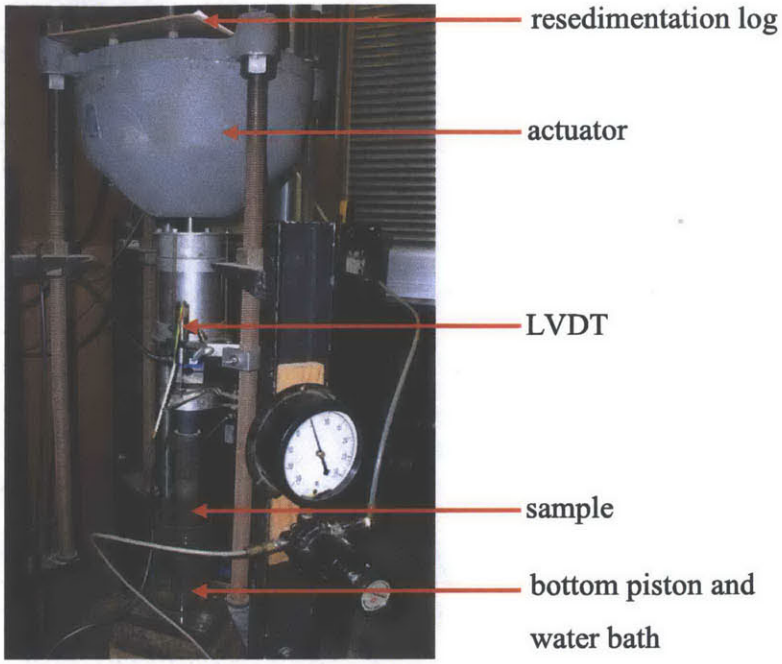

Figure 3-9: Pneumatic actuator used for resedimenting samples to $\sigma'_p = 10$ MPa

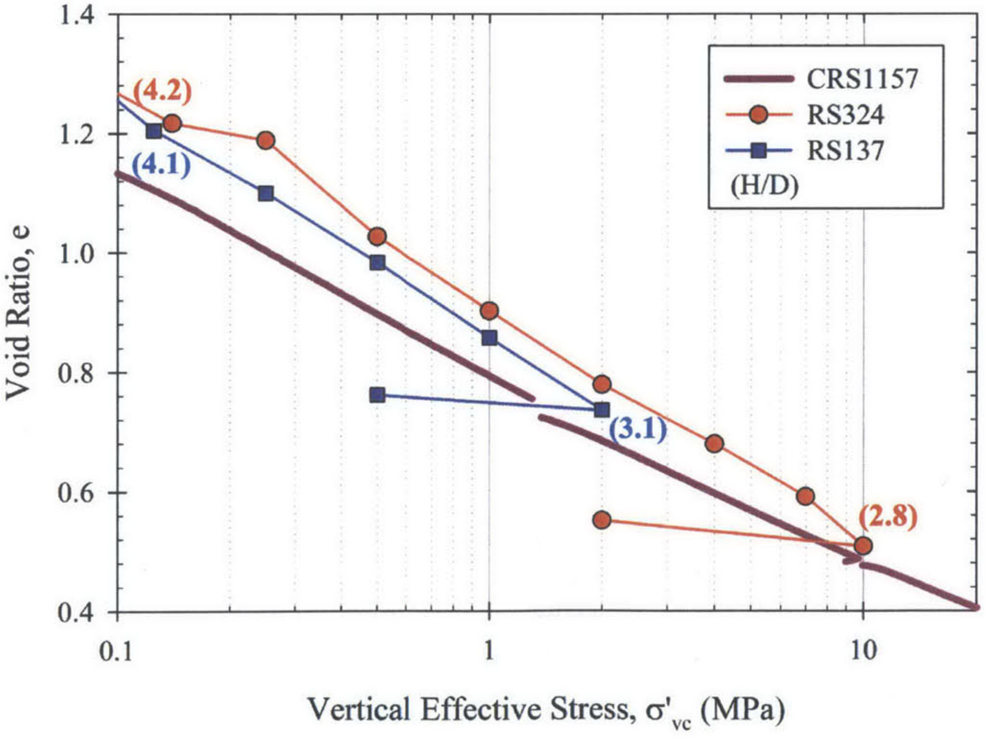

Figure 3-10: Comparison of virgin compression curves for RBBC as measured in a typical CRS test and during resedimentation in consolidometers

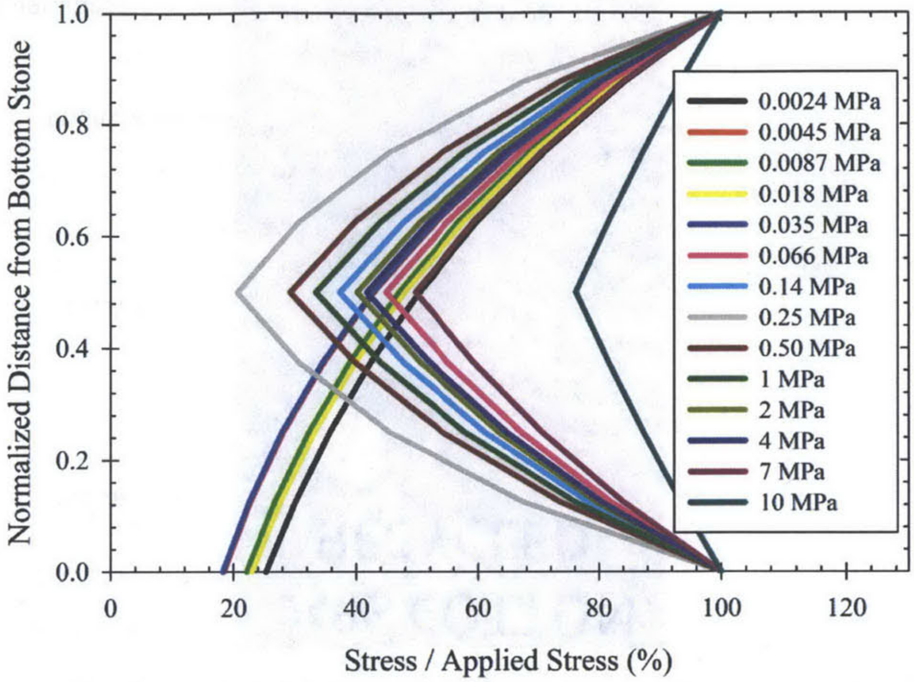

Figure 3-11: The ratio of vertical stresses within sample RS324 normalized with respect to the applied vertical stress as the sample undergoes resedimentation

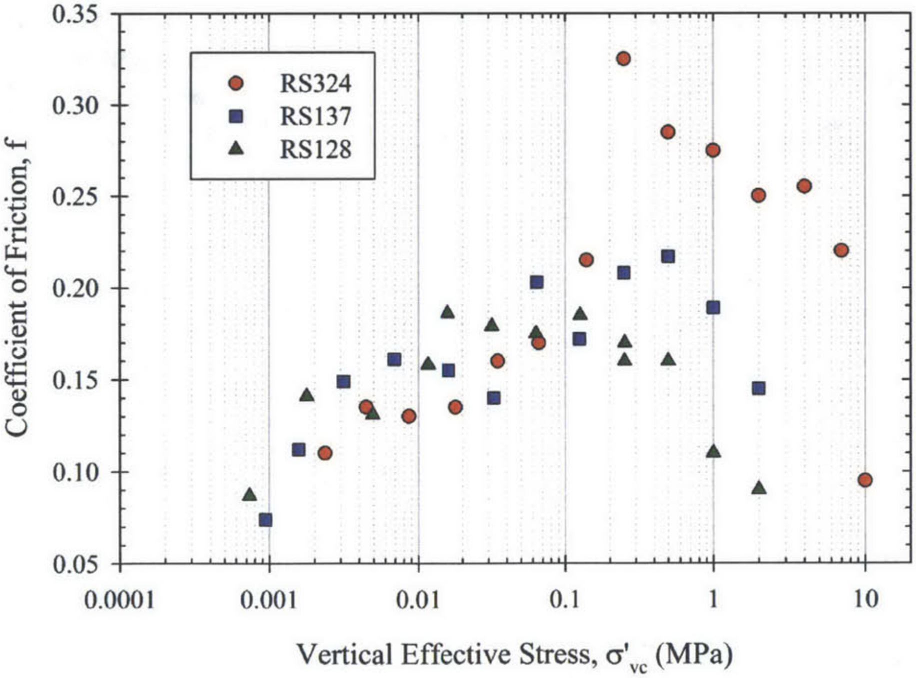

Figure 3-12: Variation in the calculated coefficients of friction as a function of stress level for three samples undergoing resedimentation

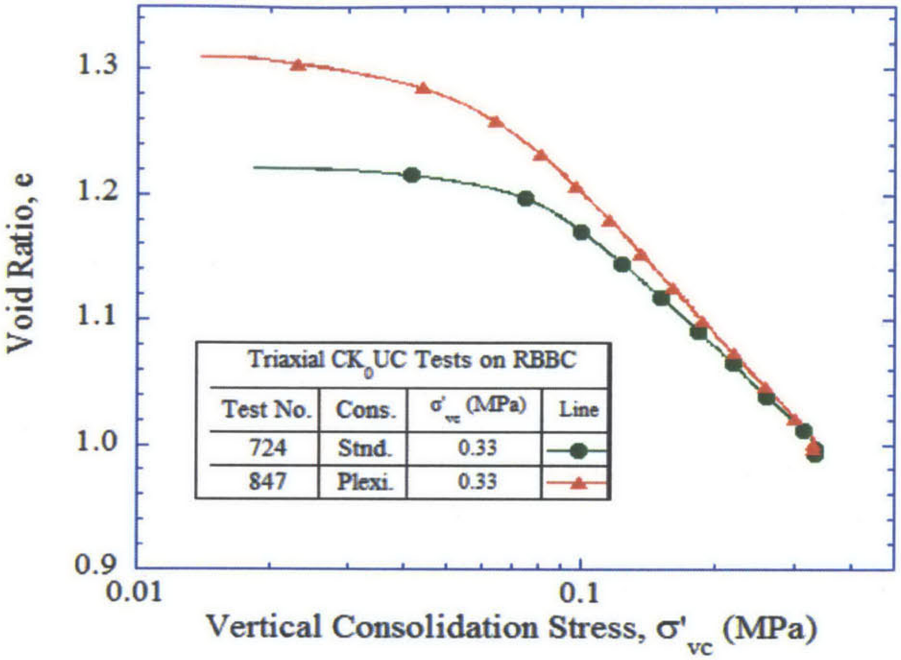

Figure 3-13: Comparison of compression behaviors measured during the K_O-consolidation phase of triaxial tests for RBBC samples prepared in 3.45 cm diameter ('Plexi.') and 6.35 cm diameter consolidometers ('Stnd.') (Abdulhadi 2009)

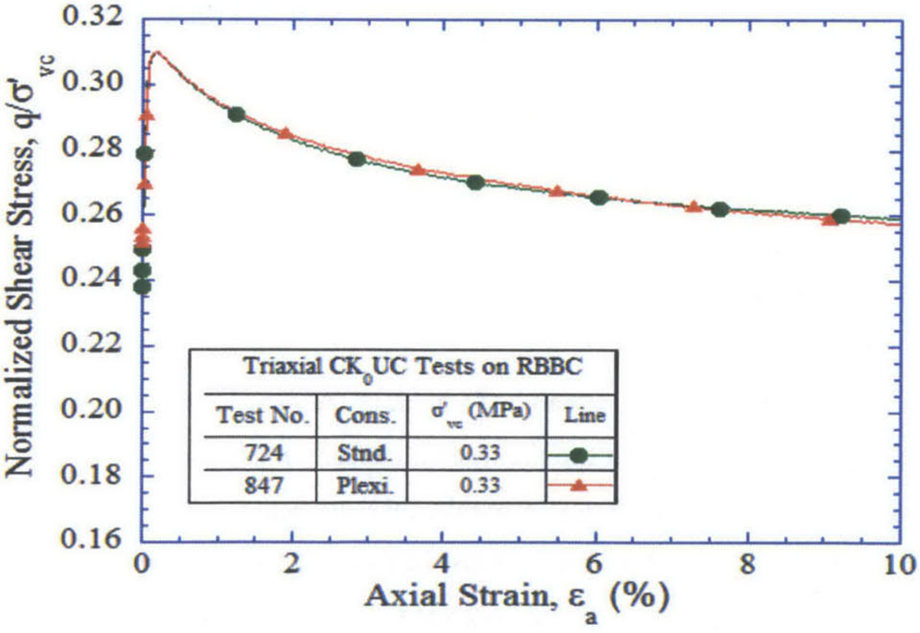

Figure 3-14: Comparison of shear stress-strain responses measured during the undrained shear phase of triaxial tests for RBBC samples prepared in 3.45 cm diameter ('Plexi.') and 6.35 cm diameter consolidometers ('Stnd.') (Abdulhadi 2009)

4 EQUIPMENT AND PROCEDURES

4.1 INTRODUCTION

This chapter describes the equipment and procedures used in a triaxial testing program that involved fine-grained specimens consolidated over a very wide range of effective stresses. Since a single triaxial system could not be used to test specimens over this entire stress range successfully, three different automated triaxial systems designed for low, medium, and high stresses were used throughout the testing program. All three triaxial systems were designed and built within the MIT Geotechnical Engineering Laboratory. Section 4.2 describes these triaxial systems and provides a detailed discussion of the triaxial cells, end platen design, pressure volume actuators (PVAs), automated control system and data acquisition. Section 4.2 also discusses the issue of apparatus compressibility in relation to the pore fluid drainage system and the impact of this compressibility on measurements of pore pressure. Section 4.3 evaluates the reproducibility and reliability of test results obtained using the three types of triaxial system. The procedures adopted in the testing program are described in Section 4.4.

4.2 TRIAXIAL EQUIPMENT

4.2.1 Overview of Triaxial Systems

In order to investigate how the mechanical behaviour of fine-grained sediments varies over a very wide range of consolidation stresses, three different automated triaxial systems were employed during the course of the research. To achieve the same degree of resolution throughout the testing program, a reduction in triaxial system capacity must coincide with a corresponding increase in the precision of both test variable measurements and load/pressure application. Essentially, anticipated material properties must be matched with testing device capacity. A low pressure system was used in tests where specimens were consolidated to a maximum σ'_p of 2 MPa, a medium pressure system for tests up to 10 MPa, while a high pressure system was used for tests above 10 MPa (note that because the value of K_O during virgin consolidation typically ranges from 0.5-0.8, the maximum cell pressure reached in tests can be considerably lower than σ'_p). The low pressure system was mostly developed by Sheahan (1991) and has been progressively modified over the past two decades. The medium pressure system was initially developed for the testing of frozen sand by Anderson (1991), but was modified for the testing of fine-grained soil by Abdulhadi (2009). The high pressure system was developed as part of this research and has a maximum cell pressure capacity of 100 MPa. A detailed description of the low and medium pressure cells in their most recent state is given in Abdulhadi (2009).

Figure 4-1 shows the components associated with the low pressure triaxial system, though the general configuration is the same for all three systems. Each system consists of a triaxial cell, a load frame to apply the necessary axial load, pressure volume-actuators (PVAs) to provide the necessary cell, back, and load frame pressures, a control box containing servoamplifiers, a power supply for the transducers, a computer to run the necessary control software and provide real-time readouts of the test data, and a central data acquisition system to record the test data. The triaxial cell, load frame and PVAs are located inside an enclosure in which the temperature can be maintained within ± 0.1°C.

4.2.2 Triaxial Cells

Each of the three types of triaxial cell test standard sized specimens of 3.5 cm diameter and 8.1 cm height. Specimens are subjected to both top and bottom drainage. For the low pressure cell it is sufficient to use a transparent 6 mm acrylic cell wall to withstand the cell pressure, while the medium pressure cell requires a 10 mm zinc-plated carbon steel cell wall. The high pressure cell developed as part of this work has a 38 mm (1.5 in.) cell wall made of high strength stainless steel (type 17-4). Cross-sectional drawings of the high pressure cell are given in Figure 4-2 and Figure 4-3, and Figure 4-4 shows a photograph of the cell within its temperature controlled enclosure. The cell possesses electrical feed-through connections located at the top and base that allow for the use of an internal load cell as well as on-specimen displacement transducers (in this work, however, on-specimen displacement transducers were not used). A suction cap located between the load cell and top cap allows a negative deviator load to be applied to the specimen, thereby making it possible to perform triaxial extension tests.

Axial load in the low pressure system is applied by means of a 1.1 ton (10 kN) bench-top screw-driven mechanical load frame, as shown in Figure 4-1. Hydraulic load frames of 10 ton (89 kN) and 24 ton (214 kN) capacity are used in the medium and high pressure systems respectively. Axial strain is measured externally on all cells by means of a displacement transducer, and volume strain is measured by means of a displacement transducer located on the back pressure PVA. In the case of the low and medium pressure systems these displacement transducers are in the form of an LVDT, while the high pressure cell utilizes string pots. Cell and pore pressures are measured using diaphragm type gauge pressure transducers that have a capacity of 1.4 MPa and 7 MPa in the low and medium pressure cells respectively. For the high pressure cell, different capacity transducers are used depending on the maximum pressure to be reached in a test. For tests with $\sigma'_p \leq 40$ MPa, cell and pore pressure measurements are made using transducers of 34 MPa and 14 MPa capacity respectively, while higher stress tests require transducers of 69 MPa and 34 MPa capacity respectively.

For each triaxial system, cell pressure is applied to the specimen using low viscosity silicone oil (Dow-Corning® 200 fluid, 20 centistokes). This oil is transparent, non-toxic, chemically inert, and does not degrade the seals or latex membranes used in testing. Silicon oil was initially used instead of water because, unlike water, the oil does not permeate through latex membranes over long periods of testing (Bellwald 1990). Another important benefit of using the oil is that it is electrically non-conductive, thereby allowing electronic devices such as a load cell or displacement transducer to be located inside the cell chamber. The latex membranes used to seal the soil specimen from the silicon oil are different for each triaxial cell. Condoms are used in the low pressure cell due to their high reliability, but have been found to leak at pressures above about 3 MPa (Abdulhadi 2009). For the medium and high pressure cells, commercial latex membranes of 0.30 mm and 0.64 mm thickness are used respectively. O-rings are used in each triaxial cell to seal to latex membranes to the base pedestal and top cap.

A load cell located inside each triaxial cell allows for the accurate measurement of deviator load without having to account for friction acting on the loading piston. In the low and medium pressure cells, Honeywell® 'S-beam' type load cells of 2.2 and 8.9 kN capacity are used respectively. The high pressure cell possesses a Futek® LCM550 threaded rod load cell of 222 kN capacity. These internal load cells should ideally have a voltage output which is unaffected by cell fluid pressure. However, this may not necessarily be the case, and can be tested by varying cell pressure while keeping the real deviator load acting on the load cell constant. Figure 4-5 shows the effect of varying cell fluid pressure on the output of a 2.2 kN load cell. The cell pressure was varied between 0 and 10 MPa for three cycles while the applied deviator load remained at zero (the initial reading of -1 N for the first loading cycle is due to submersion of the load cell in silicon oil). It can be seen that there is a large hysteretic effect within each cycle and that the output between cycles is not repeatable. Despite this, however, the load cell output varies by < 2 N (corresponding to < 0.1 % of its capacity) over the entire 10 MPa cell pressure range. This is a negligible amount compared to the shear strength of soil specimens, and can therefore be ignored in the analysis of test results. In addition, since the 8.9 kN load cell is of the same type and manufacturer, it was assumed to have a similarly negligible sensitivity to cell pressure (even assuming a calibration factor 4 times that of the 2.2 kN load cell). The 222 kN threaded rod load cell used in the high pressure cell, however, was found to have a considerable sensitivity to cell fluid pressure. Cell pressure was varied between 0 and 25 MPa for two cycles while the applied deviator load remained at zero. The results are shown in Figure 4-6, where it can be seen that increasing the cell pressure from 0 to 25 MPa reduces the load cell output by an amount corresponding to 1300 N. This is significant and must be accounted for in the calculation of axial stress. Fortunately, the load cell output between cycles is repeatable and there is no significant hysteresis within cycles. The effect of cell pressure on the load cell output can therefore be defined very accurately using a second order polynomial function:

$$\Delta N = 0.308\sigma_c^2 - 57.12\sigma_c \qquad \text{4-1}$$

where ΔN is the change in load cell output (N) and σ_c is cell pressure (MPa). This correction is applied to the load cell output in both the high pressure triaxial systems' local control computer, as well as in the analysis of test results.

4.2.3 End Platens

Different end platen configurations are used in the low, medium and high pressure triaxial cells. The low pressure cell possesses a standard type end platen configuration with a base pedestal and top cap of the same diameter as the specimen. Brass porous stones of 2.8 mm thickness are placed in contact with the base pedestal and top cap, and nylon filter paper is placed between the porous stones and the soil. This type of end platen configuration is considered 'fixed' because it prevents radial straining of the specimen at the top and bottom, which in turn results in non-uniform stresses and strains being developed during the shearing phase of triaxial tests. In an effort to minimize these non-uniformities at higher stresses, a smooth end platen design was used in many tests performed in the medium pressure cell as part of the author's earlier research (Casey 2011). This smooth end platen design is shown in cross-section in Figure 4-7. An exploded view of the membranes, filter paper strips and O-rings is given for clarity. Pore pressure is measured by connecting a pore pressure transducer to the bottom drainage line and radial drainage is provided by 16 vertical filter paper strips each of 6 mm width. The porous stones are relatively coarse, high permeability stones made from 54 grit vitrified bond stone. These smooth end platens were partially successful in increasing specimen uniformity during undrained shearing and prevented the occurrence of slip surfaces (Casey 2011). However, little change in the observed soil response could be detected between tests with smooth and fixed ends, and it was decided that the extra complication did not justify their use in future testing.

Not all tests performed in the medium pressure cell used the smooth end platen configuration. The remainder of tests instead used a fixed end configuration identical to that in the low pressure cell. However, it was found for tests performed using fixed ends close to the upper limit of cell, i.e. 10 MPa, that specimens would sometimes fail during K_O-consolidation. This failure was due to the soil specimen extruding out and around either the top cap or base pedestal. An example of a soil specimen which failed in this manner is shown in Figure 4-8. It was therefore decided that the high pressure cell would be designed such that the soil specimen could be slightly recessed within the base pedestal and top cap (Figure 4-3), thereby reducing the possibility of this type of failure. When using a 6.4 mm porous stone, the specimen is recessed 2 mm. This design is fundamentally the same as that used in the low pressure cell, in so far as it prevents radial straining of the specimen at top and bottom (i.e. a fixed end condition), but has been successful is preventing any premature failure of specimens during consolidation.

4.2.4 Pressure Volume Actuators

Custom-built PVAs are used to generate the necessary cell and back pressures for each system. For the medium and high pressure systems, a third PVA is also necessary to drive a hydraulic load frame. Two main types of PVA have been used during the course of the testing program. Both types of PVA essentially consist of a pressure chamber containing silicon oil or water, that on one end is connected to a reservoir and the triaxial cell, and on the opposite end is pressurized by a moving piston. The first type of PVA has long been used in the MIT Geotechnical Engineering Laboratory as part of a variety of test systems, including triaxial, constant rate of strain (CRS) and flow-through permeability. This type of PVA is versatile, compact, has a maximum pressure capacity of 14 MPa and a volume capacity of 47 cm^3. The PVAs accommodate a 0.5 ton Duff-Norton® inverted ball screw jack, which can be driven by a Maxon Motors® servomotor with 80 mNm continuous output (geared at 84:1). PVAs of this type are used in both the low and medium pressure systems. The high pressure triaxial system also uses one of these PVAs to generate back pressure.

A second type of PVA of much higher capacity has been developed as part of this research. This PVA type possesses a 10 ton Duff-Norton® inverted ball screw jack driven by a Maxon Motors® servomotor with 184 mNm continuous output (geared at 113:1). One PVA of this type is used in the high pressure system to generate cell pressure, and is shown in Figure 4-9. It has a piston diameter of 3.18 cm, resulting in a maximum pressure capacity of 110 MPA and a volume capacity of 200 cm^3. A second PVA of this type was built to drive the 24 ton hydraulic load frame. While this PVA has a very similar design to the first and possesses the same model of ball screw jack and servomotor, the large fluid displacement needed to drive the 24 ton load frame requires the PVA to have a much larger volume capacity but a lower maximum pressure. This is achieved by using a 6.35 cm piston, giving the PVA a maximum pressure capacity of 28 MPa and a volume capacity of 800 cm^3. To prevent damage in the case of the piston running out of stroke within the chamber, both PVAs possess limit switches which can shut off the power to the servomotor.

4.2.5 Control System

The low and medium pressure triaxial systems are automated using control hardware and software that was originally developed by Sheahan (1991). However, this original system is antiquated and contains some electronic components that are no longer commercially available. An upgraded version of the control system possessing modern components was developed as part of this research for inclusion in the new high pressure triaxial system, and can be described as follows. Measurement of test variables such as force, pressure and displacement is performed by transducers located both inside and outside the triaxial cell. The analogue output from each transducer is converted to a digital signal using a multichannel analogue-to-digital converter (MADC) device originally developed at MIT by Sheahan (1991). This MADC device is housed within a box and ported to a USB interface card (Figure 4-10), the digital output of which is conveyed to a netbook computer. The computer runs a control program written in QBASIC and is capable of performing all aspects of a triaxial test including initial pressure-up, back pressure saturation, consolidation (K_O or stress path) and shearing. The program compares the actual measurements from the transducers with the time-dependent target values and determines the corrective action required to reduce the difference between the two values. The program uses either intermittent proportional or continuous proportional-integral-derivative (PID) control to generate a digital signal which is sent to a commercial 12 bit digital-to-analogue converter by means of the USB interface card (Figure 4-10). The analogue output from this converter is then sent to a custom designed control card, located within a control box together with servoamplifiers, a 50 V dc power supply, and a fan (Figure 4-11). The control card is responsible for routing all signals originating from the digital-to-analogue converter, from limit switches located on the PVAs, and from control switches located on the front panel of the box to three Maxon Motors® ADS 50/5 servoamplifiers. By utilizing the signals from the control card together with energy from the power supply and tachometer feedback from the motors, the servoamplifiers energize the motors (by means of pulse width modulation) and allow for continuous and very precise control of cell pressure, pore pressure and axial load.

4.2.6 Data Acquisition

The control system described above incorporates two data acquisition systems; a central system used to record all data in the laboratory for subsequent analysis, and a local one for each triaxial system based around the MADC device. For the MADC device, a key component is an Analog Devices® AD1170 analogue-to-digital converter. The AD1170 is a very high resolution, integration-type converter which allows for user specified integration times (from 1 to 350 ms) and a maximum resolution of 22 bits. At a 10 V scale (±5 V), this corresponds to a maximum precision of 0.0024 mV. However, because the maximum output from pressure transducers and load cells is typically in the range of 2 – 150 mV, the analogue output from these devices can be amplified using a channel specific AD624 instrumentation amplifier by a factor of 10, 100 or 1000 prior to digital conversion, thereby increasing the precision to 0.00024 mV, 0.000024 mV or 0.0000024 mV respectively. This is more than sufficient to provide accurate readings for closed loop feedback control of the system. The high degree of signal averaging provided by the integration-type AD1170 converter helps eliminate noise from the input signal and thus provide stable readings of test variables.

The central data acquisition system present in the MIT Geotechnical Laboratory is based around a Hewlett Packard HP3497A data acquisition unit interfaced with a desktop computer. This system uses an integration-type analogue-to-digital converter with auto-ranging signal amplification to four voltages scales; 0.1, 1, 10, 100 V. This auto-ranging capability removes the need for any amplification of analogue input signals. In addition, because this central system is not used for feedback control of any testing equipment, it is not necessary for its resolution to be as high as that of the MADC device. The system is currently set up to monitor and record 180 channels simultaneously at a maximum rate of 1 Hz.

For each triaxial system, Table 4-1 summarizes the precision of both the central data acquisition system and the MADC device (in engineering values and voltages) as well as the corresponding resolutions for each device. For axial displacements and specimen volume, resolutions are based on specimen dimensions. For cell pressure, pore pressure and load cell force, resolutions are based on the maximum range of the transducer during a typical test. For the high pressure system, cell and pore pressure transducers of 69 MPa and 34 MPa capacity were assumed respectively (as these were the highest capacities used). To achieve a comparable degree of resolution across each triaxial system, axial load, cell pressure and pore pressure must be measured with far greater precision when testing at lower stresses. In reality, the MADC device can typically perform analogue-to-digital conversion with greather precision than measurements can be taken using commercially available transducers. As a result, the resolution of test variables may be controlled by the transducers used, and would be lower than the values quoted in Table 4-1.

4.2.7 Apparatus Compressibility

During the undrained shear phase of triaxial tests, excess pore pressure is generated within the specimen. To determine the effective stress acting on the soil, the specimen must be hydraulically connected to a pore pressure measuring device, i.e. a pressure transducer. These hydraulic connections also allow for drainage of the pore fluid during consolidation. However, the drainage lines, the valves and the water contained within them necessarily involve a finite compressibility. This is referred to as apparatus compressibility and it will alter the excess pore pressure generated in the specimen from its true value, since some amount of pore fluid must inevitably drain from the specimen into the drainage lines when the pore pressure increases (Wissa 1969, Bishop 1976).

One way in which the effect of apparatus compressibility on the observed soil behavior can be evaluated is to compare the specimen's B-value that can be measured using a triaxial device, B_{meas}, (Equation 2-9) against its theoretically true value, B_{true} (Equation 2-8). As discussed in Section 2.6, the true B-value of a soil is a function of its porosity, the compressibility of the pore fluid, the compressibility of the soil grains, and the compressibility of the soil skeleton with respect to a change in consolidation stress, C. In addition to these factors, the value of B_{meas} is a function of the testing device, and will always be lower than B_{true} by an amount depending on apparatus compressibility. Figure 4-12 compares the calculated true and measurable B-values of RBBC (assuming an OCR = 1) for the three triaxial systems as a function of stress level. The decrease in B_{true} of the soil with increasing stress level is almost entirely due to the dramatic change in C, which decreases from approximately 0.02 MPa^{-1} at σ'_{vc} = 0.1 MPa (estimated from data in Santagata 1998), to 0.0001 MPa^{-1} at σ'_{vc} = 100 MPa (estimated from results presented in Chapter 6 of this thesis). The graph also shows the ratio of

B_{meas} to B_{true}. It was suggested by Bishop (1976) that testing should ideally involve $B_{meas}/B_{true} >$ 90 %, in order to obtain the most accurate picture of the undrained behavior of the soil. To achieve this, triaxial cells developed for testing at higher pressures must possess a drainage system that is considerably stiffer, and stores a smaller volume of free water, than cells used at lower pressures. However, there is no scientific justification behind Bishop's specific threshold value of 90 %, and it is essentially arbitrary. For the high pressure triaxial cell developed during the course of this research, system compliance was reduced by using 0.69 mm (internal diameter) stainless steel tubes and by locating the drainage valves and pore pressure transducer at the base of the triaxial cell as close as practically possible to the specimen. Despite these measures, Figure 4-12 shows that the high pressure triaxial cell cannot achieve values of $B_{meas}/B_{true} > 90$ % at stresses above about 30 MPa. Calculations show that the apparatus compressibility associated with the high pressure cell is caused almost entirely by the compression of free water within the drainage lines and porous stones.

The analysis presented above does not imply that undrained conditions are not satisfactorily achieved during shearing. Rather than using B-value as an indicator of undrained conditions, which is not particularly useful, it is more illustrative to look at the amount of drainage required from a specimen in order to develop its drained strength and to compare that to the volume of flow caused by apparatus compressibility.

Figure 4-13 shows the ratio $\Delta V_{app}/\Delta V_{shear}$ versus stress level, where ΔV_{app} is the volume of pore fluid which flows from the specimen into the drainage lines at the point of undrained failure (due to compression of water in the drainage lines and porous stones), and ΔV_{shear} is the volume of pore fluid which must drain from the specimen in order to fully develop its drained strength. The figure is drawn assuming RBBC at OCR = 1. The value of ΔV_{shear} changes with stress level and is calculated based on the critical state behavior of RBBC, as determined from triaxial test results that are presented in Chapter 6 of this thesis. The ratio $\Delta V_{app}/\Delta V_{shear}$ increases exponentially with increasing stress level, but remains < 0.25 % at $\sigma'_{vc} = 10$ MPa and is still < 3.5 % at $\sigma'_{vc} = 100$ MPa. In addition to the increasing compression of water within the drainage lines at higher pressures, the dramatic rise in $\Delta V_{app}/\Delta V_{shear}$ also reflects the fact that the *normalized* excess pore pressures at the point of undrained failure increase rapidly for NC RBBC with increasing stress level (as will be discussed in Chapter 6), thereby dramatically increasing the value of ΔV_{app}.

4.3 EVALUATION OF TRIAXIAL EQUIPMENT

4.3.1 Introduction

It is important to demonstrate that reproducible test results can be obtained using the different triaxial systems employed during the course of the research. This is necessary to ensure that observed trends in soil properties, such as a systematic variation in strength with increasing stress level, reflect a true soil behaviour and are not influenced by the testing equipment. To demonstrate reproducibility, the results of tests performed on samples of the same composition and under the same test conditions must be compared for the three triaxial systems. The resedimentation technique is ideal for this purpose as it can produce identical saturated samples consolidated to any desired preconsolidation stress. This section compares the consolidation and undrained shear results of triaxial tests performed on samples of RBBC using the low, medium and high pressure triaxial systems.

4.3.2 Consolidation

The compression behaviour of RBBC determined from the K_O-consolidation phase of typical triaxial tests is illustrated in Figure 4-14. The figure shows the virgin compression behaviour of the soil from 0.1 MPa up to 40 MPa and includes two tests performed with both the medium and high pressure systems, as well as a test performed with the low pressure system by Abdulhadi (2009). Any swelling data from these tests are excluded from the figure for clarity. Following an initial recompression phase up the preconsolidation stress imposed during resedimentation, each of the tests can be seen to follow a unique virgin compression line. Figure 4-14 also includes the compression behaviour observed during a typical CRS test (in which σ'_p of the resedimented sample was 0.1 MPa). Excellent agreement is observed between the compression behavior determined using the CRS device and using each of the triaxial systems.

The compression index (C_c) of the soil decreases with stress level, from about 0.35 in the 0.1 – 1 MPa stress range, to 0.33 in the range of 1 – 10 MPa, to 0.23 in the range of 10 – 40 MPa.

The change in the value of K_O during consolidation is shown in Figure 4-15, which includes data from the same tests as given in Figure 4-14. In some cases a small deviator load is present on the specimen at the end of back pressure saturation, and as a result the consolidation phase of these tests does not begin under hydrostatic conditions (i.e. with $K_O = 1$). The value of K_O decreases during the recompression phase before reaching a fairly stable value of normally consolidated K_O (K_{ONC}) during virgin consolidation. Although there is a small amount of scatter in the values of K_{ONC} between tests, there is a general trend for K_{ONC} to increase with stress level. The results of triaxial tests carried out as part of this research and that of Abdulhadi (2009) show a consistent increase in K_{ONC} of RBBC from about 0.51 at 0.1 MPa to 0.60 at 100 MPa.

4.3.3 Undrained Shear

Normalized shear stress-strain responses measured during undrained shearing of NC RBBC are plotted in Figure 4-16 for axial strains up to 2 %. The behaviour measured using the low and medium pressure systems is compared at a low stress level (Figure 4-16a) while the behavior measured using the medium and high pressure systems is compared at a high stress level (Figure 4-16b). The test in the low pressure system was performed by Horan (2012). At the higher stress level, almost identical responses are measured when using the high and medium pressure systems. At the lower stress level, very similar responses are also observed between the medium and low pressure systems, although the test performed in the low pressure system displays a slightly lower peak strength. Figure 4-17 compares the critical state friction angles measured during the same tests. At the lower stress level (Figure 4-17a) friction angles of approximately 31° and 32° are measured in the medium and low pressure systems respectively. At the higher stress level (Figure 4-17b) both tests reach a very similar friction angle of about 30°. Slight differences can be seen in the normalized shear induced pore pressures measured at a given strain between the tests at both the low stress level (Figure 4-18a) and at the high stress level (Figure 4-18b). The relatively small differences in undrained shear results observed between the triaxial systems are within the range of experimental non-repeatability that could be expected between different tests from a single device. It is concluded that a very satisfactory degree of reproducibility can be achieved across the triaxial systems employed for the author's research. Furthermore, any observed systematic changes in soil properties with stress level can be assumed to reflect true soil behaviour, as they are not significantly influenced by the triaxial equipment used.

4.4 TESTING PROCEDURES

This section describes the procedures for setting up and performing triaxial tests, specifically in the high pressure triaxial system. These procedures are similar to those for testing in the low and medium pressure triaxial systems, which are already described in detail in Abdulhadi (2009) and Casey (2011) respectively and will not be repeated here.

Test specimens are prepared using the resedimentation process, as described in Chapter 3. After the resedimented sample has been extruded from the consolidometer it is placed in an aluminum mold. The ends of the sample are trimmed off using a razor to produce a specimen of 8.1 cm height. It is then removed from the mold and its dimensions measured with a calipers. The specimen is then placed on a moist porous stone which sits within the recess of the triaxial cell base pedestal. A piece of nylon filter paper is positioned between the porous stone and specimen. A second piece of nylon filter paper is then placed on top of the specimen, followed by a porous stone and the top cap. Filter paper strips may now be placed around the specimen in order to speed up the rate of consolidation for soils having low values of c_v, e.g. Resedimented London Clay. The first (inner) latex membrane is then placed over the specimen using a membrane stretcher connected to a vacuum. The second (outer) membrane is then placed in the same way. Two O-rings are positioned between the inner and outer membranes at both the top cap and base pedestal. A third O-ring is then positioned between the first two, but this O-ring is located outside the outer membrane. The top drainage line, which spirals around the specimen, is then connected at the cell base and top cap.

The steel cell chamber is now placed in position using a ceiling-mounted gantry crane and bolted to the cell base. The zero value of the load cell is recorded and the load cell is then brought into contact with the top cap. The whole cell can now be placed in the load frame using a manual fork-lift. Following this the cell is filled with silicone oil. Once filled, the cell oil is pressurized slightly to prevent the specimen from swelling once the drainage lines are flushed with water. The magnitude of the cell pressure needed to prevent the specimen from changing volume at this time (so that it neither swells nor consolidates) is estimated to be about 1.5 MPa for specimens resedimented to σ'_p = 10 MPa, though this value is difficult to establish. The drainage lines then are vacuumed (under approximately 20 inches Hg) for approximately 5 minutes to remove air before being flushed with water. The pore pressure transducer is placed and the drainage valves are closed. At this point the cell pressure is increased further, typically to a value equal to the rebound pressure applied during resedimentation (though no higher than this value). The specimen is allowed to equilibrate overnight and the following day the sampling effective stress is recorded. The specimen is then back-pressure saturated, typically to about 1 MPa, while the sampling effective stress is held constant. At the end of back-pressure saturation a B-value check is performed using a cell pressure increment of 0.1 MPa. If a suction cap is not being used in the test, a small deviator load of approximately 100 kPa is maintained on the specimen throughout the initial pressure-up and back-pressure saturation phases. This is done so that any axial strain which the specimen undergoes can be measured using the external string pot.

During K_O-consolidation specimens are consolidated to at least twice the stress level applied during resedimentation, as per the standard SHANSEP method of laboratory reconsolidation (discussed in Section 2.4.4). The K_O-consolidation algorithm used to control the triaxial system applies a constant axial rate of strain and ensures zero radial strain of the specimen by continuously adjusting cell pressure to keep volumetric and axial strains equal. The appropriate axial strain rate to be used depends on the permeability of the soil, with low permeability soils requiring slower rates to prevent large excess pore pressures from developing within the specimen (e.g. 0.15 %/hr is sufficiently slow for RBBC). At the end of K_O virgin consolidation specimens are allowed at least 24 hrs of [drained] secondary compression. For tests conducted in the overconsolidated range, specimens are K_O-swelled to the desired OCR and then allowed further time for secondary swelling. Prior to shearing, a leak check is performed by closing the drainage valves and monitoring the pore pressure. Provided no internal or external leak is detected, the specimen is sheared undrained using an axial strain rate of 0.5 %/hr. Shearing is carried out to $\varepsilon_a > 12$ % in each test, by which point a steady critical state friction angle is reached.

The raw test data are analyzed using a QBASIC computer program. The program converts the transducer voltages recorded by the central data acquisition system into engineering values of deviator load, axial displacement, volume change, cell and pore pressures, which are in turn used to compute effective stresses and strains. The area of the specimen is calculated using either a right cylinder or parabolic area correction. During the consolidation phase of tests a right cylinder correction is used to compute the area ($A_{cylindrical}$), defined as:

$$A_{cylindrical} = A_o(1/(1-\varepsilon_a)) \qquad 4-2$$

where A_o is the initial specimen area. During the shear phase of tests a parabolic area correction is typically used to compute area ($A_{parabolic}$), defined for an undrained test as (Germaine and Ladd, 1988):

$$A_{parabolic} = A_o\left\{-0.25 + \frac{\sqrt{25-20\varepsilon_a-5\varepsilon_a^2}}{4(1-\varepsilon_a)}\right\}^2 \qquad 4-3$$

where A_o is the pre-shear specimen area and ε_a is the axial strain since the beginning of shearing. In addition, the computations of axial and radial stresses involve a correction for membrane resistance using the method of Berre (1985). For tests in which filter paper strips are used to speed up consolidation, axial stress is further modified using the filter paper correction of Bishop and Henkel (1962).

Table 4-1: Precision of the central data acquisition system and MADC device together with the corresponding resolutions for each device. For axial displacements and specimen volume, resolutions are based on specimen dimensions. For cell pressure, pore pressure and load cell force, resolutions are based on the typical range of the transducer utilized during testing.

Transducer	**Working Range**	**Precision**		**Resolution**	
		MADC	**Central acq.**	**MADC**	**Central acq.**
Low Pressure					
Axial displacement	1.8 cm	0.00001 mm (0.0024 mV)	0.00045 mm (0.1 mV)	0.00001%	0.00056%
Specimen volume	47 cm^3	0.01 mm^3 (0.0024 mV)	0.41 mm^3 (0.1 mV)	0.00001%	0.00055%
Cell pressure	1.4 MPa	0.003 kPa (0.00024 mV)	0.012 kPa (0.001 mV)	0.0002%	0.0009%
Pore pressure	1.4 MPa	0.003 kPa (0.00024 mV)	0.012 kPa (0.001 mV)	0.0003%	0.0014%
Load cell	2.2 kN	0.001 N (0.00024 mV)	0.005 N (0.001 mV)	0.0001%	0.0004%
Medium Pressure					
Axial displacement	3 cm	0.00001 mm (0.0024 mV)	0.00060 mm (0.1 mV)	0.00002%	0.00074%
Specimen volume	47 cm^3	0.01 mm^3 (0.0024 mV)	0.40 mm^3 (0.1 mV)	0.00001%	0.00054%
Cell pressure	7 MPa	0.015 kPa (0.00024 mV)	0.063 kPa (0.001 mV)	0.0002%	0.0009%
Pore pressure	7 MPa	0.015 kPa (0.00024 mV)	0.063 kPa (0.001 mV)	0.0004%	0.0018%
Load cell	8.9 kN	0.012 N (0.00024 mV)	0.050 N (0.001 mV)	0.0002%	0.0009%
High Pressure					
Axial displacement	7.6 cm	0.00003 mm (0.0024 mV)	0.0014 mm (0.1 mV)	0.00004%	0.00174%
Specimen volume	47 cm^3	0.04 mm^3 (0.0024 mV)	1.75 mm^3 (0.1 mV)	0.00006%	0.00233%
Cell pressure	69 MPa	1.45 kPa (0.00024 mV)	6.03 kPa (0.001 mV)	0.0021%	0.0087%
Pore pressure	34 MPa	0.08 kPa (0.00024 mV)	0.31 kPa (0.001 mV)	0.0002%	0.0010%
Load cell	222 kN	0.040 N (0.0000024 mV)	18.6 N (0.001 mV)	0.0001%	0.0317%

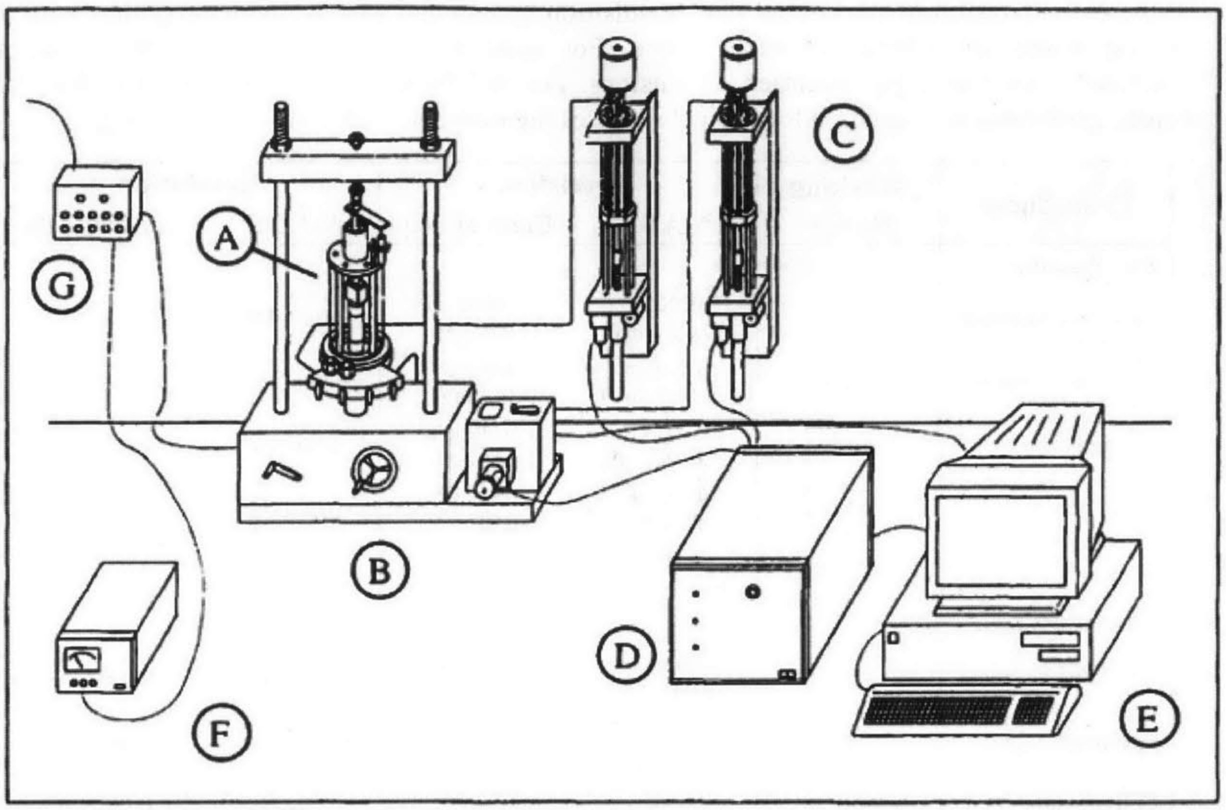

A - Triaxial Cell
B - Load Frame
C - Pressure/Volume Controllers
D - Motor Control Box
E - Personal Computer
F - DC Power Supply
G - Data Acquisition Channels

Figure 4-1: Schematic of the standard automated triaxial testing system used in the MIT Geotechnical Engineering Laboratory (from Santagata, 1998)

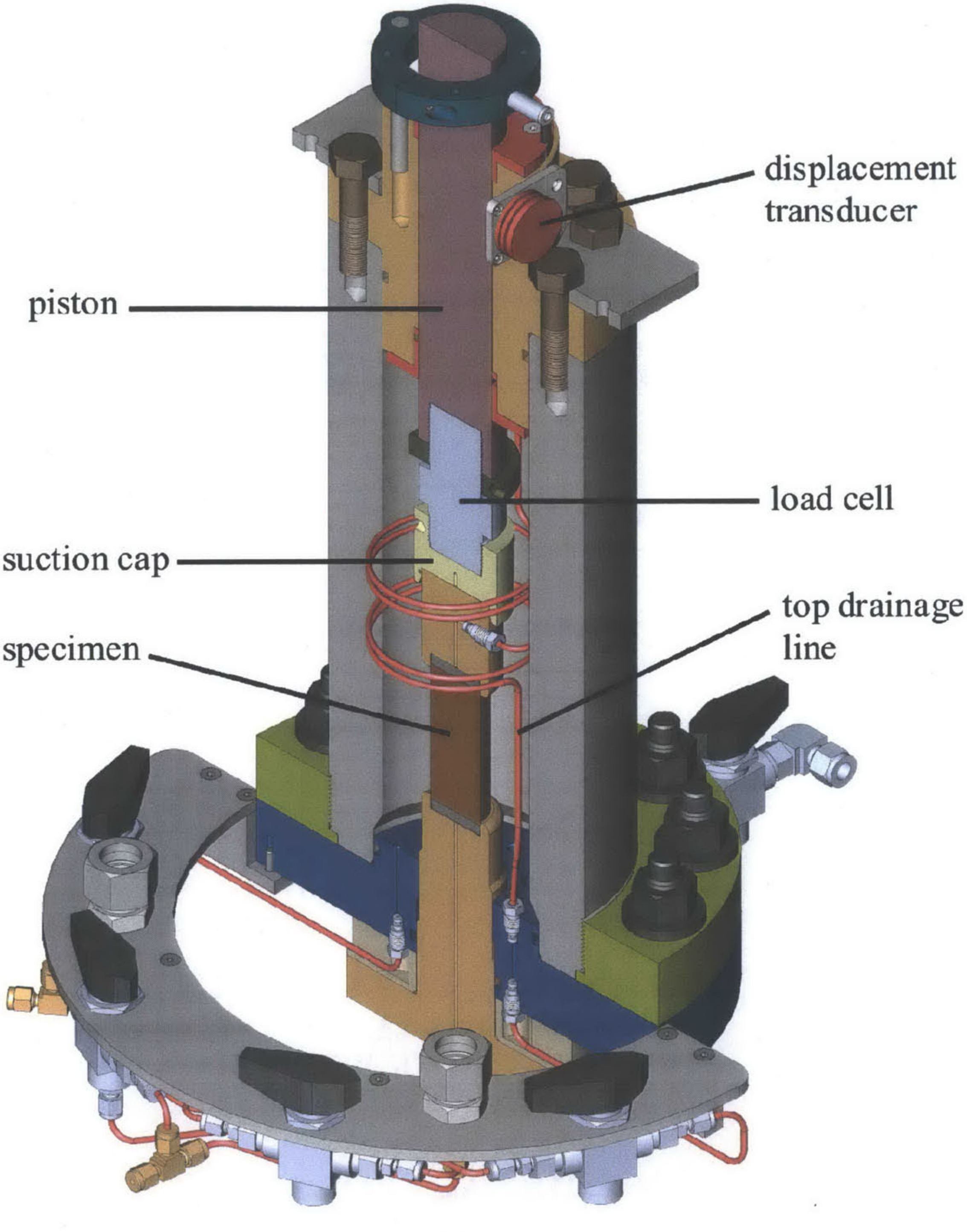

Figure 4-2: Cross-section of high pressure triaxial cell

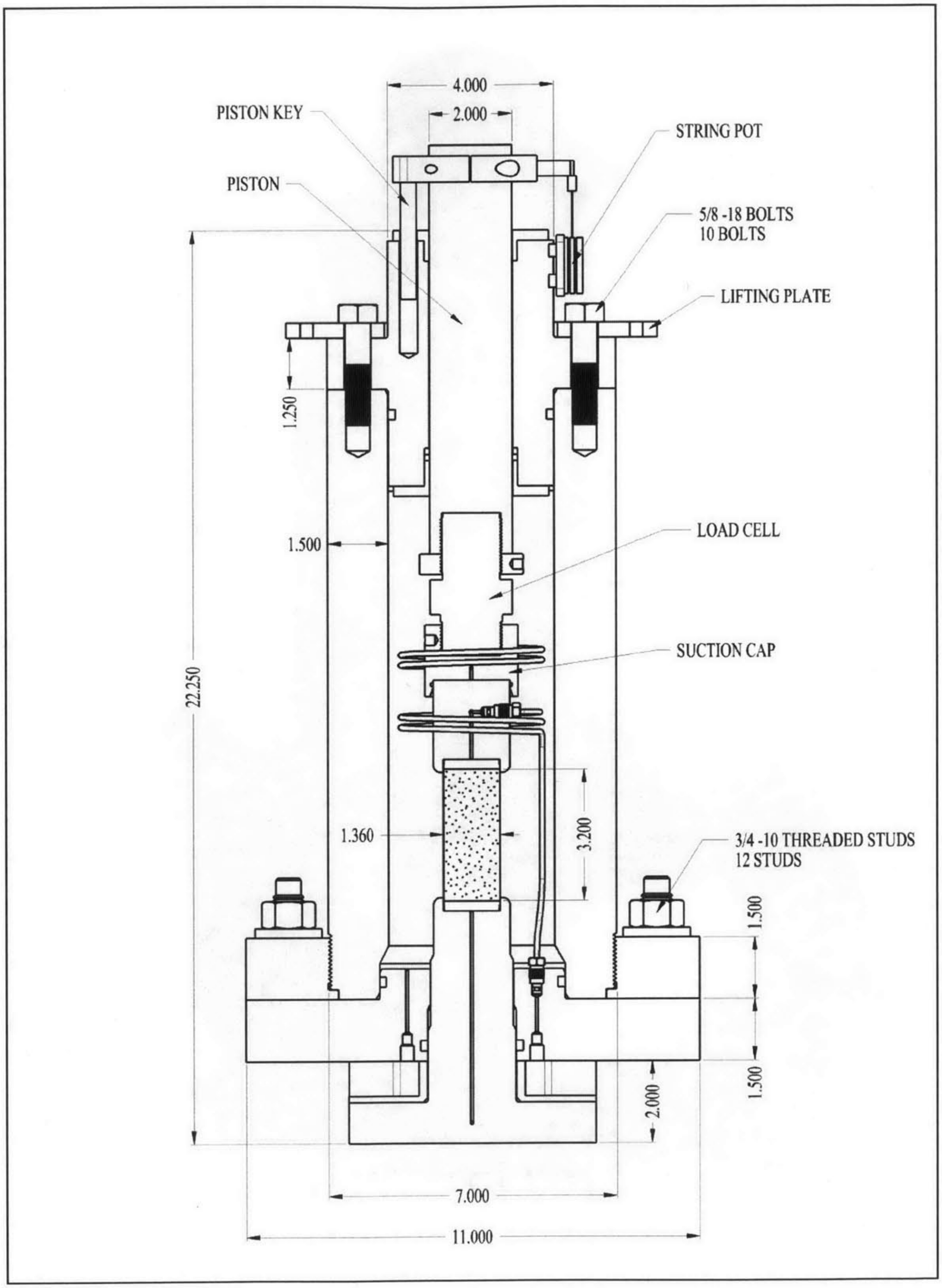

Figure 4-3: Cross-section and dimensions of high pressure triaxial cell. Note all dimensions are given in inches

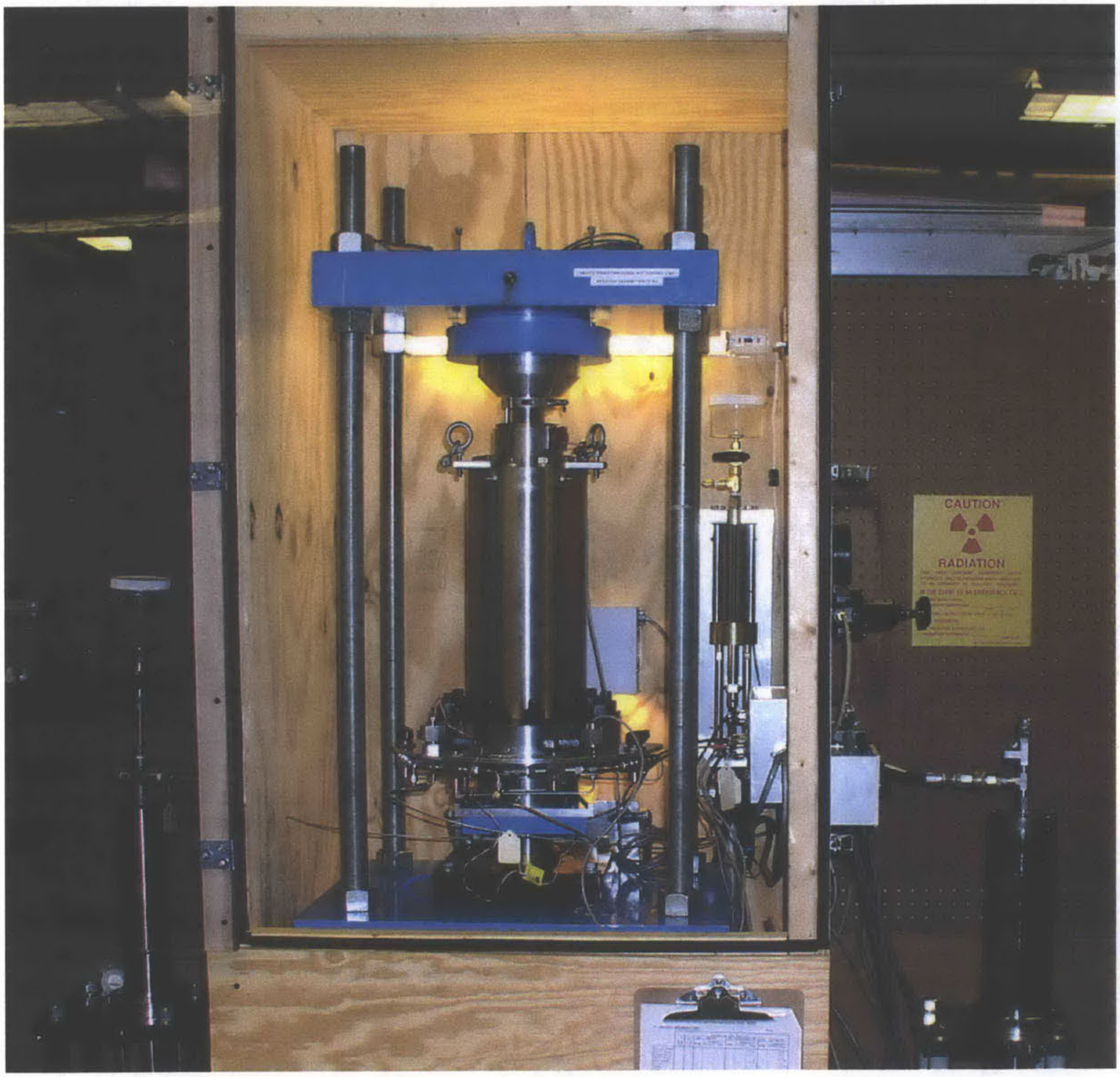

Figure 4-4: High pressure triaxial cell within a temperature controlled enclosure

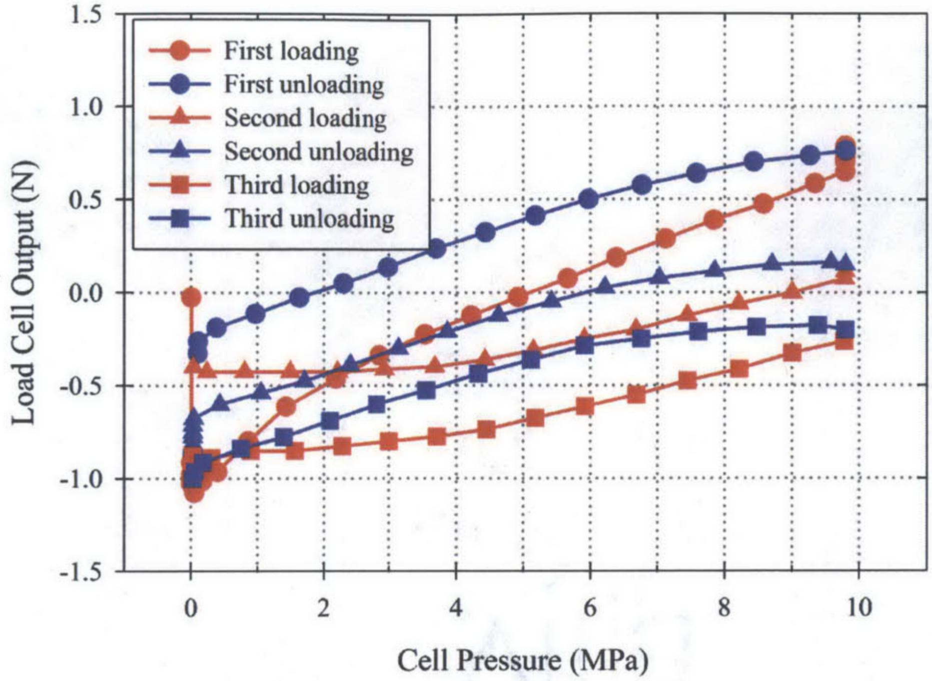

Figure 4-5: The effect of cell fluid pressure on the output of a 2.2 kN Honeywell® S-beam load cell

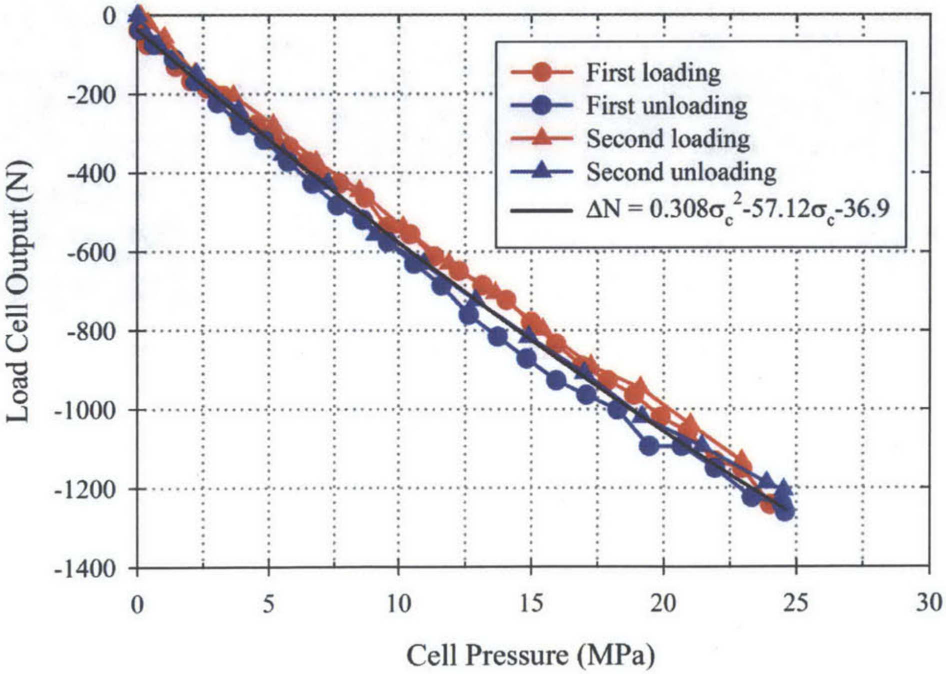

Figure 4-6: The effect of cell fluid pressure on the output of a 222 kN Futek® LCM550 threaded rod load cell

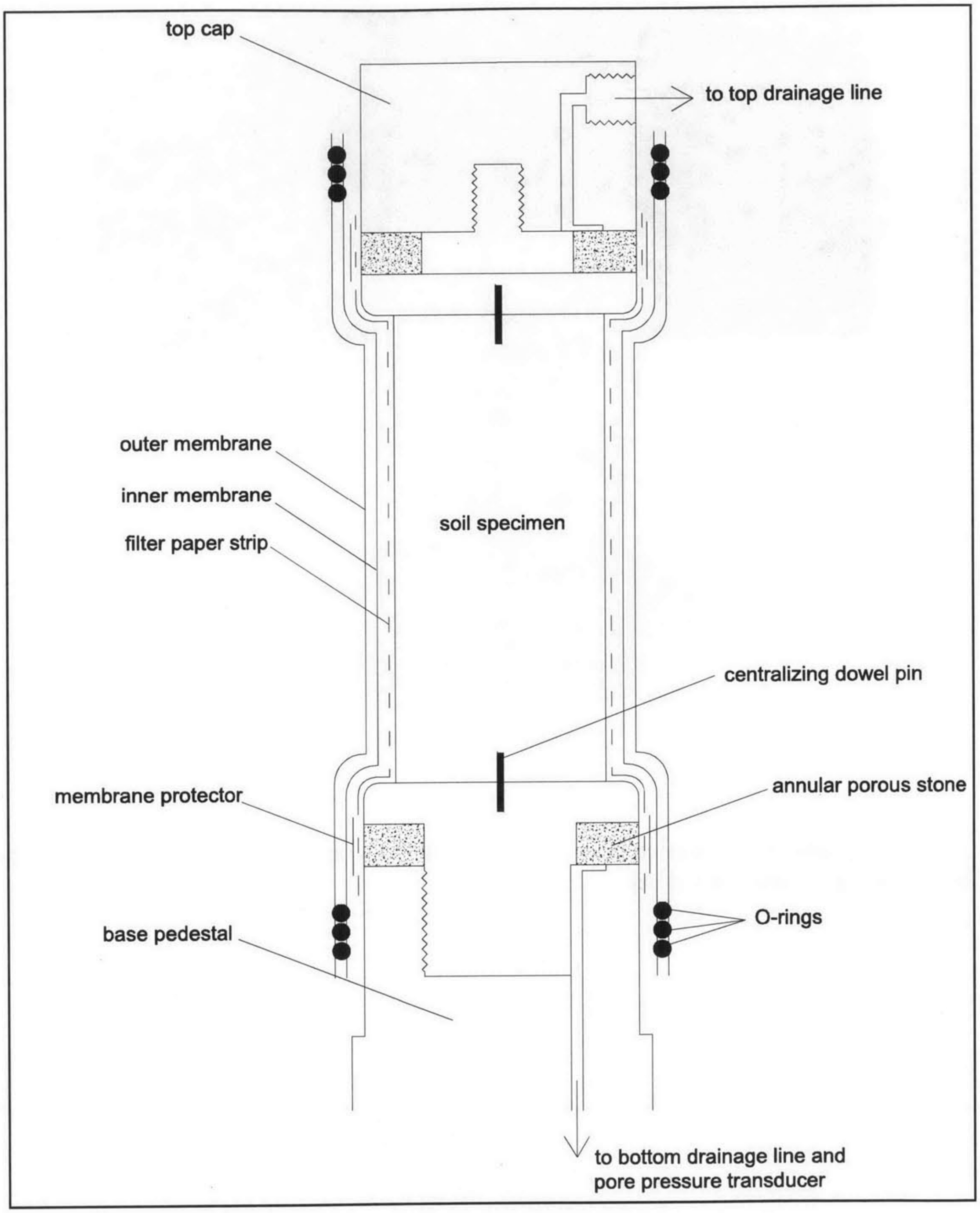

Figure 4-7: Cross-section of smooth end platen configuration

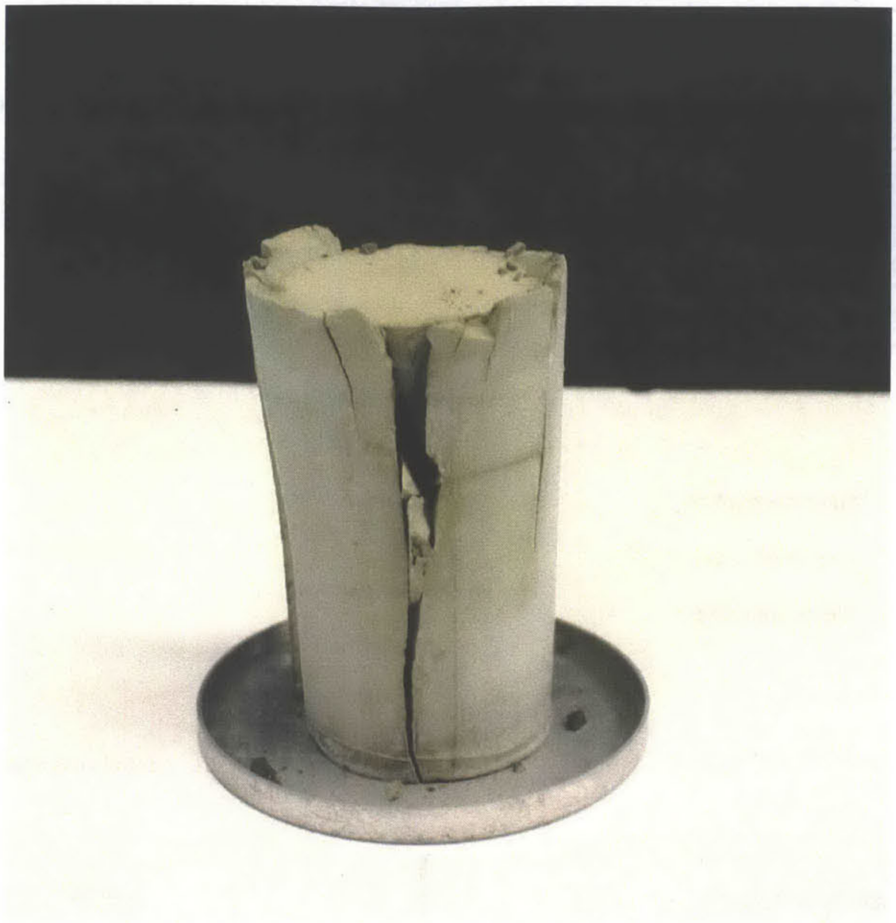

Figure 4-8: Example of a specimen which failed during K_O-consolidation in the medium pressure cell by extruding around the top cap

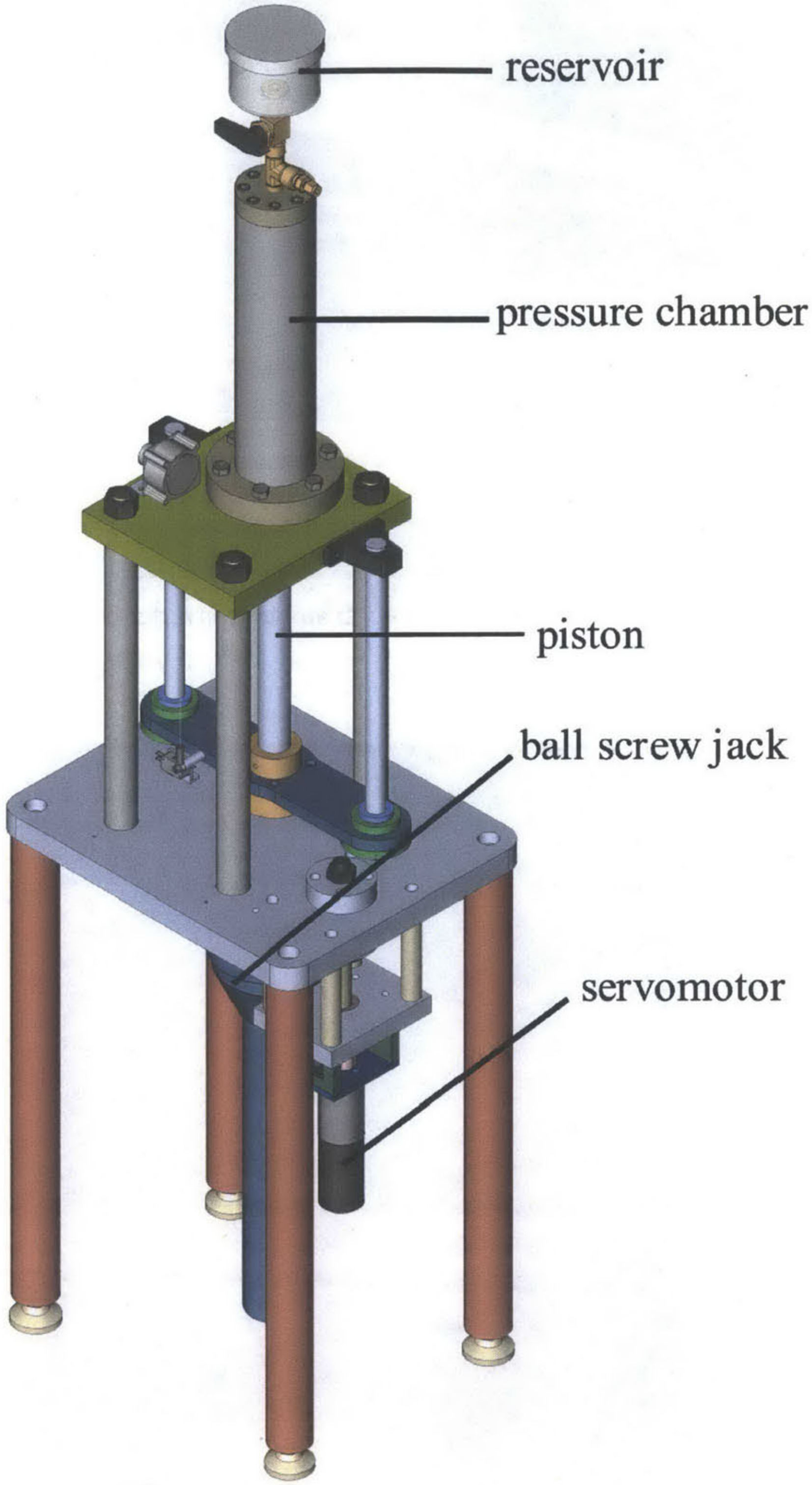

Figure 4-9: High pressure triaxial system PVA

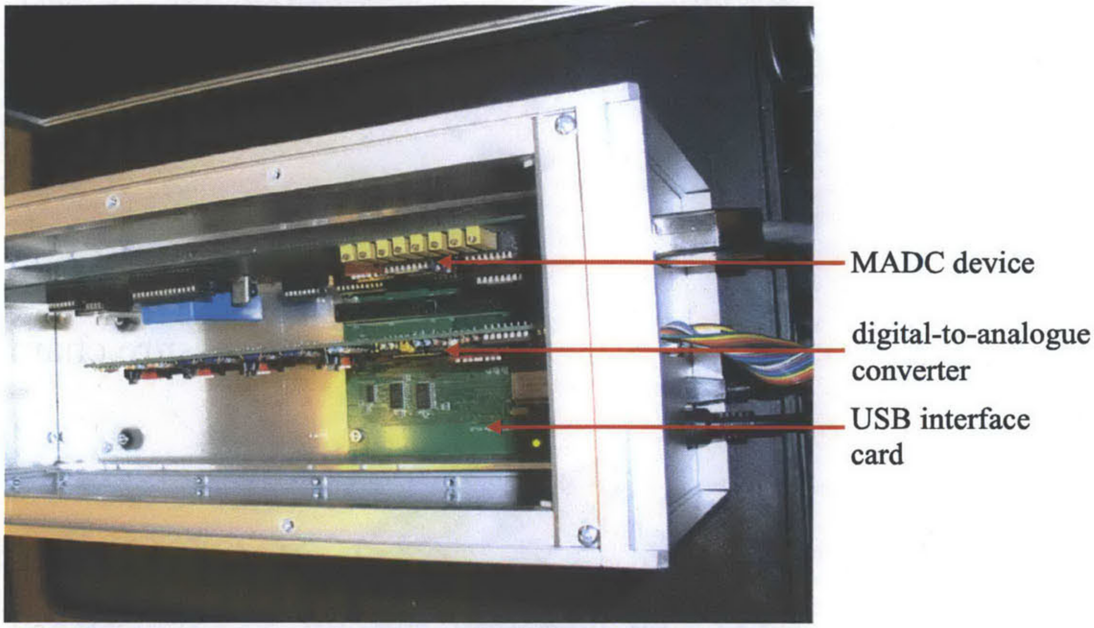

Figure 4-10: MADC device and 12 bit digital-to-analogue converter ported to a USB interface card

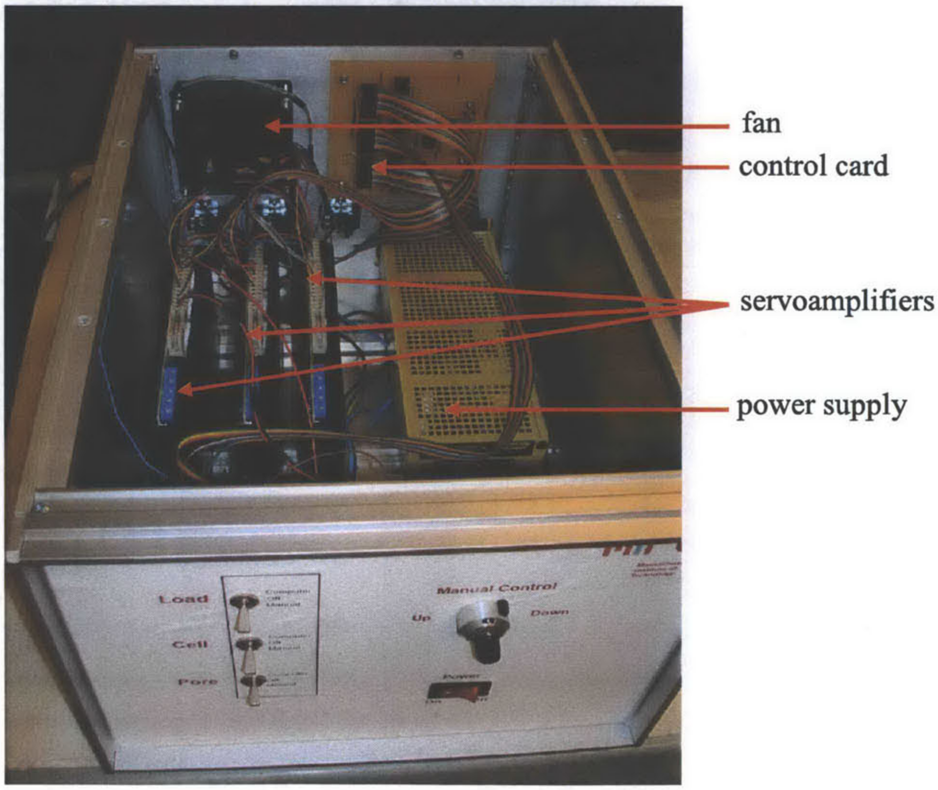

Figure 4-11: Control box containing a control card, servoamplifiers, a 50 V dc power supply and a fan

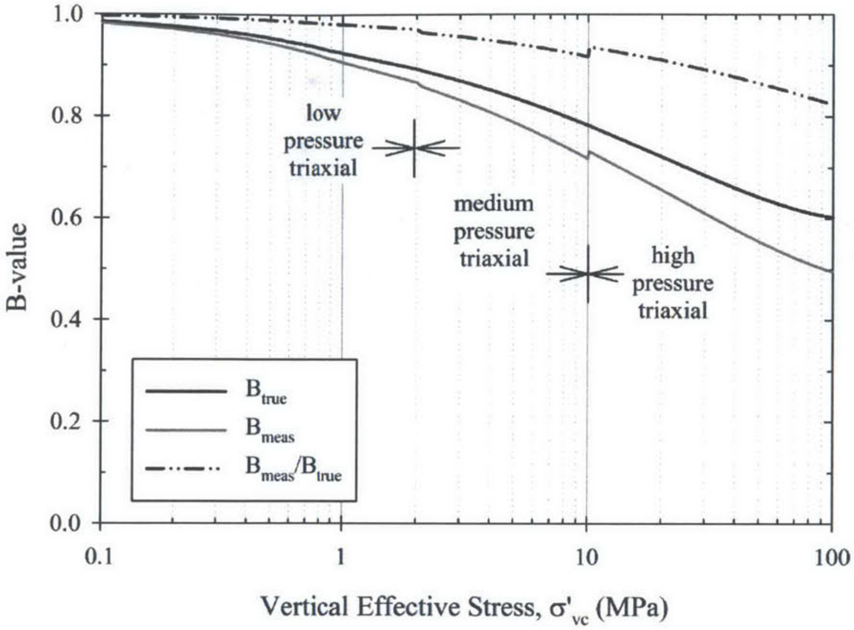

Figure 4-12: True and measurable B-values for triaxial systems. B-values are calculated assuming NC RBBC

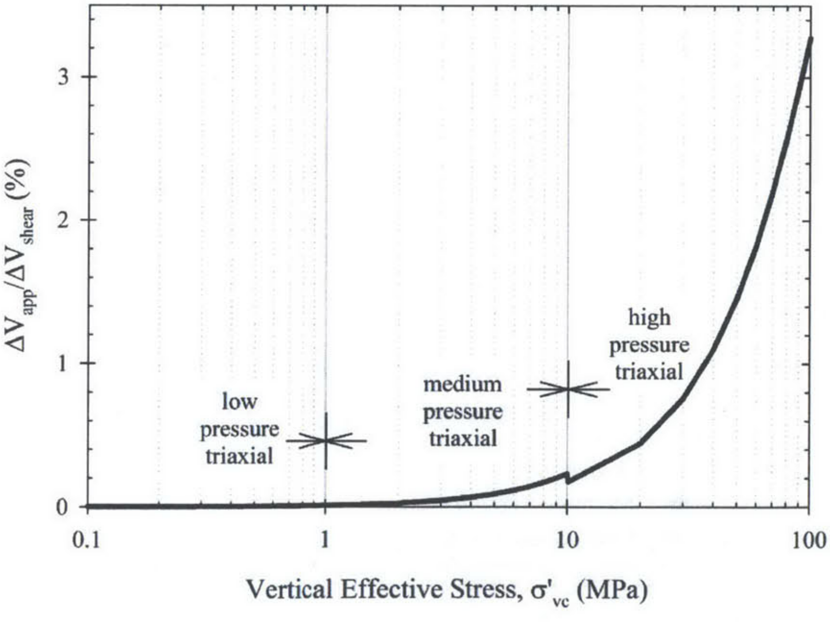

Figure 4-13: The ratio $\Delta V_{app}/\Delta V_{shear}$ versus stress level, where ΔV_{app} is the volume of pore fluid which flows from the specimen into the drainage lines at the point of undrained failure (due to compression of water in the drainage lines), and ΔV_{shear} is the volume of fluid which must drain from the specimen to develop its drained strength. The figure is drawn assuming NC RBBC

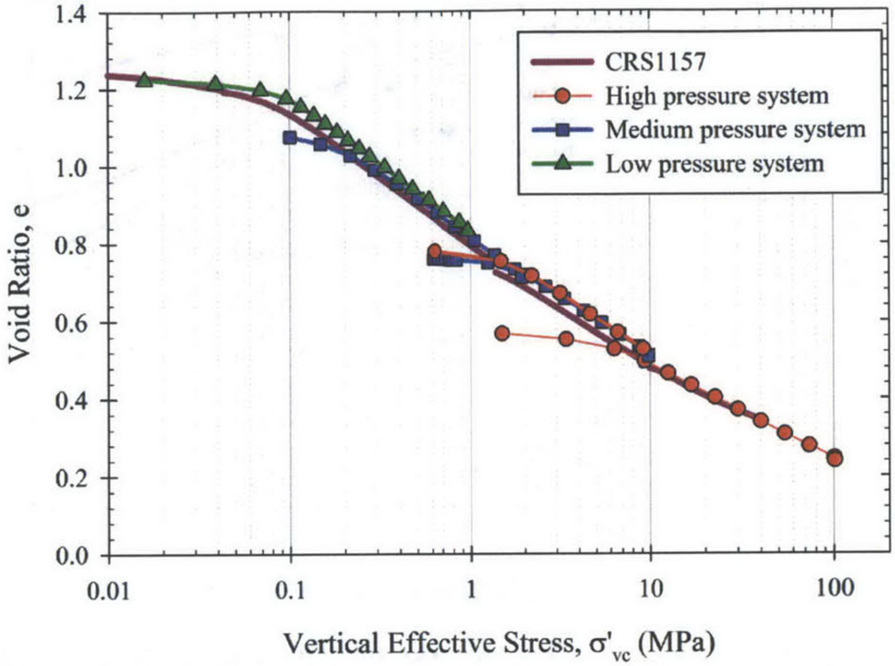

Figure 4-14: Compression behavior of RBBC as measured using the low, medium and high pressure triaxial systems and a CRS device

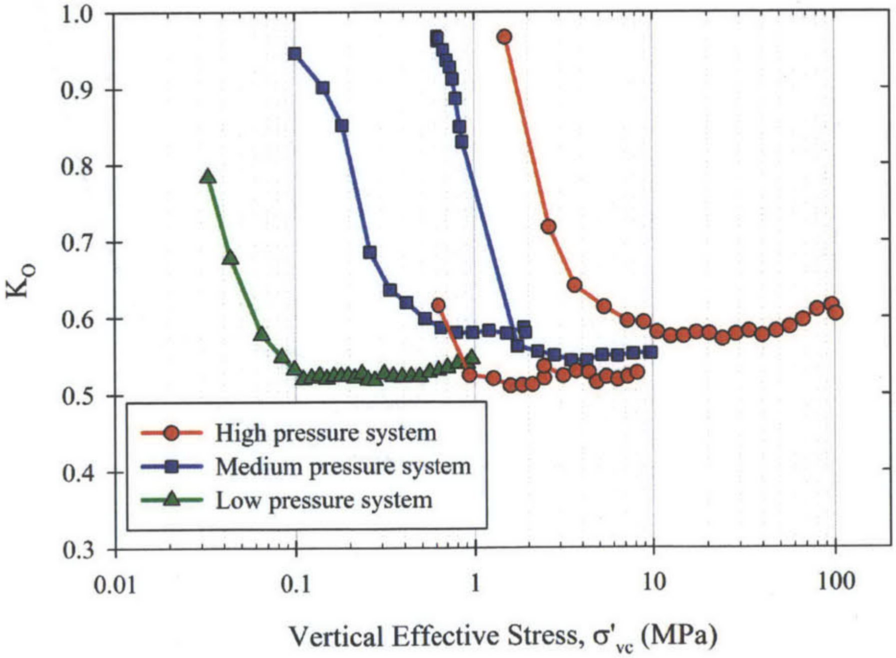

Figure 4-15: Change in K_O of RBBC during the consolidation phase of triaxial tests using the low, medium and high pressure triaxial systems

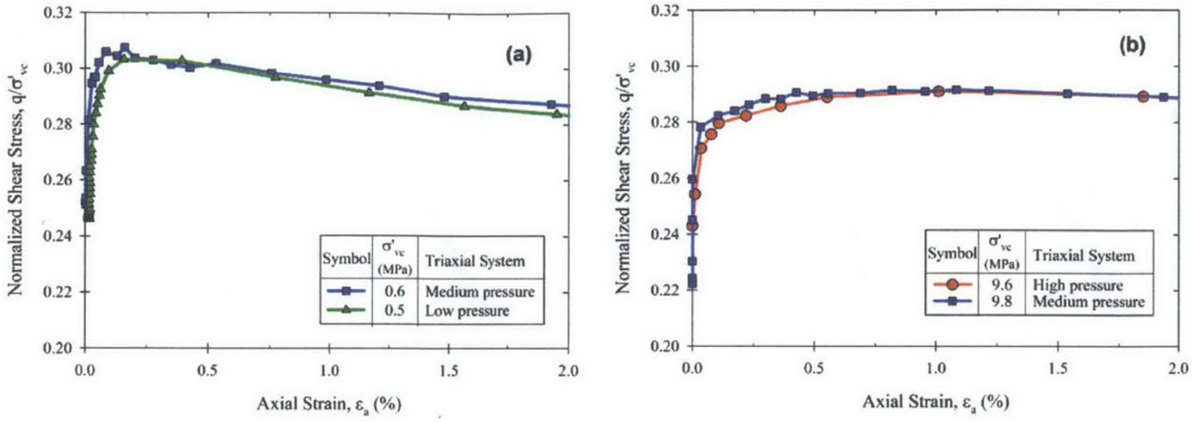

Figure 4-16 (a) and (b): Comparison of shear stress-strain responses measured during undrained shearing of NC RBBC with the low and medium pressure triaxial systems (a), and with the medium and high pressure systems (b)

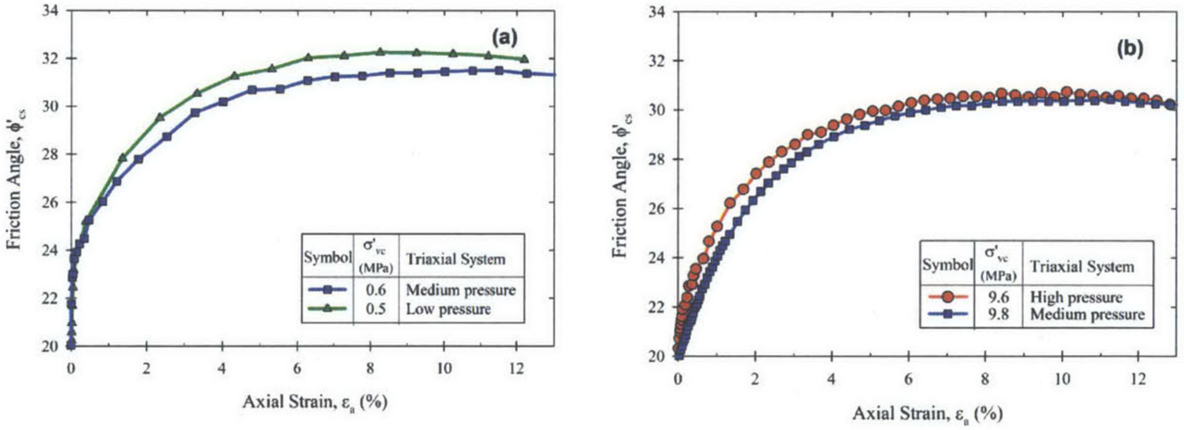

Figure 4-17 (a) and (b): Comparison of friction angles of NC RBBC measured using the low and medium pressure triaxial systems (a), and using the medium and high pressure systems (b)

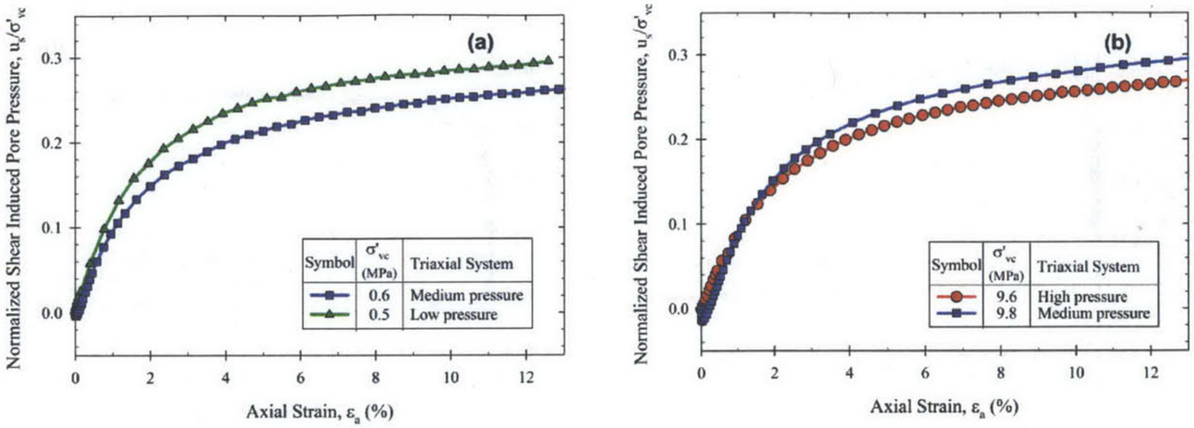

Figure 4-18 (a) and (b): Comparison of shear induced pore pressures of NC RBBC measured using the low and medium pressure triaxial systems (a), and using the medium and high pressure systems (b)

5 CONSOLIDATION RESULTS

5.1 INTRODUCTION

This chapter presents and discusses the consolidation properties of soils investigated during the research. These properties are determined from results of resedimentation, CRS tests, as well as the K_O-consolidation phase of triaxial tests. Section 5.2 presents the one dimensional virgin compression behavior of the soils and describes how this behavior changes as a function of soil type and stress level. Section 5.3 discusses the permeability behavior of the soils and shows how the permeability-porosity relationships of wide range of different soils can be successfully correlated to liquid limit. Comparisons made between the measured permeabilities of intact samples of Boston Blue Clay and Gulf of Mexico Ursa Clay against those predicted using the liquid limit correlations are used to demonstrate the value of the correlations for predicting in situ permeability. Section 5.3 also presents data on the coefficient of consolidation during virgin compression (c_{VNC}) and discusses how this parameter changes over a very wide range of effective stresses. Finally, Section 5.4 presents data on the K_O of soils as determined from triaxial tests and discusses the dependence of K_O on soil type, stress level and OCR.

Table 5-1 provides a summary of consolidation results for all triaxial tests performed during the course of the research, including triaxial system used, soil tested, resedimented sample number, initial specimen phase relations, maximum effective stress conditions during consolidation, and pre-shear effective stresses.

5.2 COMPRESSION BEHAVIOR

5.2.1 Experimental Results

Figure 5-1 shows the compression data measured during the K_O-consolidation phase of all triaxial tests performed by the author during the course of the research. The figure plots both void ratio (linear scale) and porosity (non-linear scale) as a function of vertical effective stress (logarithmic scale). To compare the compression behavior of the soils more easily, Figure 5-2 shows the K_O compression behavior of soils as measured during selected CRS and triaxial tests. Data from the recompression and swelling phases of tests are omitted from Figure 5-2 for clarity. Figure 5-3 plots the virgin compression behavior for all of the soils investigated as part of the research. The Skibbereen Silt is not included in Figure 5-3, however, as this soil is found to display very different compression behaviors depending on whether it is prepared using resedimentation or using undercompaction at different dry densities. It can be observed from Figure 5-2 and Figure 5-3 that higher plasticity, smectite rich soils (such as RGoM EI and RLC) possess much larger void ratios at low stresses compared to more silty, low plasticity soils (such as RPC). As the soils undergo consolidation to higher stresses, however, higher plasticity soils display a much greater compressibility and a corresponding larger loss in void ratio compared to lower plasticity soils. As a result, the void ratios of all the soils tend to converge into a much narrower range at high stresses. It can also be seen that many of the soils, particularly those of high plasticity, display a decreasing compression index (C_c) with increasing stress level, where C_c is the slope of the VCL in void ratio-[log] effective stress space.

The behaviors described above are illustrated more clearly in Figure 5-4 and Figure 5-5. Figure 5-4 plots the C_c of the soils shown in Figure 5-3 versus liquid limit, where C_c is defined over a stress range of 0.1 – 1 MPa, 1 – 10 MPa and 10 – 100 MPa, although not all soils have been tested fully over each stress range. It can be seen that there is a very clear trend of increasing C_c with increasing w_L in the 0.1 – 1 MPa stress range. For comparison, Figure 5-4 also includes the correlation between C_c and w_L proposed by Burland (1990), who studied the compression behavior of a large number of resedimented clays over a similar low stress range. It can be seen that the form of the correlation is the same for both this study and Burland (1990), although Burland's correlation predicts lower compressibilities for high plasticity clays. At higher stresses the C_c of the high plasticity clays decreases considerably, indicating a significant curvature to the VCL of these materials. There is much less of a decrease in the C_c of the low plasticity clays, with the C_c of RPC even displaying very slight increase with increasing stress level. The overall result of this behavior is that, at the highest stress range of 10 – 100 MPa, the compression indices of the soils tested fall to a constant value of 0.21 (standard deviation of 0.018), with no dependence on w_L being present.

Figure 5-5 plots the void ratios of the soils measured at σ'_{vc} = 0.1, 1, 10 and 40 MPa against liquid limit. It can be seen that, at a stress of 0.1 MPa, high plasticity soils possess dramatically larger void ratios than low plasticity soils. However, this tendency reduces with increasing stress level, and at 10 MPa the void ratios of all the soils in the dataset fall within a narrow range with no clear dependence on w_L. A similar result is observed at 40 MPa, albeit with all soils possessing lower void ratios (mean of 0.29 and standard deviation of 0.05). Given that liquid limit is a very strong indicator of clay composition, the results presented in Figure 5-4 and Figure 5-5 indicate that, at high stresses, all clay soils display a very similar compression behavior in terms of compressibility and void ratio, regardless of their composition. However, at low stresses the compression behavior of these materials is strongly controlled by their composition.

5.2.2 Comparison of Compression Models

In the previous section the virgin compression behavior of the soils was examined in terms of compression index, which describes a log-linear relationship between void ratio and vertical effective stress. Compression index is the most common way in which the virgin compression behavior of fine-grained soils is analyzed in the field of geotechnical engineering. However, other models of compression behavior exist to describe the volume reduction of sediments due to mechanical loading. Several of the most common models have been applied to the experimental data presented in Section 5.2.1, and these models are compared to evaluate how closely they describe the measured data. This was done by comparing the goodness of fit (i.e. the r^2 value) for the various function forms of compression model applied to the experimental data. The compression models evaluated include:

1. The assumption of a log-linear relationship between void ratio and σ'_v, where compression index is the slope of the VCL. This is the typical assumption made in geotechnical engineering practice, and the compression indices of the various soils were described in detail in Section 5.2.1.
2. The assumption of a log-log relationship between (1 + void ratio) and σ'_v. This model was proposed by Butterfield (1979), but is rarely used in engineering practice.

3. The assumption of a log-linear relationship between porosity and σ'_v. This model has not previously been proposed (as the author is aware) to describe the compression behavior of sediments, but is included here because it works well for many soils when their behavior is viewed over a very wide stress range.
4. The assumption of an exponential relationship between porosity and σ'_v. This compression model is very common in the field of petroleum geology. It was proposed by Rubey and Hubbert (1959) and was supported more recently by Hart et al. (1995) based on data from field measurements.

For all soils, the assumption of an exponential relationship between porosity and σ'_v as proposed by Rubey and Hubbert (1959) was found to give an extremely poor fit to the experimental data. The results of the comparison between the remaining three models of compression behavior are summarized in Table 5-2, where the most and least appropriate models to capture each soil's virgin compression behavior is provided. In general it is found that the assumption of a log-linear relationship between void ratio and σ'_v works best for low plasticity soils with $w_L < 50$ %. For higher plasticity soils, their behavior is generally best described by assuming a log-linear relationship between porosity and σ'_v. As discussed in Section 5.2.1, the compression indices of high plasticity soils decrease considerably when viewed over a wide range of stresses, with the result that their behavior is poorly described by a constant value of compression index. The assumption of a log-log relationship between (1 + void ratio) and σ'_v proposed by Butterfield (1979) does not work best for any particular soil type and only provides the most accurate description of compression behavior for three of the soils in the dataset. However, the Butterfield method is never the least appropriate fit for any of the soils investigated, and provides a reasonably good description of behavior for all of the soils. This model may therefore be the most appropriate to adopt in situations in which the approximate plasticity of the sediment is unknown.

5.3 PERMEABILITY BEHAVIOR

5.3.1 Introduction

At a given porosity, major factors recognized to influence permeability are pore size distribution (or equivalently particle size distribution), particle shape and orientation, and the presence of double layers around clay particles. For laminar flow through tubes of equal diameter, Poiseuille's Law states that permeability is proportional to the square of the diameter. Since the pore size distribution of a sediment intuitively is linked to its particle size distribution, it could therefore be expected that permeability would decrease rapidly as mean particle size reduces. This has been well demonstrated by Yang and Aplin (2010) and is the basis for many theoretical and empirical formulas for permeability, e.g. Hazen's formula (Hazen 1892, in Carrier 2003).

Clay mineralogy has a major effect on permeability through its influence on particle shape, or aspect ratio. Clay particles typically have a very platy shape. Particles of smectite are approximately 1-10 nm thick and have diameter-to-thickness ratios greater than 100. Illite particles are approximately 10-200 nm thick with diameter-to-thickness ratios of about 10, while for kaolinite these values increase to about 30-1000 nm and 3-10 respectively (Lambe and Whitman 1969). Quartz particles, feldspar particles and lithic fragments are typically much larger and more equi-dimensional. As effective stress increases and porosity reduces, platy clay particles become increasingly aligned perpendicular to the direction of major loading (Day-Stirrat et al. 2012), resulting in a more tortuous flow path in this direction and the development of a significant permeability anisotropy (Quigley and Thompson 1966, Daigle and Dugan 2011, Adams et al. 2013). For example, Figure 5-6 adapted from Adams (2014) shows the reduction in the mean particle orientation of RBBC with increasing vertical effective stress.

It has long been recognized in the field of soil mechanics that clay particles in water will typically be surrounded by a layer of water which is electrostatically bound to the surface of the particles, referred to as a 'diffuse double layer' or simply 'double layer'. The relative thickness and influence of this double layer depends on the clay mineralogy, increasing dramatically from chlorite to kaolinite to illite to smectite (Van Olphen 1963). Although the quantitative effect of double layers on permeability is not well understood, they are known to reduce the 'effective porosity' available for flow, thereby leading to a decrease in permeability (Mesri and Olson 1971). Double layers can also influence permeability by having a strong control over the initial sediment fabric which develops during deposition, such as the creation of clay floccules when deposition occurs in a saline environment (Lambe and Whitman 1969, O'Brien 1971). Increasing salt concentration in the pore fluid can influence permeability by reducing the thickness of double layers. For most natural clays, however, variations in NaCl concentration within the range typically encountered in a marine environment have a relatively small effect on permeability at a given porosity (Horan 2012, Cavello et al. 2005). Although practically less relevant, the valence of cations present in the pore fluid, rather than their concentration, is found to have a more significant influence on permeability by affecting double layer formation (Mesri and Olson 1971).

Figure 5-7 illustrates the effect of clay mineralogy on permeability. At similar porosities, the permeability of smectite is about 200 times lower than that of illite and about 100,000 times lower than that of kaolinite. The differences in the permeabilities of the three minerals at the same porosity may be explained by a combination of the factors described above, i.e. differences in pore size distribution, particle shape and orientation, as well as the relative influence of double layers.

Work similar to the author's was performed by Yang and Aplin (2010) who correlated the permeability of 303 samples of fine-grained sediments from 5 different sources to the clay fraction of the samples, where clay fraction is defined as the portion of particles by mass with an equivalent diameter < 2 μm. Permeability measurements were taken on about a quarter of the samples and included constant head, constant flow and transient pulse decay tests, or derivation from consolidation tests. The remainder of the permeability values included in the study were not directly measured but estimated from pore size distribution data using a procedure proposed by Yang and Aplin (1998). Yang and Aplin (2010) did not consider the effects of clay mineralogy. Furthermore, clay fraction can only be relied upon to provide a relative indicator of the particle size distribution of a sediment, (i.e. a high clay fraction probably indicates a relatively small mean particle size and vice versa) and does not capture important differences in the shape of particle size distribution curves between different sediments, especially for particle sizes < 2 μm. For example, the < 2 μm fractions of the illite and smectite tested by Mesri and Olson (1971) and given in Figure 5-7 are 100 % and 97 % respectively, though the actual particle size distributions of these two minerals are very different and their permeabilities differ by 5 orders of magnitude.

The permeability measurements presented below, except for those of the Skibbereen Silt, were determined by either one of two well established methods. The first involved the application of Terzaghi's one-dimensional consolidation theory (Terzaghi 1943) to load increments during resedimentation. In this approach permeability is determined at discrete intervals corresponding to each individual load increment. Permeability may be measured at very high porosities over 0.75. The second and primary method of measuring permeability was through the use of CRS consolidation tests performed on resedimented samples. The CRS test data were analyzed using standard linear theory (Wissa et al. 1971, ASTM D4186). Unlike incremental loading, CRS testing allows one to measure permeability on a continuous basis with very small intervals between measurements. Permeability measurements were made using several different CRS cells capable of testing specimens from 3.4 to 6.4 cm in diameter. A Trautwein CRS cell which tests 3.4 cm diameter specimens was employed in the M.I.T. Geotechnical Engineering Laboratory for CRS testing at axial effective stresses up to 40 MPa. Due to its relatively higher permeability, the permeability of the Skibbereen Silt was measured with several flow-through experiments over a relatively small range of porosities by Grennan (2010). For each experimental method used, permeability is measured on homogenous specimens in the direction of major principal loading, i.e. it is a bedding perpendicular permeability.

5.3.2 Permeability Results and Correlations with Liquid Limit

Figure 5-8 plots the bedding perpendicular permeability-porosity relationships for soils tested by the author. The figure also includes the Skibbereen Silt tested by Grennan (2010). It can be seen that, at a porosity of 0.4, the permeability of the R. London Clay is almost 5 orders of magnitude lower than that of the Skibbereen Silt. For each material tested, the permeability-porosity relationship is essentially log-linear over the porosity range 0.20 – 0.75. Yang and Aplin (2010) reported that at lower porosities the relationship may deviate slightly from log-linear as the permeability-porosity curves begin to flatten out.

For many of the soils tested, permeability data from both CRS tests and incremental loading are available. Good agreement is generally observed between the results obtained using the two methods. For a small number of cases, however, noticeably lower permeabilities were measured during incremental loading compared to CRS testing at the same porosity, e.g. the RLC at a porosity of 0.6 in Figure 5-8. This could possibly be attributed to Terzaghi's one-dimensional consolidation theory underestimating the true permeability of the soil (Taylor 1942, in Mesri and Olson 1971) or an error in the calculated porosity of the sample during incremental loading (in such cases the more relevant low porosity CRS data is adopted for use in the correlations presented below).

To model the behavior shown in Figure 5-8, regression lines are fitted through the experimental data. These regression lines are shown in Figure 5-9, together with regression lines for other soils that are included in the study but where the tests were not carried out by the author (the contributing researchers, together with appropriate references, are given in Table 3-1). The change in permeability (k) as a function of porosity (n) for each soil is described by an equation of the form:

$$\log_{10}(k) = \gamma(n - 0.5) + \log_{10}(k_{0.5}) \qquad 5 - 1$$

where γ is the slope of the regression line and $k_{0.5}$ is the permeability at $n = 0.5$.

The permeability-porosity relationship of a soil, as defined by γ and $k_{0.5}$, is strongly correlated to its liquid limit. Figure 5-10 shows the correlation between $\log_{10}(k_{0.5})$ and w_L. It can be seen from Figure 5-10 that, as expected, high plasticity soils display a dramatically lower permeability than more silty, low plasticity soils at the same porosity (in this case a porosity of 0.5). The permeability of a soil at a porosity of 0.5 is approximated by:

$$\log_{10}(k_{0.5}) = -7.55\log_{10}(w_{L[\%]}) - 3.4 \qquad 5 - 2$$

An r^2 value of 0.90 demonstrates the high quality of the correlation.

Figure 5-11 shows that the slope of the [log]permeability-porosity relationship (i.e. γ) increases linearly with w_L, indicating that high plasticity soils display a more rapid reduction in permeability with decreasing porosity (this fact can also be seen from the data shown in Figure 5-9). The value of γ is approximated by:

$$\gamma = 0.067w_{L[\%]} + 5.1 \qquad 5-3$$

The Resedimented Nankai Clay (RNC) and Cornwall Kaolin (CK) are the most significant outliers in Figure 5-11. The high value of γ for the RNC implies an unusually rapid reduction in permeability with decreasing porosity for this material, while the low value of γ for the CK implies the opposite. The presence of these outliers results in an r^2 value of 0.75 for the correlation (an r^2 of 0.86 is achieved if these data points are removed from the regression).

5.3.3 Discussion of Permeability Correlations

An explanation for the correlations between liquid limit and the parameters $k_{0.5}$ and γ is as follows. Increasing liquid limit is associated with a larger quantity of clay minerals present in a soil, particularly minerals such as smectite and to a lesser extent illite. Increasing liquid limit is therefore linked to a decrease in mean pore size, to an increase in the influence of double layers around clay particles, and to a greater likelihood for platy shaped clay particles to be oriented perpendicular to the direction of major loading. These factors combined mean that, at a given porosity, bedding perpendicular permeability decreases with increasing liquid limit (Figure 5-10). Furthermore, as effective stress increases and porosity decreases, these factors will become more pronounced. That is, the progressive re-orientation of platy clay particles perpendicular to the direction of major loading, together with a relative increase in the influence of double layers on effective porosity loss, will result in a more rapid reduction in bedding perpendicular permeability for high liquid limit soils as porosity decreases. This is illustrated in Figure 5-11 as an increasing value of γ with increasing liquid limit.

To illustrate the accuracy of the correlations presented, the measured permeabilities of the soils are compared against their permeabilities as predicted using Equations 5-1, 5-2 and 5-3. This comparison is shown in Figure 5-12, where it can be seen that the predicted permeabilities all fall within ±5 times the measured values and most fall within ±3 times the measured values.

For comparison, Figure 5-13 and Figure 5-14 plot the relationships between $\log_{10}(k_{0.5})$ and clay fraction and between γ and clay fraction respectively, where clay fraction is the percentage of particles < 2 μm. The correlations with clay fraction are clearly of much lower quality than those with liquid limit (r^2 values of 0.73 and 0.21 are achieved for clay fraction correlated to $\log_{10}(k_{0.5})$ and γ respectively). There are two reasons for this. Firstly, the very significant effect of mineralogy on permeability (e.g. Figure 5-7) is not taken into account when clay fraction is used as the correlating material property. Secondly, the use of the 2 μm size boundary as a definition of clay fraction is somewhat arbitrary, as many clay mineral particles are larger than 2 μm and many particles smaller than 2 μm are not clay minerals. Combined with some testing uncertainty, this helps explain why the relative proportions of clay minerals reported in Table 3-2 for a bulk sample and the < 2 μm fraction (of the same soil) are often inconsistent. Some chlorite, kaolinite and even illite particles will undoubtedly be larger than 2 μm and therefore not included the < 2 μm fraction, while illite-smectite is often very much finer and will therefore be concentrated in the < 2 μm fraction. The same reasoning helps explain why the total fraction of clay minerals determined through XRPD (last column of Table 3-2) can be significantly different from the < 2 μm fraction determined by sedimentation (Table 3-1). This provides cautionary evidence against the use of the 2 μm size boundary as a measure of the quantity of clay in a soil.

The correlations developed here are empirical rather than fundamental, and as such they are not claimed to be of value for material types which differ significantly from those included in the study. The correlations are not recommended for soils with $w_L < 25\%$ or $w_L > 100\ \%$. Soils with $w_L < 25\ \%$ are typically very silty and are likely to possess permeabilities much higher than those considered here. Soils with $w_L > 100\ \%$ may contain appreciable amounts of pure smectite, and for such materials the salt concentration of the pore fluid could play a significant role in affecting permeability. Furthermore, the stresses imposed on the resedimented samples during resedimentation and CRS testing can be considered representative of mechanical compression and do not include any effects of diagenesis. The correlations therefore may not be appropriate for soils possessing porosities significantly below 0.20 as a result of diagenesis/lithification.

Although the correlations presented here do not involve soils with $w_L > 100\ \%$, the permeability behavior of such materials has been investigated by Pandian et al. (1995) and provides a good comparison with the author's data. Pandian et al. (1995) examined the consolidation properties of bentonite mixed in various proportions with sand and two high plasticity clays ($w_L = 62\ \%$ and $84\ \%$). The mixtures were prepared at close to their liquid limit and placed in a modified oedometer in which the permeability was directly measured at the end of each load increment by means of a falling head type permeability test. The values of $k_{0.5}$ and γ interpreted from the results of Pandian et al. are plotted against liquid limit in Figure 5-15 and Figure 5-16 respectively, together with the values of $k_{0.5}$ and γ from the author's study. It can be seen that the form of the relationships between $k_{0.5}$ and w_L and between γ and w_L from the study of Pandian et al. compare quite well with those of the author discussed above, i.e. a logarithmic decrease in the value of $\log_{10}(k_{0.5})$ with increasing w_L (Figure 5-15) and an approximately linear increase in the value of γ with increasing w_L (Figure 5-16). For comparison, the correlations given in Equations 5-2 and 5-3 based on the author's data are also plotted in Figure 5-15 and Figure 5-16 respectively. It can be seen from Figure 5-15 that the $\log_{10}(k_{0.5})$ values from the work of Pandian et al. compare very well with the author's results at similar w_L, and that the regression line extrapolated from the author's data falls reasonable close to the data of Pandian et al. at $w_L >> 100$ %. The values of γ from Pandian et al., shown in Figure 5-16, display slightly less favorable agreement with the author's data, falling somewhat below that the author's values at similar w_L. In addition, the regression line extrapolated from the author's data tends to overpredict the γ values from Pandian et al. at $w_L >> 100$ %. A possible reason for this observation is that Pandian et al. only measured the permeability of each sample over a relatively narrow range of porosities, typically less than about 20 %. Since γ is defined as the slope of the [log]permeability-porosity relationship, the γ values interpreted from the tests of Pandian et al. are somewhat less reliable and subject to more scatter compared to the author's data, where γ values are interpreted over a much wider range of porosities. Overall, however, the data of Pandian et al. (1995) provide encouraging support for the permeability correlations proposed in this work.

5.3.4 Predicting in situ Permeability

It is useful to demonstrate the applicability of the permeability correlations, which were formulated from the results of experiments performed on resedimented soils, to the prediction of in situ permeability. Neuzil (1994) has shown that while transmissive fractures or other heterogeneities may control the large-scale permeability of certain geologic units, the permeability of many other units is scale independent. Permeability measurements made on good quality intact core samples can therefore often be taken to be representative of in situ permeability. Using three example datasets, we compare permeabilities measured on intact core to the permeabilities predicted using liquid limit (Equations 5-1, 5-2 and 5-3). The examples are from relatively shallow depths as data for much deeper sediments were not available. The first example utilizes data obtained during the site investigation for the foundation of Simmons residence hall on the MIT campus (Haley & Aldrich Inc. 2002, House 2012). Boreholes were sunk through the underlying deposit of Boston Blue Clay and measurements of porosity and liquid limit were taken at various depths down to 35 m in borehole B99-2. In addition, laboratory CRS tests were carried out on intact samples obtained from this borehole in order to determine the compression and permeability behavior of the deposit as a function of depth. The measured permeability-porosity relationship determined for each sample was extrapolated back to the in situ porosity to establish in situ permeability. Using values of liquid limit measured within approximately 1 m of the samples on which CRS tests were performed, the permeability of these samples is predicted using Equations 5-1, 5-2 and 5-3. Figure 5-17 compares these predicted permeabilities to the actual measured permeabilities of the samples. Most, but not all, of the predicted permeabilities fall within ± 5 times the measured values.

Measurements of liquid limit are routinely made as part of geotechnical site investigations, but are traditionally less common in well drilling operations. However, a useful example is provided by data retrieved from Integrated Ocean Drilling Program (IODP) Expedition 308 in the Ursa Basin (the RGoM Ursa Clay tested as part of the author's research is derived from the same expedition). The Ursa Basin is located in the northern deepwater Gulf of Mexico, approximately 210 km southeast of New Orleans. Reece et al. (2012) report the results of a large number of CRS tests performed on intact core collected at sites U1322 and U1324 (located approximately 9 km apart). A single liquid limit test with $w_L = 81\%$ was performed on material collected from a depth of 41.5 mbsf at site U1322. Together with in situ porosities (calculated from logging-while-drilling bulk density log), the measured liquid limit was used to predict the in situ permeabilities of intact samples taken from the first 100 m of basin sediment on which laboratory CRS tests were performed. A comparison of the predicted and measured permeabilities of these samples is given in Figure 5-17. It can be seen that all of the predicted permeabilities fall within ± 5 times the measured permeabilities.

A third example is provided by a dataset of permeability results from a proprietary location in the Ursa Basin of the Gulf of Mexico. At this location CRS tests were performed on intact core samples obtained from the seafloor down to 125 mbsf. Porosity and liquid limit measurements were also performed on these same core samples. Liquid limits ranged from 87 % to 46 %, with values generally decreasing with depth. A comparison of the measured permeabilities with those predicted using the liquid limit correlations is included in Figure 5-17, where it can be seen that all of the predicted permeabilities fall within ± 5 times the measured permeabilities.

An important factor in determining the accuracy of the liquid limit correlations for predicting in situ permeability is the amount of spatial variability (in terms of composition) that exists in a deposit. The sediment present at sites U1322 and U1324 in the Ursa Basin is relatively homogenous with depth and location (John and Adatte 2009, Sawyer et al. 2008), with the result that a single measurement of liquid limit is capable of providing a reasonable estimate of permeability for a 100 m section of sediment (provided that porosity data are also available). In comparison, in situ Boston Blue Clay displays significant compositional variability with depth (Berman 1993). The predicted permeabilities for the clay therefore show more deviation from the measured values, despite the fact that liquid limits measured within 1 m of the CRS test samples were used.

5.3.5 Coefficient of Consolidation

The changes in c_{VNC} for soils tested by the author are shown in Figure 5-18, which plots c_{VNC} on a logarithmic scale versus vertical effective stress on a logarithmic scale. The figure shows changes in c_{VNC} over almost 5 orders of magnitude of stress. In addition to data from CRS tests, Figure 5-18 also includes c_{VNC} values calculated from incremental loading that occurs during resedimentation. This allows values of c_{VNC} to be calculated at very low stresses corresponding to the early stages of resedimentation. It can be observed from

Figure 5-18 that, at stresses below about 10 kPa, the c_{VNC} values of all the soils fall within a relatively narrow range. Furthermore, there is no clear trend in c_{VNC} with soil type at these low stresses. As the soils consolidate to higher stresses, however, their c_{VNC} values diverge significantly and a clear trend with soil type emerges. Low plasticity soils display an increasing c_{VNC} with increasing stress level while high plasticity soils display a decreasing c_{VNC}. At σ'_{vc} = 10 MPa for example, the c_{VNC} of RPC (w_L = 33.1 %) has risen to approximately 100 times that of RLC (w_L = 73.8 %). This behavior explains why a load increment applied to a typical resedimented sample prepared for triaxial testing may take several days to reach end of primary consolidation in the case of RLC, though a similar sample of RPC may take less than an hour.

A noticeable feature of the results presented in Figure 5-18 is that, for some of the soils, the value of c_{VNC} calculated from CRS testing is significantly higher than the corresponding value calculated from incremental loading at the same stress level. This can be seen to be the case for RLC, RGoM Ursa, RUC and, to a lesser extent, RBBC. For example, in the 0.1 – 1 MPa stress range, the c_{VNC} values calculated for RLC from CRS testing are about twice as high as the values calculated from incremental loading. The exact reason for this discrepancy is unknown. However, given the significant impact of side wall friction on the compression behavior of samples undergoing resedimentation (discussed in Section 3.3.4.), the CRS data could be taken to provide more accurate values of c_V.

5.4 FACTORS INFLUENCING K_O

5.4.1 Effect of Stress Level and Composition on K_{ONC}

The K_O-consolidation procedure used in the research allows one to continuously measure the K_O value of a specimen throughout the consolidation phase of a triaxial test. The control algorithm applies a constant axial rate of strain and ensures zero radial strain of the specimen by continuously adjusting cell pressure to keep volumetric and axial strains equal. Figure 5-19 shows the variations in K_O during the consolidation phase of triaxial tests carried out on RBBC. Data obtained during the swelling portion of tests are omitted from Figure 5-19 for clarity. The wide range of starting points for the tests reflects the different preconsolidation stresses which specimens are subjected to during resedimentation. Specimens were typically resedimented to nominal preconsolidation stresses of 0.1, 2 or 10 MPa (though side wall friction reduces the actual preconsolidation stress imposed on specimens, as discussed in Section 3.3.4.) before being swelled to OCR = 5 prior to extrusion. The change in K_O during consolidation follows the same trend in all tests. During the initial pressure-up and back-pressure saturation phases of a test, the OC specimen is subjected to almost isotropic stress conditions. The value of K_O is therefore close to unity at the beginning of consolidation. It decreases rapidly during recompression to the

σ'_p imposed during resedimentation, before reaching a stable value during normal consolidation. While the value of K_{ONC} remains fairly constant for each test, it can be seen from Figure 5-19 that there is an overall trend for K_{ONC} to increase slightly with stress level. For RBBC, K_{ONC} increases logarithmically from approximately 0.51 at 0.1 MPa to 0.60 at 100 MPa. As discussed in Chapter 2 and shown in Figure 2-6, a very similar result was reported by Abdulhadi (2009) who tested RBBC up to 10 MPa. An anomalous K_O response was measured during TX1030, and this is clearly in error.

Figure 5-20 shows the variation in K_O during consolidation for all soils investigated during the course of the research. The figure includes representative tests for each soil. The same general behavior is observed for all soils and is the same as that described above, i.e. a rapidly decreasing K_O during recompression followed by a less rapid change during normal consolidation. However, the magnitude of K_{ONC}, and the direction and degree to which it changes during consolidation depend strongly on the type of soil in question. For example, the R. Presumpscot Clay possesses the lowest value of K_{ONC} and this value increases very slightly with increasing stress level. On the other hand, the R. London Clay possesses a much higher value of K_{ONC} which increases rapidly with increasing stress level. This behavior is illustrated more clearly in Figure 5-21, which plots the values of K_{ONC} measured at the end of normal consolidation for all tests performed during the course of the research. The figure also includes data for Skibbereen Silt, R. Ugnu Clay and R. Gulf of Mexico Eugene Island Clay from Grennan (2010), Jones (2010) and Fahy (2014) respectively. The figure does not include any K_O data for R. San Francisco Bay Mud from Kontopoulos (2012) as these data display a large amount of scatter.

To model the behavior shown in Figure 5-21, power-law regression lines are fitted through the experimental data. These regression lines are presented in Figure 5-22, where one can detect a systematic trend in behavior (a regression line for RSFBM is not included in Figure 5-22 as there is an insufficient amount of reliable data available for this soil). It can be observed that soils possessing high liquid limits tend to have a higher K_{ONC}, and that this K_{ONC} increases more rapidly, when compared to soils with low liquid limits. The soil with the highest liquid limit, RGoM EI, displays a very rapid increase in K_{ONC} with increasing stress level. On the other hand, the soil with the lowest liquid limit, SS, displays a rapid reduction in K_{ONC} with increasing stress. A soil with a medium liquid limit, such as RBBC, displays a moderate increase in K_{ONC}. At $\sigma'_{vc} = 10$ MPa, RGoM EI possesses the highest K_{ONC} of approximately 0.79, RBBC possesses a medium K_{ONC} of 0.56, while RPC (which has the lowest liquid limit of the soils tested at $\sigma'_{vc} =$ 10 MPa) has the lowest K_{ONC} of 0.52. For a given soil, the variation in K_{ONC} as a function of stress level can be approximated using a power-law function of the form:

$$K_{ONC} = K_{O10}(0.1\sigma'_{vc[MPa]})^{J} \qquad 5\text{ - }4$$

where K_{O10} is the value of K_{ONC} at $\sigma'_{vc} = 10$ MPa and J is an exponent which describes the change in K_{ONC} as a function of effective stress level, with higher values of J implying a more rapid increase in K_{ONC} with increasing stress level. The relationship between K_{O10} and w_L is plotted in Figure 5-23, where it can be seen that a strong linear correlation exists between the two parameters that can be approximately by:

$$K_{O10} = 0.0056w_{L[\%]} + 0.33 \qquad 5\text{ - }5$$

An r^2 value of 0.92 demonstrates the reasonably high accuracy of the correlation. Figure 5-24 plots the relationship between the parameter J and w_L, which can be approximated by a log-linear equation of the form:

$$J = 0.257\log_{10}(w_{L[\%]}) - 0.398 \qquad 5\text{ - }6$$

Once again, an r^2 value of 0.83 reflects the relatively good quality of the correlation. As is the case for the correlations with permeability (discussed in Section 5.3), Equations 5-5 and 5-6 are not claimed to be valid for soil types which differ significantly from those investigated in this work. The correlations are not recommended for soils with $w_L < 25\%$ or $w_L > 90$ %, or for soils possessing a bonded microstructure such as that caused by cementation.

Previous empirical correlations for estimating K_{ONC} have been proposed by Jâky (1944, 1948) (in Mesri and Hayat 1993), Brooker and Ireland (1965) and Bolton (1991). All of these studies involved correlating K_{ONC} to ϕ'_{cs}, where ϕ'_{cs} is assumed to be constant. However, it will be demonstrated in Chapter 6 that ϕ'_{cs} can vary considerably for a given soil as a function of effective stress level. In addition, liquid limit is a more practically useful correlating parameter as it is considerably less complicated and less expensive to measure compared to $\phi'_{cs.}$

5.4.2 Effect of OCR on K_O

The K_O-consolidation algorithm used to control the triaxial system can be less effective during the swelling portion of tests. This is due to backlash of the axial loading mechanism (particularly in the low and medium pressure systems) combined with the relatively small changes in axial strain involved in swelling compared to virgin consolidation. This issue manifests itself as erratic changes in K_O during the initial portions of swelling (below an OCR of roughly 1.5), though K_O tends to become more stable as swelling progresses and the control system achieves true one-dimensional conditions. As a result of this issue, previous researchers who have examined the behavior of OC soil in the MIT Geotechnical Engineering Laboratory (e.g. Sheahan 1991, Santagata 1998, Abdulhadi 2009, Casey 2011) have typically relied on stress path swelling rather than K_O-swelling. However, a small number of tests were performed during the course of this research which involved successful K_O-swelling followed by K_O-recompression back to a normal condition. These tests were performed on RBBC, RPC, RSFBM and RLC, and the results are shown in Figure 5-25. At a given OCR, the RLC has a higher K_O than the other soils, and this especially so at higher OCRs. At OCR = 8 for example, RLC has a K_O of approximately 1.9, compared to a K_O of just 1.1 for RBBC and RPC. This behavior appears to be consistent with that observed in the NC range, discussed above, as RLC has a significantly higher liquid limit than the RPC or RBBC. It should be kept in mind, however, that the results shown in Figure 5-25 involve triaxial tests performed at different stress levels. The tests performed on RPC, RSFBM and RLC had preconsolidation stresses of 4.73 MPa, 14.1 MPa and 0.38 MPa respectively prior to swelling, while the tests performed on RBBC had preconsolidation stresses of 9.81 MPa (TX1061) and 40.1 MPa (TX1185).

In Figure 5-26, the change in K_O during swelling and subsequent recompression is shown for RLC alone. The value of K_O during the swelling phase (K_{OS}) can be approximated by a function originally proposed by Schmidt (1966):

$$K_{OS} = K_{ONC}(OCR)^{a} \qquad 5-7$$

where a is a constant and equal to 0.51 for the RLC specimen. This form of equation has since been widely accepted to describe the variation in K_O during swelling/unloading for both clays and sands (e.g. Mesri and Hayat 1993). The variation in K_O during recompression (K_{OR}) is less well established, and the author proposes the following function to describe the variation in K_O for a soil during this phase:

$$K_{OR} = K_{ONC} + 0.5K_{ONC}(OCR_{MAX}^{a} - 1)\left(\frac{OCR-1}{OCR_{MAX}-1}\right)\left(\frac{OCR-1}{OCR_{MAX}-1} + 1\right) \qquad 5 - 8$$

where $OCR_{MAX} = 9.23$ in the case of the RLC specimen. Although cumbersome, the function is straightforward to apply and does not require any empirical parameters other than *a*. A function similar to that given in Equation 5 – 8 was proposed by Mayne and Kulhawy (1982) but requires the use of an additional fitting parameter. Figure 5-27, Figure 5-28 and Figure 5-29 show the change in K_O during both the swelling and recompression phases of triaxial tests performed on specimens on RBBC, RPC and RSFBM respectively. The variations in K_O for RBBC and RPC can be well approximated by Equations 5-7 and 5-8 for swelling and recompression respectively, with both RBBC and RPC having $a = 0.39$. For the test performed on RSFBM, K_O conditions were not controlled with sufficient accuracy at all times during the swelling and recompression phases. As a result, much of the K_O data, particularly for the recompression phase, are not considered reliable and therefore not included in Figure 5-29. A value of $a = 0.38$ was interpreted for RSFBM based on the available data. Unfortunately, the limited number of triaxial tests in which K_O was measured in the OC range means that sufficient information is not available to determine the effects, if any, of composition and stress level on the value of *a*.

Empirical correlations between the parameters *a* and ϕ'_{cs} have been proposed by Schmidt (1966) and Mayne and Kulhawy (1982). The correlation of Schmidt ($a = 1.2\sin\phi'_{cs}$) predicts *a* values of 0.64, 0.59, 0.47 and 0.42 for RPC, RBBC, RSFBM and RLC respectively at the relevant stress levels. The correlation of Mayne and Kulhawy ($a = 0.018 + 0.974\sin\phi'_{cs}$) predicts *a* values of 0.54, 0.50, 0.40 and 0.36 for RPC, RBBC, RSFBM and RLC respectively at the relevant stress levels. However, the correlations of both Schmidt (1966) and Mayne and Kulhawy (1982) show a great deal of scatter. This is likely due to their incorrect assumption of a constant ϕ'_{cs} for each of the soils included in their studies, in that measured *a* parameters were correlated to stress dependent values of ϕ'_{cs}, with this stress level dependence not being considered.

Table 5-1: Summary of triaxial consolidation results

Test no.	TX System	Soil	Sample no.	Initial		At Max. Stress		OCR	Pre-Shear		
				w_c	e_o	σ'_p (MPa)	K_{ONC}		σ'_{vc} (MPa)	e	K
TX1030^	MIT07	RBBC	RS127	27.2	0.756	9.812	0.557	1.00	9.812	0.447	0.557
TX1031^	MIT07	RBBC	RS128	26.5	0.737	5.870	0.521	1.00	5.870	0.550	0.521
TX1034^	MIT07	RBBC	RS130	27.2	0.757	9.817	0.601	4.02	2.442	0.508	1.003
TX1036^	MIT07	RBBC	RS132	39.3	1.093	0.557	0.493	1.00	0.557	0.872	0.493
TX1040^	MIT07	RBBC	RS137	27.4	0.762	9.805	0.554	2.01	4.881	0.517	0.743
TX1041^*	MIT07	RBBC	RS142	41.2	1.146	0.629	0.580	1.00	0.629	0.918	0.580
TX1042^	MIT07	RBBC	RS138	30.9	0.860	1.939	0.557	4.13	0.469	0.731	1.032
TX1043^*	MIT07	RBBC	RS159	38.7	1.075	0.572	0.546	1.00	0.572	0.879	0.546
TX1046^	MIT07	RBBC	RS162	39.3	1.092	1.925	0.581	4.18	0.461	0.740	1.027
TX1053^*	MIT07	RBBC	RS169			0.587	0.510	1.00	0.587	0.864	0.510
TX1057^	MIT07	RBBC	RS168	27.6	0.766	9.813	0.525	3.97	2.472	0.518	0.992
TX1059^	MIT07	RBBC	RS171	27.5	0.764	9.567	0.510	1.00	9.567	0.504	0.510
TX1061^	MIT07	RBBC	RS172	27.4	0.761	9.811	0.532	8.03	1.222	0.533	0.989
TX1070^	MIT07	RBBC	RS196	40.0	1.110	0.555	0.517	1.00	0.555	0.885	0.517
TX1073^	MIT13	RBBC	RS198	41.5	1.153	0.563	0.492	1.00	0.563	0.832	0.492
TX1115^E	MIT07	RBBC	RS256	27.2	0.755	6.941	0.557	1.00	6.941	0.536	0.557
TX1119^E	MIT03	RBBC	RS264	44.2	1.229	0.198	0.495	1.00	0.198	1.069	0.495
TX1120	MIT07	RBBC	RS263	20.4	0.568	13.100	0.550	15.80	0.829	0.540	0.961
TX1124^	MIT07	RBBC	RS284	31.8	0.883	5.857	1.000	1.00	5.857	0.559	1.000
TX1147	MIT09	RBBC	RS283	28.4	0.790	9.610		1.00	9.610	0.513	0.000
TX1160	MIT09	RBBC	RS324	19.9	0.552	20.05	0.586	1.00	20.05	0.401	0.586
TX1162	MIT09	RBBC	RS337	21.9	0.607	40.53	0.585	1.00	40.53	0.347	0.585
TX1163	MIT09	RBBC	RS338	20.0	0.556	40.29	0.556	4.12	9.77	0.348	0.952
TX1166	MIT09	RBBC	RS340	20.5	0.569	40.30	0.580	2.01	20.05	0.345	0.750
TX1185	MIT09	RBBC	RS322	20.0	0.556	40.11	0.577	8.41	4.77	0.382	1.157
TX1193	MIT09	RBBC	RS341	20.7	0.576	101.25	0.595	1.00	101.25	0.239	0.595
TX1204	MIT09	RBBC	RS388	20.4	0.566	103.07	0.605	2.03	50.77	0.261	0.605
TX1093	MIT07	RPC	RS228	22.0	0.611	9.464	0.470	1.00	9.464	0.423	0.470
TX1096	MIT02	RPC	RS236	28.1	0.780	0.241	0.510	1.00	0.241	0.686	0.510
TX1111	MIT01	RPC	RS254	26.2	0.726	0.990	0.460	1.00	0.990	0.586	0.460
TX1208	MIT09	RPC	RS403	17.9	0.495	101.30	0.581	1.00	101.30	0.226	0.581
TX1210	MIT03	RPC	RS404	27.3	0.757	0.579	0.485	1.00	0.579	0.615	0.485
TX1072	MIT07	RGoM Ursa	RS183	25.3	0.676	9.600	0.645	1.00	9.600	0.386	0.645
TX1077	MIT13	RGoM Ursa	RS191	38.9	1.038	0.625	0.596	1.00	0.625	0.752	0.596
TX1106	MIT01	RGoM Ursa	RS244	42.9	1.145	0.188	0.517	1.00	0.188	0.961	0.517
TX1218	MIT09	RGoM Ursa	RS407	18.1	0.482	84.8		1.00	84.8	0.209	
TX1092	MIT07	RUC	RS226	24.0	0.646	9.783	0.605	1.00	9.783	0.382	0.605
TX1198	MIT09	RUC	RS360	16.0	0.432	105.30	0.726	1.00	105.30	0.150	0.726
TX1079	MIT07	RSFBM	RS204	31.6	0.849	9.540	0.562	1.00	9.540	0.492	0.562
TX1216	MIT09	RSFBM	RS408	21.9	0.590	83.00	0.739	1.00	83.00	0.268	0.739
TX1123	MIT03	RLC	RS278	52.7	1.476	0.153	~0.56	1.00	0.153	1.193	~0.56
TX1127	MIT03	RLC	RS279	45.8	1.282	0.379	0.604	1.00	0.379	1.028	0.604
TX1129	MIT03	RLC	RS280	39.2	1.097	1.395	0.680	1.00	1.395	0.745	0.680
TX1137$^\$$	MIT03	RLC	RS297	36.2	1.015	0.671	0.647	1.00	0.671	0.894	0.647
TX1189	MIT09	RLC	RS358	24.7	0.691	11.82	0.790	1.00	11.82	0.459	0.790
TX1209	MIT09	RGoM EI	RS379	20.8	0.577	63.47	0.917	1.00	63.47	0.311	0.917

^ test performed with smooth end platens; *specimen consolidated under high u_b; ^{E} triaxial extension test; $ likely error in w_c and e_o

Table 5-2: Comparison of the accuracy of various compression models to measured behavior. For each soil, the most appropriate model to capture the soil's virgin compression behavior is indicated by '✓', while the least appropriate model is indicated by '**X**'

Soil	w_L **(%)**	**USCS classification**	**e-log(**σ'_v**)**	**ln(1+e)-log(**σ'_v**)**	**n-log(**σ'_v**)**
Presumpscot Clay	33.1	CL	✓		X
Boston Blue Clay	46.5	CL	X	✓	
Cornwall Kaolin	48	ML	✓		X
Villanova Tulo W. Kaolin	49.0	ML	✓		X
GoM Ursa Clay	51.7	CH		✓	X
Ugnu Clay	56.4	CH	X		✓
San Francisco Bay Mud	60.2	MH	X		✓
Edgar Plastic Kaolin	68	MH	X		✓
Nankai Clay	68	CH	X		✓
London Clay	73.8	CH	X	✓	
GoM Eugene Island Clay	85.8	CH	X		✓
GoM Clay A	70.4	CH	X		✓
GoM Clay B	90.2	CH	X		✓
GoM Lower Clay	62.7	CH	X		✓
GoM Upper Clay	64.7	CH	X		✓

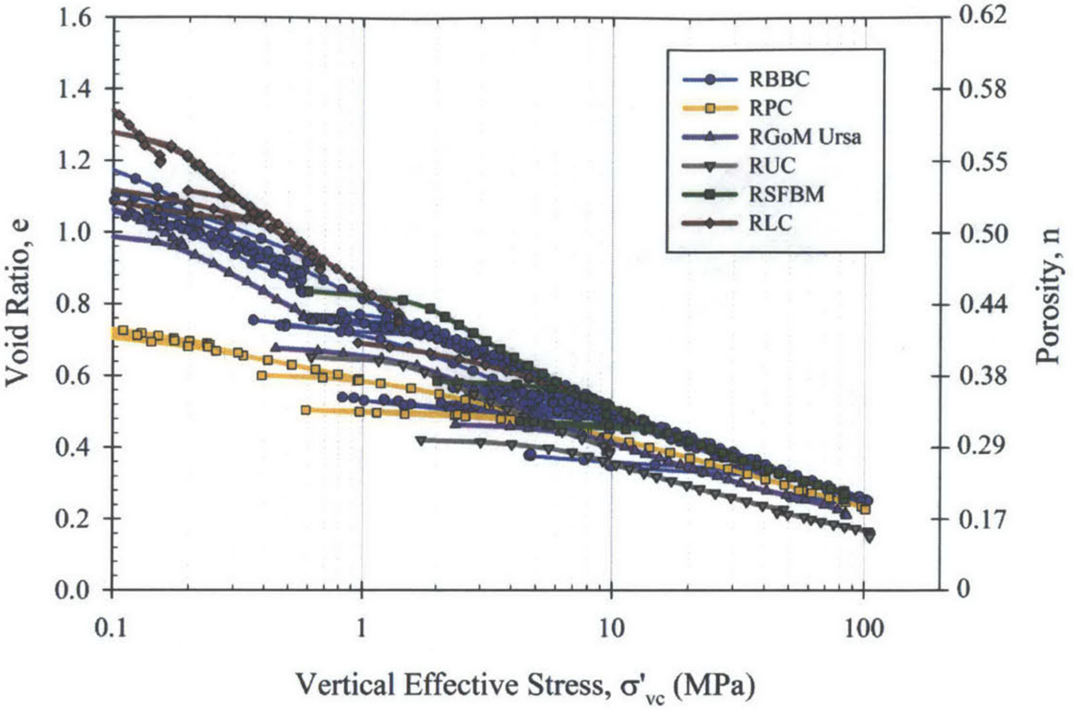

Figure 5-1: Compression data measured during the K_O-consolidation phase of triaxial tests

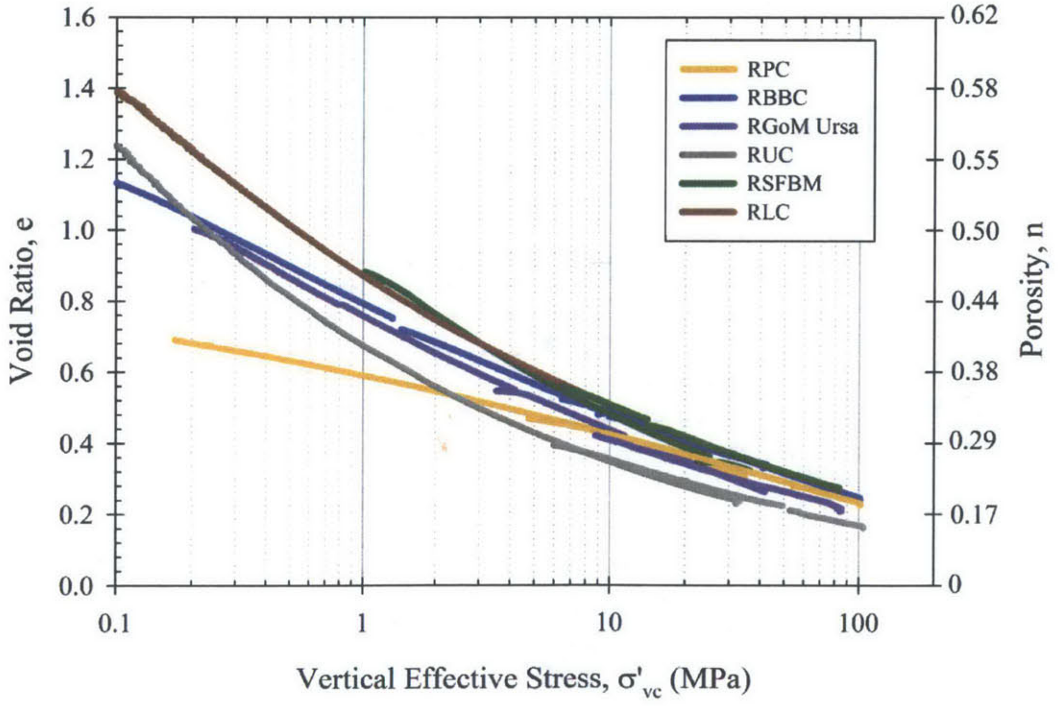

Figure 5-2: One dimensional virgin compression behavior of soils tested by the author

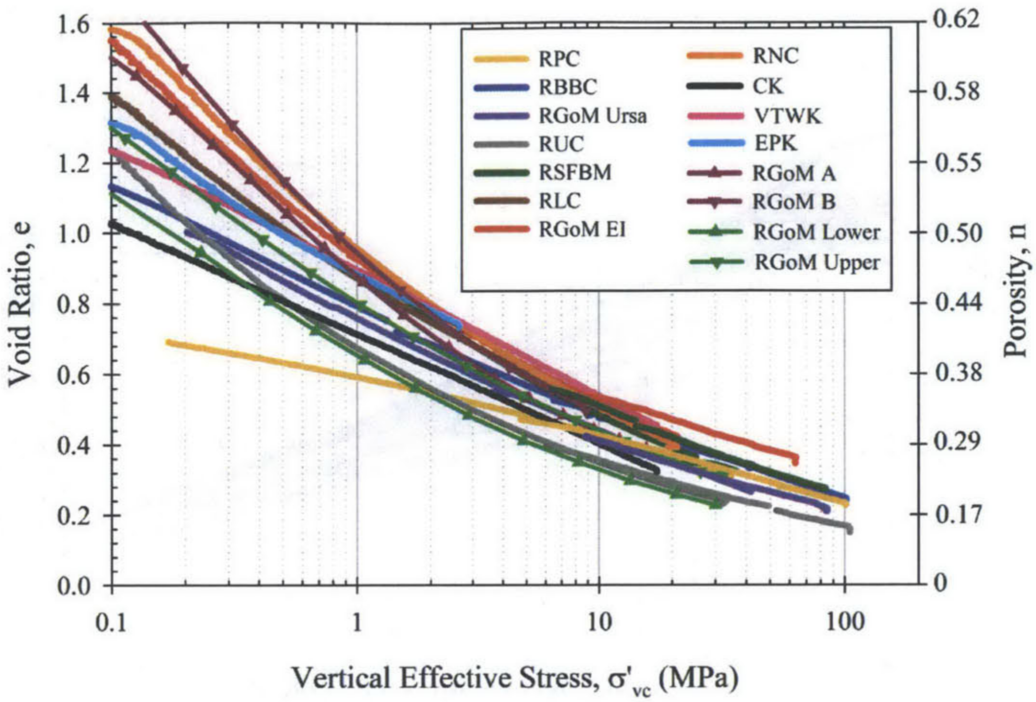

Figure 5-3: One dimensional virgin compression behavior of all soils included in the research

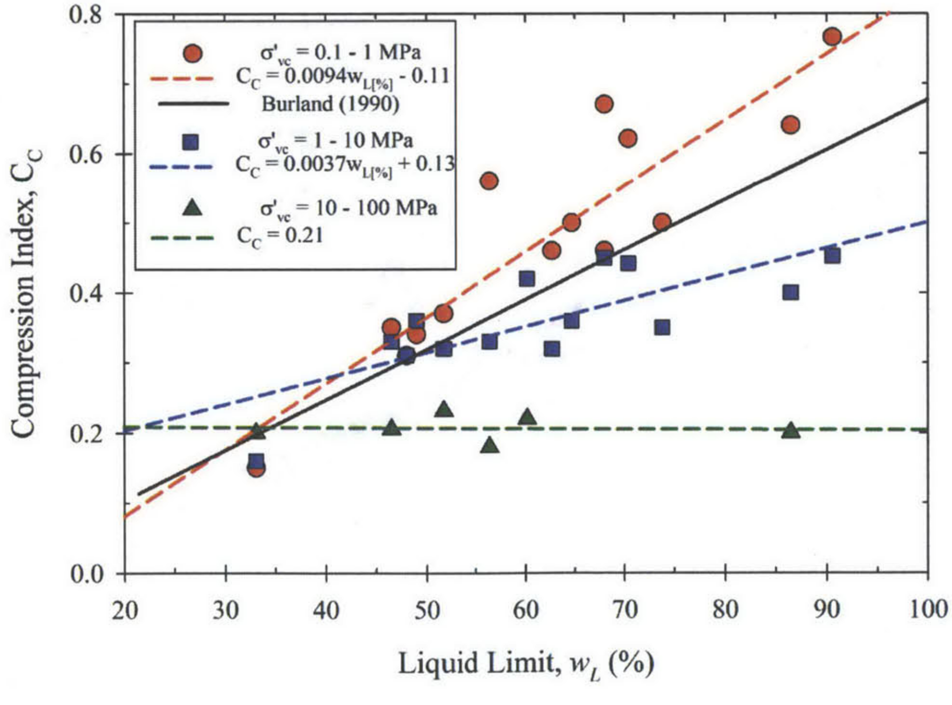

Figure 5-4: Compression indices of all soils included in the research plotted as a function of liquid limit and stress level

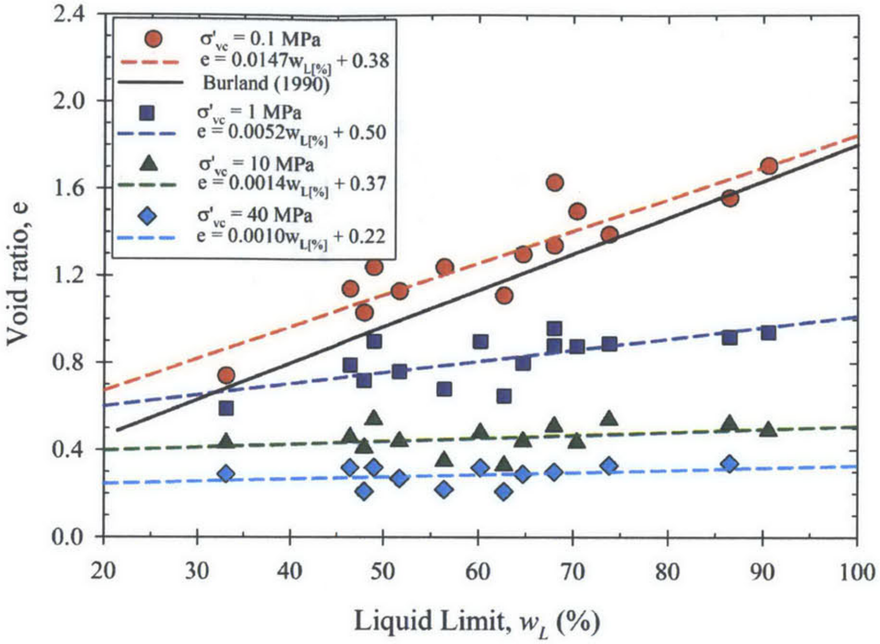

Figure 5-5: Void ratios at specific stresses for all soils included in the research plotted as a function of liquid limit

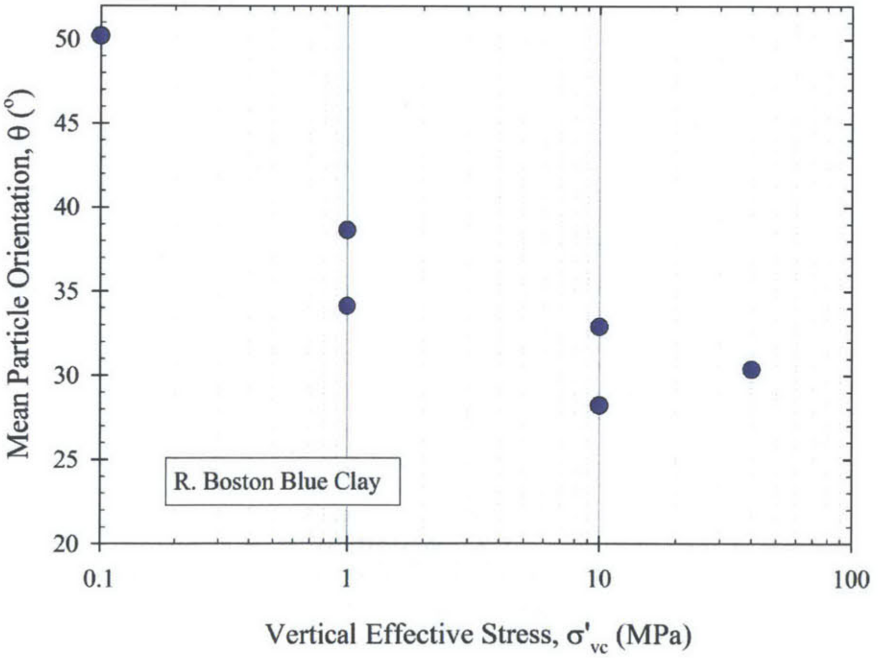

Figure 5-6: The reduction in the mean particle orientation (from horizontal) of RBBC with increasing vertical effective stress. Multiple data points at a given σ'_{vc} reflect experimental scatter as well as differences in imaging techniques (adapted from Adams 2014)

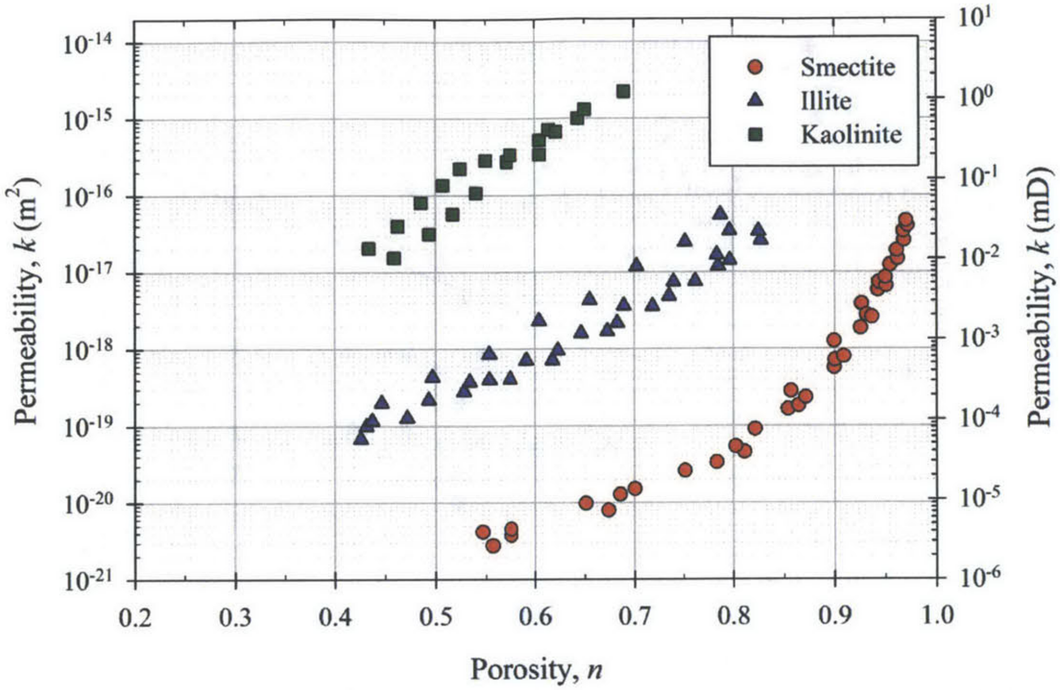

Figure 5-7: Permeabilities of smectite, illite and kaolinite clay minerals (adapted from Mesri and Olson 1971)

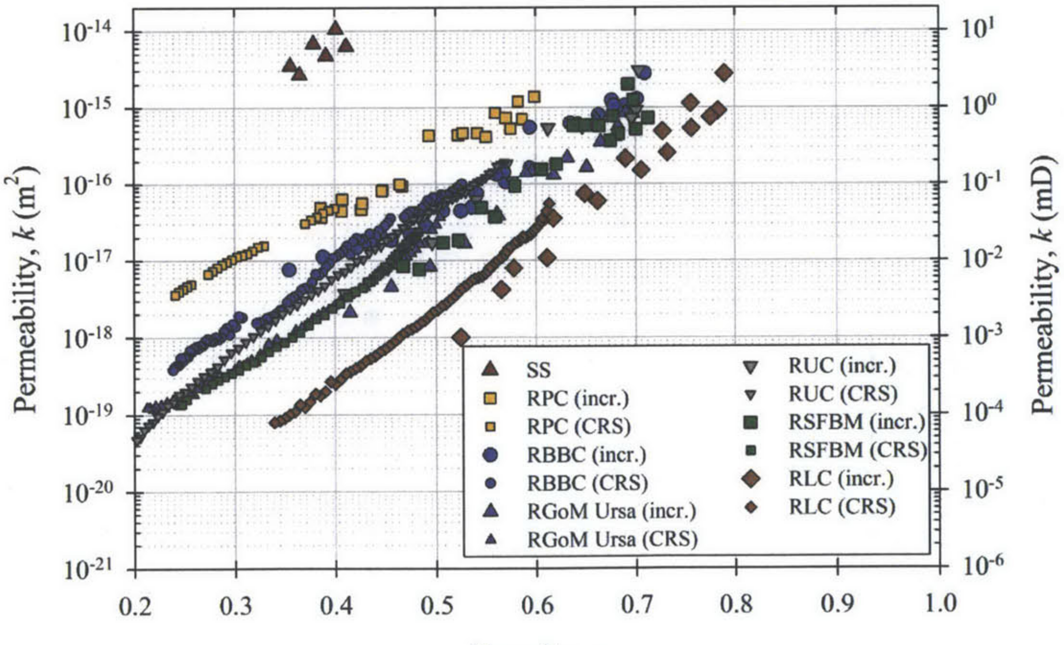

Figure 5-8: Changes in the permeability of soils with porosity as measured during resedimentation and CRS tests

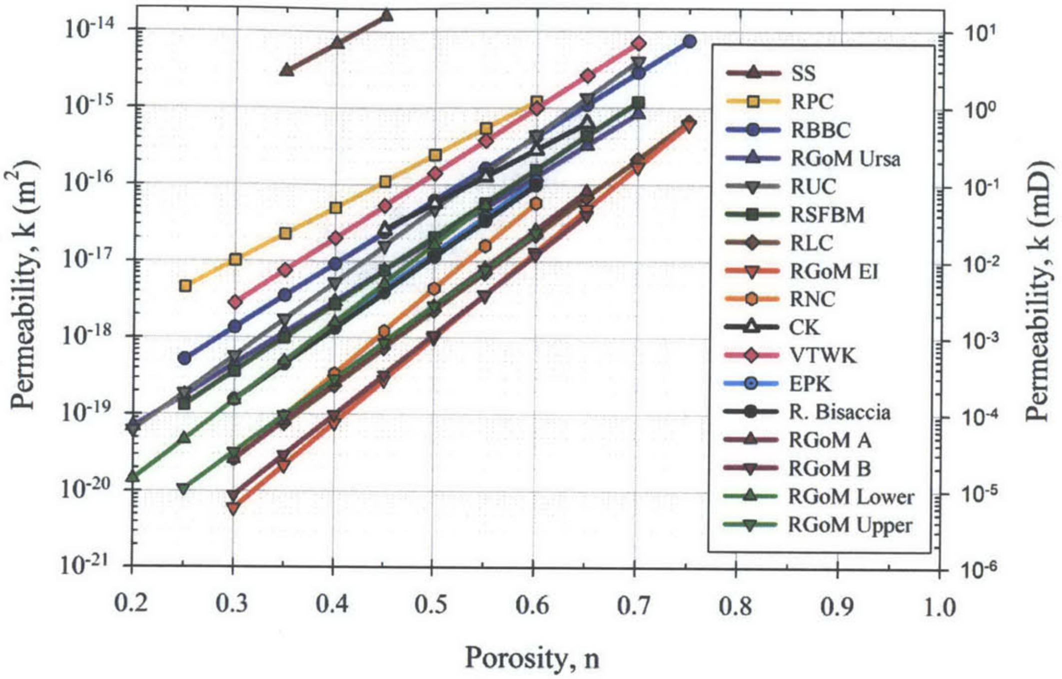

Figure 5-9: Permeability-porosity relationships for all of the soils included in the research. The experimental data are represented using regression lines. The limits of the regression lines represent the limits of the measured data

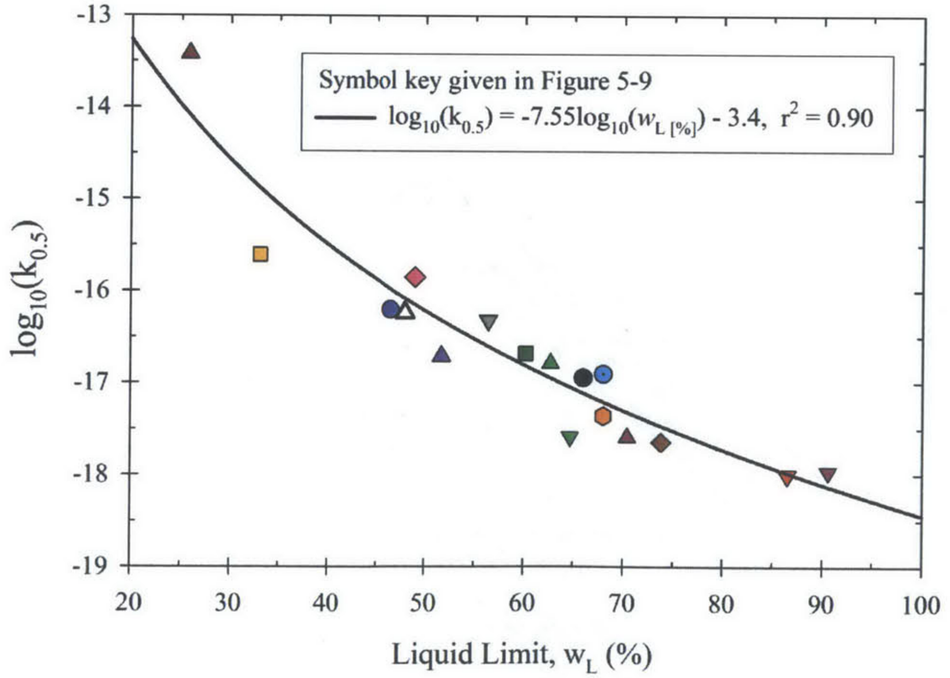

Figure 5-10: Correlation between $\log_{10}(k_{0.5})$ and liquid limit

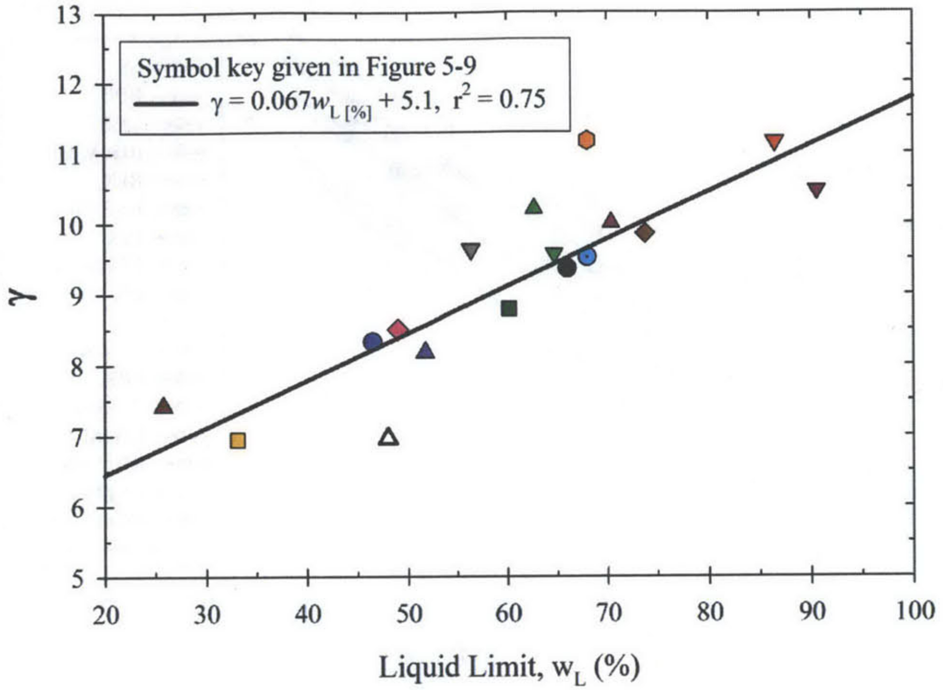

Figure 5-11: Correlation between the parameter γ and liquid limit

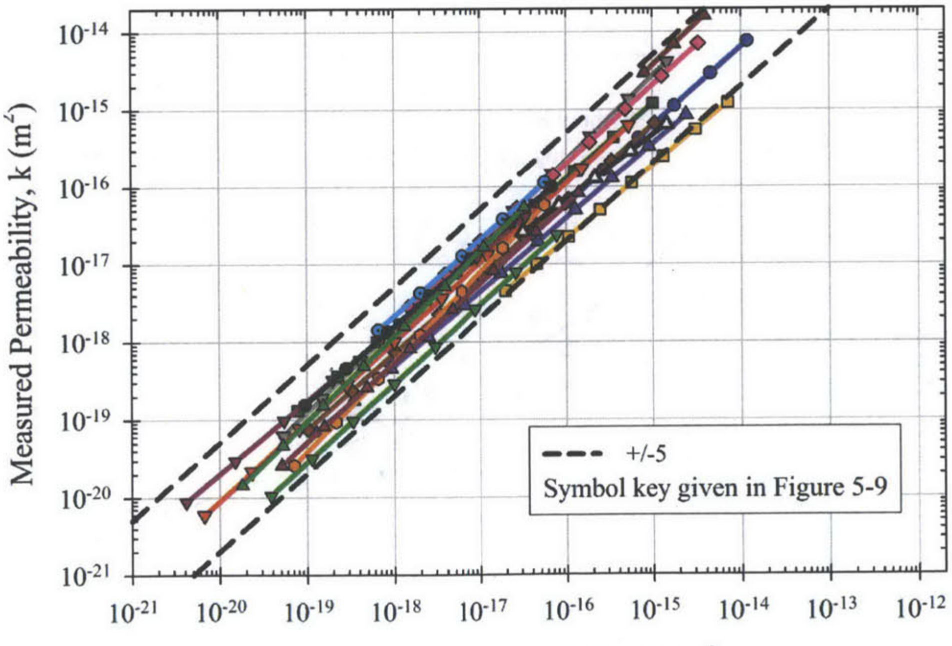

Figure 5-12: Comparison of measured permeabilities with those predicted using the liquid limit correlations. The predicted permeabilities all fall within ±5 times the measured values

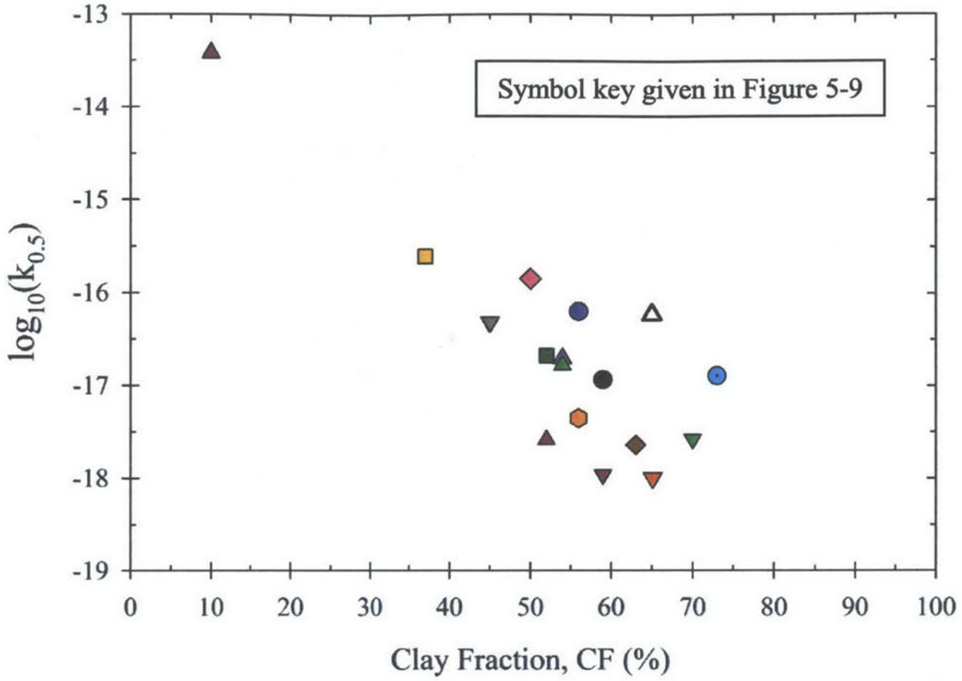

Figure 5-13: Relationship between $\log_{10}(k_{0.5})$ and clay fraction, where clay fraction is defined as the percentage of particles < 2 μm

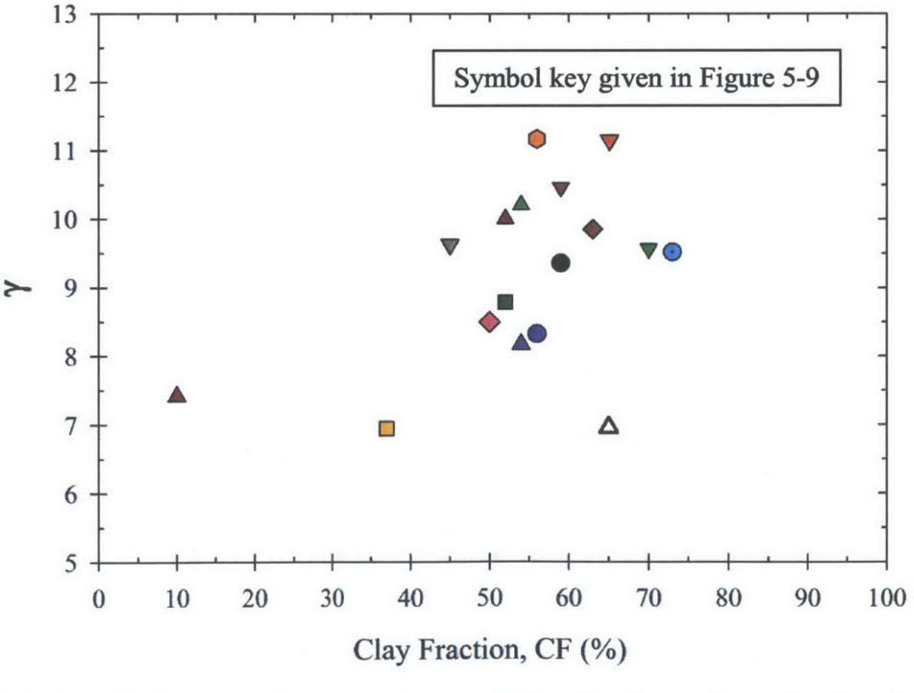

Figure 5-14: Relationship between the parameter γ and clay fraction, where clay fraction is defined as the percentage of particles < 2 μm

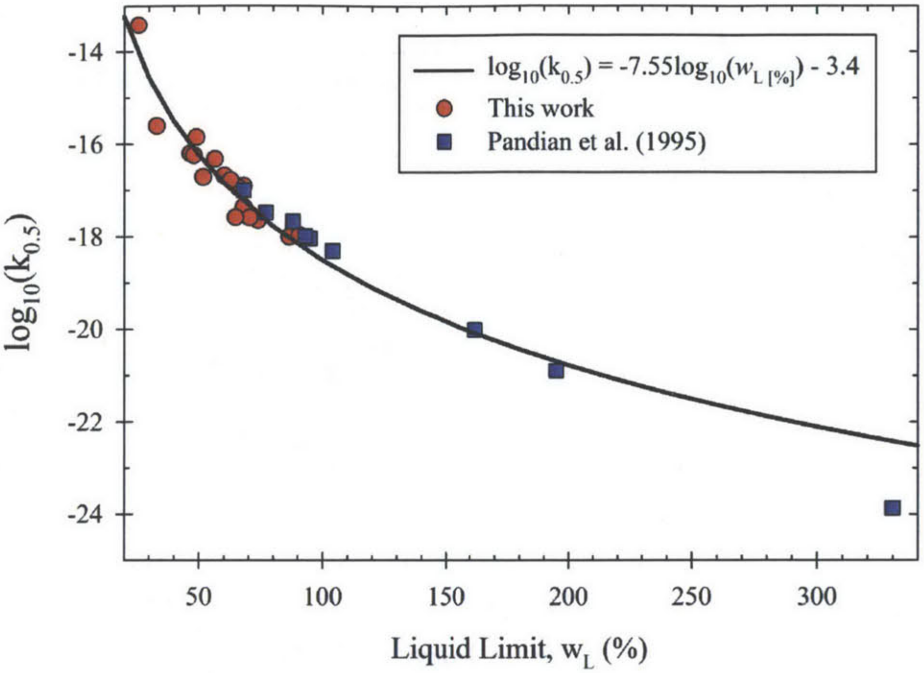

Figure 5-15: Values of $\log_{10}(k_{0.5})$ from this work as well as from Pandian et al. (1995) plotted against liquid limit

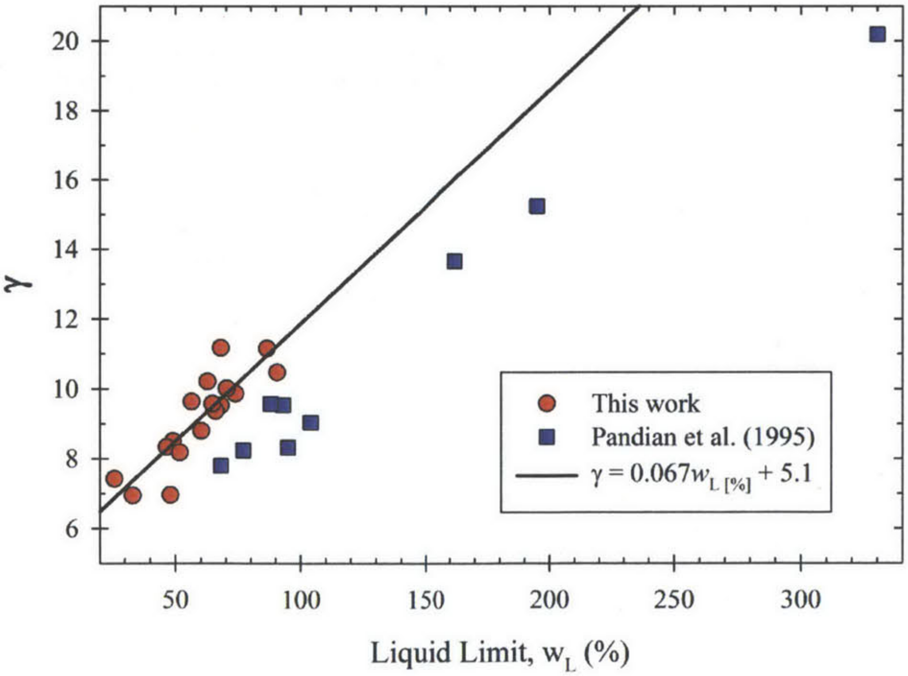

Figure 5-16: Values of γ from this work as well as from Pandian et al. (1995) plotted against liquid limit

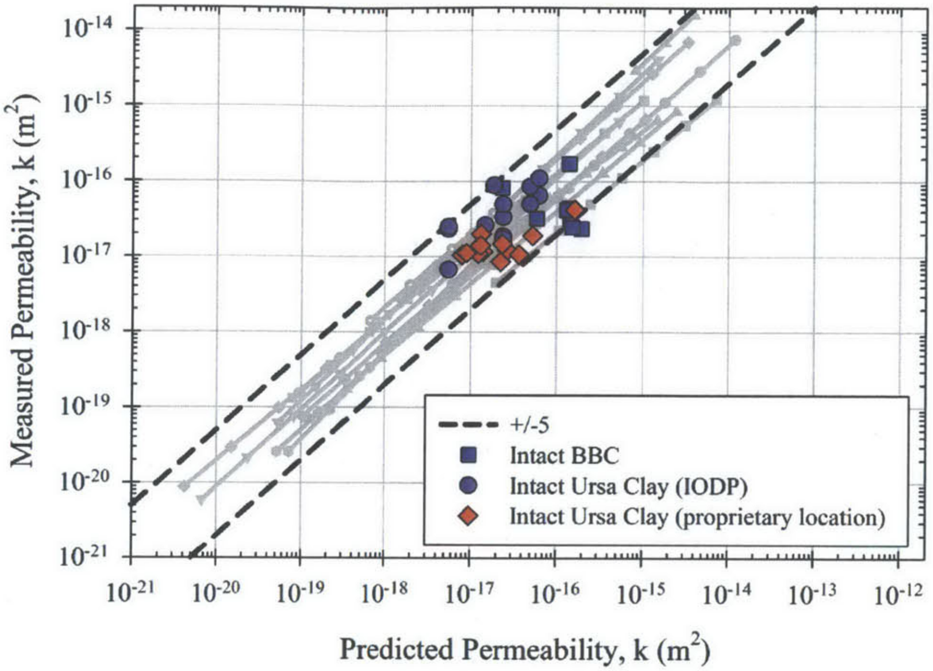

Figure 5-17: Comparison of measured permeabilities with those predicted using the liquid limit correlations for samples of intact Boston Blue Clay and intact GOM Ursa Clay. The permeability data included in Figure 5-12 are shown in grey in the background

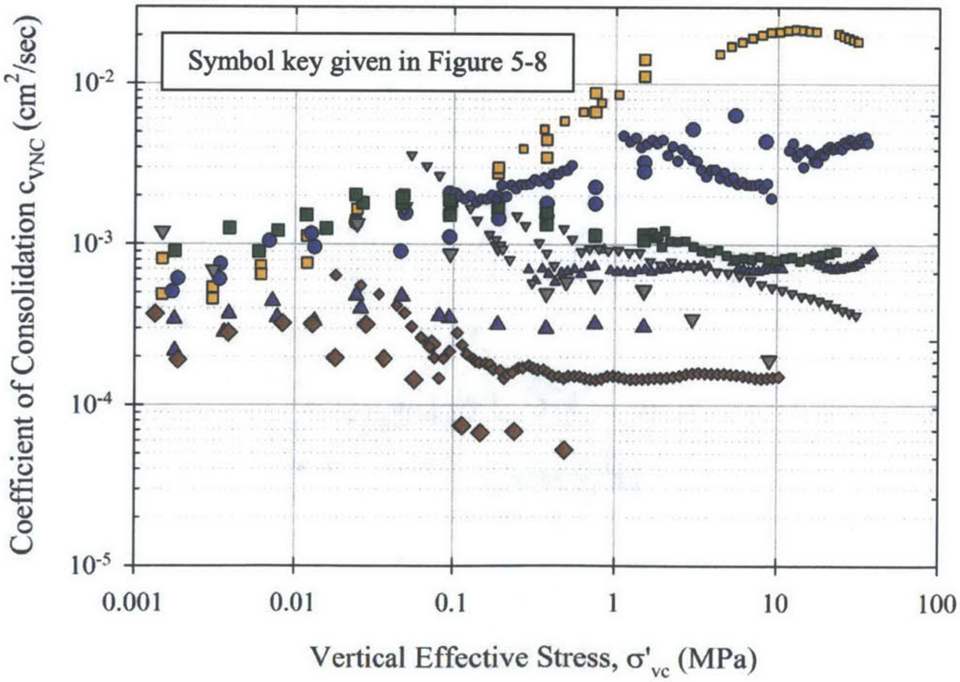

Figure 5-18: The change in c_{VNC} of soils over a very wide range of effective stress

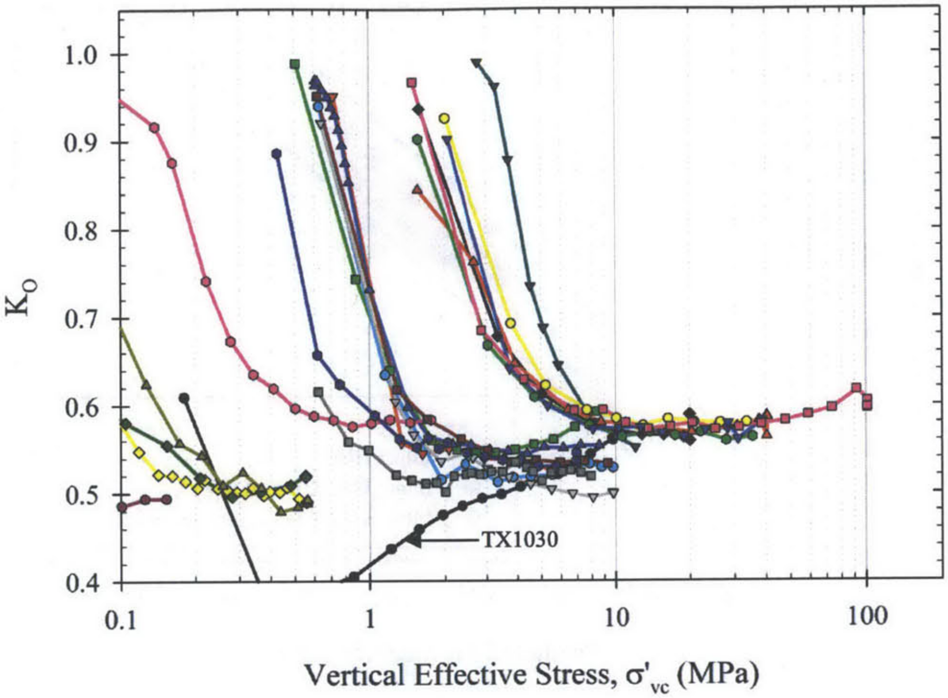

Figure 5-19: The change in K_O measured during the consolidation phase of triaxial tests performed on RBBC. Each line represents a different test

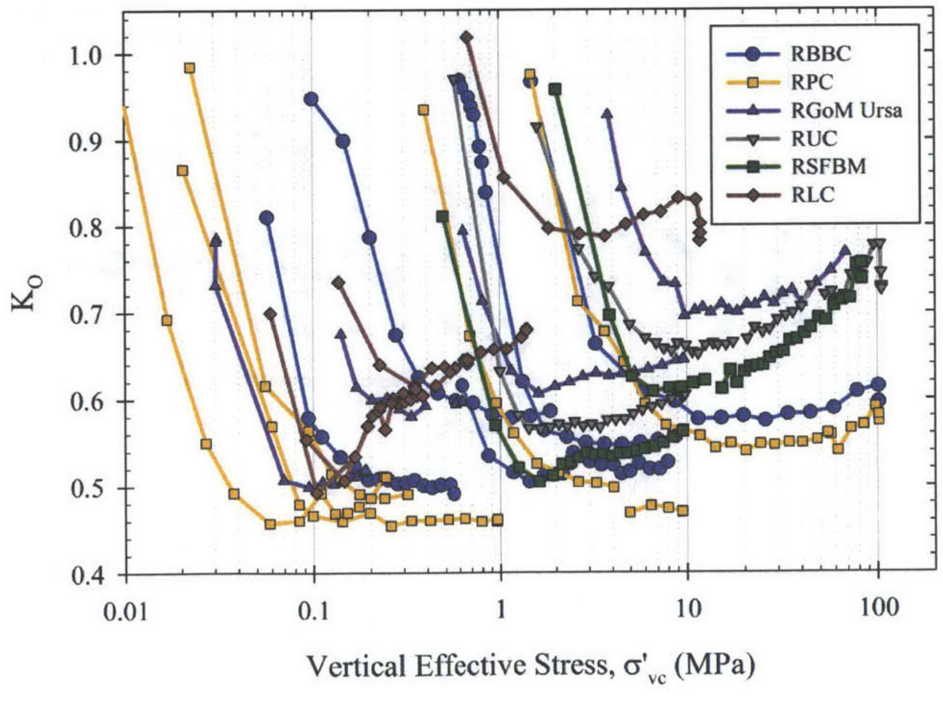

Figure 5-20: The change in K_O measured during the consolidation phase of selected triaxial tests

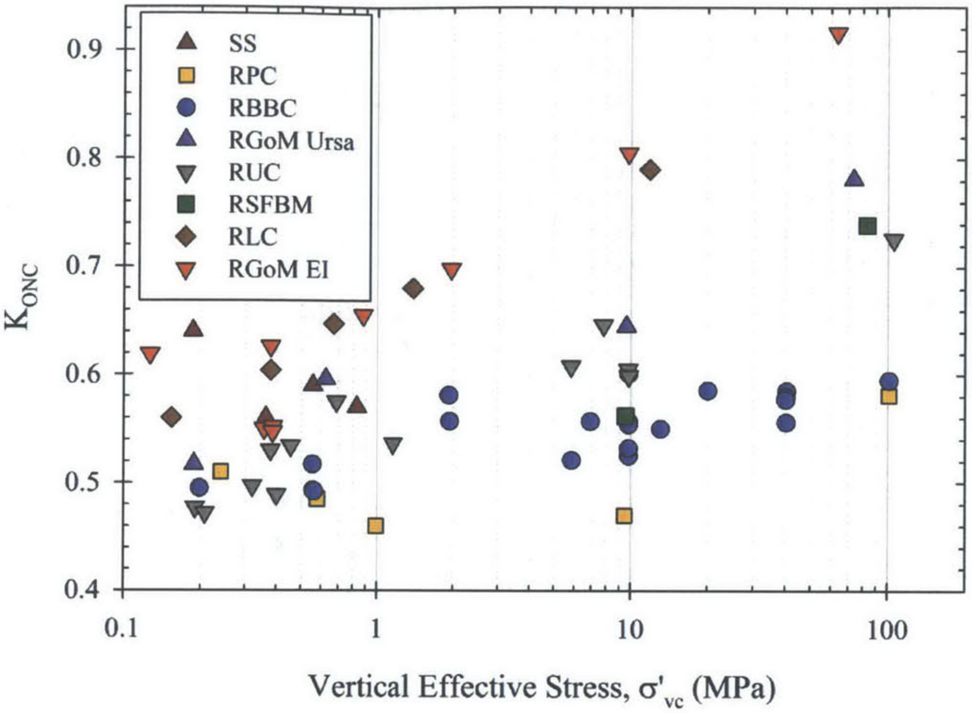

Figure 5-21: Values of K_{ONC} measured at the end of the consolidation phase of triaxial tests

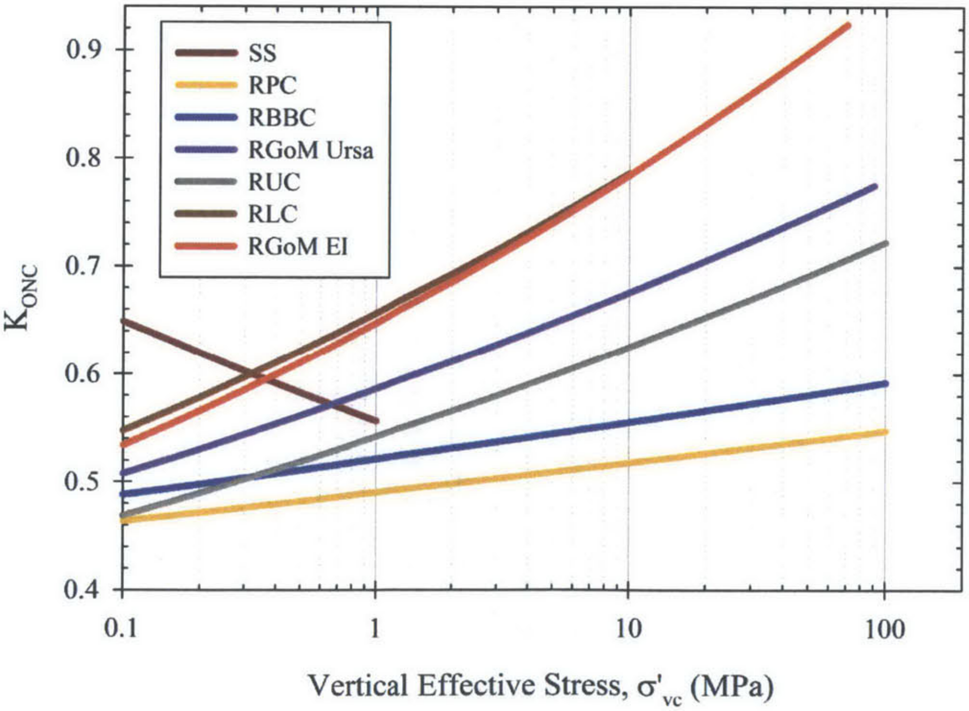

Figure 5-22: Power-law regressions through the K_{ONC} data presented in Figure 5-21

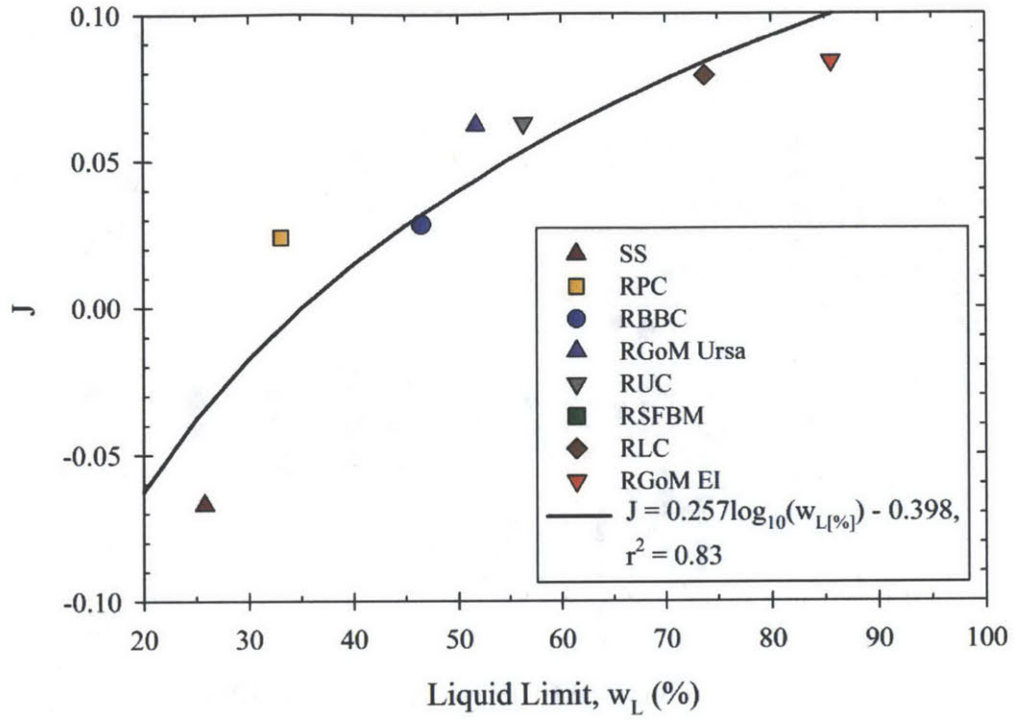

Figure 5-23: Correlation between the parameter K_{O10} and liquid limit

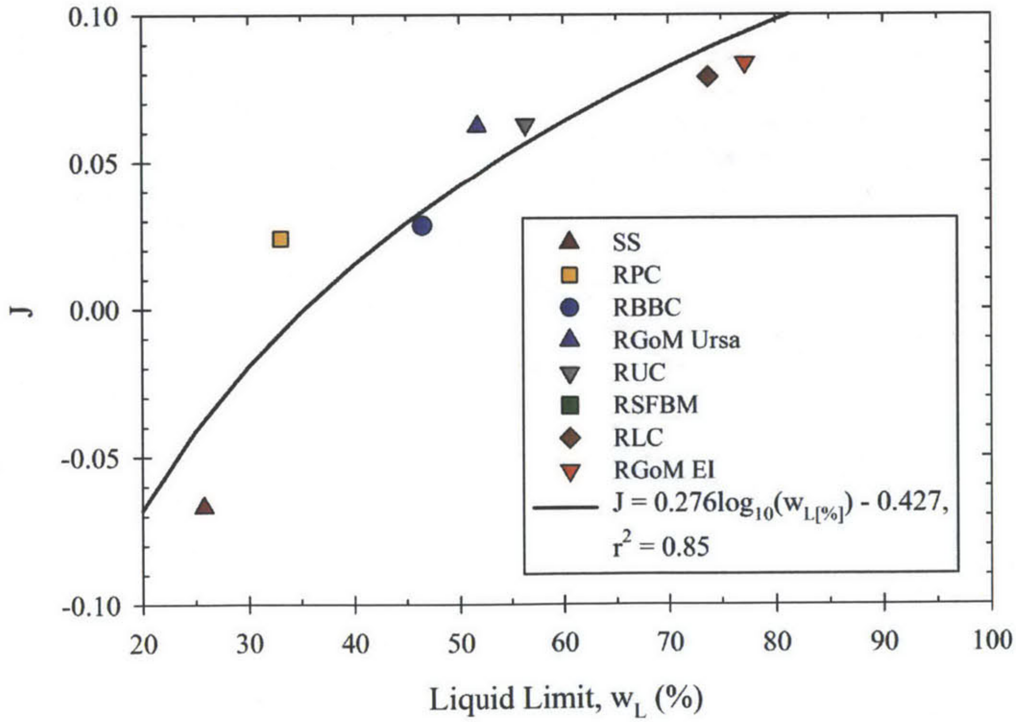

Figure 5-24: Correlation between the parameter J and liquid limit

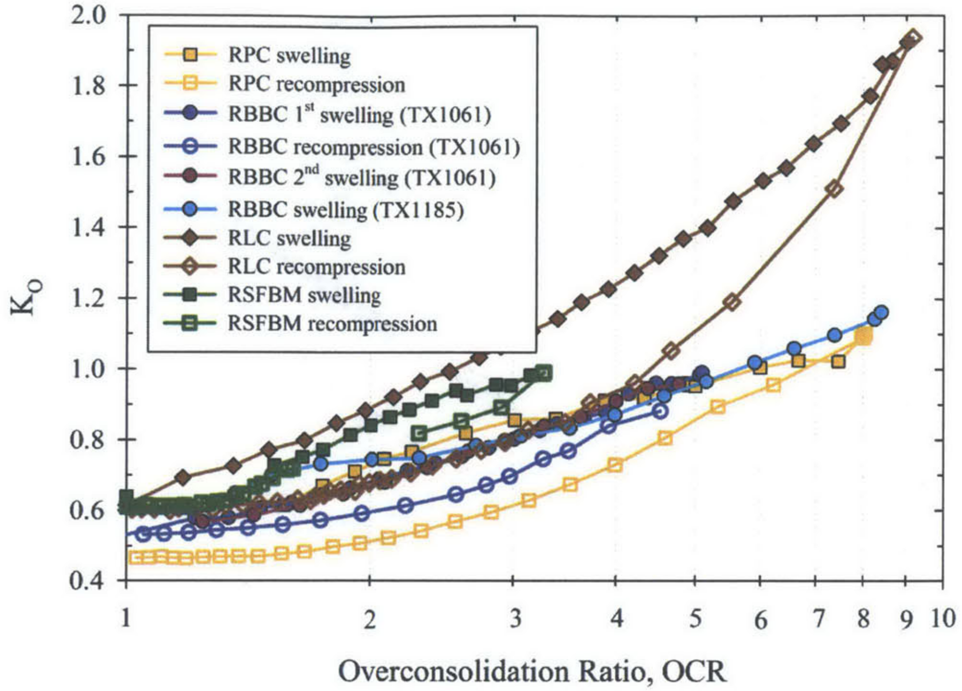

Figure 5-25: The change in K_O measured during the swelling portion of triaxial tests

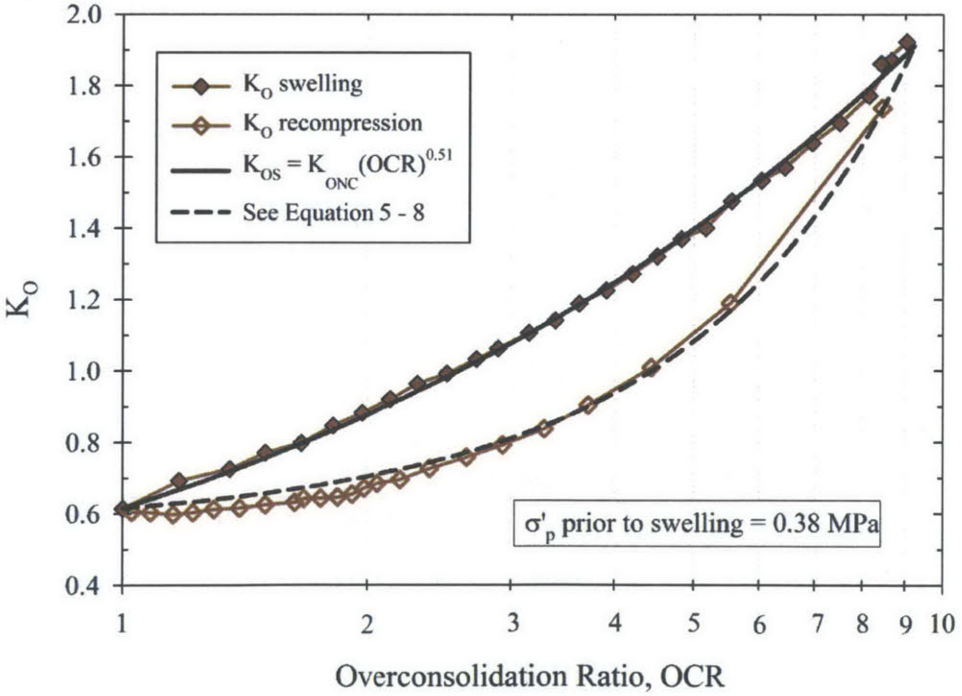

Figure 5-26: The change in K_O measured during the swelling and recompression portions of a triaxial test performed on RLC

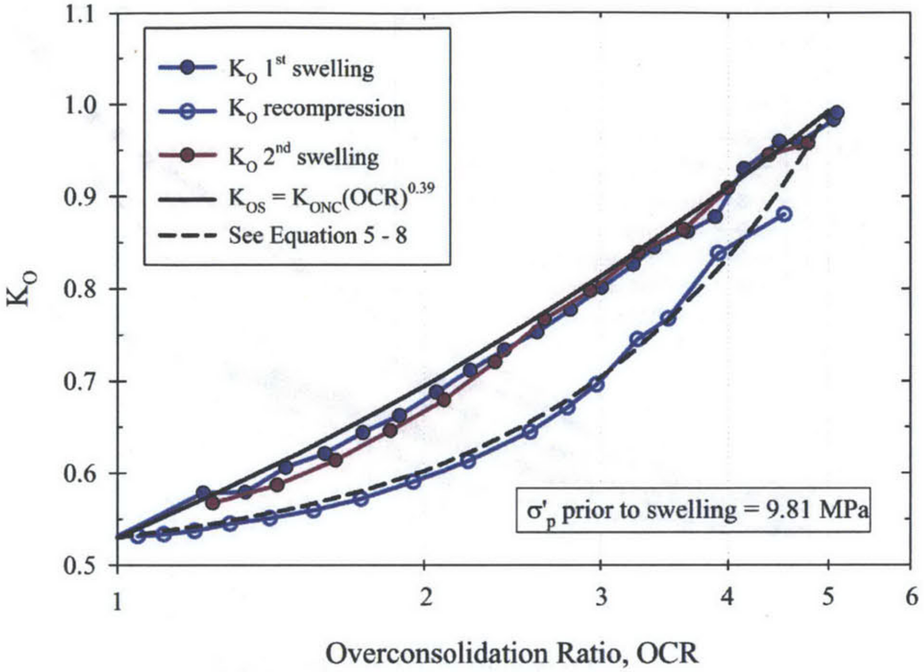

Figure 5-27: The change in K_O measured during the swelling and recompression portions of a triaxial test performed on RBBC

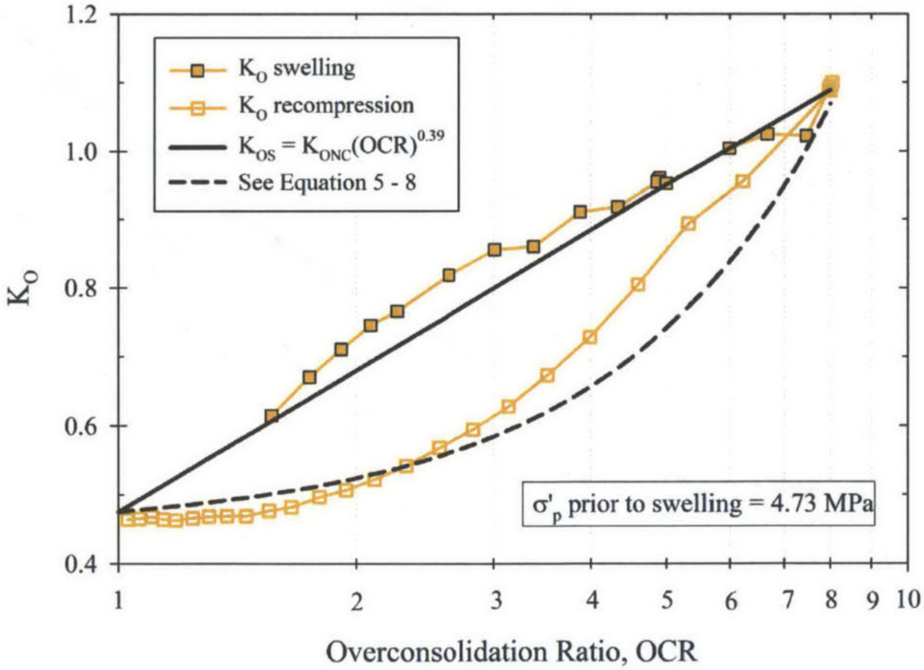

Figure 5-28: The change in K_O measured during the swelling and recompression portions of a triaxial test performed on RPC

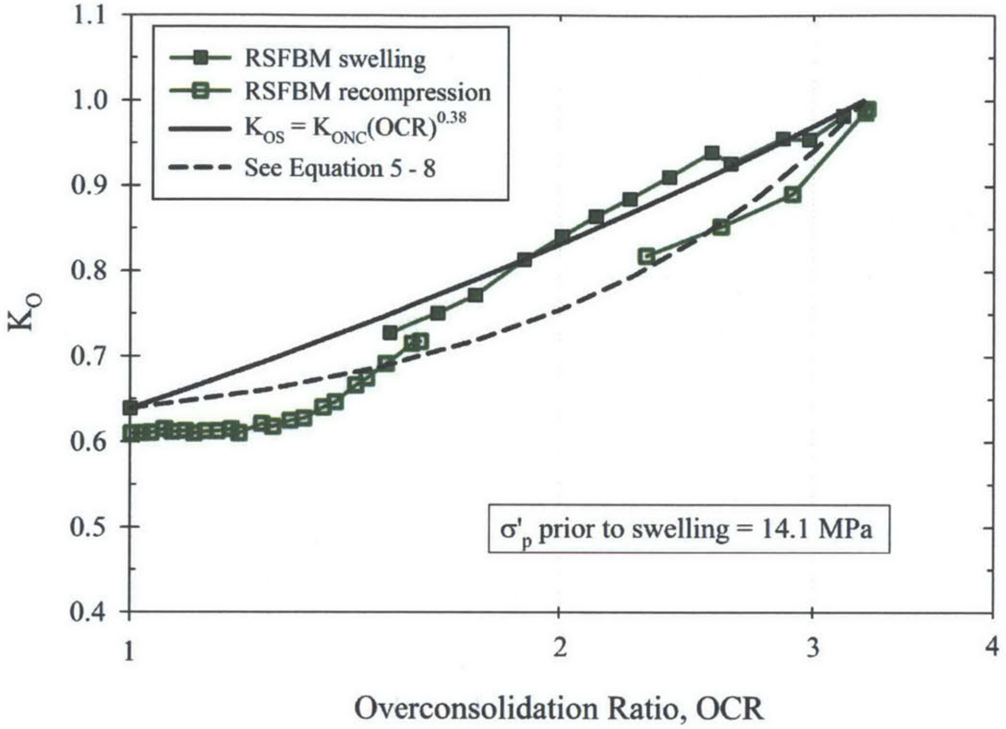

Figure 5-29: The change in K_O measured during the swelling and recompression portions of a triaxial test performed on RSFBM

6 UNDRAINED SHEAR RESULTS

6.1 INTRODUCTION

This chapter presents the results obtained during the undrained shear phase of triaxial tests carried out during the course of the research. These tests were carried out at effective stresses ranging from 0.1 MPa up to 100 MPa, generally in triaxial compression mode of shear. Section 6.2 first discusses the results of triaxial tests carried out specially to examine the validity of the Terzaghi definition of effective stress at high pore pressures. This was necessary to ensure that the results of triaxial tests carried out over a very wide range of consolidation stresses but with a relatively low laboratory back-pressure are relevant to a field situation in which the in situ pore pressures are much higher. Section 6.3 presents the undrained shear behavior of RBBC, including shear stress-strain response, shear induced pore pressure generation, strength properties, and Young's modulus, as well as how these vary as a function of both effective stress level and OCR. Section 6.3 also discusses the critical state behavior of RBBC. The results are generally presented in a normalized format to allow for an easier and more meaningful examination of behavior over a wide range of stresses. Triaxial tests performed on soils other than RBBC only involved testing at OCR = 1. The undrained shear behaviors at OCR = 1 of R. Presumpscot Clay, R. GoM Ursa Clay, R. Ugnu Clay, R. San Francisco Bay Mud and R. London Clay are presented in Sections 6.4, 6.5, 6.6, 6.7 and 6.8 respectively.

Section 6.9 summarizes and compares the undrained shear behaviors of the different soils. Emphasis is placed on systematic stress level changes in strength properties as a function of soil composition. Correlations are presented which relate variations in the undrained strength ratio and critical state friction angle of soils to liquid limit, where liquid limit can be regarded as a proxy for soil composition. Section 6.9 also compares the critical state behavior of the soils tested, as well as the important link observed between K_O and strength properties.

The anisotropic nature of soil means that its behavior is different depending on the orientation and relative magnitudes of the principal stresses. However, significantly less strength data are available for modes of shear other than triaxial compression. Section 6.10 presents the limited data available on undrained shear behavior in triaxial extension and direct simple shear. These results are limited to OCR = 1.

The author's experimental program has involved 74 triaxial tests carried out using low, medium and high pressure triaxial systems. Of these, however, only 48 tests were successful and provide results which could be included in this thesis. The remainder of the tests encountered catastrophic failure, the most common causes being a control program malfunction (particularly in the medium pressure triaxial system) or the development of a leak in the drainage lines. Internal leakage was a particular problem in the early stages of testing in the new high pressure triaxial system. Table 6-1 provides a summary of the shear results from all triaxial tests performed during the course of the research, including the soil tested, pre-shear effective stresses, stress conditions at peak shear strength, and stress conditions at critical state. Table 6-1 also specifies if a failure plane was visible on the sheared specimen after testing. A failure plane was not observed in the majority of tests, and no systematic trend could be detected for tests in which one was. Furthermore, no difference in shear behavior could be found between tests which did and did not develop failure planes. Additional data on pre-shear values of K_O and void ratio are given in Table 5-1.

6.2 EFFECTIVE STRESS TESTS

Several triaxial compression tests were carried out to examine the validity of Terzaghi's definition of effective stress at pore pressures much higher than those typically encountered in geotechnical engineering practice. These tests were carried using a procedure similar to that adopted by Bishop and Skinner (1977) and described in Section 2.5.3. The procedure consists of the observation of strength changes resulting from large changes in confining pressure and pore pressure but with the difference between these pressures (i.e. the effective stress under Terzaghi's definition) kept constant. If interparticle contact area has an impact on effective stress, this would be detected as an increase in shear strength for tests performed under higher pore pressures.

Figure 6-1 shows the normalized shear stress-strain responses measured during undrained shearing of RBBC for axial strains up to 2 %. All tests were performed at a consolidation stress of approximately 0.6 MPa and at OCR = 1. Tests TX1036, TX1070 and TX1073 were carried out using a low back-pressure as is typical for laboratory testing. In tests TX1041 and TX1043, the specimens were K_O-consolidated with back-pressures (u_b) of 9.80 MPa and 4.90 MPa respectively and then sheared undrained, with larger excess pore pressures generated during undrained shearing. This method is slightly different to that of Bishop and Skinner (1977) in that the magnitude of u_b is not varied during the undrained shear phase of individual tests. Based on the results of these initial tests, it appears that higher pore pressures in fact lead to a decrease in undrained strength (which in theory should not be possible). However, these tests also possess significantly different pre-shear values of K_{ONC}, and it is known that K_{ONC} can have a dramatic effect on undrained strength ratio (Santagata 1994, Abdulhadi 2009, and Section 6.9.4). This variation in K_{ONC} for tests consolidated under different back-pressures is believed to be due the triaxial pore pressure system operating at considerably higher pressures than for what it was designed, and is not believed to reflect a true soil behavior. Test TX1053 was therefore carried out with u_b = 9.80 MPa but using stress path consolidation to produce a pre-shear K = 0.51, i.e. a value similar to tests carried out with a standard low back-pressure. It can be seen from Figure 6-1 that test TX1053 produces a much higher strength than both TX1041 and TX1043. It is therefore concluded that the differences in undrained strength ratios for the tests presented in Figure 6-1 are caused by variations in the pre-shear K, and are not noticeably influenced by the magnitude of the pore pressure.

Figure 6-2 plots the friction angles mobilized in the same tests as mentioned above, where friction angle is calculated using the Terzaghi definition of effective stress. The friction angles calculated at large strains, i.e. at critical state, vary between approximately 32° to 34°, with no clear trend with the magnitude of u_b being present. In TX1070 the confining pressure and pore pressure were together increased by a relatively large amount *during* undrained shearing. The test was K_O-consolidated using a standard low u_b and undrained shearing was commenced in the typical fashion. At ε_a = 6.7 % the pore pressure was increased to approximately 4.8 MPa, with a further increase to 9.7 MPa at ε_a = 9.7 % (this was achieved by increasing the confining pressure under undrained conditions, thereby causing the pore pressure in the specimen to increase by essentially the same amount). It can be seen that these large increases in pore pressure appear to have no detectable effect on the shear strength of the soil (and therefore on effective stress). To investigate if the same behavior is associated with other soils, a similar test (TX1077) was performed on RGoM Ursa, the results of which are also included in Figure 6-2. Again, it can be seen that large variations in pore pressure do not appear to have any effect on the strength of RGoM Ursa. Based on the results presented in Figure 6-1 and Figure 6-2, it is concluded that the magnitude of pore pressure in itself has no detectable influence on the shearing behavior of fine-grained soils. Modification of the conventional Terzaghi definition of effective stress is therefore not necessary to describe the behavior of these materials at high stresses.

6.3 RESEDIMENTED BOSTON BLUE CLAY

6.3.1 Normally Consolidated Behavior

Figure 6-3 shows the shear stress-strain responses ($q = (\sigma_v - \sigma_h)/2$ vs. ε_a) measured during undrained shearing for 5 tests performed on NC RBBC at consolidation stresses ranging from 0.56 MPa to 40.5 MPa. As expected, undrained strength increases with increasing consolidation stress. In each test a peak strength is reached following by strain softening, a behavior which would be expected for a NC soil. This behavior is illustrated more clearly in Figure 6-4, where the shear stresses measured in each test have been normalized with respect to the pre-shear vertical consolidation stress. It is observed from Figure 6-4 that there is a decrease in the undrained strength ratio, i.e. the peak point of the normalized stress-strain curve, with increasing stress level, reducing from 0.310 at 0.56 MPa to 0.287 at 40.5 MPa. It can also be seen from Figure 6-4 that the stress-strain response becomes more ductile with increasing consolidation stress as the strain to failure increases and there is a reduction in post-peak strain softening. This increase in ductility can be observed more clearly in Figure 6-5, where the normalized stress-strain responses are plotted only for axial strains up to 2 %.

The reduction in the normalized strength of NC RBBC is illustrated in Figure 6-6, which plots the undrained strength ratio of the soil versus stress level. The figure also includes the results of Abdulhadi (2009), as well as two tests carried out at $\sigma'_p = 0.3$ MPa by Sheahan (1991). Overall, there is a clear decrease in the undrained strength ratio from about 0.32 at 0.3 MPa to 0.29 at 40 MPa. This result contradicts the common belief that NC soils exhibit a constant normalized undrained strength independent of consolidation stress. At a given stress level, however, it can be seen from Figure 6-6 that the undrained strength ratios determined by the author (and Sheahan) are typically higher than those determined by Abdulhadi (2009) (although the rate of decrease was calculated to be essentially the same for both datasets). This could be attributed to a systematic difference in operator setup procedure. Another possible explanation for this inconsistency is the effect of specimen end condition. Abdulhadi (2009) exclusively used fixed ends in the low and medium pressure triaxial cells (i.e. up to 10 MPa), whereas both the author and Sheahan (1991) used smooth end platens in these triaxial cells. The use of smooth end platens is believed to result in a more ideal shearing condition for NC soil in the triaxial device, as discussed in greater detail in Casey (2011). As a result, the undrained strength ratios measured for NC RBBC by the author and Sheahan (1991) are believed to be more accurate, and are fitted with a power-law regression of the form:

$$s_u/\sigma'_{vc} = S_1(1000\sigma'_{p\,[MPa]})^T \qquad 6-1$$

where S_1 and T are fitting parameters equal to 0.366 and -0.024 respectively. The parameter S_1 is an apparent intercept value produced by extrapolating the regression to $\sigma'_{vc} = 1$ kPa. A stress level of 1 kPa is chosen as an intercept value simply because it allows a consistent trend in S_1 as a function of soil type to be detected, as will be discussed in Section 6.9.1. The parameter T describes the change in undrained strength ratio with stress, so that a lower value of T (i.e. more negative) indicates a faster reduction in strength ratio with increasing stress.

Figure 6-7 plots curves of normalized secant Young's modulus versus axial strain on log scales for the tests performed in this work. The axial strain measurements were only performed externally using either an LVDT (low and medium pressure cells) or a string pot (high pressure cell). As a result, values of Young's modulus below $\varepsilon_a = 0.01$ % show a large amount of scatter (particularly for the string pot) and are therefore not included in Figure 6-7. In general, Figure 6-7 illustrates that the soil exhibits strong non-linearity and that yielding occurs at small strains. Increasing consolidation stress causes a reduction in the normalized initial Young's modulus of the soil. It also tends to produce a larger strain range of linear behavior. These observations are to be expected, with similar findings reported by Santagata (1998) and Abdulhadi (2009). Tests TX1030 and TX1031 performed at $\sigma'_{vc} = 9.81$ and 5.87 MPa respectively are not included in Figure 6-7 because the calculated Young's moduli are significantly affected by apparatus compressibility and are believed to be in error.

Figure 6-8 plots the normalized shear induced pore pressures measured in the tests. As expected for a NC soil, positive shear induced pore pressures are generated during shearing indicating contractive behavior. It can be seen that there is very good repeatability between tests, although TX1030 does show slightly higher pore pressures at a given axial strain compared to the other tests. Stress level does not appear to have any effect on the normalized shear induced pore pressures generated. At large strains the pore pressures tend to level off as a critical state condition is developed, with values of u_s/σ'_{vc} ranging between about 0.25 – 0.29. This is in contrast to the finding of Abdulhadi (2009), who reported normalized shear induced pore pressures at critical state which decreased consistently from about 0.35 at 0.1 MPa to 0.30 at 10 MPa.

Combining stress-strain and pore pressure data, Figure 6-9 plots the effective stress paths for the tests on NC RBBC. The stress paths are drawn in normalized MIT q-p' space, i.e. $(\sigma_v - \sigma_h)/2\sigma'_{vc}$ versus $(\sigma'_v + \sigma'_h)/2\sigma'_{vc}$. Different starting points for the tests are due to an increasing pre-shear K_{ONC} with increasing stress level, a behavior discussed previously in Section 5.4. However, the general shape of the effective stress path followed in each test remains very similar. The generation initially of low shear induced pore pressures causes the stress path to rise slightly to the right. A clear yield point is then reached, after which the generation of large shear induced pore pressures causes the effective stress to decrease and the stress path to travel to the left before reaching the large strain Mohr-Coulomb failure envelope. Consistent with what is observed in Figure 6-4, increasing stress level causes the effective stress paths to reach lower normalized strengths. In addition, at low stress the yield point of the stress path coincides with peak shear strength. At higher stresses, on the other hand, the point of peak shear strength occurs further down the stress path and does not coincide with the yield point, i.e. peak shear strength occurs at a lower normalized effective stress. Increasing stress level also causes the stress paths to reach lower Mohr-Coulomb failure envelopes, with φ'_{cs} reducing from an average of about 31.7° at 0.56 MPa to 29.0° at 40.5 MPa. The reductions in both normalized shear stress and effective stress at failure explains why the secant friction angle at peak shear strength (φ'_p) does not display any clear dependence on stress level, remaining in the range of 23.5° to 26.2° for the 5 tests.

Figure 6-10 shows the relationships between normalized undrained strength and pre-shear K_O for NC RBBC as found in this work, Abdulhadi (2009) and Santagata (1994). In each case a trend of decreasing s_u/σ'_{vc} with increasing K_{ONC} is observed, although linear regressions through the data of each experimental program yield slightly different equations. It should be noted that Santagata's relationship is based on results from triaxial tests performed on RBBC Series III, with some tests involving K_O consolidation and others involving stress path consolidation with a prescribed value of K. However, it can be seen that the relationship determined in this work is more similar to that of Santagata (1994) than that of Abdulhadi (2009), who predicts a much greater sensitivity of undrained strength to K_{ONC}. Figure 6-10 also includes an aggregate correlation based on a combination of the data from all three studies. The relationship between s_u/σ'_{vc} and K_{ONC} is discussed further in Section 6.9.4, where similar results for other soils are presented and compared.

6.3.2 Overconsolidated Behavior

Figure 6-11 shows the shear stress-strain responses measured in representative tests carried out on RBBC at OCRs 1, 2, 4 and 8. For each OCR, tests at a low (0.6 MPa) and high (40 MPa) preconsolidation stress are presented. The low stress tests on OC RBBC (TX16, TX40 and TX47) were performed by Sheahan (1991). As expected, when normalized with respect to the pre-shear vertical effective stress, undrained strength increases considerably with increasing OCR. Increasing OCR also leads to a more ductile behavior for RBBC, with strain to failure increasing and post-peak strain softening reducing. At a given OCR, increasing effective stress leads to a reduction in undrained strength ratio and an increase in strain to failure. The effects of both stress level and OCR on the strain to failure are illustrated more clearly in Figure 6-12, which plots strain to failure versus OCR for $\sigma'_p = 0.2$, 10 and 40 MPa. At a given stress level, ε_f increases approximately linearly with increasing OCR, as indicated by regression lines through the experimental data. The results presented in Figure 6-12 also demonstrate that the increase in strain to failure associated with stress level occurs to essentially the same extent at each OCR.

With regard to the effect of stress level on undrained strength ratio, Figure 6-11 shows that it is the same as that observed for OCR = 1 and discussed in Section 6.3.1., i.e. increasing consolidation stress leads to a reduction in undrained strength ratio at a given OCR. This is demonstrated more clearly in Figure 6-13, which plots the variation in the undrained strength ratio of RBBC at OCRs 1, 2, 4 and 8 versus preconsolidation stress. Figure 6-13 includes a compilation of data from this work, Sheahan (1991) and Abdulhadi (2009). The variation in strength ratio at each OCR is described by a regression of the same form as given in Equation 6-1. It can be seen that the values of the T parameter determined at each OCR vary by a relatively small amount and show no trend with OCR. This result indicates that increasing consolidation stress reduces undrained strength ratio by essentially the same proportion at each OCR. A similar conclusion was reached by Abdulhadi (2009). The consistency of the results presented in Figure 6-13 is quite impressive when one considers that they were obtained by three different researchers using different triaxial systems over an approximately 25 year time period.

As discussed in Chapter 2, the SHANSEP normalization procedure developed by Ladd and Foott (1974) assumes a constant undrained strength ratio for a soil at a given OCR. Abdulhadi (2009) has shown that for RBBC the procedure breaks down because the soil exhibits a consistent variation in strength ratio when viewed over a significant stress range. The effect of stress level on the SHANSEP S and m parameters is summarized in Figure 6-14. Again, the figure includes a compilation of data from this work, from Sheahan (1991) and from Abdulhadi (2009). Consistent with the results presented above, increasing stress level leads to a reduction in the S parameter. The value of S reduces from 0.311 at 0.6 MPa to 0.291 at 40 MPa. Figure 6-14 also seems to indicate that increasing stress causes a reduction in the m parameter of RBBC. However, this variation in the m parameter is believed instead to be the result of random scatter in the OC data at the particular stress levels included in Figure 6-14. As discussed above, regression lines through all of the available data at each OCR indicate that increasing consolidation stress reduces undrained strength ratio by essentially the same proportion at each OCR, a result which points to an m parameter that is independent of stress level. The m parameters presented in Figure 6-14 for the three selected stress levels are also quite low when compared to previously quoted values, e.g. from Ladd (1991) and Abdulhadi (2009).

Based on the data shown in Figure 6-13, a weighted average value of T = -0.025 was calculated from the undrained strength ratios at all OCRs. The regression lines through the data at each OCR are therefore modified and forced to have T = -0.025, which in turn changes the equivalent values of S_1 at each OCR (henceforth denoted as S_{1OC}) from those given in Figure 6-13. The modified regression lines are shown in Figure 6-15, which plots best-fit power-law functions through the experimental data with the constraint that T has a value of -0.025. The values of S_{1OC} given in Figure 6-15 are plotted against OCR in Figure 6-16. Figure 6-16 is similar to the typical SHANSEP method for presenting results of a laboratory shear test program, and a regression line through the data in Figure 6-16 yields an equation of the form:

$$S_{1OC} = S_1(OCR)^m \qquad 6-2$$

where S_1 for NC RBBC is 0.368 and m = 0.73. While Equation 6-2 is similar to the conventional SHANSEP equation (Equation 2-1), it is important to keep in mind that the data points shown in Figure 6-16 are not measured undrained strength ratios, rather they are values obtained using the curve fitting procedure described above. While the SHANSEP S parameter is a physically measured strength ratio, the S_1 parameter used in the modified procedure is an apparent value determined by extrapolating the regression line (given by Equation 6-1) to $\sigma'_{vc} = 1$ kPa (the S_1 parameter can be thought of as being similar to an apparent cohesion intercept c'). A stress level of 1 kPa is chosen as an intercept value simply because it allows a consistent trend in S_1 as a function of soil type to be detected, as will be discussed in Section 6.9.1.

Figure 6-17 plots curves of normalized secant Young's modulus versus axial strain on log scales for OCRs 1, 2, 4 and 8. The figure includes data from the same high stress tests as shown in Figure 6-11 (unfortunately low stress E_u data were not reported by Sheahan (1991)). As expected, when normalized with respect to σ'_{vc}, Young's modulus increases considerably with increasing OCR. At $\varepsilon_a = 0.01$ % for example, E_u/σ'_{vc} increases from approximately 150 at OCR = 1 to over 1,000 at OCR = 8. Most of this increase is associated with the transition from the NC to OC regimes as the pre-shear condition moves inside the yield surface, with less increase being associated with further increasing OCR. The shape of the curves remains essentially the same at each OCR.

The effect of stress level on normalized Young's modulus is illustrated in Figure 6-18, which plots values of E_u/σ'_{vc} measured at $\varepsilon_a = 0.01$ % versus consolidation stress for OCRs 1, 2, 4 and 8. At a given OCR, the normalized modulus of the soil can be seen to decrease with increasing stress. For NC RBBC, E_u/σ'_{vc} at $\varepsilon_a = 0.01$ % decreases from approximately 500 at low stresses to 70 at 100 MPa. The tendency for the normalized modulus of RBBC to decrease with increasing consolidation stress is to be expected, with a similar finding reported previously by both Santagata (1998) and Abdulhadi (2009). Figure 6-18 also includes the relationship for the initial maximum Young's modulus (E_{uMAX}) of RBBC proposed by Santagata (1998):

$$E_{uMAX} = 270e^{-2.45}\sigma'_{vc}{}^{0.43} \text{ (MPa)} \qquad 6-3$$

Santagata (1998) performed a large number of tests to investigate the small strain behavior of RBBC up to approximately 2 MPa using internal strain measurement. Figure 6-18 also includes the extrapolation of this relationship for stresses up to 100 MPa. The relationship is plotted assuming a particular VCL for RBBC based on the results of a CRS test (CRS1157) performed by the author, i.e. it assumes OCR = 1 (similar relationships for OCRs > 1 would lie above the line plotted in Figure 6-18). It is important to keep in mind that the values of E_u/σ'_{vc} determined at $\varepsilon_a = 0.01$ % by the author are not directly comparable to the E_{uMAX} relationship proposed by Santagata (1998). The reliance on external strain measurement in the author's work means that values of E_u are difficult to interpret at $\varepsilon_a < 0.01$ %. However, internal strain measurement allowed Santagata to measure Young's modulus at strains as low as 0.0001 %, and it was demonstrated that RBBC typically exhibits modulus degradation at strains $\varepsilon_a < 0.01$ %. For OC RBBC, E_u drops to about 95 % of its initial maximum value at $\varepsilon_a = 0.01$ %. At OCR = 1, however, yielding can begin at strains as low as 0.001 % and Young's modulus is reduced to about 75 % of its initial maximum value at $\varepsilon_a = 0.01$ % (Santagata 1998). Despite this, the author's limited data at OCR = 1 appear to be consistent with the relationship proposed by Santagata for $\sigma'_p < 10$ MPa. At higher stresses, however, Santagata's relationship tends to greatly overpredict the measured data. This is not surprising given that Santagata only measured data up to 2 MPa, and the author's results are believed to more accurately reflect behavior at higher stresses.

The Young's moduli measured in many of the triaxial tests performed in the medium pressure triaxial cell at $\sigma'_p = 10$ MPa are not included in Figure 6-18. This is because apparatus compressibility in the medium pressure triaxial system has a significant effect on the small strains calculated at the very beginning of shearing (when the axial load increases rapidly), even after a correction is applied to account for apparatus compressibility. As a result, reliable values of Young's modulus often cannot be interpreted from these tests.

Figure 6-19 plots the normalized shear induced pore pressures measured in the same tests as shown in Figure 6-11. As expected, the shear induced pore pressures change from positive for the NC soil to increasingly negative at greater OCRs. This reflects a shift from entirely contractive behavior at OCR = 1 to increasing dilative behavior with increasing overconsolidation. Increasing stress level tends to reduce the absolute value of u_s/σ'_{vc} for the OC soil at small strains. This effect is observed most clearly at OCR = 8, where at $\varepsilon_a = 2$ % the normalized pore pressure generated at 40 MPa is less than half that generated at 0.6 MPa. However, as a critical state condition is developed at large strains the normalized pore pressures converge at each OCR and become less affected by stress level.

Combining stress-strain and pore pressure data, Figure 6-20 plots the effective stress paths for the same tests. The stress paths are normalized with respect to σ'_p (unlike Figure 6-11, Figure 6-17 and Figure 6-19 where stresses are normalized with respect to σ'_{vc}). At OCR = 1 the soil exhibits entirely contractive behavior and the stress paths travel far to the left before reaching the Mohr-Coulomb failure envelope at large strains. Upon reaching the failure envelope, the stress paths travel down the envelope. At OCRs 4 and 8 the soil exhibits dilative behavior as negative shear induced pore pressures are generated and the stress paths travel up the envelope prior to reaching a peak shear strength. An intermediate type behavior is observed at OCR = 2. Regardless of the OCR, all tests for a given σ'_p reach a fairly common failure envelope at critical state. However, this failure envelope exhibits significant curvature, decreasing from an average φ'_{cs} of 33.6° at 0.6 MPa to 27.8° at 40 MPa (note that these are secant values of friction angle). For the OC soil, the larger (i.e. more negative) normalized shear induced pore pressures generated at low stress also cause the stress paths for these tests to be pushed further to the right when compared to the stress paths at high stress.

The reduction in the critical state friction angle of RBBC with stress level is illustrated in Figure 6-21, where stress level is defined in terms of σ'_p. The figure includes a compilation of data from this work, Sheahan (1991) and Abdulhadi (2009). The friction angle reduces from almost 40° at 0.15 MPa to as low as 27° at 100 MPa[6], indicating a failure envelope which possesses significant curvature. Most of the decrease in φ'_{cs} occurs at stresses < 1 MPa. In general, when viewed at a given stress level, φ'_{cs} shows no dependence OCR. However, the

---

[6] The test performed at $\sigma'_p = 100$ MPa and OCR = 1 (TX1193) exhibited a small external leak during undrained shearing. As a result, the undrained behavior of the soil in this test could not be determined, although a friction angle could be obtained.

results at OCR = 8 do not appear to follow this behavior and display only a slight decrease in φ'_{cs} with stress, remaining significantly above the lower OCR data at high stresses. The variation in φ'_{cs} as a function of stress level can be described by a power-law regression through the data at OCR = 1:

$$\varphi'_{cs} = A(0.001\sigma'_{p\,[MPa]})^B \qquad 6-4$$

where A and B are fitting parameters equal to 24.0 and -0.044 for RBBC respectively. The A parameter is an apparent intercept value produced by extrapolating the regression to σ'_{vc} = 1 GPa. A stress level of 1 GPa is chosen as an intercept value as it allows for a consistent trend in A as a function of soil type to be detected, as will be discussed in Section 6.9.2. The parameter B describes the change in friction angle with stress, so that a lower value of B (i.e. more negative) indicates a faster reduction in friction angle with increasing stress.

6.3.3 Critical State Behavior

Critical state soil mechanics is based on an idealized soil behavior in which, at sufficiently large strains, shearing progresses without any change in pore pressure (or volume in the case of drained conditions), effective stress or shearing resistance. For triaxial testing in the laboratory, this idealized behaviour is difficult to achieve with certainty as non-uniform stresses and localized deformations occur at moderate strains and it becomes difficult to calculate the exact area of the specimen (and hence stresses) with accuracy. This being said, triaxial tests performed on resedimented materials typically do approximate this idealized behavior. Figure 6-22 plots the mean effective stresses ($p'_m = (\sigma'_1+\sigma'_2+\sigma'_3)/3$) and shear stresses at critical state for RBBC in void ratio-[log]stress space. The figure excludes the results of test TX1030 where the calculated void ratio is believed to be in error. The results of two triaxial extension tests performed by the author (discussed in more detail in Section 6.10.1) are also included in Figure 6-22[7]. Regression lines plotted through the data points yield the critical state lines (CSLs) of effective stress and shear stress for the soil. Figure 6-22 also includes the K_O virgin compression line of RBBC as determined from representative triaxial tests (TX727 performed by Abdulhadi 2009). According to critical state soil mechanics theory, the virgin compression line and critical

---

[7] Since the value of q at critical state is negative for extension tests, absolute values of q are plotted in Figure 6-22

state lines of a soil should remain log-linear and parallel to one another. However, the highest stress data points in Figure 6-22 indicate that the critical state and virgin compression lines of RBBC begin to flatten out at void ratios below about 0.35, deviating from a log-linear relationship. Furthermore, the CSLs of effective stress and shear stress tend to diverge slightly with increasing stress level. This reflects the fact that the critical state friction angle of RRBC decreases with increasing consolidation stress, as illustrated in Figure 6-21.

6.4 RESEDIMENTED PRESUMPSCOT CLAY

This section describes the undrained shear behavior of Resedimented Presumpscot Clay at OCR = 1. Figure 6-23 shows the normalized shear stress-strain responses measured during undrained shearing for the 5 tests performed on the soil at consolidation stresses ranging from 0.24 MPa to 101 MPa. In terms of the peak normalized shear strength reached in each test, there is no clear trend with consolidation stress level. This is in contrast to the behavior of RBBC where a stress level dependence of normalized strength is observed. The undrained strength ratio of RPC only varies between 0.299 and 0.317 over the entire stress range, and small differences in s_u/σ'_{vc} values between triaxial tests is likely the result of experimental non-repeatability. However, the form of the stress-strain curve for RPC displays significant stress level dependence. Similar to what was observed for RBBC, the shearing behavior of RPC becomes more ductile with increasing consolidation stress. There is a consistent and dramatic increase in strain to failure with stress level, with ε_f increasing from just 0.28 % at 0.24 MPa to almost 5 % at 101 MPa. The amount of post-peak strain softening also generally reduces with increasing stress, with almost no strain softening observed at 101 MPa. However, at the lowest stress level of 0.24 MPa the soil exhibits significant strain hardening following an initial peak stress, and the highest shear stress mobilized in the test actually occurs at large strains (although the quoted values of $s_u/\sigma'_{vc} = 0.299$ and $\varepsilon_f = 0.28$ % correspond to the initial peak in the stress-strain curve). The shearing behavior of RPC at small strains is illustrated more clearly in Figure 6-24, which plots the stress-strain responses for axial strains up to 2 %.

Figure 6-25 plots curves of normalized secant Young's modulus versus axial strain on log scales for the tests on RPC. Since axial strain measurements were performed externally, values of Young's modulus are only plotted for $\varepsilon_a > 0.01$ %. In addition, the Young's modulus of RPC measured in test TX1093 (performed in the medium pressure triaxial cell) is significantly affected by apparatus compressibility and is therefore not included in Figure 6-25. Unlike RBBC, increasing consolidation stress appears to have no consistent effect on the normalized Young's modulus of the soil, and curves of E_u/σ'_{vc} generally show good repeatability between tests. While TX1208 performed at the highest stress of 101 MPa shows a very different response compared to the other tests, this is probably due to an experimental issue and may not reflect the true behavior of the soil. A cause for the apparently erroneous measurements of Young's modulus in TX1208 could not be determined.

Figure 6-26 plots the shear induced pore pressures measured in the same tests. Unlike RBBC, which displays essentially no change in normalized pore pressure generation with stress level, RPC shows a remarkably consistent trend of decreasing u_s/σ'_{vc} with increasing consolidation stress. The value of u_s/σ'_{vc} at critical state reduces from about 0.27 at very low stresses to 0.20 at 101 MPa. This result indicates a less contractive behavior at higher stresses. For the highest stress test, the soil even produces a small negative shear induced pore pressure at the initial stages of shearing.

Figure 6-27 plots the effective stress paths for the tests carried out on NC RPC. Different starting points for the stress paths are due to inconsistent variations in the pre-shear K_{ONC} for different tests. Apart from the lowest stress test (TX1096), the shape of the stress paths is fairly similar to that observed for NC RBBC. The generation initially of low shear induced pore pressures causes the stress paths to rise slightly to the right. A clear yield point is then reached in all tests, after which the generation of large positive shear induced pore pressures causes the effective stress to decrease and the stress paths to travel to the left before reaching the large strain Mohr-Coulomb failure envelope. Increasing consolidation stress causes the stress paths to reach lower failure envelopes, with φ'_{cs} reducing from 36.7° at 0.24 MPa to 28.7° at 101 MPa. Consistent with what is observed in Figure 6-23, increasing stress level does not have any significant impact on the peak shear strength reached in the tests. Furthermore, the friction angle mobilized at peak strength does not display any clear trend with stress level, remaining in the range of 24.8° to 27.5° for the 5 tests.

Somewhat unexpected behavior is observed in the lowest stress test shown in Figure 6-27, i.e. TX1096 at 0.24 MPa. Once the stress path for this test reaches the failure envelope at large strains, it then reverses direction and travels up the failure envelope. This result is consistent with the strain hardening behavior presented in Figure 6-23 and with the decrease in shear induced pore pressures observed in the test at large strains in Figure 6-26. The behavior is similar to that which could be expected for a normally consolidated silt at low stress (Grennan 2010), and is not exceptionally unusual when one considers the fact that RPC is a low plasticity clay (w_L = 33.1 %) that possesses a large silt fraction (particles > 2μm) of 63 %.

6.5 RESEDIMENTED GoM URSA CLAY

This section describes the undrained shear behavior of Resedimented GoM Ursa Clay at OCR = 1. Figure 6-28 shows the normalized shear stress-strain responses measured during undrained shearing for the 4 tests performed on the soil at consolidation stresses ranging from 0.19 MPa to 84.8 MPa. The normalized undrained strength of the clay decreases consistently with increasing consolidation stress, from 0.311 at 0.19 MPa to 0.223 at 84.8 MPa. The response of the soil also becomes much more ductile with increasing stress. The strain to failure increases from 0.47 % at the lowest stress to 4.90 % at 84.8 MPa, and the amount of post-peak strain softening also reduces dramatically. In TX1077 the pore and cell pressures were increased by a large amount during shearing after ε_a = 6.7 %. This was done as part of an investigation into the principle of effective stress, as discussed previously is Section 6.2. The process of applying these large pressure increments in the triaxial cell produces 'jumps' in the stress-strain curve, and as a result the response is only plotted to ε_a = 6.7 %. The small strain behavior of RGoM Ursa can be observed more clearly in Figure 6-29, where the normalized stress-strain responses are plotted for axial strains only up to 2 %.

Figure 6-30 plots curves of normalized secant Young's modulus versus axial strain on log scales for tests on RGoM Ursa. The Young's modulus of the soil measured in TX1072 is significantly affected by apparatus compressibility and is therefore not included in Figure 6-30. It appears that increasing consolidation stress causes a reduction in E_u/σ'_{vc} of the soil. While two tests performed at 0.19 MPa and 0.63 MPa display a very similar normalized response, the highest stress test performed at 84.8 MPa has a much lower normalized Young's modulus.

Figure 6-31 plots the normalized shear induced pore pressures measured in the tests performed on RGoM Ursa. Stress level appears to have no effect on the normalized pore pressures for σ'_{vc} up to 10 MPa, with tests up to this stress displaying good repeatability in terms of pore pressure generation. In the highest stress test (TX1218) performed at σ'_{vc} = 84.8 MPa, however, dramatically lower normalized pore pressures are measured at the beginning of shearing. It is possible that this reflects a true behavior, with the soil becoming less contractive at high stresses (similar to what is observed for RPC). However, it is also possible that this is due to apparatus compressibility of the drainage system combined with the low permeability of the soil at this stress level (less than 10^{-19} m^2). As discussed in Section 4.2.7, apparatus compressibility of the drainage system in the high pressure triaxial cell becomes increasingly important at stresses approaching 100 MPa, as both the true and measurable B-values of the soil decrease significantly. Apparatus compressibility leads to a small quantity of pore fluid flowing from the specimen into the drainage lines during undrained shearing. Combined with the low permeability of the soil, this results in a misleadingly low excess pore pressure being measured at the beginning of shearing. At large strains, however, the normalized pore pressures measured in TX1218 approach the same as those measured in the low stress tests. This may be due to pore pressures within the specimen equilibrating and becoming more uniform as a critical state condition is developed. A similar argument could help explain the small negative shear induced pore pressures measured for RPC at the beginning of shearing, as shown in Figure 6-26. However, the considerably higher permeability of RPC at this consolidation stress means that the effect on the measured pore pressures is much smaller.

Figure 6-32 plots the effective stress paths for the tests on RGoM Ursa. Different starting points for the stress paths are due to a consistent increase in the K_{ONC} of the soil from 0.52 at 0.19 MPa to 0.78 at 73 MPa[8]. However, the general shape of the stress path followed in each test remains similar. Consistent with what is observed in Figure 6-32, increasing stress level causes the effective stress paths to reach lower normalized strengths. At low stress the yield point of the stress path coincides with peak shear strength. At higher stresses, however, the point of peak shear strength occurs much further down the stress path and does not coincide with the yield

---

[8] A control malfunction occurred in TX1218 at σ'_{vc} =73 MPa. As a result, the K_O data for this test is not considered reliable from σ'_v = 73 MPa to the end of the test at σ'_{vc} = 84.8 MPa

point. Increasing stress level also causes the stress paths to reach considerably lower Mohr-Coulomb failure envelopes, with φ'_{cs} reducing from 29.2° at 0.19 MPa to just 18.1° at 84.8 MPa. The friction angle of RGoM Ursa at peak shear strength also displays a significant stress level dependence, reducing from 24.6° at 0.19 MPa to as low as 15.9° at 84.8 MPa.

6.6 RESEDIMENTED UGNU CLAY

This section describes the undrained shear behavior of Resedimented Ugnu Clay at OCR = 1. Figure 6-33 shows the normalized shear stress-strain responses measured during undrained shearing for 4 representative tests performed on the soil at consolidation stresses ranging from 0.19 MPa to 105 MPa. The lower stress tests (TX962 and TX969) were performed by Jones (2010) while the higher stress tests were performed by the author. The normalized undrained strength of the clay decreases consistently with increasing consolidation stress, from 0.344 at 0.19 MPa to 0.215 at 105 MPa. The response of the soil also becomes more ductile with increasing stress. The strain to failure increases from 0.19 % at the lowest stress to over 5 % at 105 MPa, and the amount of post-peak strain softening reduces dramatically. In TX1092 a problem was encountered with the control system at the beginning of the test. As a result, slight fluctuations are present in the measured shear stress and the exact point of peak strength is difficult to establish. The increase in the strain to failure of the soil can be observed more clearly in Figure 6-34, where the normalized stress-strain responses are plotted only for axial strains up to 2 %.

Figure 6-35 plots curves of normalized secant Young's modulus versus axial strain on log scales for tests on RUC. The Young's modulus of RUC measured in TX1092 is significantly affected by apparatus compressibility and is therefore not included in Figure 6-35. Instead, the figure includes the results of TX918 which was performed by Jones (2010) at $\sigma'_{vc} = 9.8$ MPa. Similar to RBBC, increasing consolidation stress results in a decrease in the normalized Young's modulus of the soil, with E_u/σ'_{vc} at $\varepsilon_a = 0.01$ % decreasing from 450 at 0.19 MPa to 80 at 105 MPa. Increasing consolidation stress also produces a larger strain range of linear behavior in the soil.

Figure 6-36 plots the normalized shear induced pore pressures measured in the tests performed on RUC. Stress level appears to have no effect on the normalized pore pressures for σ'_{vc} up to 10 MPa, with tests up to this stress displaying good repeatability in terms of pore pressure generation. In the highest stress test (TX1198) performed at σ'_{vc} = 105 MPa, however, dramatically lower normalized pore pressures are measured. Similar to the results for RGoM Ursa discussed in Section 6.5, this may reflect a true behavior of the soil, or may be due to a low B-value combined with the low permeability of the soil at that stress level. The lower shear induced pressures measured in TX1216 have only a minor effect on the shape of the effective stress path for the test.

Figure 6-37 plots the effective stress paths for the selected tests on RUC. Different starting points for the stress paths are due to a considerable increase in the K_{ONC} of RUC from approximately 0.48 at 0.19 MPa to 0.73 at 105 MPa. However, the general shape of the stress path followed in each test remains similar. Consistent with what is observed in Figure 6-33, increasing stress level causes the effective stress paths to reach lower normalized strengths. In addition, at low stress the yield point of the stress path coincides with peak shear strength. At higher stresses, on the other hand, the point of peak shear strength occurs further down the stress path and does not coincide with the yield point. Increasing stress level also causes the stress paths to reach lower Mohr-Coulomb failure envelopes, with φ'_{cs} reducing from 33.2° at 0.19 MPa to 17.2° at 105 MPa. The friction angle of RUC at peak shear strength also displays a very strong stress level dependence, reducing from 27.1° at the lowest stress to just 14.8° at 105 MPa.

6.7 RESEDIMENTED SAN FRANCISCO BAY MUD

This section describes the undrained shear behavior of Resedimented San Francisco Bay Mud at OCR = 1. Figure 6-38 shows the shear stress-strain responses measured during undrained shearing for 4 representative tests performed on the soil at consolidation stresses ranging from 0.19 MPa to 83.0 MPa. The lower stress tests (TX901S1 and TX977S2) were performed by Kontopoulos (2012) while the higher stress tests were performed by the author. The nature of the research conducted by Kontopoulos (2012) meant that, in many of triaxial tests performed, undrained shearing was not carried out to large strains. The normalized undrained strength of the clay decreases consistently with increasing consolidation stress, from a relatively high value of

0.388 at 0.19 MPa to 0.236 at 83.0 MPa. The response of the soil also becomes more ductile with increasing stress. The strain to failure increases from 0.29 % at the lowest stress to 4.65 % at 83.0 MPa, and the amount of post-peak strain softening reduces dramatically. The increase in the strain to failure of the soil can be observed more clearly in Figure 6-39, where the normalized stress-strain responses are plotted only for axial strains up to 2 %.

Figure 6-40 plots curves of normalized secant Young's modulus versus axial strain on log scales for tests on RSFBM. The figure shows that the soil exhibits strong non-linearity and that yielding occurs at small strains. Increasing consolidation stress has a very large effect on the normalized Young's modulus of the soil, with E_u/σ'_{vc} at $\varepsilon_a = 0.01$ % decreasing from just over 1000 at 0.19 MPa to less than 100 at 83.0 MPa. Increasing consolidation stress also produces a much larger strain range of linear behavior for the soil. The results of TX1079 at 9.5 MPa are not consistent with these overall trends, however, displaying the same E_u/σ'_{vc} at $\varepsilon_a = 0.01$ % as the highest stress test and showing a more rapid deterioration in normalized Young's modulus at large strains compared to any other test.

Figure 6-41 plots the shear induced pore pressures measured in the same tests. Based on the limited data available from the low stress tests of Kontopoulos (2012), it appears that stress level has relatively little effect on the normalized shear induced pore pressures generated within RSFBM for stresses up to 10 MPa. However, TX1216 at $\sigma'_{vc} = 83$ MPa produced significantly lower normalized pore pressures. Similar to the results for RGoM Ursa and RUC discussed in Sections 6.5 and 6.6 respectively, this may reflect a true behavior of the soil, or may be due to a low B-value combined with the low permeability of the soil at that stress level. The lower shear induced pressures measured in TX1216 have only a minor effect on the shape of the effective stress path for the test.

Figure 6-42 plots the effective stress paths for the tests on RSFBM. Different starting points for the stress paths are due to a consistent increase in the K_{ONC} of the soil with increasing consolidation stress. However, the general shape of the stress path followed in each test remains similar. Consistent with what is observed in Figure 6-38, increasing stress level causes the effective stress paths to reach lower normalized strengths. In addition, at low stress the yield point of the stress path coincides with peak shear strength. At higher stresses, on the other hand, the point of peak shear strength occurs much further down the stress path and does not coincide with the yield point. Increasing stress level also causes the stress paths to reach considerably lower Mohr-Coulomb failure envelopes, with φ'_{cs} reducing from a relatively high value of 36.6° at 0.19 MPa to just 18.4° at 83.0 MPa. The friction angle of the soil at peak shear strength also displays a very strong stress level dependence, reducing from 32.0° at the lowest stress to 17.2° at 83.0 MPa.

6.8 RESEDIMENTED LONDON CLAY

This section describes the undrained shear behavior of Resedimented London Clay at OCR = 1. Figure 6-43 shows the stress-strain responses measured during undrained shearing for the 5 tests performed on the soil at consolidation stresses ranging from 0.15 MPa to 11.8 MPa. The normalized undrained strength of the clay decreases consistently and very dramatically with increasing consolidation stress, from 0.288 at 0.15 MPa to just 0.155 at 11.8 MPa. The response of the soil also becomes much more ductile with increasing stress. The strain to failure increases from 0.29 % at the lowest stress to 3.39 % at 11.8 MPa, and the amount of post-peak strain softening also reduces dramatically. The increase in the strain to failure of the soil can be observed more clearly in Figure 6-44, where the normalized stress-strain responses are plotted only for axial strains up to 2 %.

Figure 6-45 plots curves of normalized secant Young's modulus versus axial strain on log scales for tests on RUC. The figure shows that the soil exhibits strong non-linearity and that yielding occurs at small strains. An anomalous jump in the measured data is present in test TX1127. There is no clear effect of consolidation stress level on the initial normalized Young's modulus of the soil. The 4 tests performed at $\sigma'_{vc} < 2$ MPa show very similar normalized moduli, with values of E_u/σ'_{vc} at $\varepsilon_a = 0.01$ % between about 200 and 300. However, the test performed at the highest stress of 11.8 MPa displays a somewhat lower normalized modulus, with $E_u/\sigma'_{vc} = 130$ at $\varepsilon_a = 0.01$ %.

Figure 6-46 plots the shear induced pore pressures measured in the same tests. Similar to what is observed for Young's modulus, there is no obvious effect of stress level on the normalized shear induced pore pressures, although the highest stress test at 11.8 MPa displays the highest normalized pore pressures.

Figure 6-47 plots the effective stress paths for the tests on RLC. Different starting points for the stress paths are due to a dramatic increase in the K_{ONC} of RLC from 0.56 at 0.15 MPa to 0.79 at 11.8 MPa. However, the general shape of the stress path followed in each test remains similar. Consistent with what is observed in Figure 6-43, increasing stress level causes the effective stress paths to reach lower normalized strengths. In addition, at low stress the yield point of the stress path coincides with peak shear strength. At higher stresses, on the other hand, the point of peak shear strength occurs much further down the stress path and does not coincide with the yield point. At the highest stress level of 11.8 MPa, for example, the point of peak shear strength occurs on the failure envelope. Increasing stress level also causes the stress paths to reach considerably lower Mohr-Coulomb failure envelopes, with φ'_{cs} reducing from 24.7° at 0.15 MPa to a very low value of just 12.7° at 11.8 MPa. The friction angle of RLC at peak shear strength also displays a very strong stress level dependence, reducing from 21.5° at 0.15 MPa to as low as 11.8° at 11.8 MPa.

6.9 SUMMARY AND COMPARISON OF RESULTS

6.9.1 Undrained Strength

Figure 6-48 summarizes the variation in undrained strength ratio with stress level for the soils tested in this work. In addition to the author's results, the figure includes data from Jones (2010) for RUC, Kontopoulos (2012) for RSFBM and Sheahan (1991) and Abdulhadi (2009) for RBBC. Furthermore, Figure 6-48 includes data on Skibbereen Silt (SS) which was tested exclusively by Grennan (2010) and Resedimented GoM Eugene Island Clay (RGoM EI) which was tested exclusively by Fahy (2014) (except for TX1209 which was performed by the author). In general, there is a very wide range in undrained strength ratios across the different soil types and consolidation stresses. The soils included in the dataset originate from a very diverse set of geologic backgrounds, and cover practically the entire range of strength behaviors that would be expected for natural sedimentary fine-grained soils. As discussed previously, most soils exhibit a consistent variation in undrained strength ratio with stress level, deviating from ideal normalized behavior. These variations in strength ratio are illustrated more clearly in Figure 6-49, which plots the calculated regression lines through the data of each soil. These regression lines are of the form given in Equation 6-1.

There is in fact an underlying trend to the behavior presented in Figure 6-49. For example, the soil with the highest liquid limit, RGoM EI, displays the most rapid reduction in strength ratio with increasing stress. A soil with a medium liquid limit, such as RBBC, displays a moderate reduction in strength ratio. On the other hand, the soil with the lowest liquid limit, SS, shows a slight increase in strength ratio with increasing stress. Essentially, the direction and rate to which the normalized strength of a soil varies as a function of stress level is related to the soil's liquid limit, where liquid limit is a reflection of soil composition. Figure 6-50 and Figure 6-51 plot the S_1 and T parameters respectively for the soils against liquid limit. The correlation between S_1 and w_L presented in Figure 6-50 is closely approximated, with r^2 of 0.97, by the following log-linear equation:

$$S_1 = 0.86\log(w_{L[\%]}) - 1.04 \qquad 6\text{-}5$$

Recalling that the parameter S_1 is defined as the undrained strength ratio at $\sigma'_{vc} = 1$ kPa, the relationship presented in Figure 6-50 predicts that high plasticity soils have a much greater shear strength at very low effective stresses. However, it is important to keep in mind that measured data have only been obtained for σ'_{vc} as low as about 0.1 MPa. The S_1 parameter is an apparent value determined by extrapolation of Equation 6-1 to an effective stress two orders of magnitude lower than the measured data, and may therefore not possess a physical meaning.

The relationship between the parameter T and w_L presented in Figure 6-51 is well approximated, with r^2 of 0.95, by a log-linear equation:

$$T = -0.46\log_{10}(w_{L\,[\%]}) + 0.73 \qquad 6\text{-}6$$

Recalling that a lower value of T implies a faster reduction in strength ratio with increasing stress level, the relationship given in Figure 6-51 indicates that high plasticity soils display a more rapid reduction in normalized undrained strength with increasing consolidation stress. Equivalently, high plasticity soils show a greater sensitivity of normalized undrained strength to stress level. Table 6-2 summarizes the values of S_1 and T for the fine-grained soils included in this work, together with the r^2 values associated with each regression (where the regressions are of the form given in Equation 6-1). As discussed previously in Section 6.3.1, the value of T is constant for a given soil and does not vary with OCR.

By combining Equations 6-1 and 6-2, a modified SHANSEP equation is proposed which accounts for variations in undrained strength ratio with consolidation stress. The undrained strength ratio of a fine-grained soil at any OCR may be given by:

$$s_u/\sigma'_{vc} = S_1(1000\sigma'_{p\,[MPa]})^T(OCR)^m \qquad 6\text{-}7$$

where S_1 and T are functions of w_L as given in Equations 6-5 and 6-6 respectively. To accurately determine the SHANSEP m parameter for a soil, undrained strength data are required at several different OCRs (ideally with the same σ'_p). In this work, only RBBC has been tested at OCRs > 1. However, based on a fairly large database of homogenous CL and CH sedimentary clays (I_p = 20 – 80 %), Northeastern U.S. varved clays and sedimentary deposits of silts and organic soils (excluding peats, sensitive marine clays and clays with shells), Ladd (1991) quoted values of m ranging from 0.75 to 0.80. Without further information, assuming a value of m = 0.73 (as measured for RBBC) is not likely to result in a significant error for low or medium OCR soil[9]. Furthermore, the tests performed on OC RBBC indicate that the value of m is independent of stress level and can be assumed to be constant for a given soil.

Equation 6-7 allows one to estimate the undrained strength of a fine-grained soil in triaxial compression by knowing 3 pieces of information about the soil: the in situ vertical effective stress, the OCR and the liquid limit. Given that liquid limit is easy to measure and can be determined from disturbed sample material, Equation 6-7 therefore has great practical value as it may be used to obtain a reasonable estimate of undrained strength for a relatively large number of borehole depths/locations quickly and cheaply. This would not be possible by performing CK_OUC triaxial tests on intact samples, because the expense associated with obtaining and testing intact samples limits the number of tests which can feasibly be carried out in a typical geotechnical site investigation. Alternatively, instead of relying exclusively on liquid limit, Equation 6-7 may be used in combination with limited CK_OUC testing of intact samples in

---

[9] For example, assuming m = 0.73 instead of a much higher value of m = 0.80 would result in about a 10 % difference in the calculated undrained strength at OCR = 4. This difference is relatively small compared to other effects, such as mode of shear or errors in the interpreted σ'_p in situ

order to obtain a more accurate prediction of undrained strength. Apart from OCR, most of the remaining uncertainty in the prediction of undrained strength ratio using Equation 6-7 is associated with the value of S_1, since the m parameter is reasonably well known and the T parameter will not have a major impact on the calculated strength (provided that the test is performed at a reasonably similar stress level). The measured undrained strength from a single CK_OUC test performed on an intact sample may be used to back-calculate an accurate value of S_1 for the soil, and Equation 6-7 could then be used to calculate the undrained strength ratio of the sediment at different OCRs.

Regardless of which of the methods mentioned above are adopted, the determination of undrained strength ratio for OC soils requires an estimate of the in situ OCR, which has a very large impact on strength ratio. For shallow overconsolidated sediments, establishing an accurate profile of OCR with depth may require a significant number of laboratory one-dimensional consolidation tests performed on intact samples. However, one-dimensional consolidation tests are significantly less costly than good quality CK_OUC tests. In addition, Equation 6-7 may be particularly valuable for situations in which the determination of shear strength is of secondary importance to the determination of consolidation properties, such as two- or three-dimensional settlement analyses, for example, where an evaluation of the in situ stress history is needed regardless.

6.9.2 Friction Angle

Figure 6-52 summarizes the variation in critical state friction angle with stress level for the soils tested in this work. The figure also includes data from Jones (2010) for RUC, Kontopoulos (2012) for RSFBM, Grennan (2010) for SS, Fahy (2014) for RGoM EI and Sheahan (1991) and Abdulhadi (2009) for RBBC. As discussed previously, all of the soils which have been tested display consistent variations in friction angle with stress level. Depending on soil type, φ'_{cs} values vary from as high as 40° at 0.1 MPa to as low as 12° at 100 MPa, an extremely wide range. These consistent variations in φ'_{cs} are illustrated more clearly in Figure 6-53, which plots the calculated regression lines through the data of each soil. These regression lines are of the form given in Equation 6-4.

Similar to what was observed for undrained strength, there is an underlying trend to the behavior presented in Figure 6-53. The soil with the highest liquid limit, RGoM EI, displays the most rapid reduction in friction angle with increasing stress. A soil with a medium liquid limit, such as RBBC, displays a moderate reduction. On the other hand, the soil with the lowest liquid limit, SS, actually shows a slight increase in friction angle with increasing stress. Once again, the direction and rate to which the critical state friction angle of a soil varies as a function of stress level is related to the soil's liquid limit. Figure 6-54 and Figure 6-51 plot the A and B parameters respectively for the soils against liquid limit. The relationship between A and w_L presented in Figure 6-54 is closely approximated, with r^2 of 0.90, by the following log-linear equation:

$$A = -75\log_{10}(w_{L\,[\%]}) + 148 \qquad \text{6-8}$$

Recalling that the parameter A is defined as the φ'_{cs} of a soil at σ'_{vc} = 1 GPa, the relationship presented in Figure 6-54 predicts that high plasticity soils have a much lower friction angle at very high effective stresses. However, it is important to keep in mind that measured data have only been obtained for, at most, σ'_{vc} up to 100 MPa. The A parameter is an apparent value determined by extrapolation of Equation 6-4 to an effective stress at least one order of magnitude higher than the measured data, and may therefore not reflect actual friction angles measured at 1 GPa. In the case of Skibbereen Silt, in particular, measured data were only obtained over the stress range of 0.1 to 1 MPa.

The relationship between the parameter B and w_L presented in Figure 6-51 is well approximated, with r^2 of 0.95, by a log-linear equation:

$$B = -0.39\log_{10}(w_{L\,[\%]}) + 0.59 \qquad \text{6-9}$$

Recalling that a lower value of B implies a faster reduction in friction angle with increasing stress level, the relationship presented in Figure 6-51 indicates that high plasticity soils display a more rapid reduction in critical state friction angle with increasing consolidation stress. Equivalently, high plasticity soils show a greater sensitivity of critical state friction angle to stress level. Table 6-2 summarizes the values of A and B for the fine-grained soils investigated in this work, together with the r^2 values associated with each regression (where the regressions are of the form given in Equation 6-4). The positive value of B for Skibbereen Silt, implying an increase in critical state friction angle with increasing stress, is quite atypical and the author is not aware of any other soil exhibiting this strength behavior. Despite the peculiarity of the result, however, the observed behavior in consistent with the overall trend with plasticity.

For fine-grained soils in triaxial compression, a reasonable estimate of critical state friction angle can be obtained by using Equation 6-4 together with the σ'_p of the sediment and the values of A and B given by Equations 6-8 and 6-9 respectively. Similar to Equation 6-7 for undrained strength, Equation 6-4 can be used in isolation by providing an estimate of friction angle based only on liquid limit, or may be used in combination with limited CK_OUC testing carried out on intact samples. Regardless of which of these methods is adopted, the determination of critical state friction angle still requires a reasonable estimate of the σ'_p profile of a sediment. For high OCR sediments this may require determining σ'_p from the results of laboratory one-dimensional consolidation tests performed on intact samples. For low OCR sediments, on the other hand, the error in the calculated friction angle associated with using σ'_{vc} rather than σ'_p is not likely to have a major impact on the friction angle calculated using Equation 6-4. This would be particularly so for lower plasticity soils which display less sensitivity of φ'_{cs} to stress level.

It can be seen from Figure 6-51 that the T and B parameters of the various soils, which describe the variation in s_u/σ'_{vc} and φ'_{cs} respectively with stress, are quite similar. In addition, the forms of both correlations with liquid limit are almost identical. This result points to the fact that increasing consolidation stress decreases both the normalized undrained strength and critical state friction angle of a soil by essentially the same proportion. A decrease in normalized undrained strength is closely related to a corresponding decrease in friction angle, and vice versa.

6.9.3 Young's Modulus

Figure 6-55 summarizes the normalized secant Young's moduli measured at $\varepsilon_a = 0.01$ % for the various soils that were tested at OCR = 1. The figure also includes the relationship for E_{uMAX}/σ'_{vc} of NC RBBC proposed by Santagata (1998), discussed previously in Section 6.3.2. Unlike the strength properties of the soils, Young's modulus shows no clear dependence on soil type. For a given soil, values of E_u/σ'_{vc} also display a lot more scatter between tests. There is a general trend for normalized modulus to decrease with increasing stress, reducing from a range of about 200 - 600 at 0.1 MPa to 35 - 100 at 100 MPa. The tendency for the normalized Young's modulus of soil to decrease with increasing consolidation stress is to be expected, with a similar finding reported previously for RBBC by Santagata (1998) and Abdulhadi (2009). The relationship for E_{uMAX}/σ'_{vc} proposed by Santagata (1998) for NC RBBC (Equation 6-3) can be seen to provide a reasonable upper bound to the measured data for all the soils in Figure 6-55. This is consistent with the fact that the values of initial maximum Young's modulus obtained using internal strain measurement by Santagata (1998) would be higher than values of E_u/σ'_{vc} determined at $\varepsilon_a = 0.01$ %. Within the stress range in which it was defined, i.e. below 2 MPa, Santagata's relationship therefore works well not only for RBBC, but for all fine-grained soils. For higher stresses, however, the extrapolation of Equation 6-3 is found to predict an increase in normalized Young's modulus, a result which is not consistent with the measured data. For stresses greater than 10 MPa, in particular, the use of Equation 6-3 will likely result in a significant overestimate of the initial Young's modulus of a soil. As an improved alternative to Equation 6-3, the following simple relationship is proposed based on the author's results:

$$E_{uMAX}/\sigma'_{vc} = 500 - 175\log_{10}(\sigma'_{vc}) \qquad 6\text{-}10$$

This relationship applies to fine-grained soils at OCR = 1, and is included in Figure 6-55. At stresses below 2 MPa, Equation 6-10 follows Santagata's relationship closely, but for higher stresses it provides a more reasonable prediction of Young's modulus based on the experimental results from this work. Unlike Equation 6-3, Equation 6-10 also removes void ratio as an input parameter. This is because void ratio can vary considerably for different soils, while the data presented in Figure 6-55 suggest that Young's modulus does not have a significant dependence on soil type. It should be noted, however, that this observation is not consistent with previous work at low stresses by Foott and Ladd (1981), who reported significantly lower values of Young's modulus associated with high plasticity soils.

6.9.4 Effect of K_O on Shear Strength

Figure 6-56 plots the undrained strength ratios at OCR = 1 for all the soils included in this study versus pre-shear K_{ONC}. Although there is some scatter, there is a very clear trend of decreasing undrained strength with increasing K_{ONC}. It is quite remarkable that all of the soils in the dataset follow this same unique relationship, despite wide differences in composition, geologic origin and undrained strength at a given σ'_{vc}. The relationship is consistent with the

K_{ONC} data for the soils presented in Section 5.4.1 and with the undrained strength data presented in Section 6.9.1, i.e. higher plasticity soils display a more rapid increase in K_{ONC} and a more rapid decrease in undrained strength ratio with increasing consolidation stress. For example, particularly large values of K_{ONC} for RGoM EI at high stresses correspond with particularly low undrained strength ratios measured in the same tests. On the other hand, the decrease in K_{ONC} with stress observed for the SS coincides with an increasing undrained strength ratio. A linear regression, with $r^2 = 0.89$, through the experimental data yields the following relationship:

$$s_u/\sigma'_{vc} = 0.56 - 0.48K_{ONC} \qquad \text{6-11}$$

This equation is almost identical to the aggregate relationship for RBBC alone, as given in Figure 6-10. It is worth noting that the strong inverse correlation between K_{ONC} and strength ratio could be considered somewhat counter-intuitive. For a given σ'_{vc}, a higher K_{ONC} corresponds to a greater mean stress, which one might expect would produce a higher shear strength. However, this effect is counter-acted and outweighed by the fact that the application of a higher shear stress during consolidation has a strengthening effect on soil (De Groot 1992). Essentially, the ability of a soil to maintain a higher shear stress during one-dimensional consolidation gives it a higher strength during undrained shearing.

In the OC range, soil undergoes shearing from an initial stress state which lies within the yield surface, so the effect of the pre-shear K_O is less important. Undrained strength in the OC range is likely more influenced by the value of K_{ONC} prior to swelling, rather than the pre-shear K_O.

Figure 6-57 plots the critical state friction angles of the soils versus pre-shear K_{ONC} (in the case of RBBC, only the data at OCR = 1 is plotted). The behavior is similar to that observed for undrained strength, in that an increase in K_{ONC} corresponds with a decrease in φ'_{cs}. However, the correlation with friction angle shows more scatter than the correlation with undrained strength ratio, with friction angles varying by > 10° at a given K_{ONC}. Figure 6-57 also includes the widely known correlation of Jâky (1948) relating K_{ONC} to friction angle ($K_{ONC} = 1 - \sin\varphi'$). It can be seen that Jâky's correlation provides a reasonably good approximation to the measured data, although the data for SS lie considerably above the correlation.

The results presented in Figure 6-56 and Figure 6-57 demonstrate that unique relationships exist between K_{ONC}, critical state friction angle and undrained strength ratio. With regard to friction angle, the value of K applied during consolidation does not impact the friction angle measured at critical state. This can be concluded from the fact that the correlation of Jâky (1948) is based on independently measured values of K_{ONC} and φ'_{cs}, where φ'_{cs} was determined from isotropically consolidated triaxial tests (in contrast to the author's work in which both properties were together measured in individual triaxial tests). On the other hand, the value of K applied during consolidation does have a direct causal impact on the measured undrained strength. This can be concluded from the relationship between s_u/σ'_{vc} and K_{ONC} determined by Santagata (1994) (Figure 6-10) which is based on low stress tests (< 1 MPa) with some tests involving K_O-consolidation and other tests involving stress path consolidation with a prescribed value of K. A very similar result was found by the author in a series of tests carried out at σ'_{vc} = 0.6 MPa to examine the principal of effective stress, as discussed previously in Section 6.2. In addition, a test performed by the author on RBBC (TX1124) in which the specimen was resedimented under K_O conditions to a nominal $\sigma'_p = 1$ MPa and then isotropically consolidated in the triaxial cell to $\sigma'_{vc} = 5.9$ MPa produced $s_u/\sigma'_{vc} = 0.243$. This data point would fall far below the trend shown in Figure 6-6, indicating that the stress path followed during consolidation has a large direct impact on the measured undrained strength ratio.

6.9.5 Critical State Behavior

Figure 6-58 plots the mean effective stresses and shear stresses at critical state for RPC, RGoM Ursa, RUC, RSFBM and RLC, as well as the RBBC data presented previously in Figure 6-22. The figure does not include any data from Kontopoulos (2012) for RSFBM, from Jones (2010) for RUC, or from Fahy (2014) for RGoM EI as these datasets have an excessive amount of scatter in calculated void ratios. To make trends in the data easier to detect, Figure 6-59 plots the calculated log-linear regression lines through the experimental data. Consistent with the virgin compression behavior of the soils discussed in Section 5.2, higher plasticity soils possess larger critical state void ratios at low stresses, though they also have steeper CSLs. As a result, the CSLs for all the soils tend to converge into a narrower range at high stresses. A central assumption of the critical state soil mechanics framework is that the CSLs of effective stress and shear stress for a soil remain parallel to one another. However, it can be seen from Figure 6-59 that this is generally not the case. For high plasticity soils, such as RLC, the CSLs of effective stress and shear stress show considerable divergence with increasing consolidation stress. For medium plasticity soils, such as RBBC, the CSLs show moderate divergence. On the other hand, for a low plasticity soil such as RPC, the CSLs remain essentially parallel across the entire stress range investigated. These results are consistent with the variations in ϕ'_{cs} of the soils as discussed in Section 6.9.2, in that diverging CSLs of effective stress and shear stress indicate a reduction in ϕ'_{cs} with increasing stress, while parallel CSLs indicate a constant ϕ'_{cs} with stress.

While Figure 6-59 shows log-linear trendlines fitted through the experimental data, in reality different functional forms may provide a more accurate representation of the behavior of each soil. For example, the highest stress data points in Figure 6-22 indicate that the critical state and virgin compression lines of RBBC begin to flatten out at void ratios below about 0.35, deviating from a log-linear relationship. Furthermore, as discussed in Section 5.2, the virgin compression lines of most soils display a reduction in compression index with increasing stress, particularly high plasticity materials. Unfortunately, sufficient data are not available for soils other than RBBC to determine the exact functional form(s) of the critical state lines.

6.9.6 Particle Reorientation

It is worth considering if particle reorientation during one-dimensional compression could help explain variations in the strength properties of soils. As consolidation stress increases and porosity reduces, platy-shaped clay particles become increasingly aligned perpendicular to the direction of major loading (Day-Stirrat et al. 2012, Adams et al. 2013). This phenomenon was addressed previously in Chapter 5 in relation to its effect on permeability, and Figure 5-6 shows the effect of increasing vertical effective stress on the mean particle orientation of RBBC. Keeping in mind that failure in triaxial compression occurs along a plane oriented at $(45+\phi/2)^\circ$ to the horizontal, the results presented in Figure 6-53 suggest that, for all of the soils investigated in this work, shear failure should occur at angles of as high as 65° at 0.1 MPa to as low as 51° at 100 MPa. Particle reorientation with increasing vertical effective stress might therefore be expected to *increase* the normalized strength of a soil, because particles would become less favorably aligned with the failure plane and instead be more likely to be aligned perpendicular to the failure plane. This would be particularly so for high plasticity soils which contain a larger portion of platy shaped clay particles compared to more silty low plasticity soils. As can be seen in Figure 6-49 and Figure 6-53, however, the opposite is the case. Higher plasticity soils, which would be expected to have more pronounced particle reorientation with increasing stress level, also display the fastest reductions in normalized undrained strength and friction angle. The underlying mechanism causing a more rapid reduction in the strength properties of high plasticity soils must therefore more than offset the opposing effect of particle reorientation.

6.10 STRENGTH BEHAVIOR IN OTHER MODES OF SHEAR

6.10.1 Triaxial Extension Tests

Figure 6-60 plots the shear stress-strain responses measured during undrained shearing of NC RBBC in TE mode of shear at $\sigma'_{vc} = 0.20$ MPa and 6.94 MPa. It can be seen that the stress-strain response of the soil is very different to what is observed in triaxial compression, e.g. as shown in Figure 6-4. The response in TE is more ductile at all stresses with no clear point of peak shear strength being evident, although shear stresses tend to level off at large strains as a critical state condition is developed. There is very good repeatability between the two tests despite a large difference in pre-shear consolidation stresses. Unlike TC, there is no significant stress level dependence in the stress-strain response, with almost identical undrained strength ratios measured in the two tests. This result is in contrast to Moniz (2009) who reported a slight decrease in the undrained strength ratio of NC RBBC in TE with increasing stress for $\sigma'_p < 2$ MPa.

Figure 6-61 plots the normalized shear induced pore pressures measured in the same TE tests. As expected for a NC soil, positive shear induced pore pressures are generated during shearing indicating contractive behavior. Lower normalized pore pressures are measured in the test consolidated to 6.94 MPa. This result is different to what is observed in TC (Figure 6-8), where very similar normalized pore pressures are measured in tests consolidated to stresses ranging from 0.56 MPa to 40.5 MPa. For comparison, the normalized pore pressure response for a typical TC test (TX1031) is included in Figure 6-61. It can be seen that, even for the higher stress TE test, larger shear induced pore pressures are generated in TE than in TC. At large strains, however, the normalized shear induced pore pressures generated in both modes of shear tend to converge.

Figure 6-62 plots the effective stress paths for the TE tests. Different starting points for the two stress paths are due to the increasing K_{ONC} of RBBC with increasing consolidation stress. This initial offset in the stress paths is maintained throughout the tests. Consistent with what is observed in Figure 6-60, both tests reach very similar normalized peak shear strengths. This result suggests that the pre-shear K_{ONC} has far less of an impact, if any, on undrained strength in TE mode of shear. Both tests, however, reach very different failure envelopes at critical state. At 0.2 MPa, a relatively high φ'_{cs} of 39.4° is mobilized, though this drops to 29.1° at 6.94 MPa. This observation of a decreasing friction angle with increasing consolidation stress is consistent with Moniz (2009).

6.10.2 Summary of Undrained Strength

In addition to the triaxial extension tests performed on RBBC by the author, extension tests have also been carried out on RBBC by Moniz (2009), and direct simple shear tests have been performed on the soil by Walbaum (1988), Ahmed (1990) and Seah (1990) using the Geonor Direct Simple Shear Device. These test programs only involved testing at OCR = 1. Figure 6-63 plots the undrained strength ratios of RBBC versus stress level as determined from these test programs, together with the triaxial compression results at OCR = 1 presented previously in Section 6.3.1. While Moniz (2009) reported a slight decrease in undrained strength ratio with increasing stress based on TE tests performed at $\sigma'_p = 0.41, 0.97$ and 1.96 MPa, the TE tests performed in this work at lower and higher stresses indicate that there is essentially no change in the normalized undrained strength of the soil in this mode of shear. In addition, for the stress range in which it was measured, the undrained strength ratio in DSS mode of shear also remains constant. The observation of a DSS strength which lies between the TE and TC strengths is to be expected for a non-varved clay soil. It can be noted that the exact stress state is not defined in a DSS test as the orientation of the maximum shear stress is unknown. The undrained strength ratios given for DSS in Figure 6-63 are defined in the usual way as τ_{hMAX}/σ'_{vc}, where τ_{hMAX} is the maximum horizontal shear stress measured during shearing. Data from DSS tests are also available for Skibbereen Silt at several OCRs from Grennan (2010). Unlike RBBC, the normalized undrained strength of Skibbereen Silt increases in DSS as it does in TC, with τ_{hMAX}/σ'_{vc} rising considerably from 0.13 at $\sigma'_p = 0.2$ MPa to 0.18 at $\sigma'_p = 1.8$ MPa for OCR = 1.

Quirós et al. (2000) examined the results of 172 DSS tests performed on a wide variety of NC soils from six different locations around the world and which were carried out at five separate geotechnical laboratories. The vast majority of the test specimens were high plasticity clays and the dataset as a whole displayed a remarkably consistent trend of decreasing normalized undrained strength with increasing effective stress.

6.10.3 Summary of Friction Angle Data

Figure 6-64 presents critical state friction angle data for NC RBBC in TC, DSS and TE. A similar trend of decreasing friction angle is observed in all three modes of shear. The friction angle measured in TE is higher than the TC friction angle at low stresses but reduces to about the same value for $\sigma'_p > 1$ MPa. The friction angle values given for DSS in Figure 6-64 are defined in the usual way as $\psi'_{cs} = \arctan(\tau_h/\sigma'_v)_{max}$ (i.e. the underlying assumption being that the failure plane is horizontal). A lot of scatter can be seen in the DSS results and data are not available for $\sigma'_p > 1.2$ MPa. A clear outlier value of $\psi'_{cs} = 50.1$ is observed at $\sigma'_p = 0.14$ MPa. The DSS data available for Skibbereen Silt from Grennan (2010) show an even more dramatic increase in friction angle with stress level than the TC data for the soil, with ψ'_{cs} increasing from about 22° at $\sigma'_p = 0.2$ MPa to 35° at $\sigma'_p = 1.8$ MPa for OCR = 1. It can be noted that the results of isotropically consolidated triaxial compression tests performed on the soil did not display this trend of increasing friction angle with stress (Grennan 2010).

6.10.4 Yield Surface Evolution

Combining triaxial compression and extension data makes it possible to locate the full yield surface of a soil in two-dimensional q-p' stress space. A yield surface is a conceptual surface that defines the boundary at which a soil behaves elastically. When the stresses acting upon the soil lie on the yield surface, such as occurs during undrained shearing at OCR = 1, then the soil can undergo plastic deformation, i.e. progressive yielding. The effective stress paths followed during undrained shearing at OCR = 1 in TC and TE, together with the interpreted Mohr-Coulomb failure envelopes, can therefore be used to define the location of the entire yield surface. Figure 6-65 plots the normalized stress paths followed during undrained shearing of NC RBBC in both TC and TE for tests consolidated to low and high stress levels. The plot also includes the author's interpretation of the soil's yield surface at the low and high stress levels. At the pre-shear stress state the soil does not exist on the yield surface. This is due to the well-known phenomenon of secondary compression (a.k.a. drained creep) causing the yield surface to move out beyond the stress state achieved by primary consolidation alone (Bjerrum 1973). For the TC stress paths the point of first yield is easy to distinguish, as beyond this point the generation of large shear induced pore pressures cause the effective stress to decrease and the stress path to move to the left before reaching the large strain Mohr-Coulomb failure envelope (which also defines the yield surface). The point at which the TE stress path coincides with the yield surface is less obvious to detect, and involves some judgment on part of the author. The fact that the soils investigated in this work possess no true cohesion means that the yield surface must pass through the origin of the q-p' plot, although in reality the yield surface will be slightly curved to reflect a variation in friction angle with stress level.

The interpreted yield surfaces shown in Figure 6-65 synthesize many of the results presented previously. For RBBC, increasing consolidation stress changes the form of the yield surface such that it becomes more centered about the effective stress axis, i.e. the yield surface becomes more isotropic. This is reflected in a decrease in normalized undrained strength and friction angle and an increase in K_{ONC} with increasing consolidation stress. The yield surfaces of other soils change differently. For example, high plasticity soils such as R. London Clay display a large reduction in normalized undrained strength and friction angle and a large increase in K_{ONC} with increasing stress. This reflects a yield surface which becomes elongated about the effective stress axis as consolidation stress increases, as can be observed from the TC stress paths plotted in

Figure 6-47. On the other hand, Skibbereen Silt displays an increasing undrained strength ratio and friction angle and decreasing K_{ONC} with increasing stress level, at least for $\sigma'_p < 1$ MPa. This reflects a yield surface which is becoming more anisotropic. The strength properties and K_{ONC} of R. Presumpscot Clay remain essentially constant with stress level, reflecting a yield surface which does not change in shape. Apart from RBBC, however, these soils have only been tested in TC mode of shear, and as a result the evolution of much of the yield surface corresponding to the TE regime is not understood. However, it is believed that the same underlying mechanism which causes a rotation of the yield surface in the TC regime would have a similar effect in the TE regime.

Table 6-1: Summary of triaxial shear results

		Pre-Shear		At Peak Shear Stress				At Critical State		
Test no.	**Soil**	σ'_{vc} (MPa)	**OCR**	ϵ_f (%)	s_u/σ'_{vc}	s_u (MPa)	φ'_D (°)	φ'_{cs} (°)	p'/σ'_{vc}	q/σ'_{vc}
TX1030^	RBBC	9.812	1.00	0.92	0.292	2.865	23.8	30.4	0.491	0.246
TX1031^	RBBC	5.870	1.00	0.54	0.289	1.696	23.5	30.1	0.471	0.230
TX1036^	RBBC	0.557	1.00	0.11	0.310	0.173	24.0	31.7	0.471	0.240
TX1040^	RBBC	4.881	2.01	2.06	0.489	2.387	27.4	29.9	0.881	0.436
TX1041^*	RBBC	0.629	1.00	0.88	0.270	0.170	23.4	32.6	0.466	0.250
TX1042^	RBBC	0.469	4.13	6.16	0.821	0.385	30.5	30.9	1.502	0.760
TX1043^*	RBBC	0.572	1.00	0.24	0.291	0.167	22.7	35.0	0.466	0.264
TX1046^	RBBC	0.461	4.18	6.94	0.780	0.360	30.9	31.2	1.447	0.742
TX1053^*	RBBC	0.587	1.00	0.26	0.300	0.176	23.7	34.0	0.480	0.266
TX1057^	RBBC	2.472	3.97	6.08	0.812	2.007	30.9	31.0	1.526	0.773
TX1059^	RBBC	9.567	1.00	0.55	0.295	2.822	22.8	28.7	0.493	0.248
TX1061^	RBBC	1.222	8.03	8.01	1.326	1.620	32.4	34.1	2.491	1.296
TX1070^	RBBC	0.555	1.00	0.30	0.316	0.175	24.8	34.8	0.473	0.266
TX1073^	RBBC	0.563	1.00	0.15	0.324	0.182	24.9	34.8	0.442	0.250
TX1115^E	RBBC	6.941	1.00	-14.40	-0.166	-1.152	29.1	29.1	0.350	-0.163
TX1119^{E,F}	RBBC	0.198	1.00	-15.50	-0.164	-0.032	38.2	39.4	0.265	-0.164
TX1120^F	RBBC	0.829	15.80	9.19	1.676	1.389	30.7	34.5	*critical state not reached*	
TX1124^	RBBC	5.857	1.00	8.33	0.243	1.423	28.9	30.1	0.475	0.238
TX1147	RBBC	9.610	1.00	0.97	0.292	2.807	25.2	30.8	0.487	0.246
TX1160^F	RBBC	20.05	1.00	2.53	0.287	5.755	26.2	29.2	0.517	0.243
TX1162	RBBC	40.53	1.00	2.40	0.287	11.64	25.7	29.0	0.537	0.255
TX1163	RBBC	9.77	4.12	6.11	0.786	7.682	30.2	30.5	1.543	0.742
TX1166	RBBC	20.05	2.01	2.94	0.481	9.646	27.9	29.1	0.901	0.423
TX1185^F	RBBC	4.77	8.41	8.63	1.267	6.043	29.8	32.1	2.530	1.163
TX1193	RBBC	101.25	1.00	*external leak in test*				26.6		
TX1204	RBBC	50.77	2.03	3.56	0.488	24.7	27.0	28.1	0.981	0.454
TX1093	RPC	9.464	1.00	0.54	0.308	2.915	26.3	32.0	0.535	0.280
TX1096	RPC	0.241	1.00	0.28	0.300	0.072	26.2	36.7	0.518	0.307
TX1111	RPC	0.990	1.00	0.29	0.317	0.314	27.5	34.7	0.502	0.279
TX1208	RPC	101.30	1.00	4.86	0.305	30.88	27.3	28.7	0.616	0.293
TX1210	RPC	0.579	1.00	0.21	0.301	0.174	24.8	32.6	0.478	0.256
TX1072	RGoM Ursa	9.600	1.00	1.69	0.242	2.323	18.8	20.8	0.574	0.198
TX1077	RGoM Ursa	0.625	1.00	0.51	0.273	0.171	20.5	25.3	0.596	0.248
TX1106	RGoM Ursa	0.188	1.00	0.47	0.311	0.058	24.6	29.2	0.503	0.234
TX1218	RGoM Ursa	84.8	1.00	4.90	0.223	18.87	15.9	18.1	0.647	0.199
TX1092	RUC	9.783	1.00	0.21	0.268	2.622	19.1	24.1	0.555	0.223
TX1198	RUC	105.30	1.00	5.33	0.215	22.60	14.8	17.2	0.695	0.204
TX1079^F	RSFBM	9.540	1.00	0.84	0.291	2.776	22.3	24.7	0.546	0.214
TX1216	RSFBM	83.0	1.00	4.65	0.236	19.63	17.2	18.4	0.671	0.207
TX1123^F	RLC	0.153	1.00	0.29	0.288	0.044	21.5	24.7	*pronounced failure plane*	
TX1127	RLC	0.379	1.00	0.23	0.252	0.096	18.5	20.3	0.561	0.176
TX1129^F	RLC	1.395	1.00	0.49	0.208	0.290	14.7	16.8	0.599	0.159
TX1137	RLC	0.671	1.00	0.37	0.223	0.150	16.1	18.7	0.588	0.175
TX1189	RLC	11.82	1.00	3.39	0.155	1.831	11.8	12.7	0.642	0.140
TX1209	RGoM EI	63.47	1.00	6.90	0.110	7.000	10.4	11.9	0.500	0.103

^ test performed with smooth end platens; *specimen consolidated under high u_b; E triaxial extension test, F failure plane visible in specimen

Table 6-2: Summary of strength parameters for soils investigated in this work

Soil	Liquid Limit (%)	s_u/σ'_{vc}			φ'_{cs}		
		S_1	T	r^2	A	B	r^2
Skibbereen Silt	25.8	0.15	0.104	0.86	48.5	0.053	0.90
R. Presumpscot Clay	33.1	0.30	0.001	0.02	26.7	-0.035	0.85
R. Boston Blue Clay	46.5	0.37	-0.024	0.92	24.0	-0.044	0.82
R. Ursa Clay	51.7	0.39	-0.052	0.96	14.8	-0.077	0.99
R. Ugnu Clay	56.4	0.48	-0.067	0.95	14.7	-0.095	0.96
R. San Francisco Bay Mud	60.2	0.52	-0.066	0.72	14.2	-0.113	0.95
R. London Clay	73.8	0.58	-0.142	0.99	6.5	-0.148	0.99
R. Eugene Island Clay	85.8	0.60	-0.148	0.91	6.8	-0.159	0.91

*Based on data at OCR=1

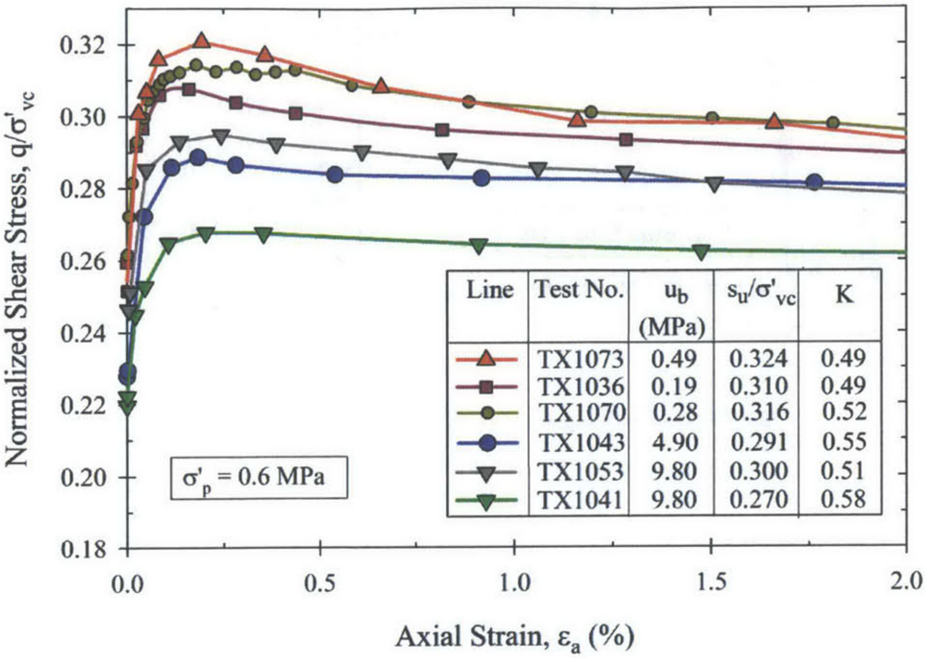

Figure 6-1: Stress-strain responses measured during undrained shearing of NC RBBC with a wide range in the magnitude of pore pressures

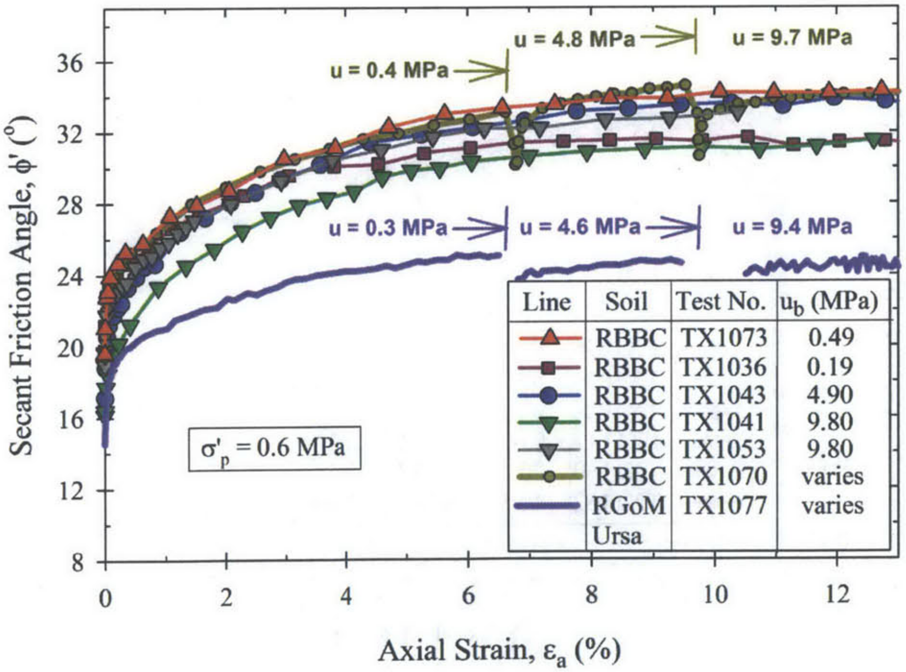

Figure 6-2: Friction angles measured during undrained shearing of NC RBBC and NC RGoM Ursa with a wide range in the magnitude of pore pressures

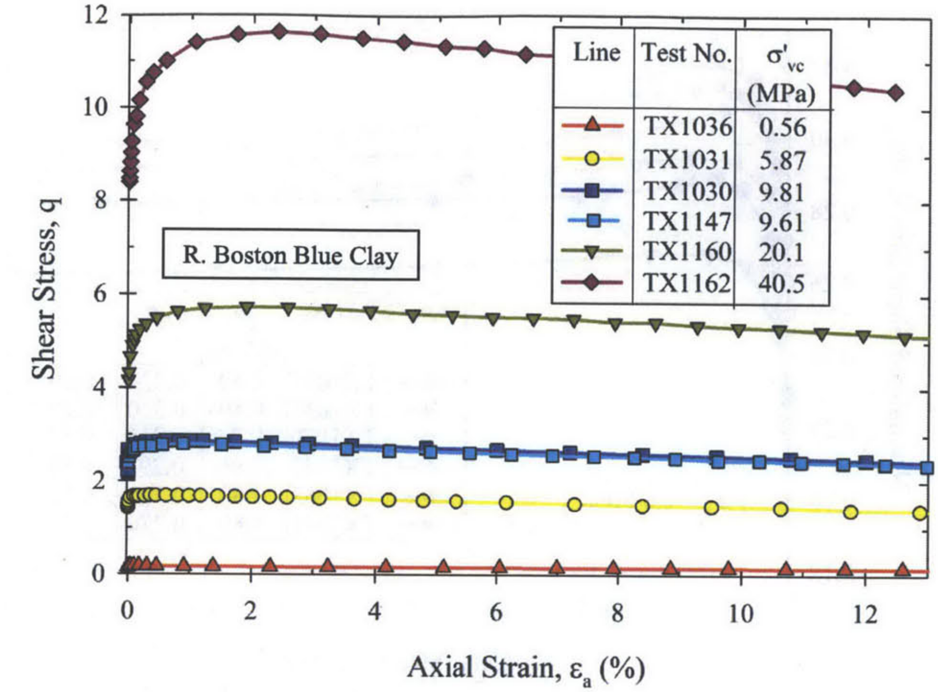

Figure 6-3: Stress-strain responses measured during undrained shearing of NC RBBC

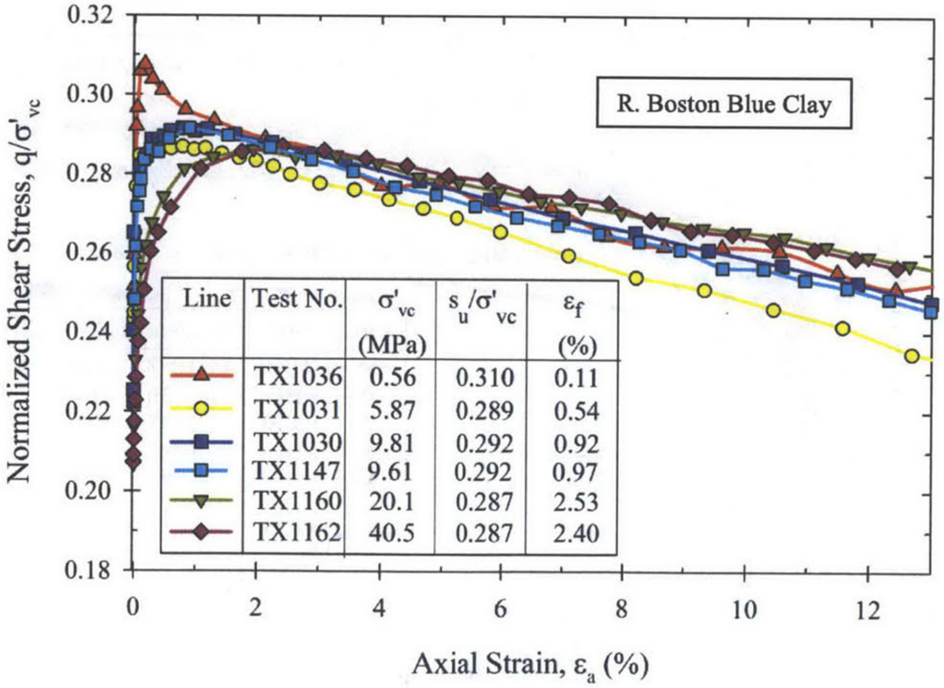

Figure 6-4: Normalized stress-strain responses measured during undrained shearing of NC RBBC

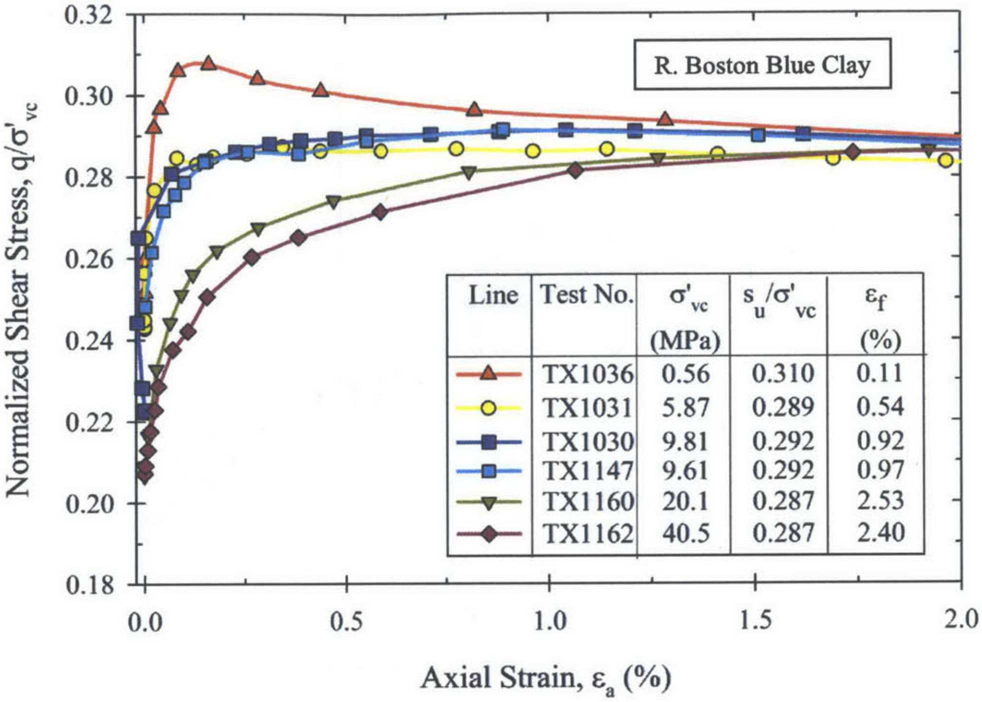

Figure 6-5: Normalized stress-strain responses measured during undrained shearing of NC RBBC for axial strains up to 2 %

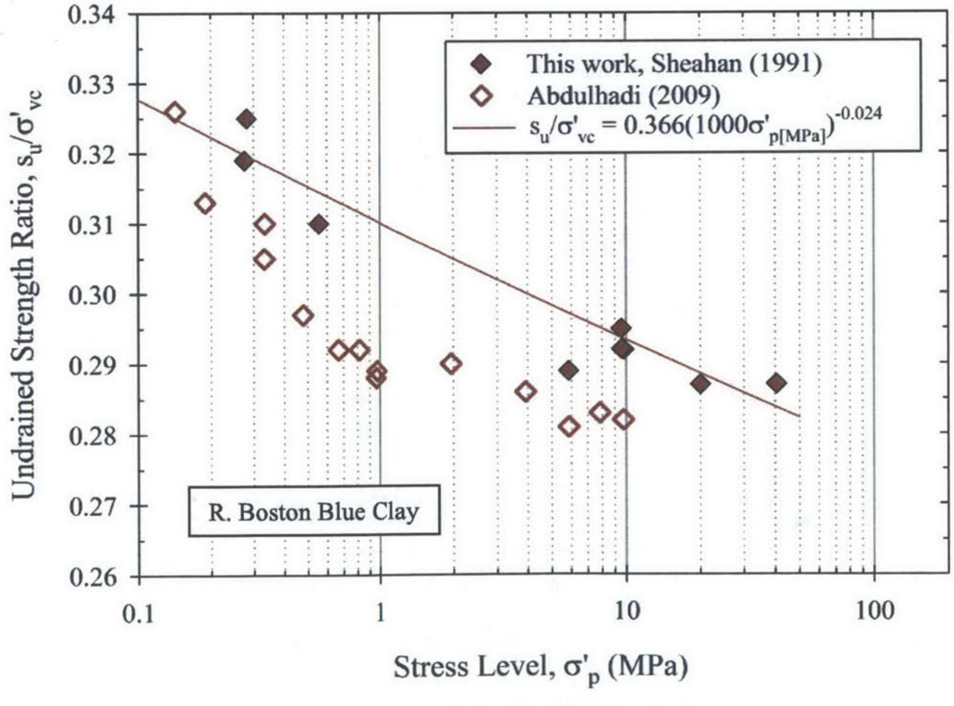

Figure 6-6: The variation in the undrained strength ratio of NC RBBC with stress level

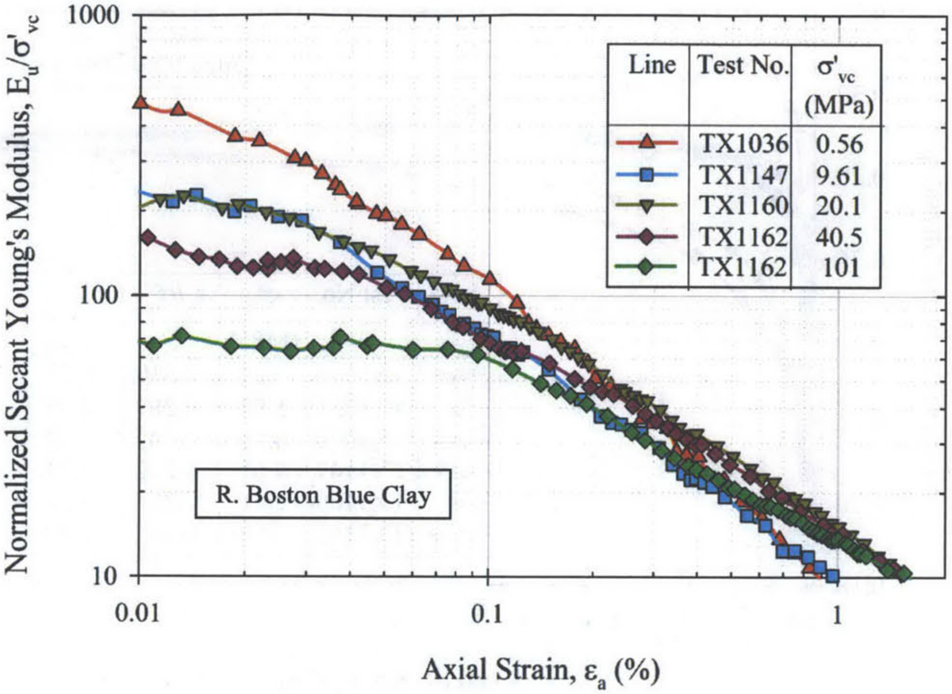

Figure 6-7: The variation in normalized secant Young's modulus with axial strain measured during undrained shearing of NC RBBC

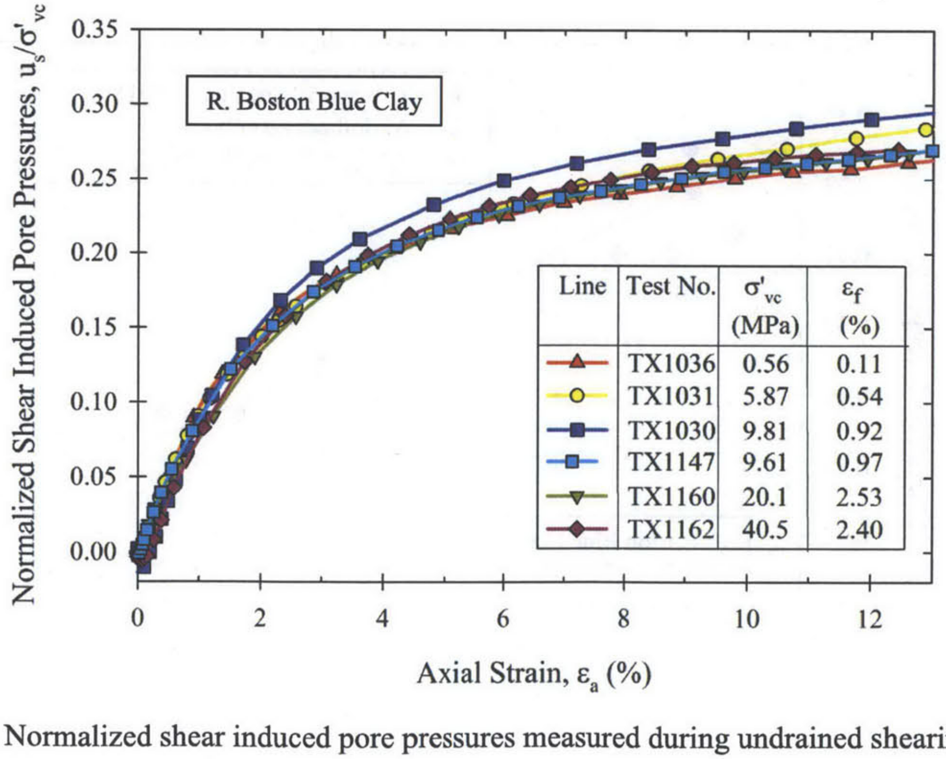

Figure 6-8: Normalized shear induced pore pressures measured during undrained shearing of NC RBBC

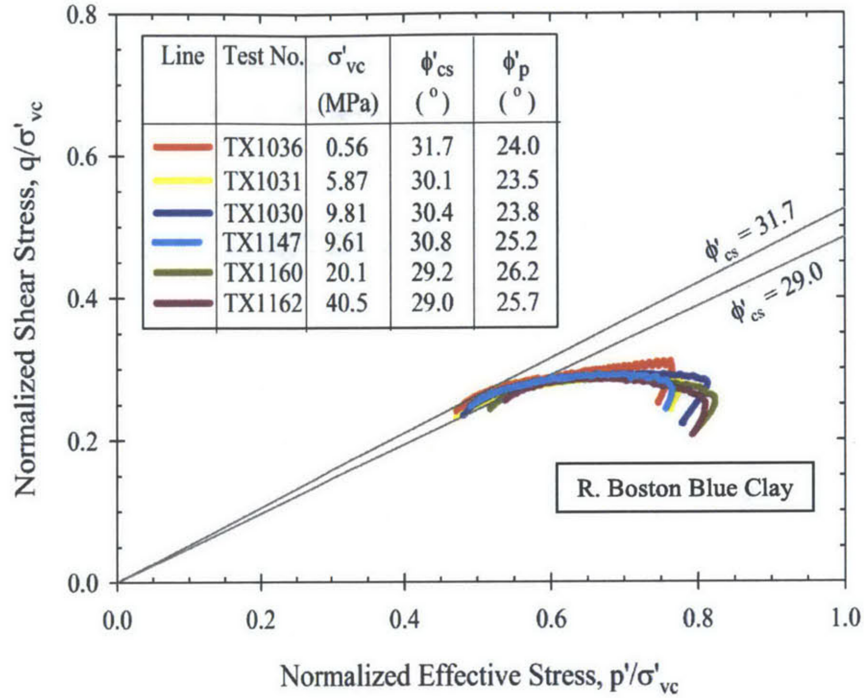

Figure 6-9: Effective stress paths followed during undrained shearing of NC RBBC over a wide range of consolidation stresses

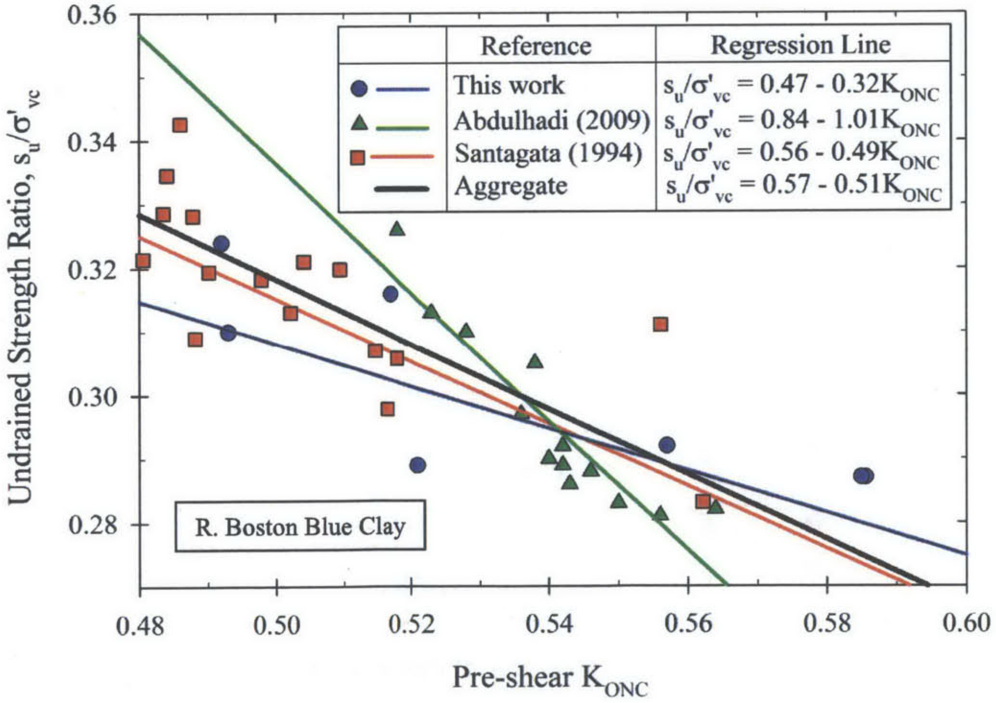

Figure 6-10: The variation in undrained strength ratio of RBBC as a function of pre-shear K_{ONC}

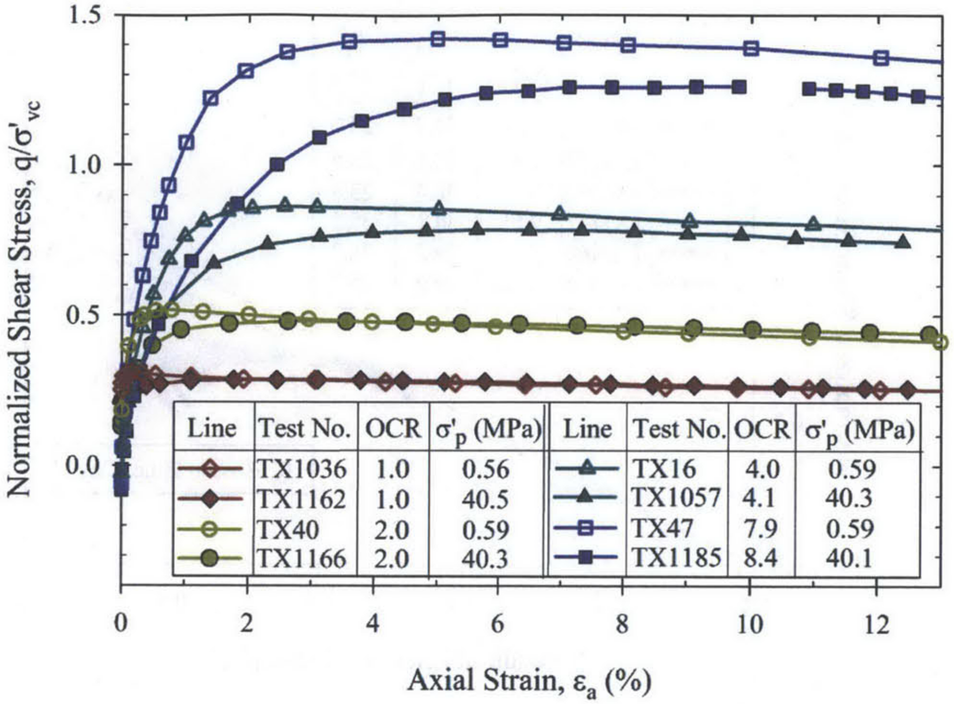

Figure 6-11: Stress-strain responses measured during undrained shearing of RBBC at OCRs 1, 2, 4, and 8 for a low and high stress level

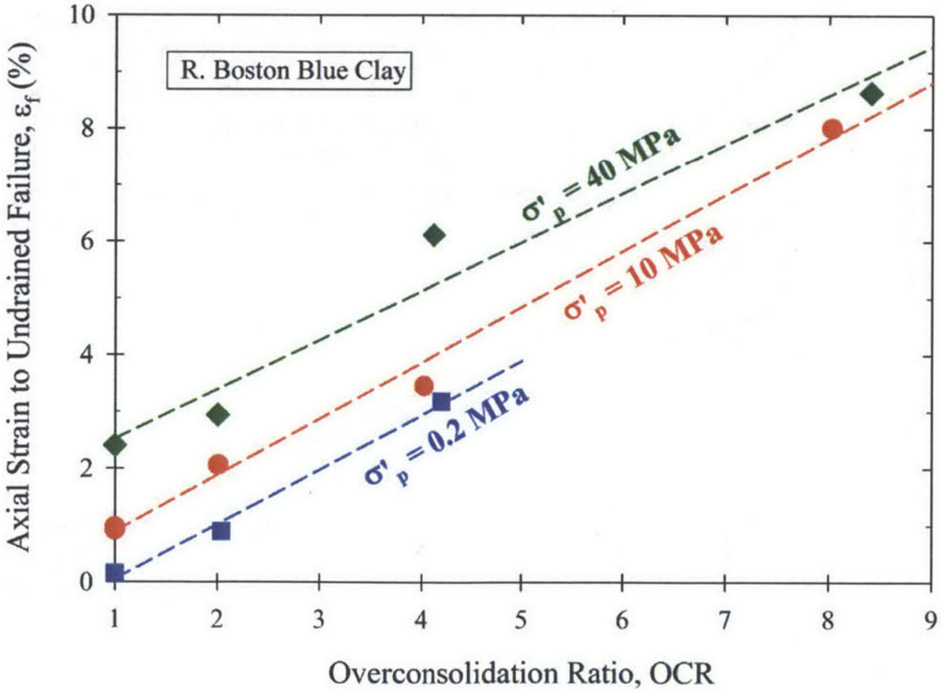

Figure 6-12: The effect of OCR and stress level on the axial strain to undrained failure

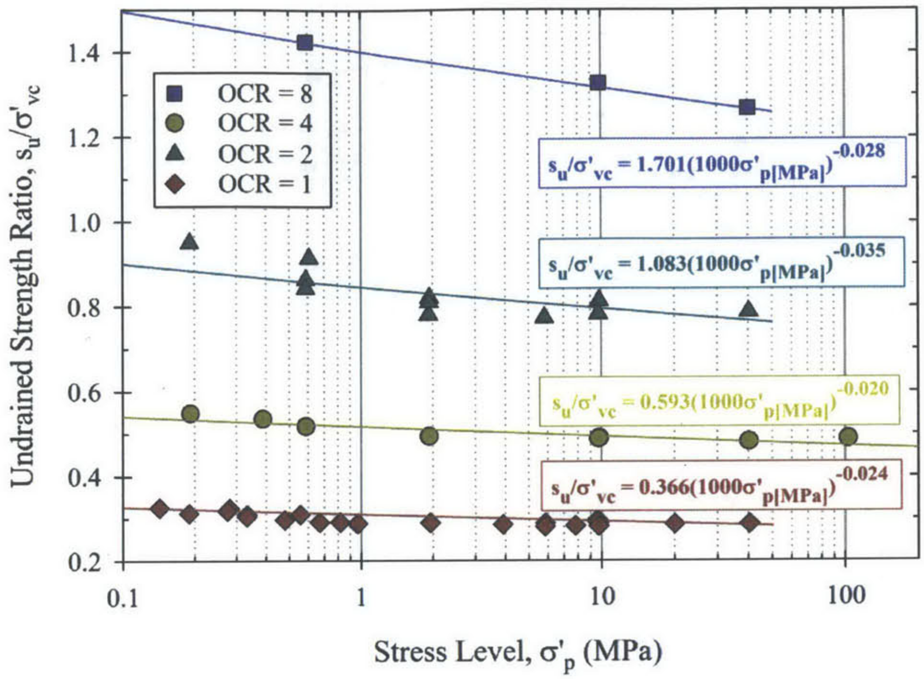

Figure 6-13: The variation in the undrained strength ratio of RBBC with stress level at OCRs 1, 2, 4 and 8. Best-fit power-law functions are fitted through the experimental data

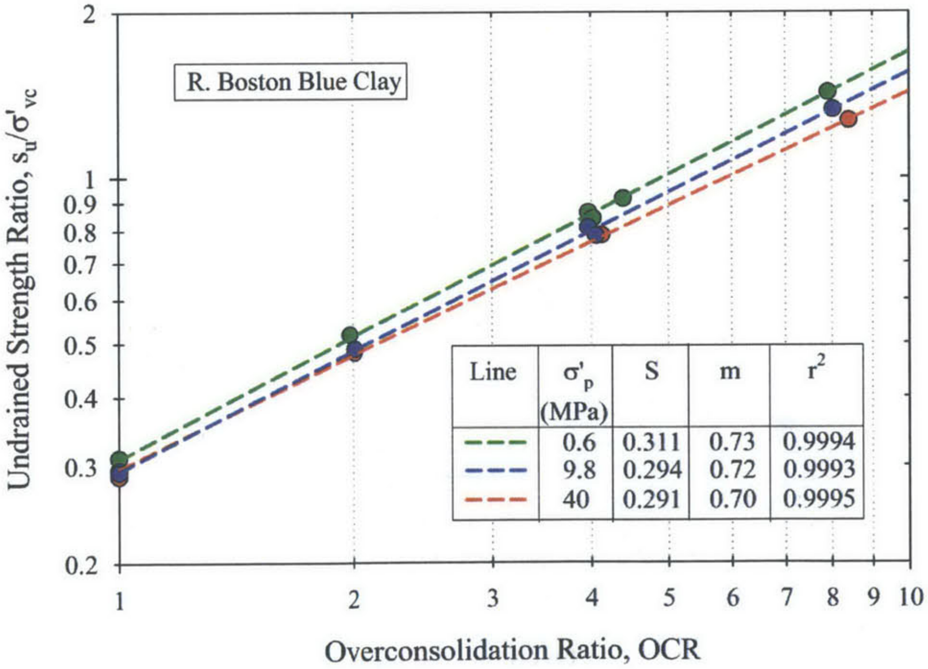

Figure 6-14: The variation in the SHANSEP S and m parameters for RBBC as a function of stress level

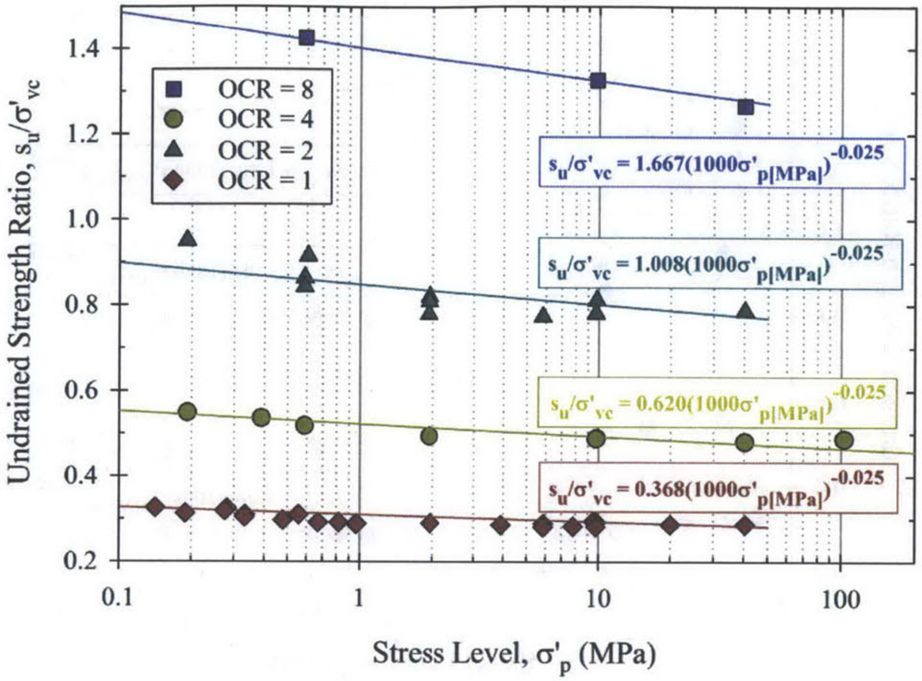

Figure 6-15: The variation in the undrained strength ratio of RBBC with stress level at OCRs 1, 2, 4 and 8. Best-fit power-law functions are fitted through the experimental data with the constraint that T = -0.025

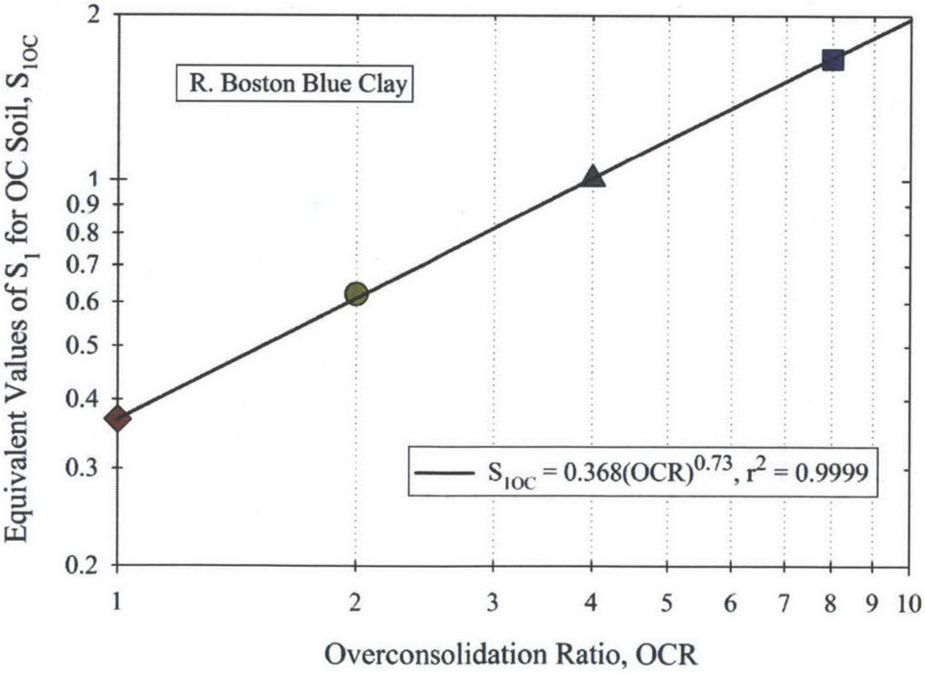

Figure 6-16: Equivalent values of S_1 for OC RBBC as a function of OCR

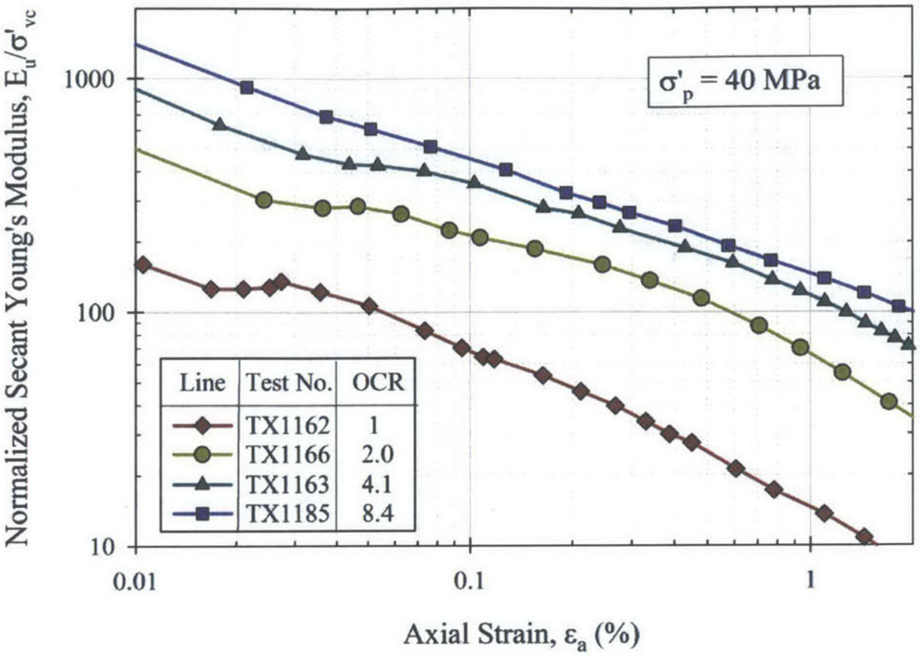

Figure 6-17: The variation in normalized secant Young's modulus with axial strain measured during undrained shearing of RBBC at OCRs 1, 2, 4, and 8

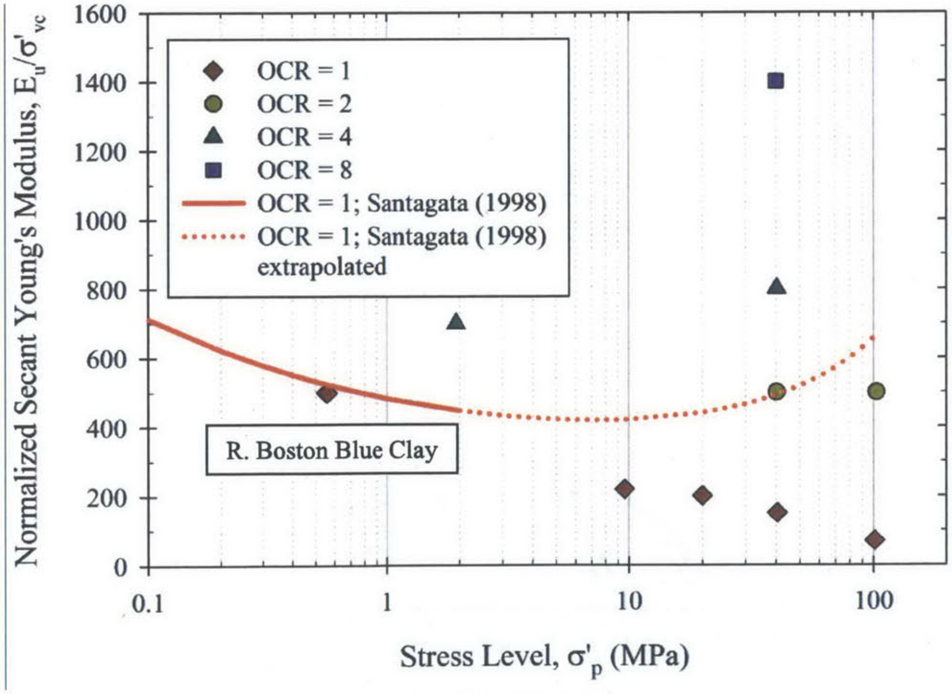

Figure 6-18: The variation in normalized secant Young's modulus as a function of OCR and consolidation stress level for RBBC. The author's measured data define E_u/σ'_{vc} at $\varepsilon_a = 0.01$ %, while the relationship of Santagata (1998) defines E_u/σ'_{vc} at its initial maximum value

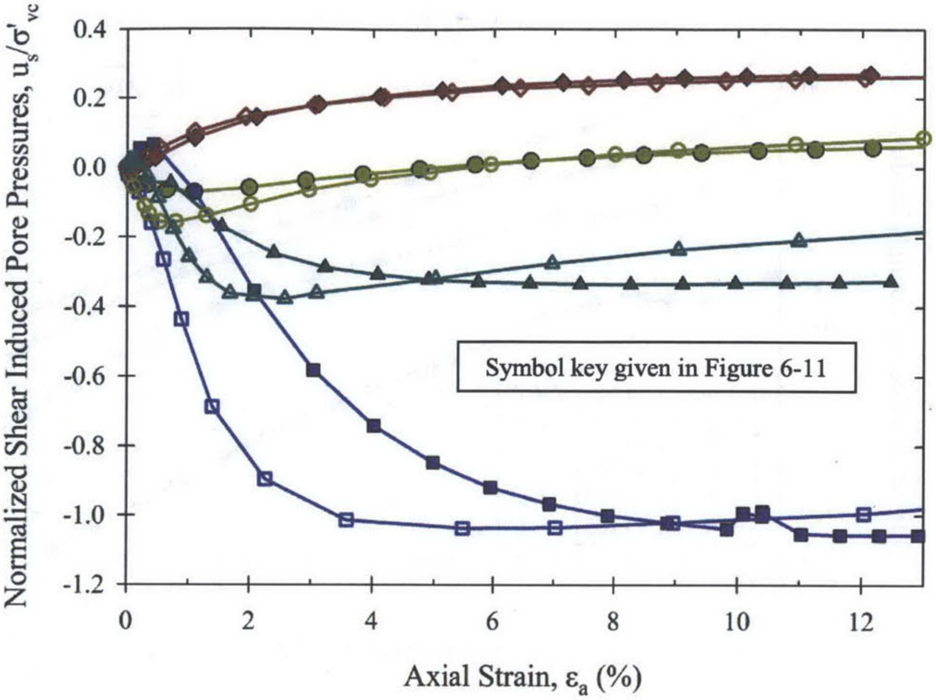

Figure 6-19: Normalized shear induced pore pressures measured during undrained shearing of RBBC at OCRs 1, 2, 4, and 8 for a low and high stress level

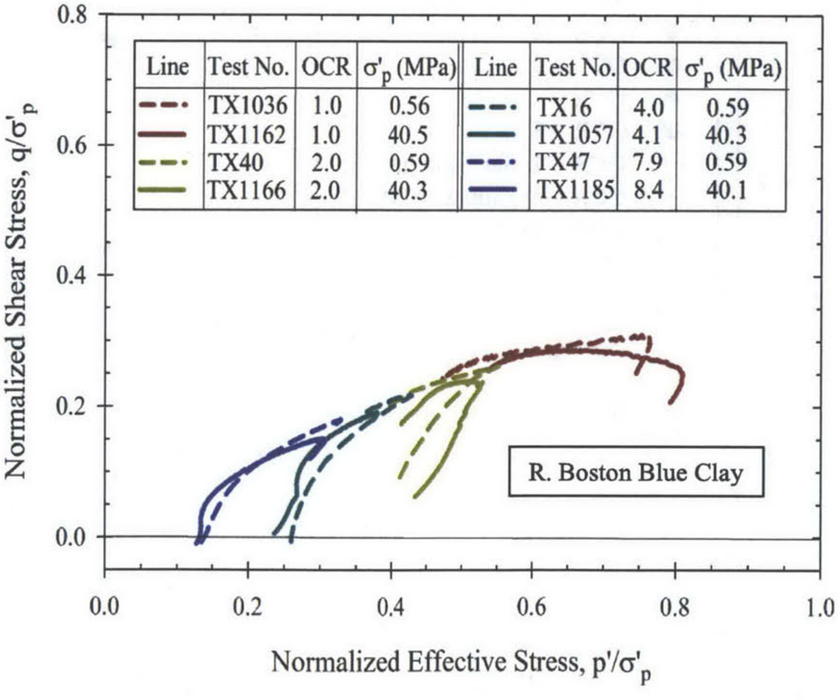

Figure 6-20: Effective stress paths followed during undrained shearing of RBBC at OCRs 1, 2, 4, and 8 for a low and high stress level

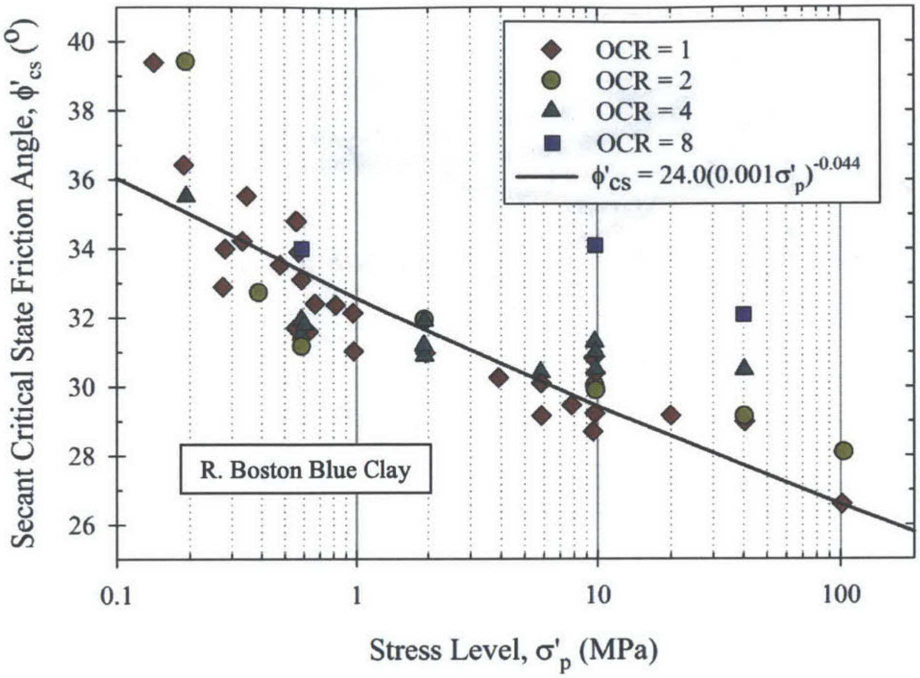

Figure 6-21: The variation in the critical state friction angle of RBBC with stress level

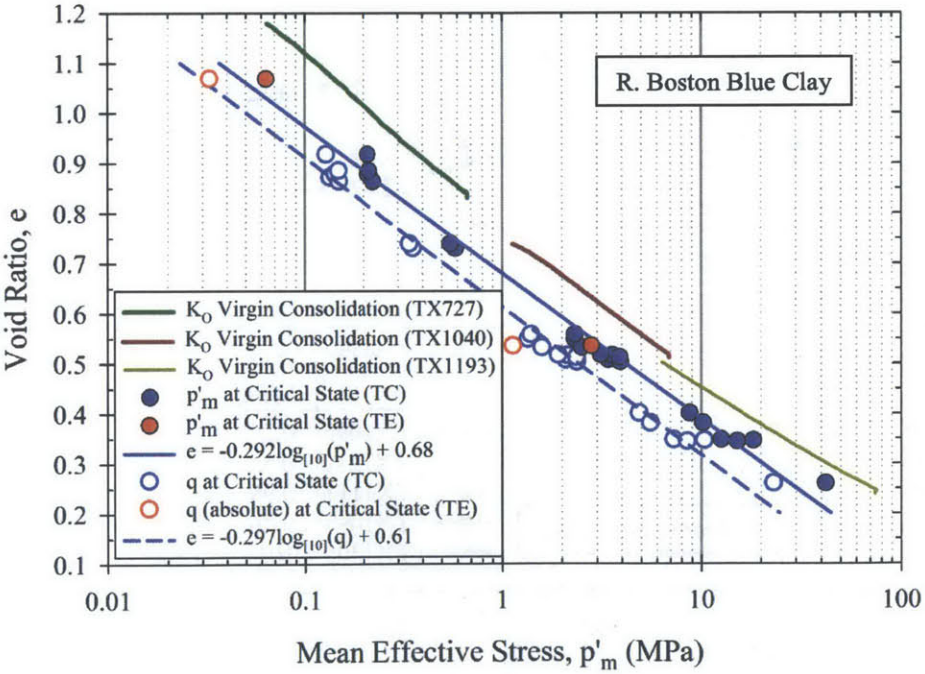

Figure 6-22: Mean effective stresses and shear stresses at critical state for RBBC. The figure shows the K_O virgin compression behavior of the soil as determined from representative triaxial tests. Results from two triaxial extension tests are also included.

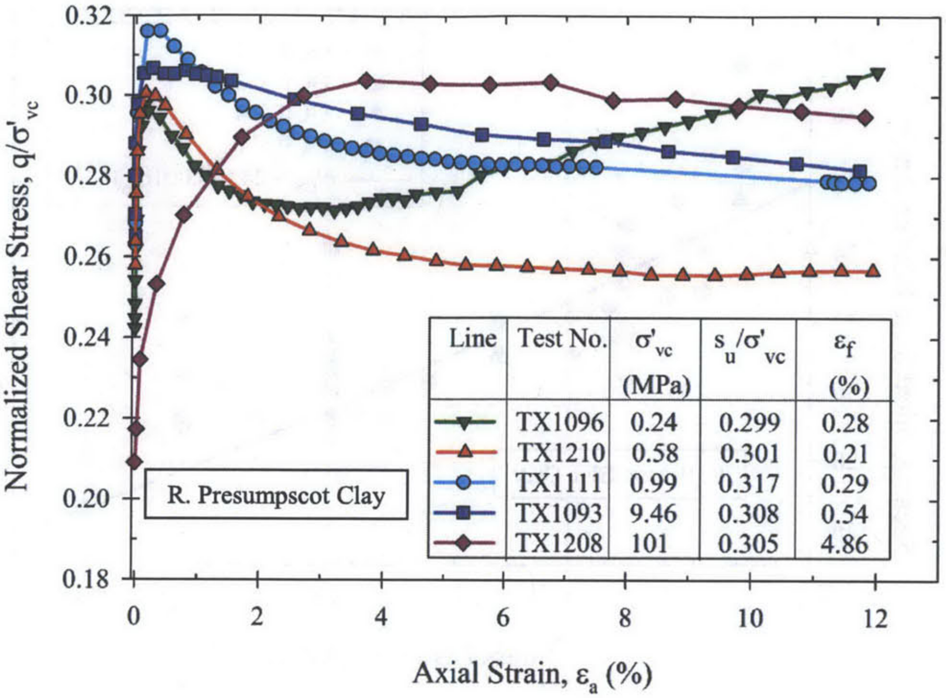

Figure 6-23: Normalized stress-strain responses measured during undrained shearing of NC RPC

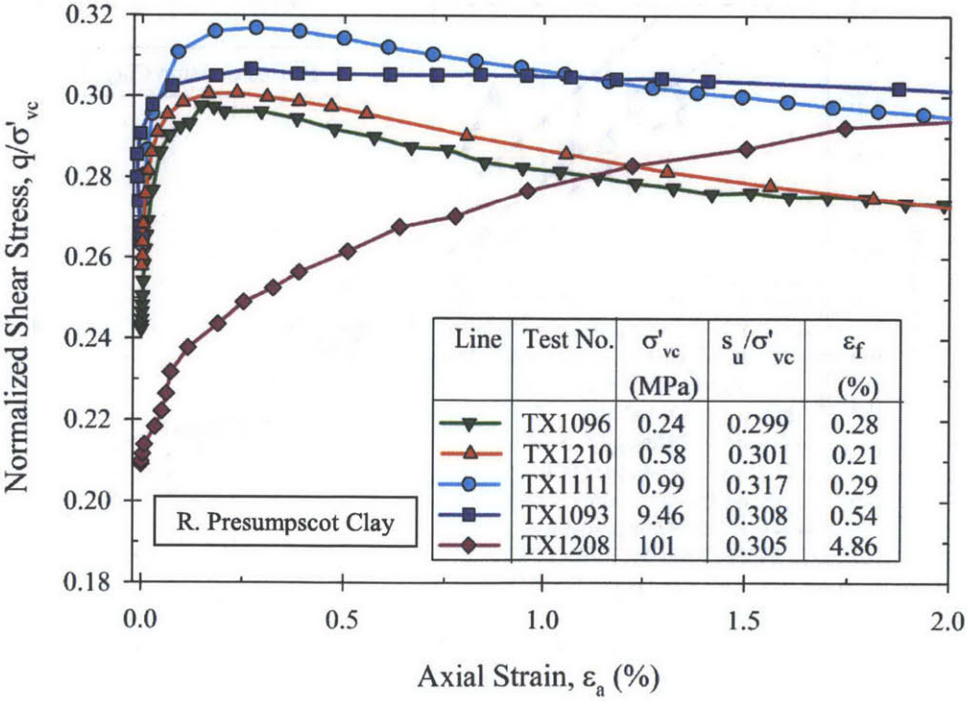

Figure 6-24: Normalized stress-strain responses measured during undrained shearing of NC RPC for axial strains up to 2 %

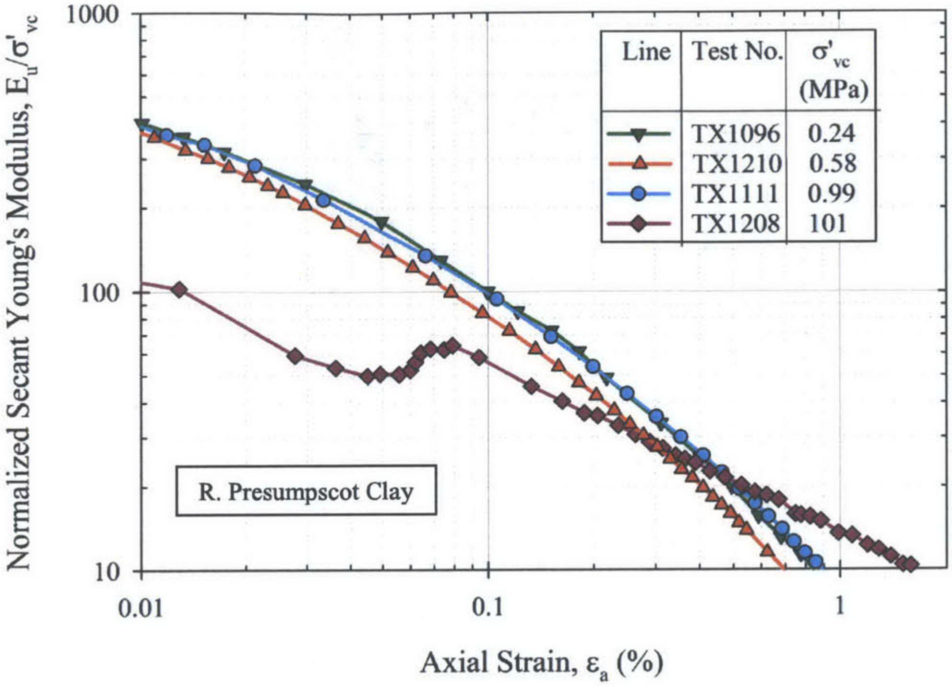

Figure 6-25: The variation in normalized secant Young's modulus with axial strain measured during undrained shearing of NC RPC

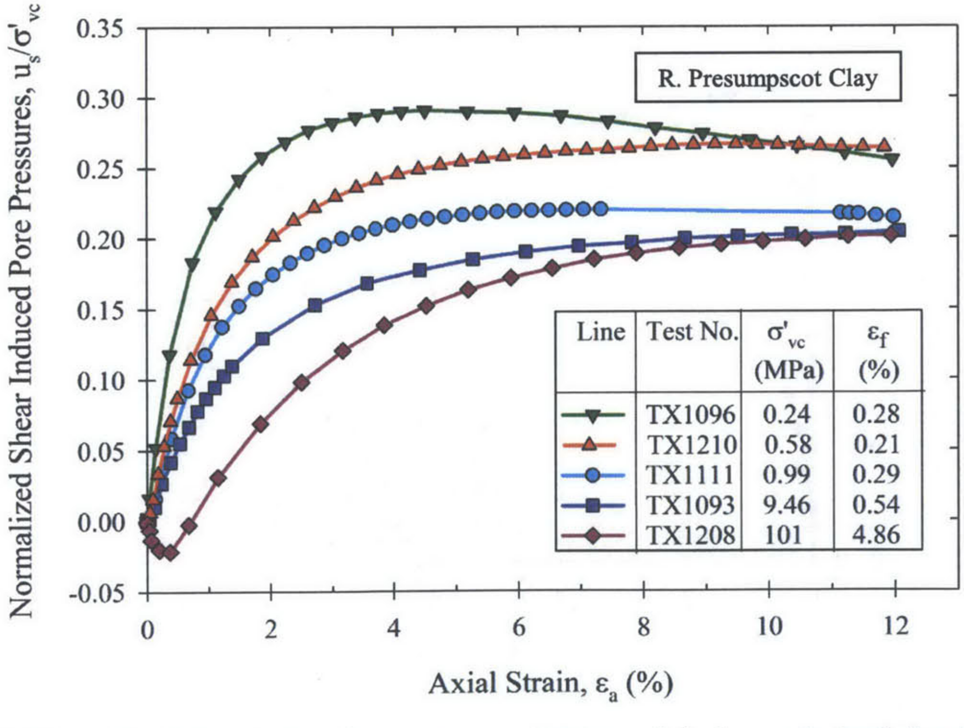

Figure 6-26: Normalized shear induced pore pressures measured during undrained shearing of NC RPC

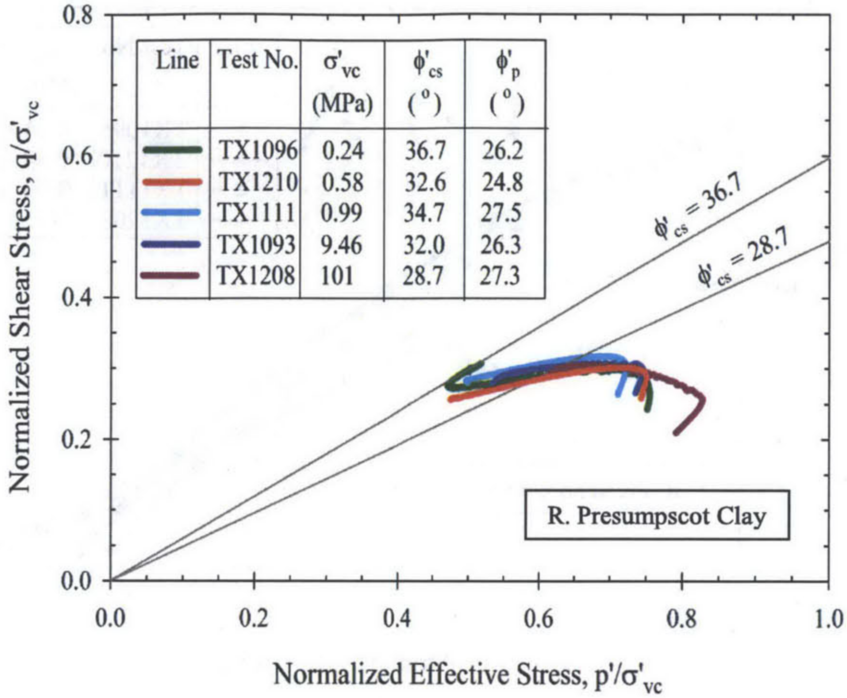

Figure 6-27: Effective stress paths followed during undrained shearing of NC RPC

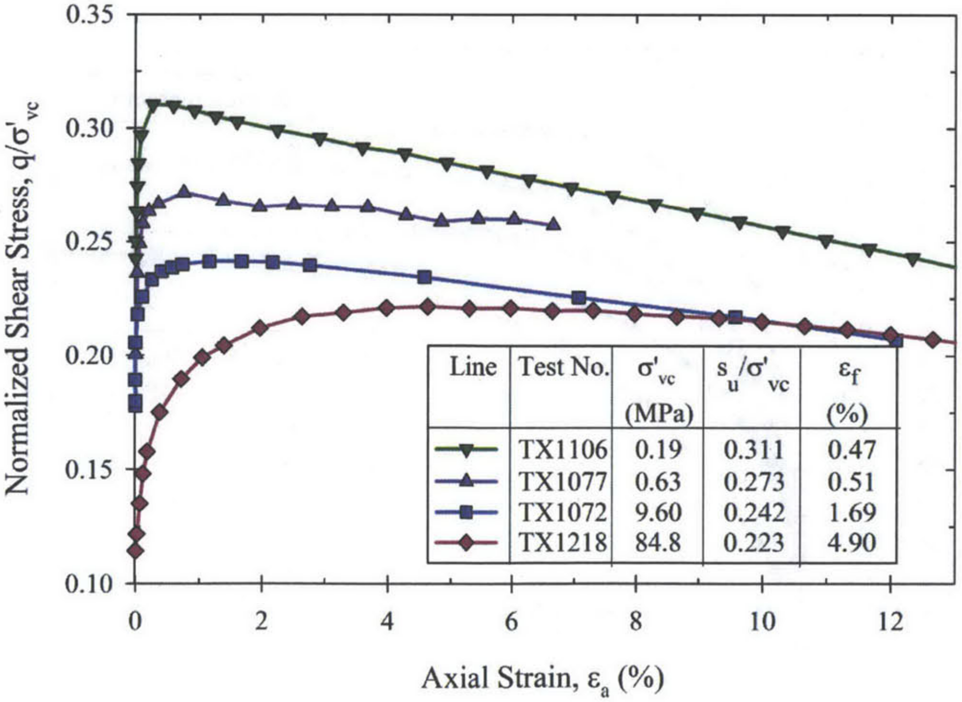

Figure 6-28: Normalized stress-strain responses measured during undrained shearing of NC RGoM Ursa

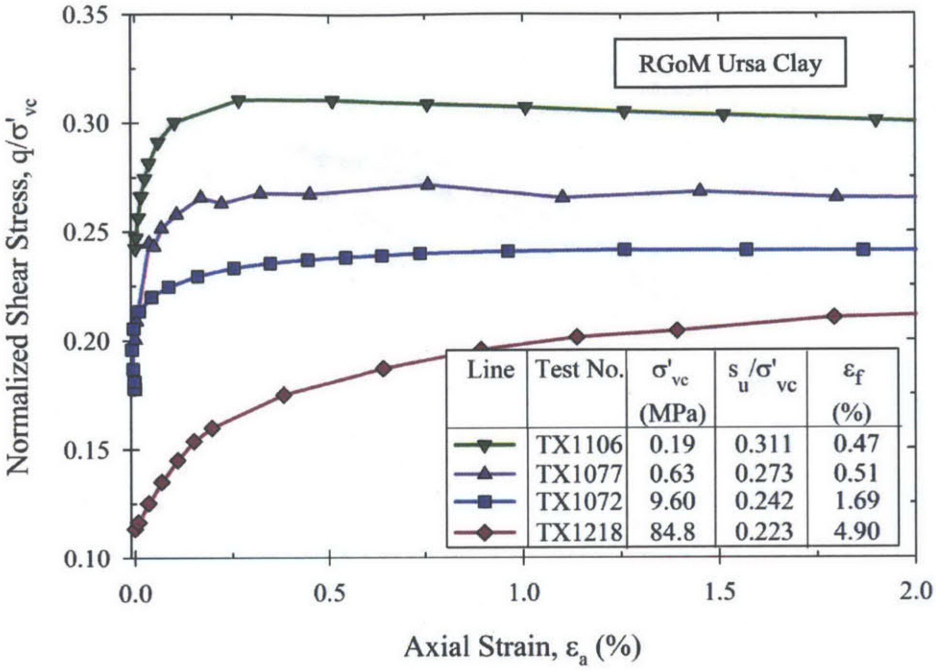

Figure 6-29: Normalized stress-strain responses measured during undrained shearing of NC RGoM Ursa for axial strains up to 2 %

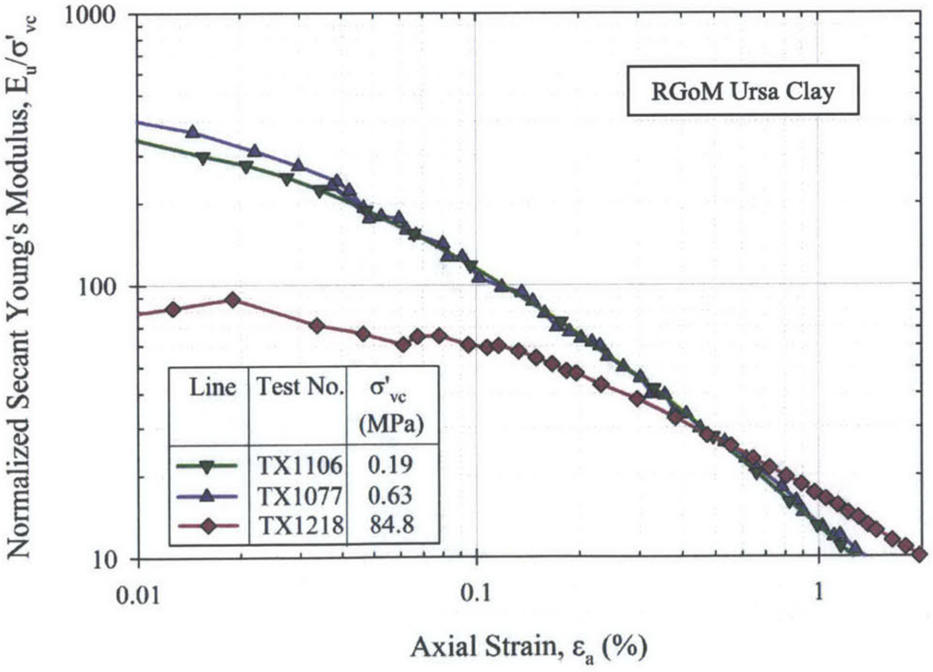

Figure 6-30: The variation in normalized secant Young's modulus with axial strain measured during undrained shearing of NC RGoM Ursa

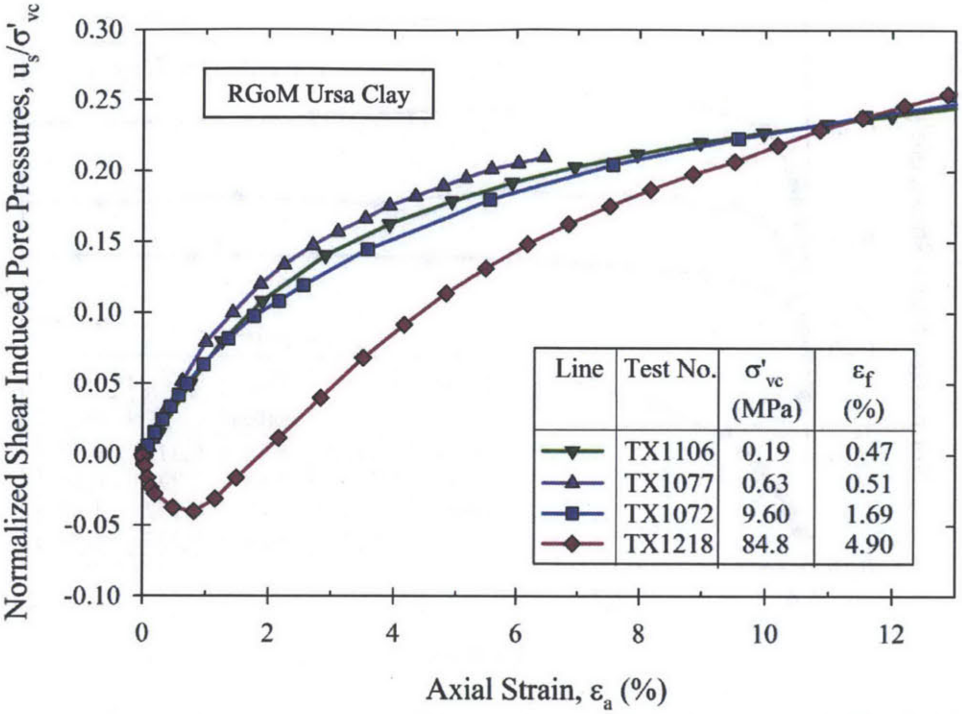

Figure 6-31: Normalized shear induced pore pressures measured during undrained shearing of NC RGoM Ursa

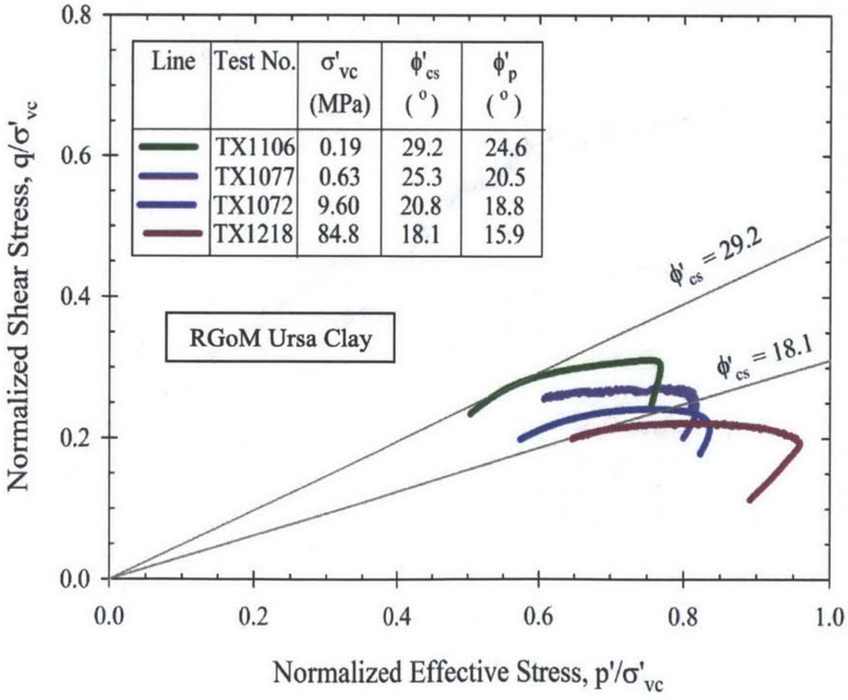

Figure 6-32: Effective stress paths followed during undrained shearing of NC RGoM Ursa

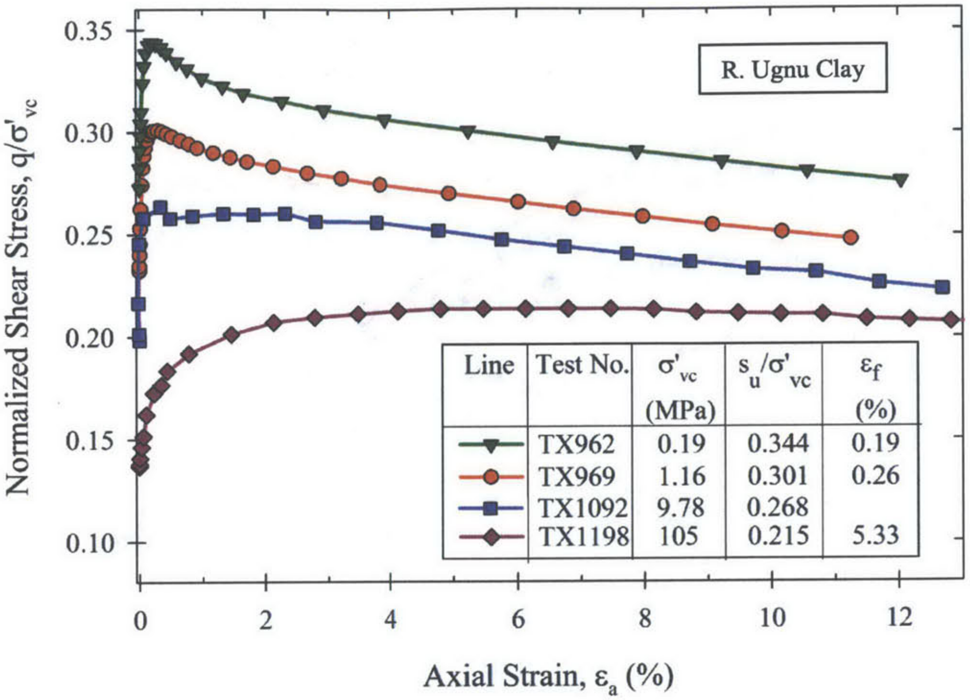

Figure 6-33: Normalized stress-strain responses measured during undrained shearing of NC RUC

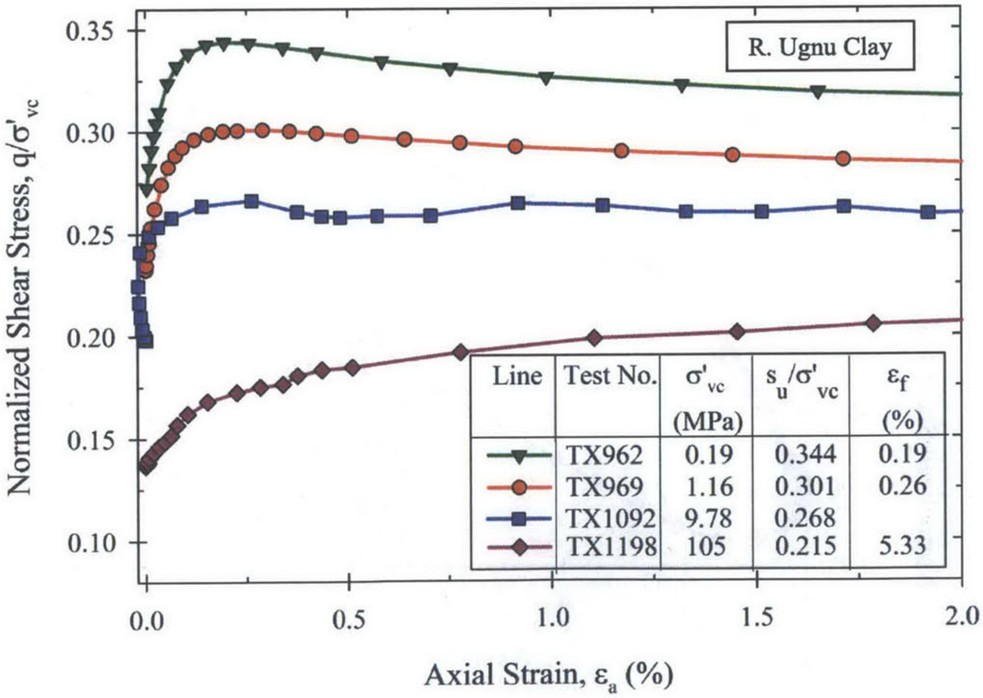

Figure 6-34: Normalized stress-strain responses measured during undrained shearing of NC RUC for axial strains up to 2 %

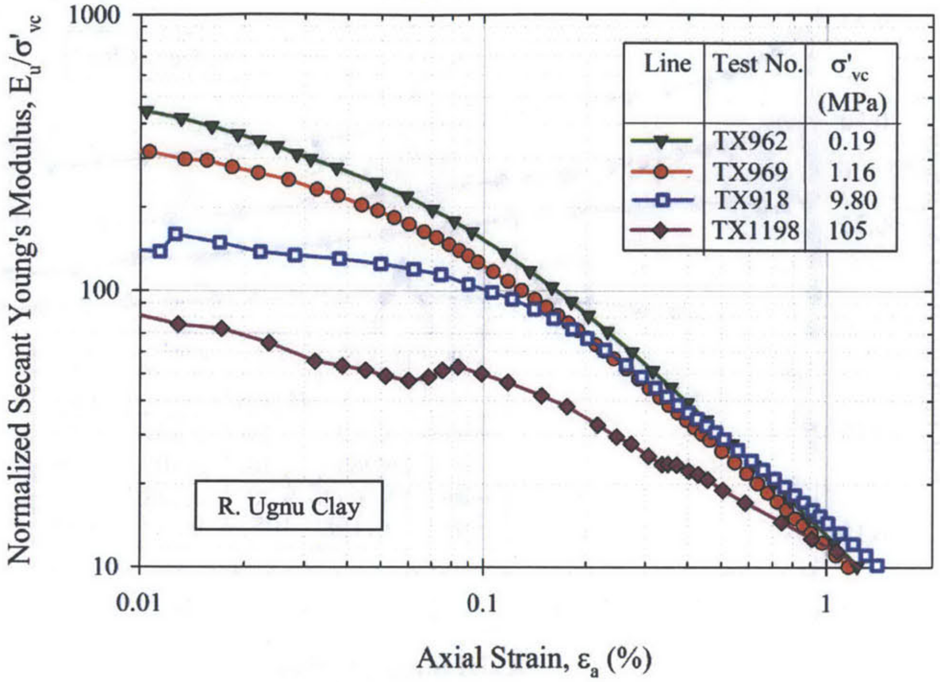

Figure 6-35: The variation in normalized secant Young's modulus with axial strain measured during undrained shearing of NC RUC

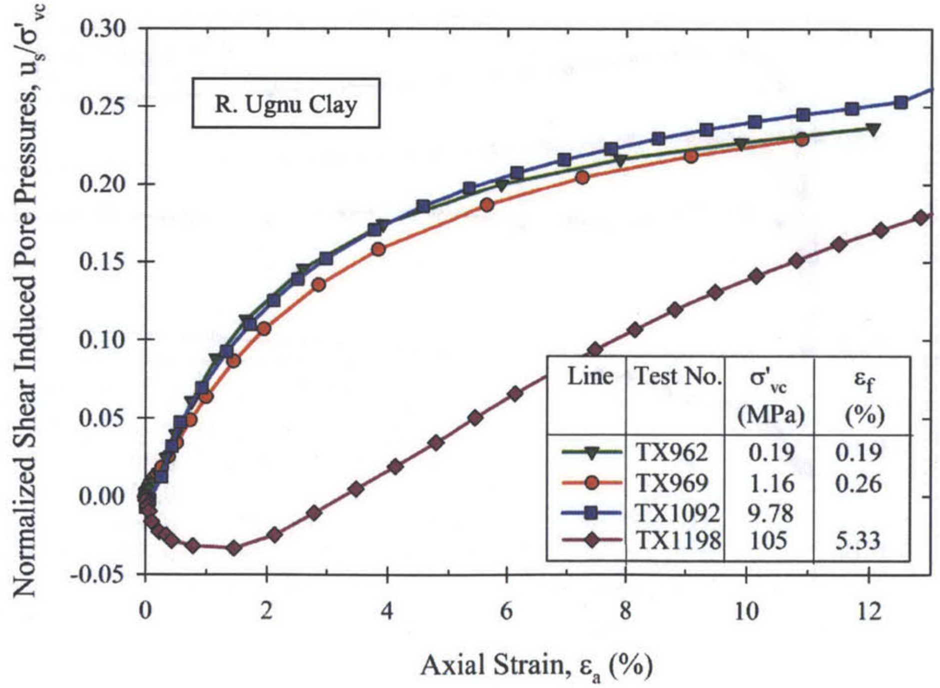

Figure 6-36: Normalized shear induced pore pressures measured during undrained shearing of NC RUC

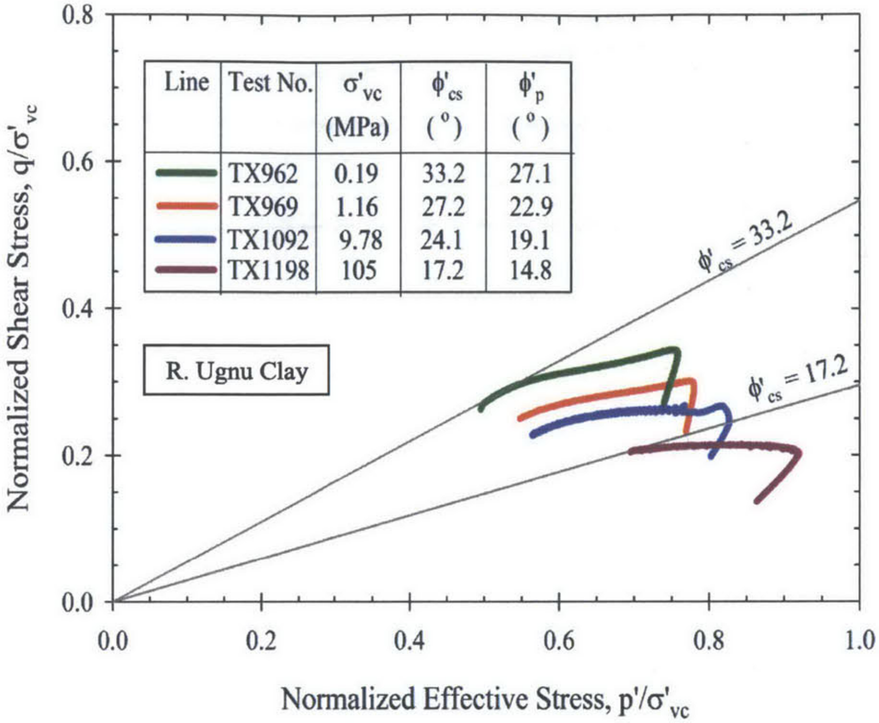

Figure 6-37: Effective stress paths followed during undrained shearing of NC RUC

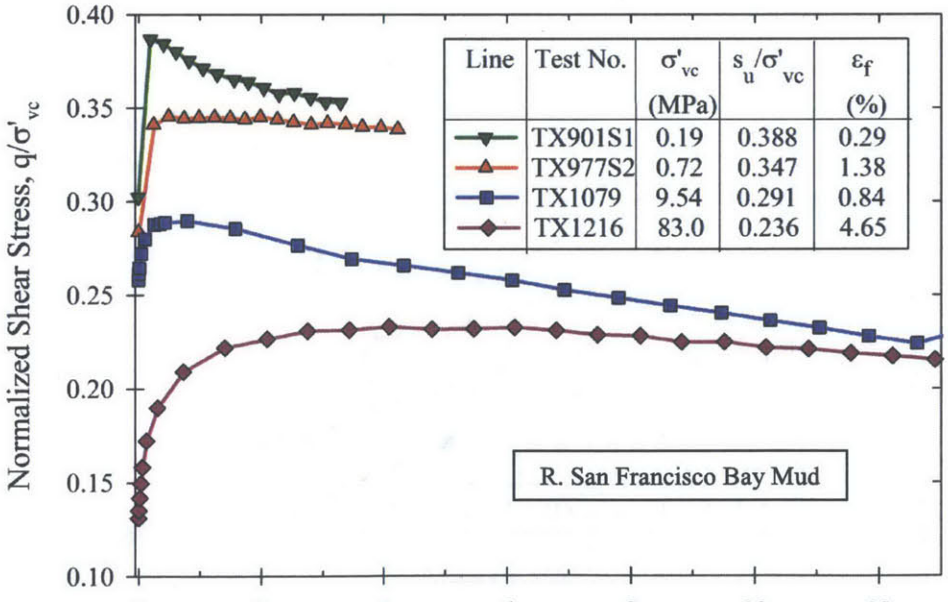

Figure 6-38: Normalized stress-strain responses measured during undrained shearing of NC RSFBM

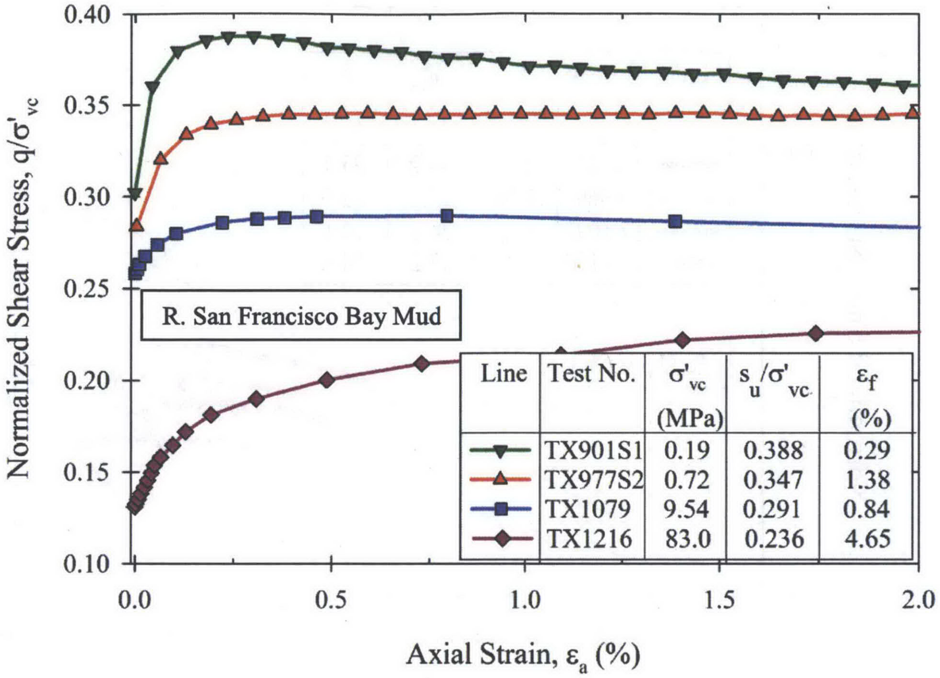

Figure 6-39: Normalized stress-strain responses measured during undrained shearing of NC RSFBM for axial strains up to 2 %

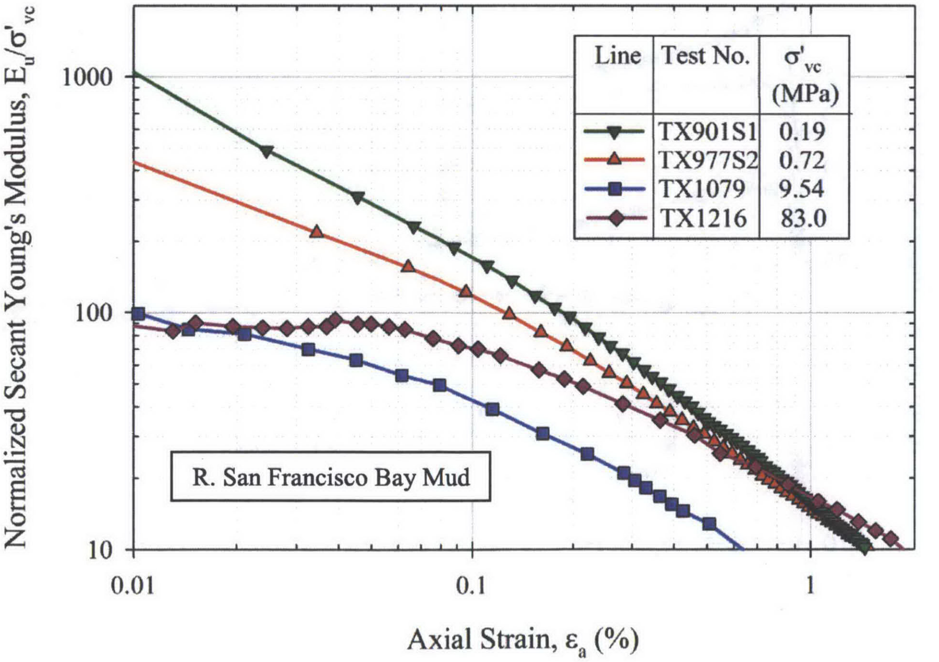

Figure 6-40: The variation in normalized secant Young's modulus with axial strain measured during undrained shearing of NC RSFBM

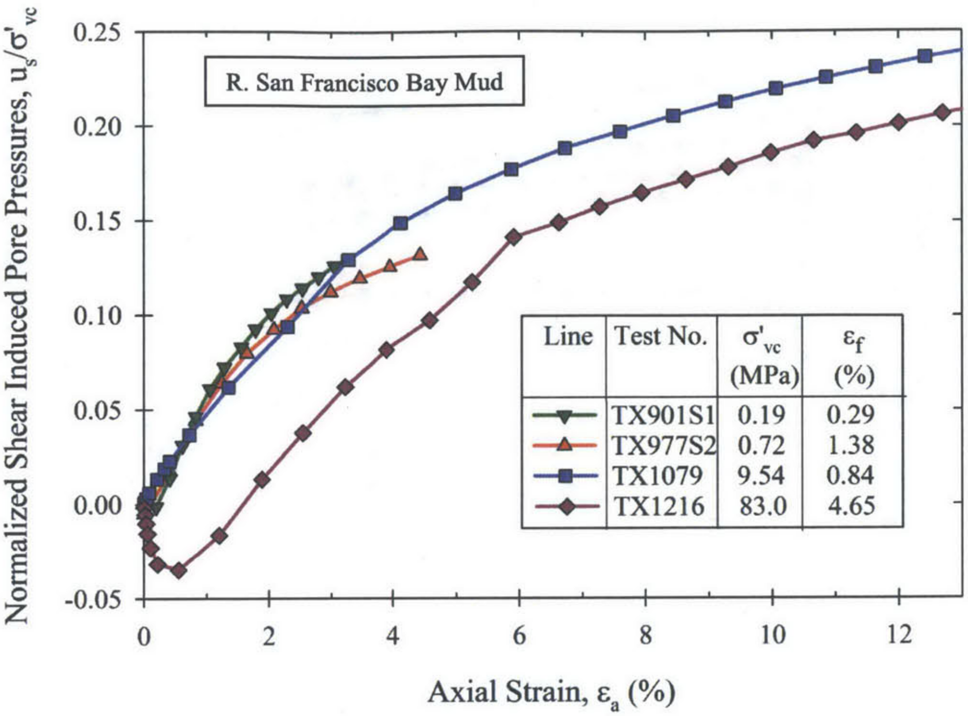

Figure 6-41: Normalized shear induced pore pressures measured during undrained shearing of NC RSFBM

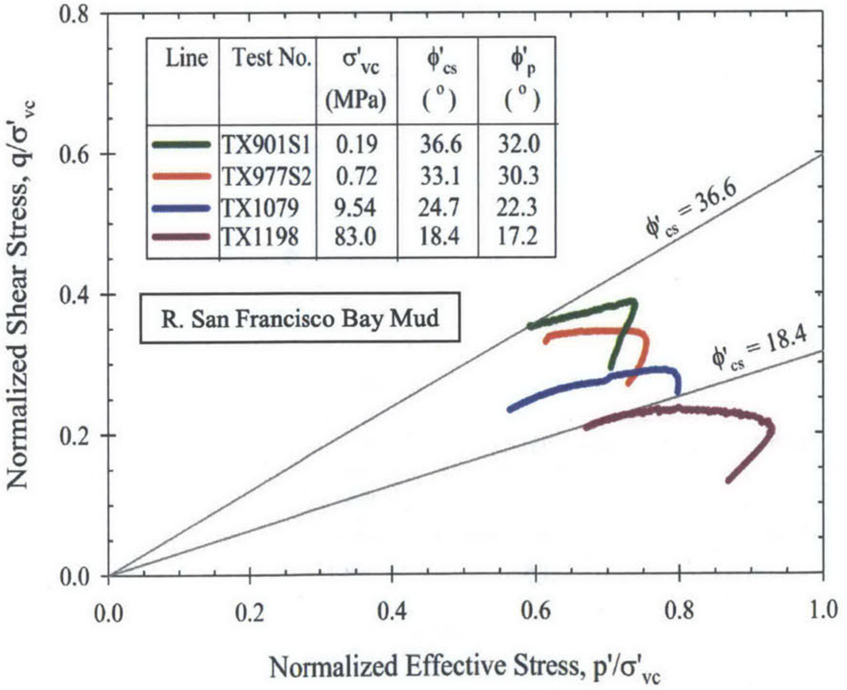

Figure 6-42: Effective stress paths followed during undrained shearing of NC RSFBM

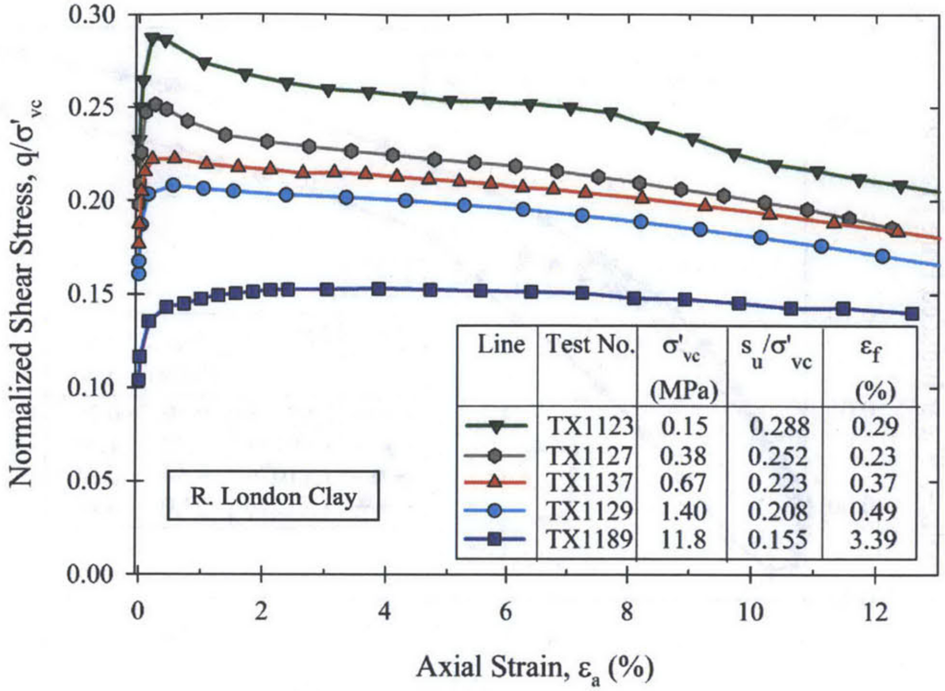

Figure 6-43: Normalized stress-strain responses measured during undrained shearing of NC RLC over a wide range of consolidation stresses

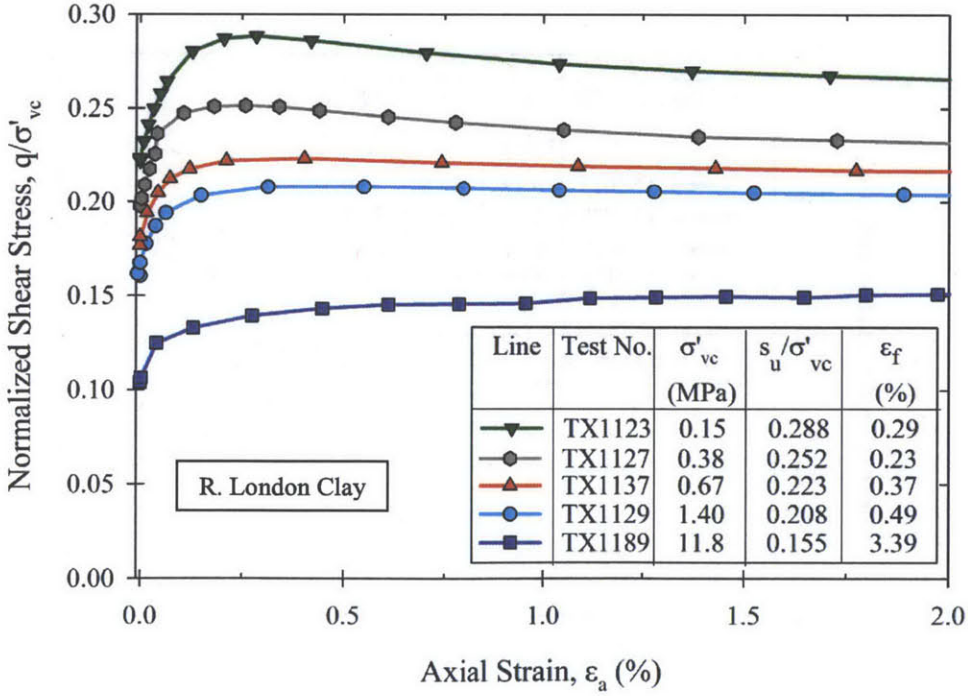

Figure 6-44: Normalized stress-strain responses measured during undrained shearing of NC RLC over a wide range of consolidation stresses for axial strains up to 2 %

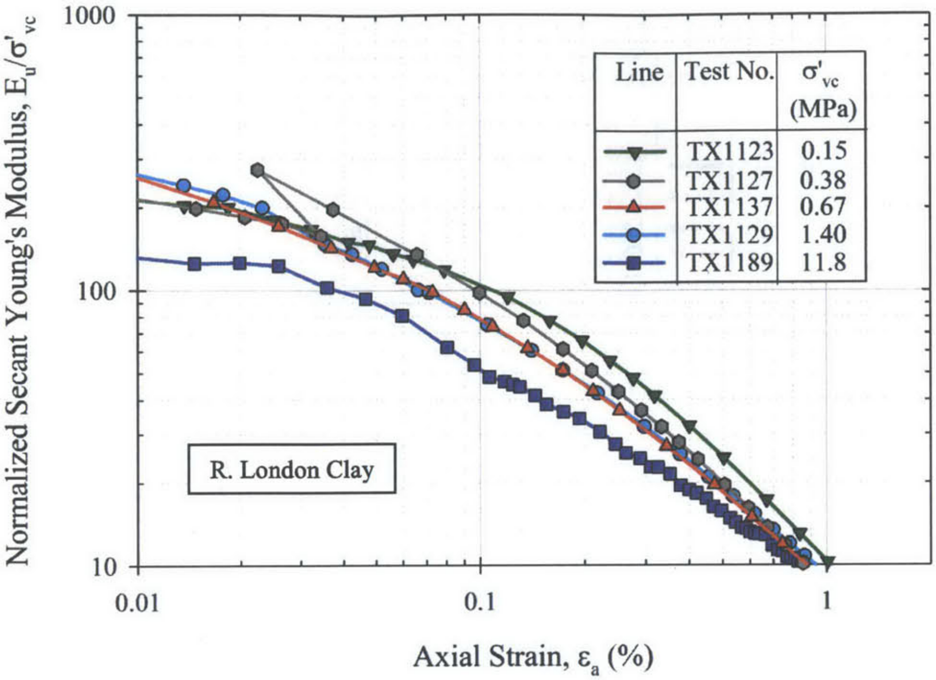

Figure 6-45: The variation in normalized secant Young's modulus with axial strain measured during undrained shearing of NC RLC

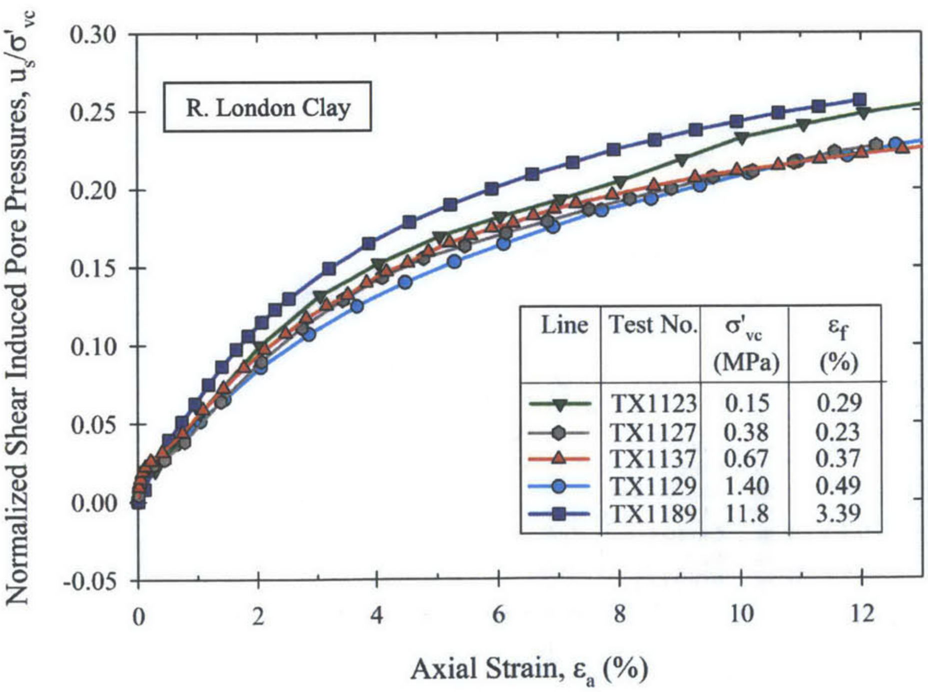

Figure 6-46: Normalized shear induced pore pressures measured during undrained shearing of NC RLC over a wide range of consolidation stresses

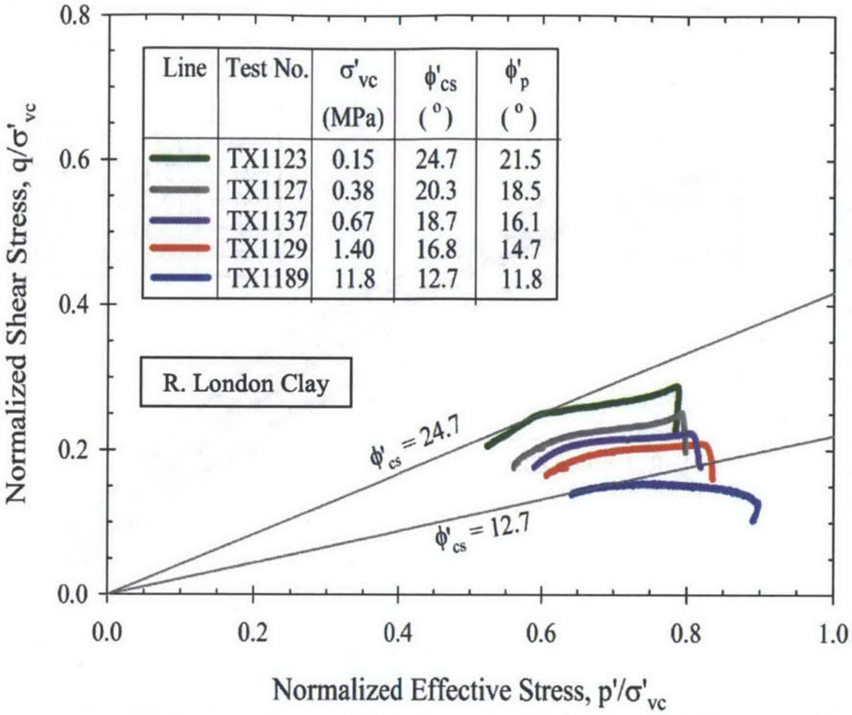

Figure 6-47: Effective stress paths followed during undrained shearing of NC RLC over a wide range of consolidation stresses

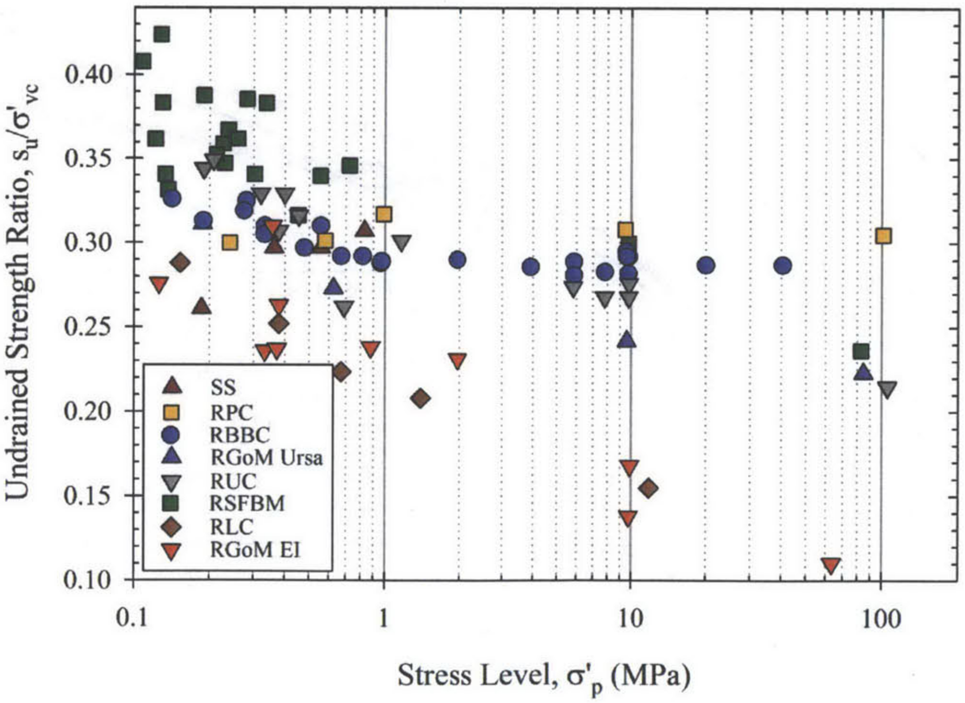

Figure 6-48: Undrained strength ratios of soils plotted as a function of stress level

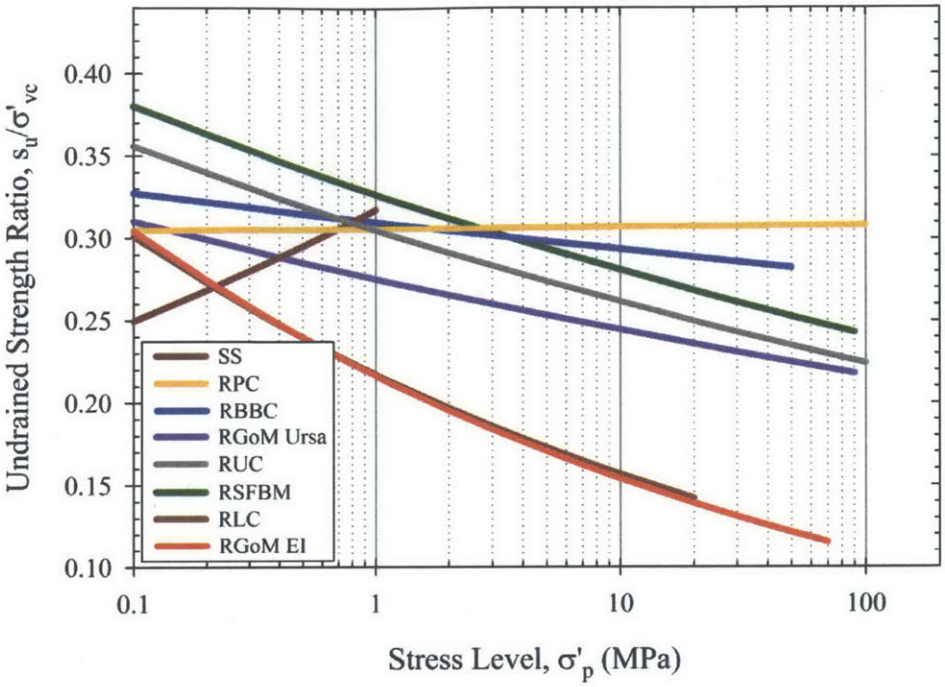

Figure 6-49: Regression lines for the experimental data presented in Figure 6-48. The regression lines are of the form $s_u/\sigma'_{vc} = S_1(1000\sigma'_{p\,[MPa]})^T$

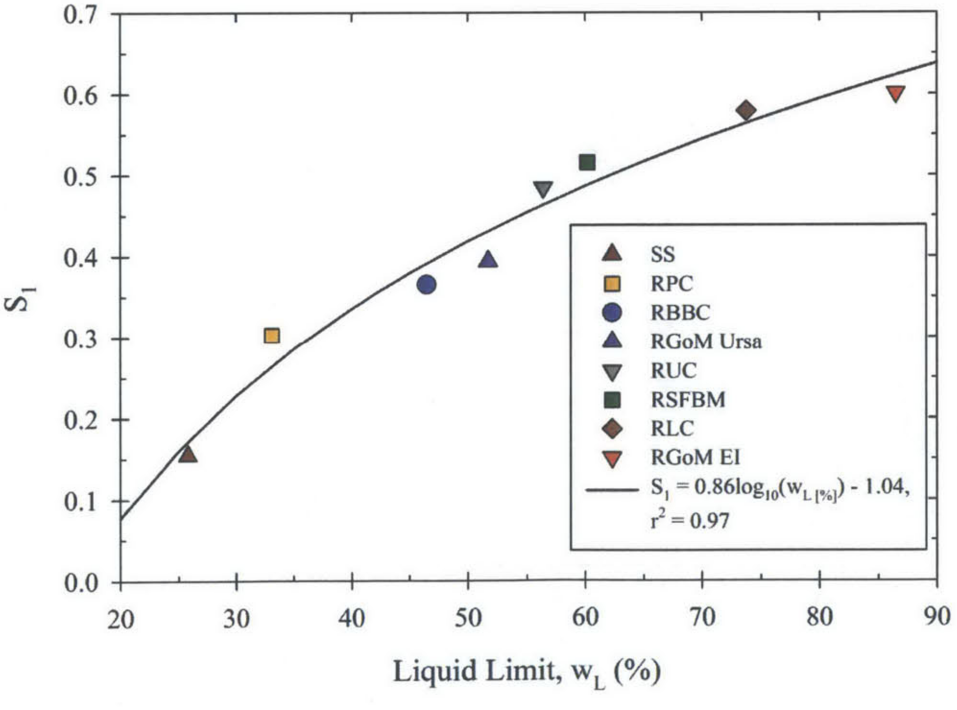

Figure 6-50: Correlation between the parameter S_1 and liquid limit

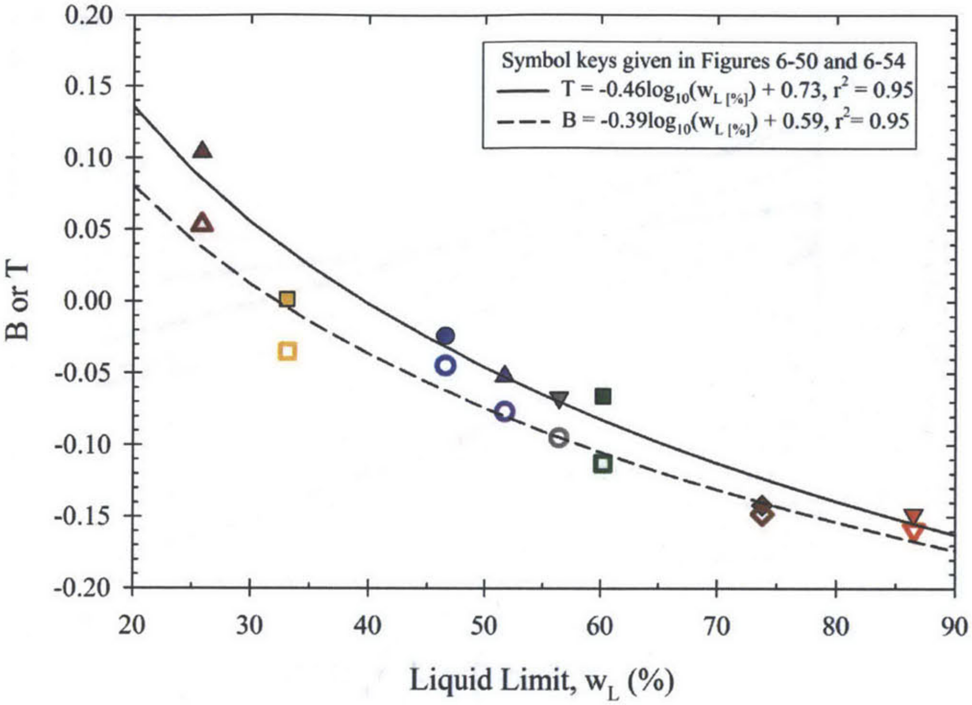

Figure 6-51: Correlations between the parameters T and B with liquid limit

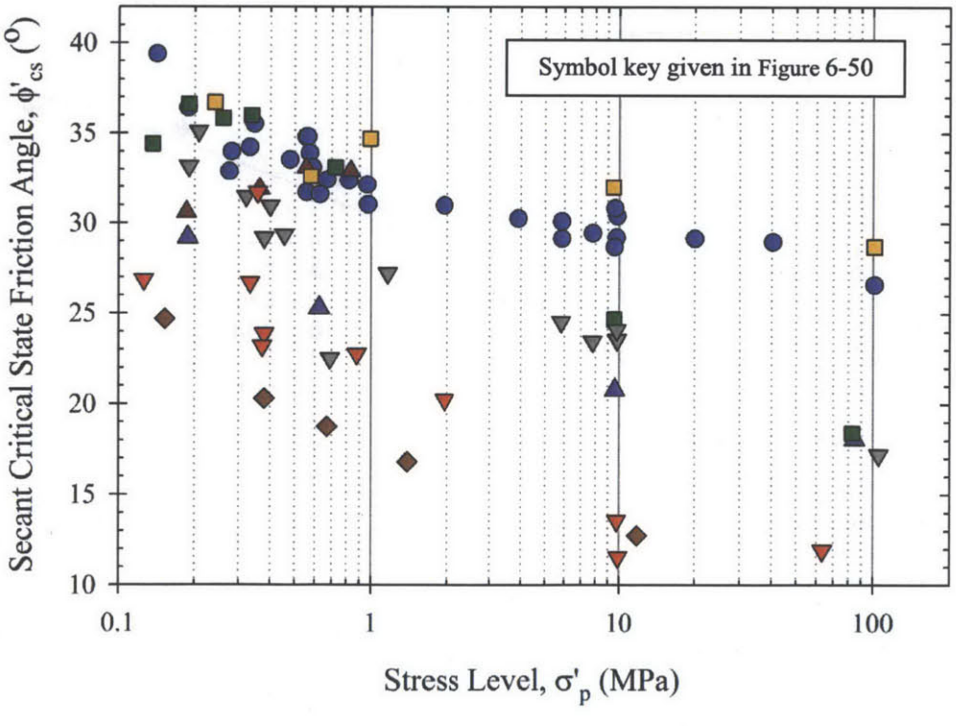

Figure 6-52: Critical state friction angles of soils plotted as a function of stress level

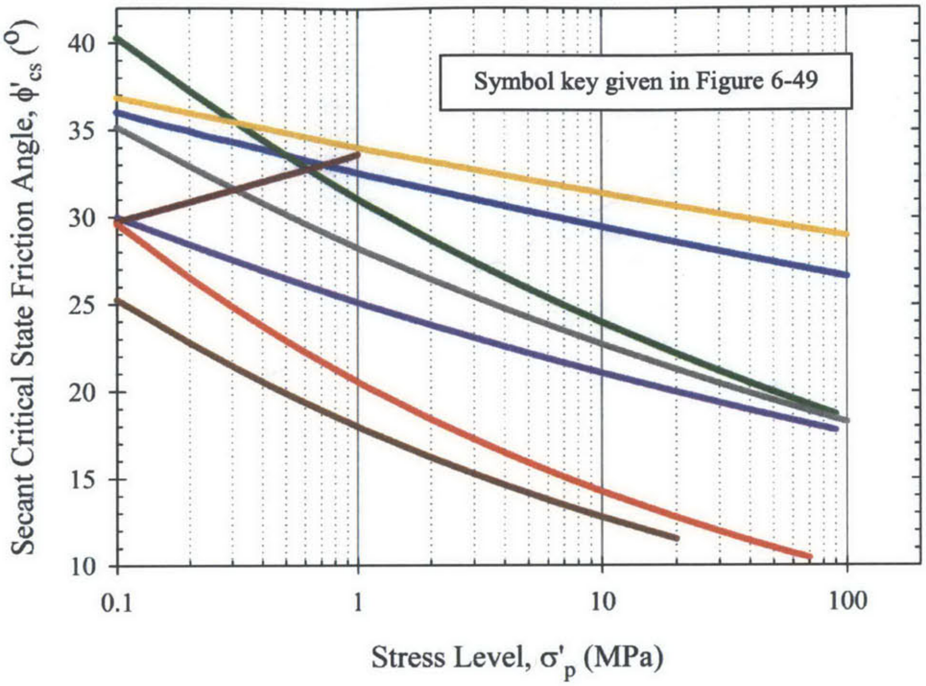

Figure 6-53: Regression lines for the experimental data presented in Figure 6-52. The regression lines are of the form $\varphi'_{cs} = A(0.001\sigma'_{p\,[MPa]})^B$

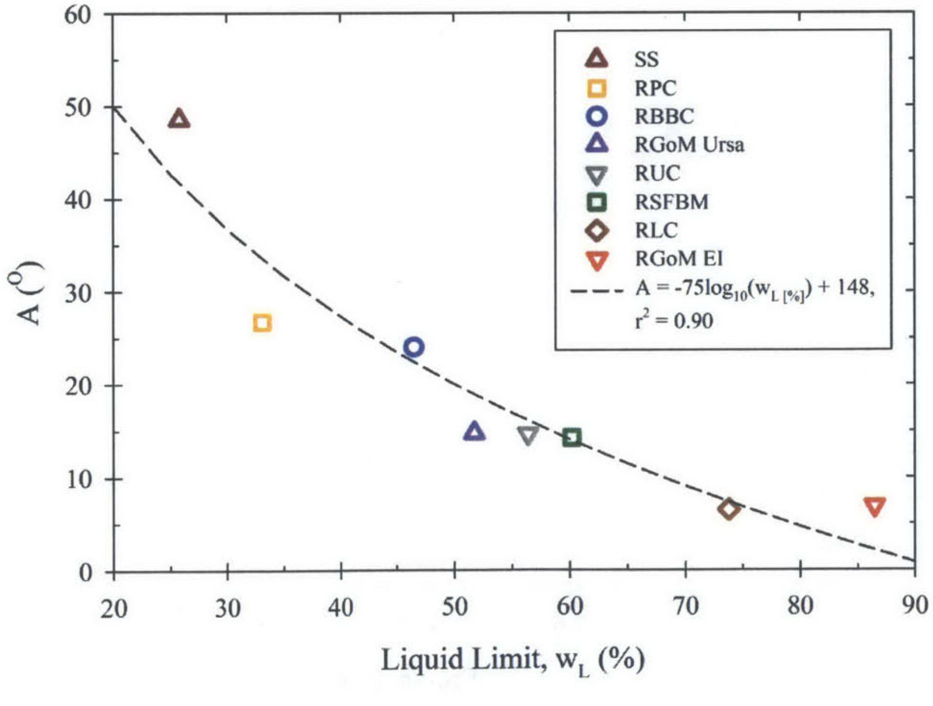

Figure 6-54: Correlation between the parameter A and liquid limit

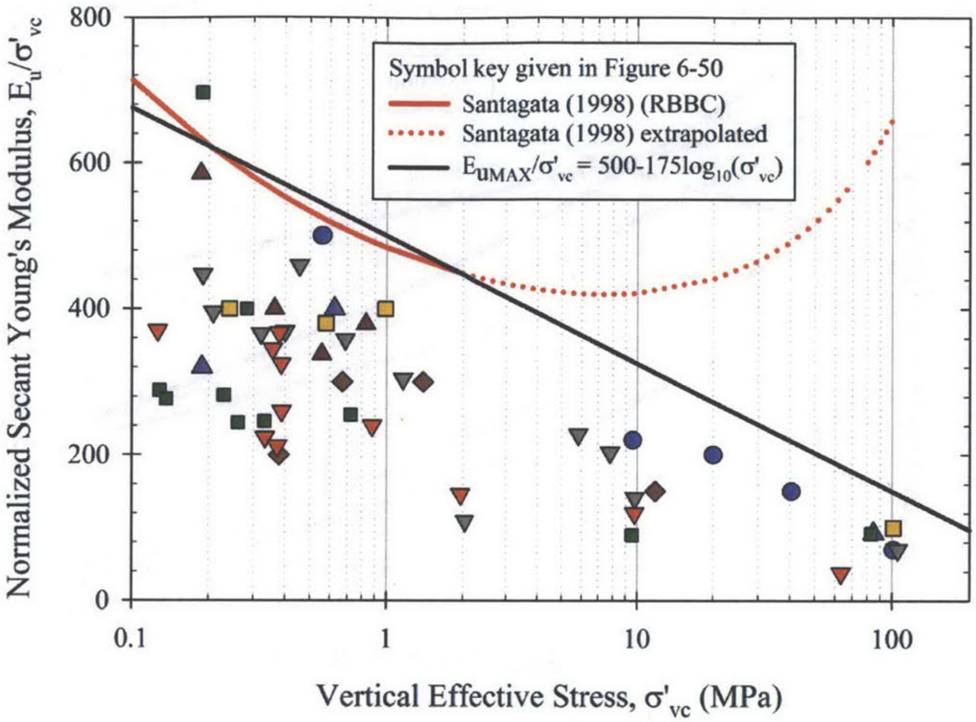

Figure 6-55: Normalized secant Young's moduli of soils measured at $\varepsilon_a = 0.01$ % and OCR = 1. The relationship for E_{uMAX}/σ'_{vc} developed for NC RBBC by Santagata (1998) is also plotted

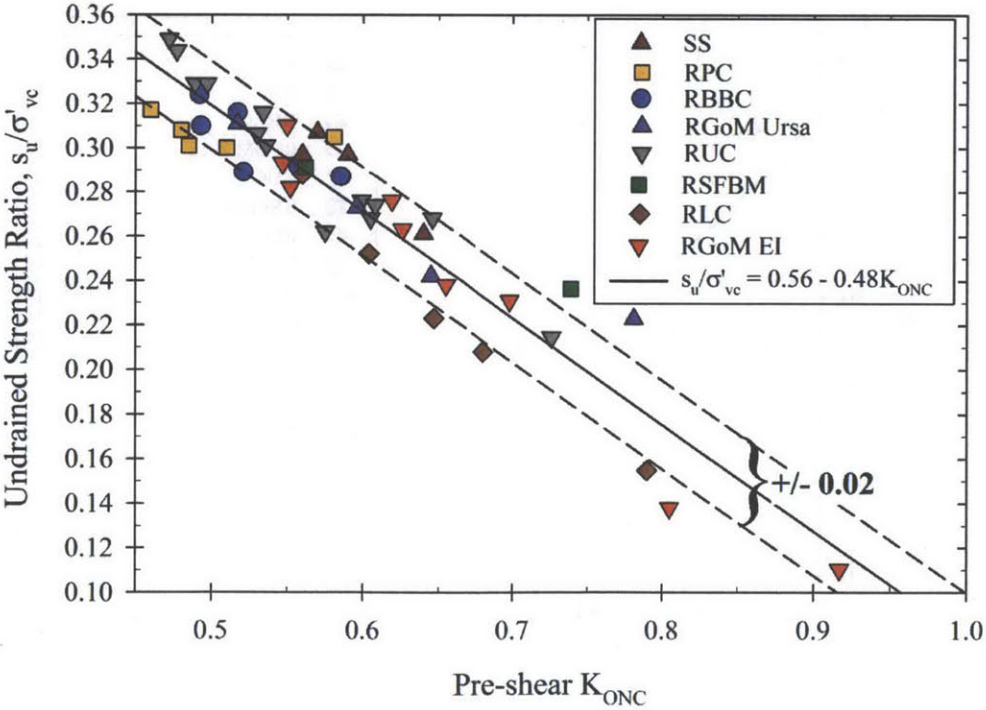

Figure 6-56: Relationship between the pre-shear K_{ONC} and undrained strength ratio of soils

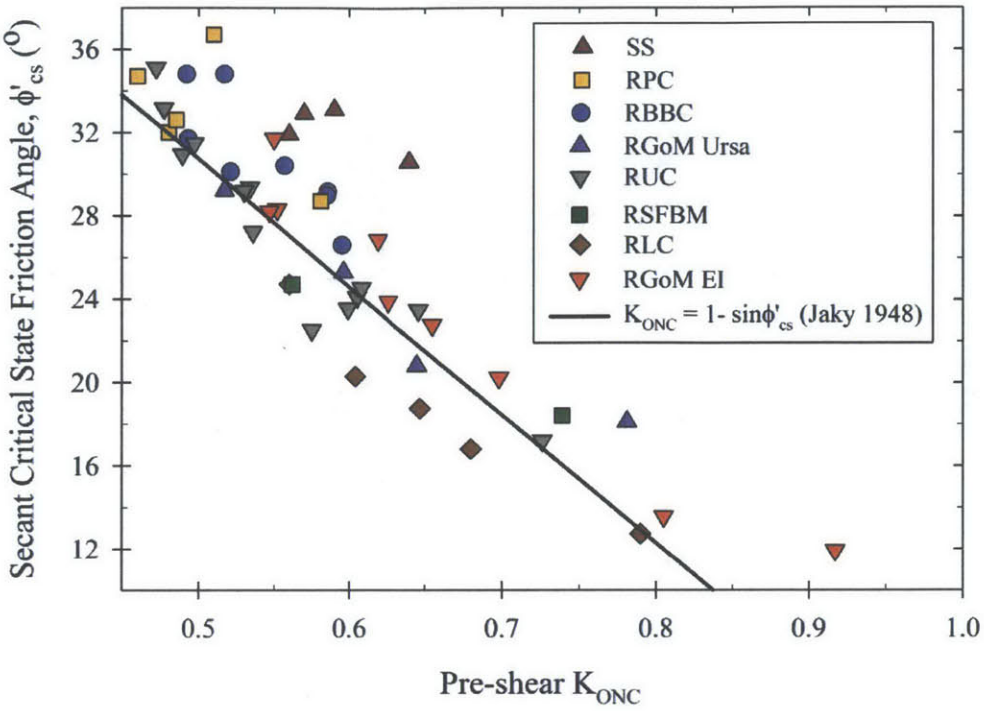

Figure 6-57: Correlation between the pre-shear K_{ONC} and friction angle of soils

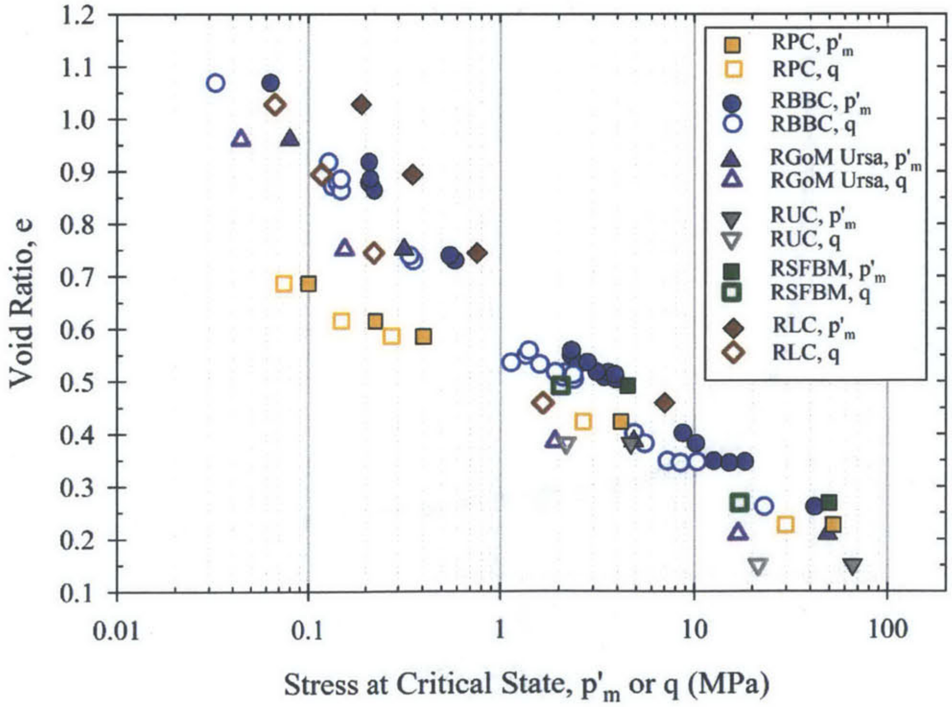

Figure 6-58: Mean effective stresses and shear stresses at critical state for various soils

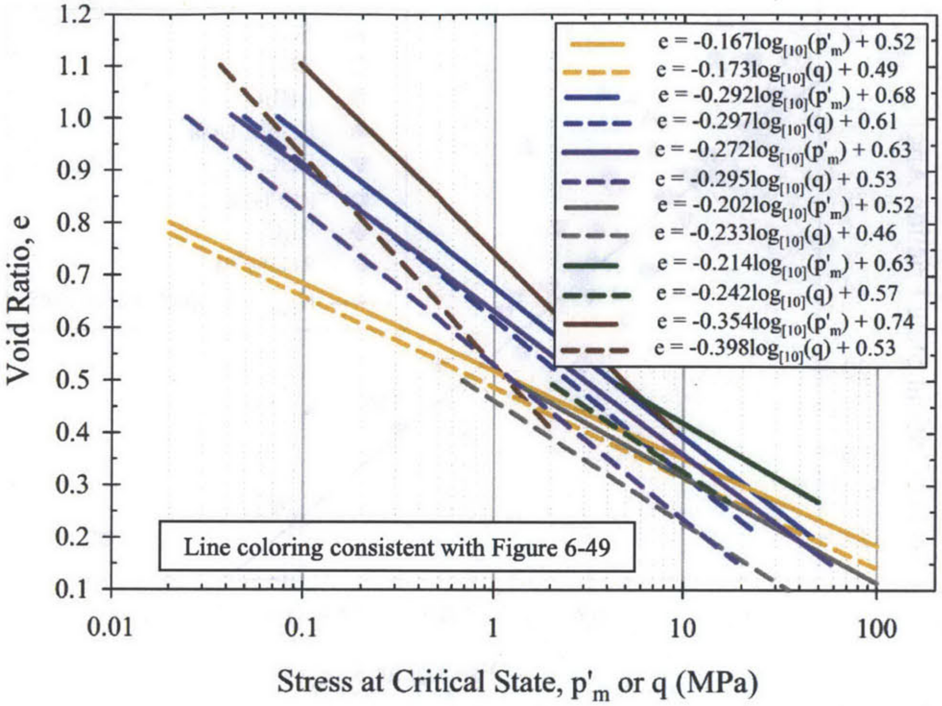

Figure 6-59: Critical state lines of mean effective stress and shear stress for various soils

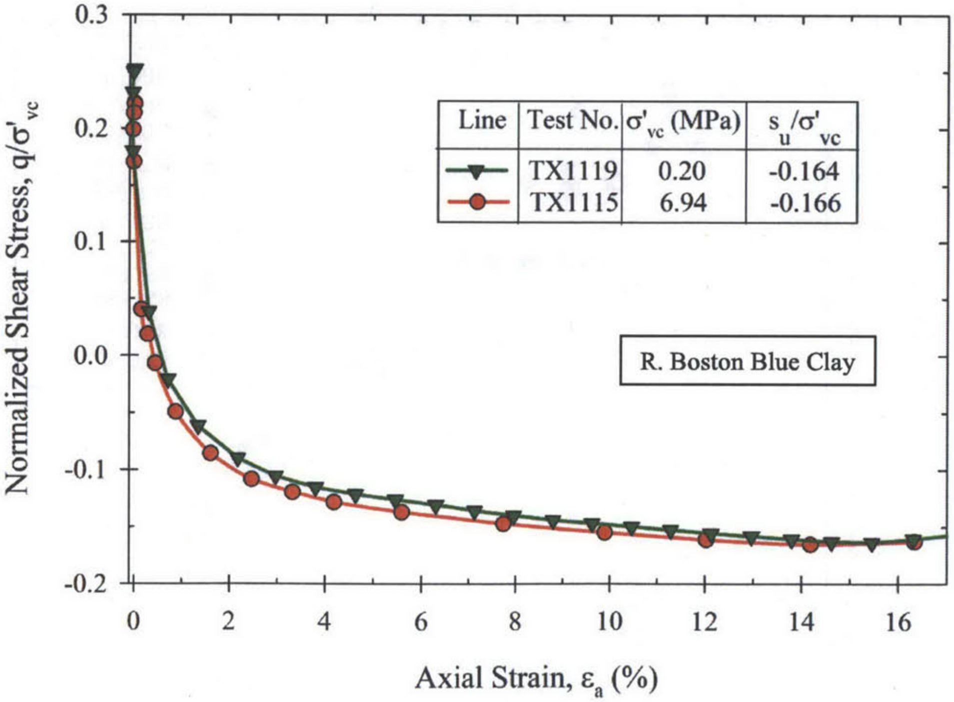

Figure 6-60: Normalized stress-strain responses measured during undrained shearing of NC RBBC in triaxial extension mode of shear at a low and high consolidation stress level

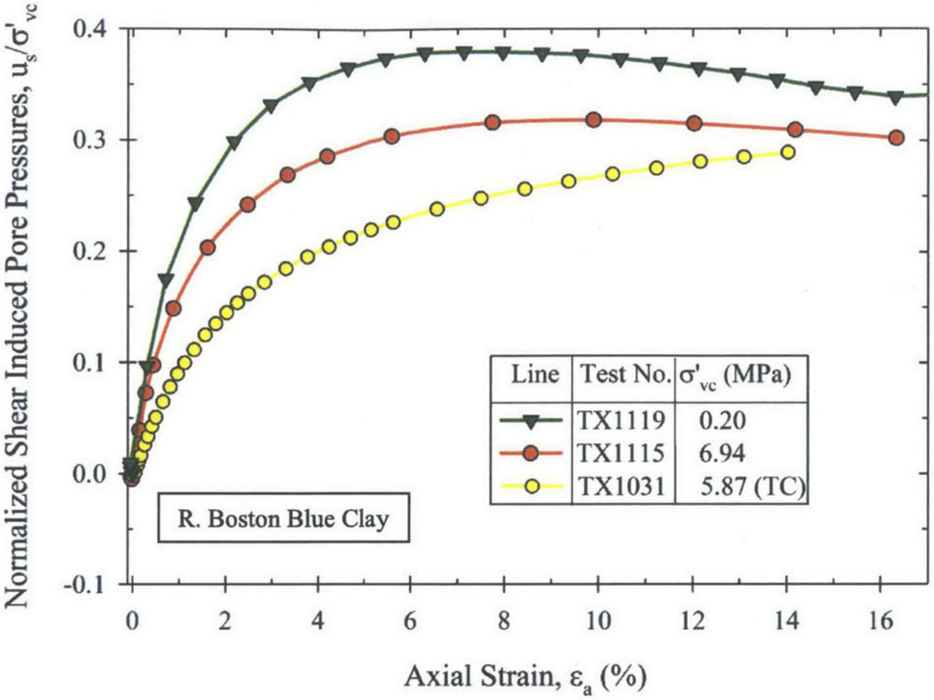

Figure 6-61: Normalized shear induced pore pressures measured during undrained shearing of NC RBBC in triaxial extension mode of shear at a low and high consolidation stress level

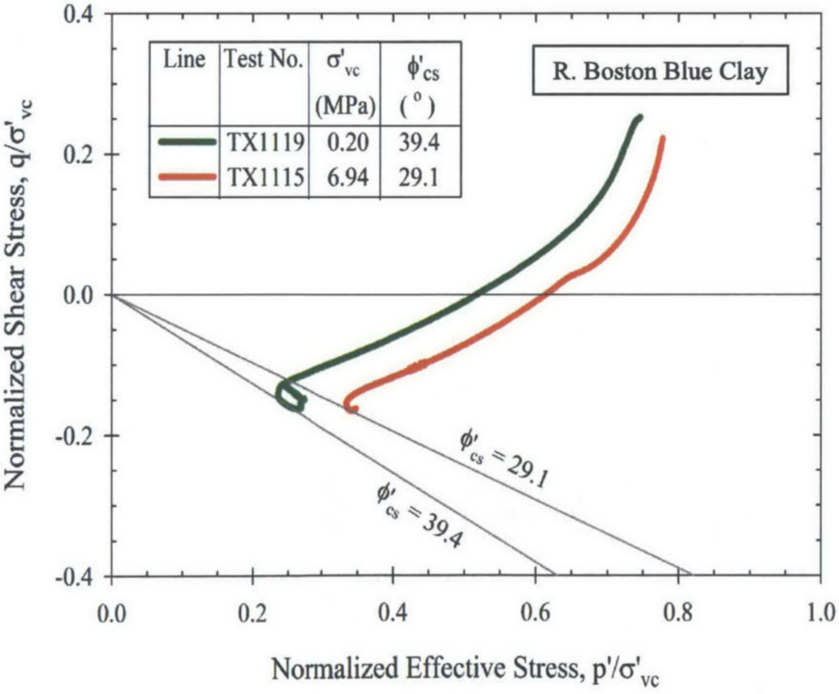

Figure 6-62: Effective stress paths followed during undrained shearing of NC RBBC in triaxial extension mode of shear at a low and high consolidation stress level

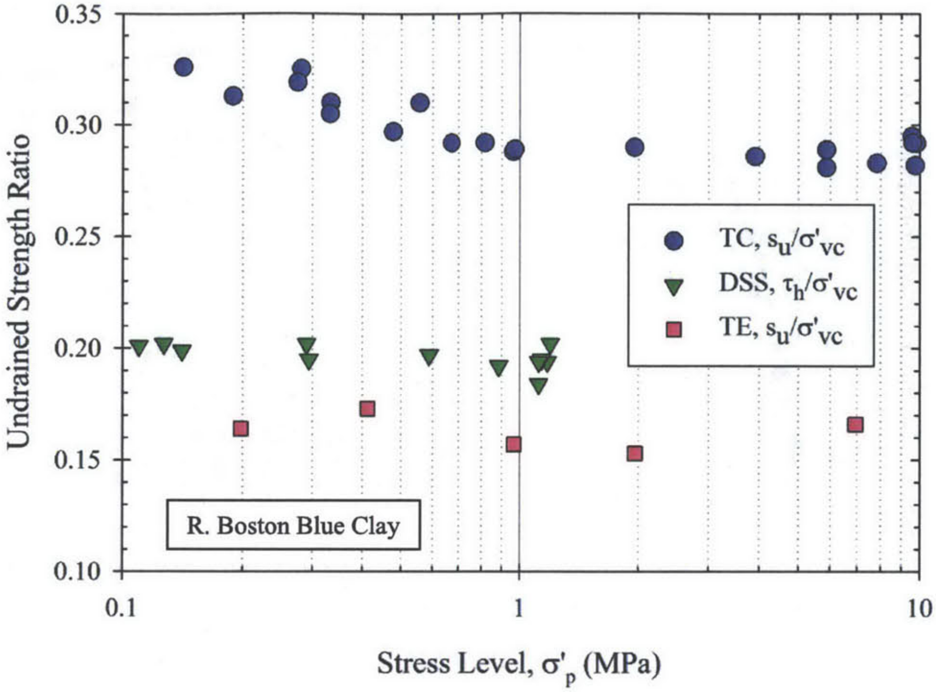

Figure 6-63: The variation in the undrained strength ratio of NC RBBC with consolidation stress level for TC, DSS and TE modes of shear

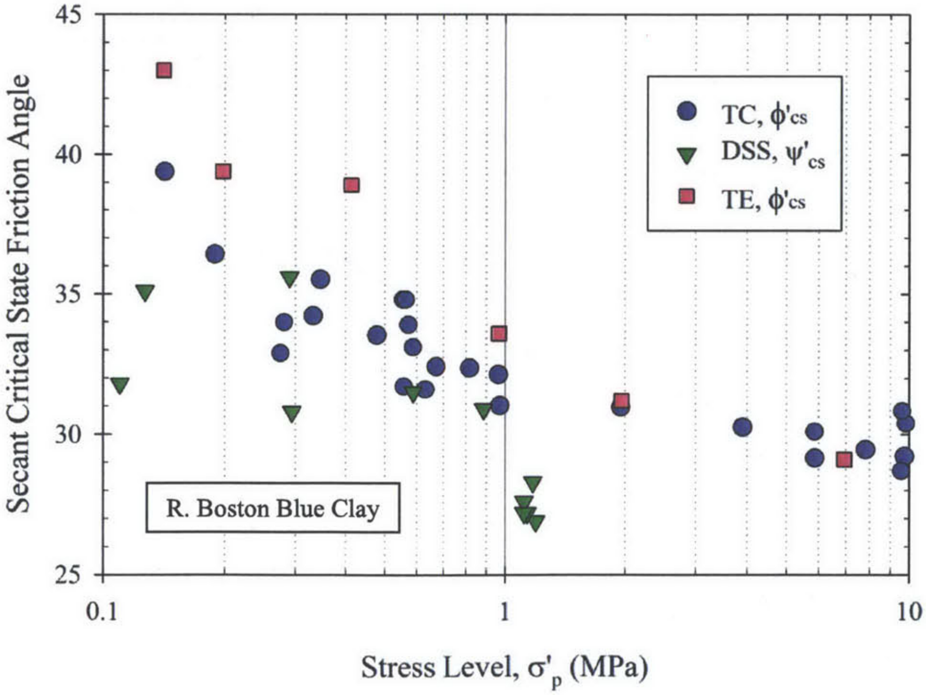

Figure 6-64: The variation in the critical state friction angle of RBBC with consolidation stress level for TC, DSS and TE modes of shear

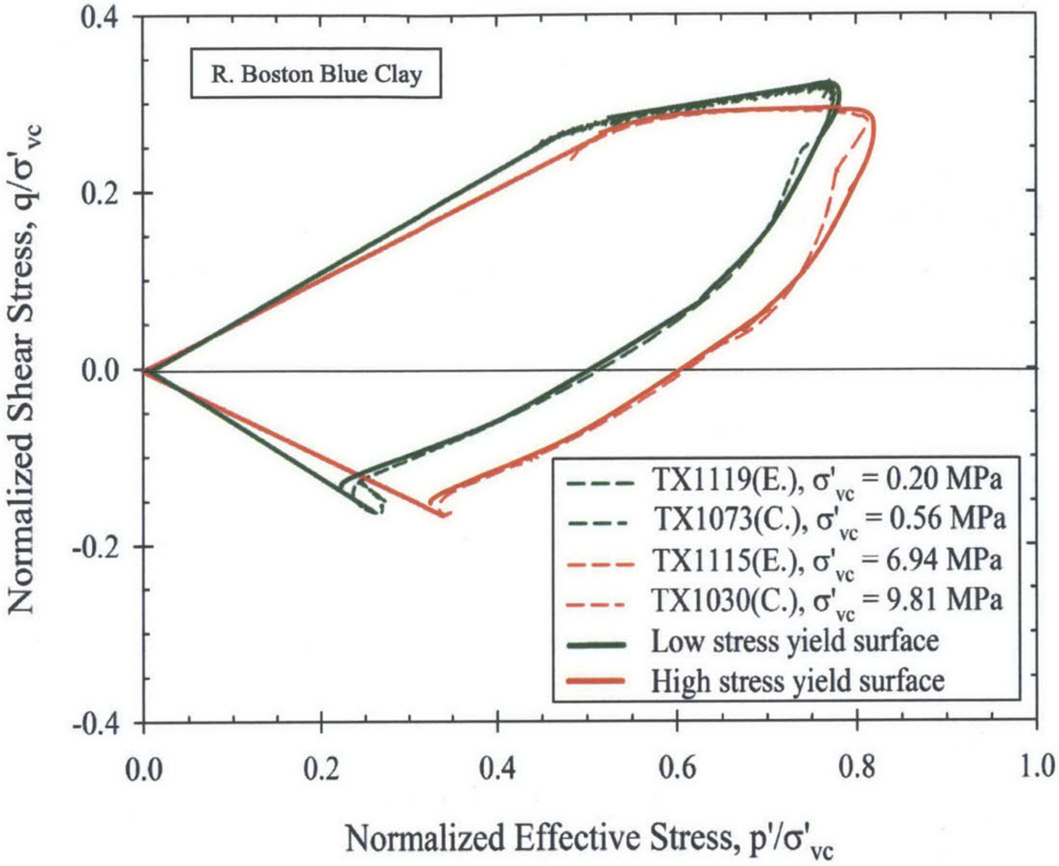

Figure 6-65: Interpreted yield surfaces of RBBC at low and high consolidation stresses based on the results of TE and TC tests performed on the soil at OCR = 1

7 CONCLUSIONS AND RECOMMENDATIONS

7.1 RESEDIMENTATION

The research presented in this thesis makes use of soil samples which are resedimented in the laboratory from natural source materials. These source materials are derived from a wide range of geologic origins in order to encompass close to the full spectrum of behaviors that would be encountered for natural sedimentary fine-grained soils. From a practical viewpoint, resedimented samples are far easier and less expensive to obtain than good quality intact samples, particularly for deep sediments subjected to very high in situ pressures that are a special focus of the research. In addition to considerable practical benefits, however, resedimentation is also a technical necessity. The author's research involves the isolation of various factors influencing mechanical behavior (e.g. soil composition, consolidation stress, OCR) so that they can be systematically quantified. This is not possible with the use of intact samples, since no two intact samples, even of the same sediment, will possess an identical composition and stress history. In addition, intact samples of a similar composition and OCR do not exist over a significant range of in situ consolidation stresses. For these reasons, the use of resedimentation is a technical requirement for the research.

Very limited previous research has investigated shear strength behavior over a wide range of consolidation stresses using resedimented soil. The most relevant work up to this point has been that of Abdulhadi (2009). Abdulhadi carried out a comprehensive experimental investigation to systematically quantify the effects of stress history and stress level on behavior for stresses up to 10 MPa, though only for a single material (Resedimented Boston Blue Clay). Studies which have examined behavior at stresses higher than 10 MPa using resedimented soil include Bishop et al. (1975), Yassir (1989), Nüesch (1991), Berre (1992) and William (2007). However, these studies provide very limited and isolated results.

7.2 CONSOLIDATION BEHAVIOR

The mechanical behavior of fine-grained soils has been investigated by combining the results of laboratory tests performed by the author with those of other researchers over the stress range of 0.1 to 100 MPa. With regard to K_O-virgin compression behavior, it has been found that high plasticity, smectite rich soils possess much larger void ratios at low stresses compared to more silty, low plasticity soils. This result is generally to be expected, and is consistent with the findings of previous studies. As soils undergo consolidation to higher stresses, however, higher plasticity soils display a much greater compressibility and a corresponding larger loss in void ratio compared to lower plasticity soils. As a result of these two trends, the void ratios of all fine-grained soils tend to converge into a much narrower range above about 10 MPa, and compression indices reach an approximately constant value of 0.21. It is concluded that at high stresses all fine-grained soils display a similar compression behavior regardless of their composition, though at low stresses their compression behavior is strongly controlled by composition.

Several models used to describe the compression behavior of fine-grained soils have been evaluated by comparing the model predictions with experimental data over a very wide range of effective stresses. It is found that the virgin compression behavior of low plasticity soils, (with w_L below about 50 %) is best described by assuming a log-linear relationship between void ratio and σ'_v. For higher plasticity soils, their behavior is better described by assuming a log-linear relationship between porosity and σ'_v. The assumption of a log-log relationship between (1 + void ratio) and σ'_v proposed by Butterfield (1979) is not the most appropriate for any particular soil type, but gives a reasonably good description of compression behavior for all soils. It is therefore ideal for situations in which the plasticity of a sediment is unknown. For all soils, the assumption of an exponential relationship between porosity and σ'_v gives a very poor fit to the experimental data.

Measurements of K_O made continuously throughout the consolidation phase of triaxial tests demonstrate that the value of K_{ONC} changes systematically with stress level for most soils. This result is consistent with the behavior reported by Abdulhadi (2009) for RBBC. The author's K_O measurements also show systematic behavior in terms of soil composition, with high plasticity soils displaying a rapid increase in K_{ONC} with increasing stress. For example, values of

K_{ONC} in excess of 0.80 have been measured for R. Eugene Island Clay at very high stresses, these being higher than any previously reported values that the author is aware of. Medium plasticity soils display a moderate increase in K_{ONC} with increasing stress. On the other hand, very low plasticity soils can display a decrease in K_{ONC} with increasing stress. This is the first time that such a systematic behavior in K_{ONC} as a function of both stress level and soil type has been reported. Correlations have been developed which allow K_{ONC} for a fine-grained soil to be estimated based on liquid limit. Limited data are also available for the K_O of soils in the OC regime, and an original equation (Equation 5-8) is proposed based on the author's results to describe the variation in K_O observed during recompression.

The permeability of 17 resedimented natural soils has been investigated over a permeability range of 10^{-14} m^2 to 10^{-20} m^2, effective stresses up to 100 MPa and a porosity range of about 0.75 to 0.20. A log-linear relationship between bedding perpendicular permeability and porosity has been observed over this range. The permeability-porosity relationship for a soil can be related to its liquid limit, which provides a robust indicator of the combined effects of pore size distribution and clay mineralogy on behavior. At a given porosity, permeability can vary by up to 5 orders of magnitude and decreases as the liquid limit of a soil increases. This is due to an increase in liquid limit being associated with a decrease in mean pore size, with an increase in the influence of double layers around clay particles as well as with a greater likelihood for platy-shaped clay particles to be oriented perpendicular to the direction of major loading, thereby increasing tortuosity. As effective stress increases and porosity decreases these factors become more pronounced, resulting in a more rapid reduction in permeability for soils with high liquid limits. Correlations have been developed which allow the permeability of a soil to be estimated based on its porosity and liquid limit. The permeabilities predicted using these correlations fall within ±5 times the measured values and most fall within ±3 times the measured values. A comparison of permeabilities measured on intact core samples of Boston Blue Clay and GoM Ursa Clay against those predicted using the liquid limit correlations demonstrates the practical applicability of the correlations for estimating in situ permeability. The use of clay fraction (percentage of particles < 2 um) as a material index property for predicting permeability is found to be considerably less reliable than using liquid limit.

Many correlations are presented in this thesis which relate the mechanical properties of fine-grained soils to liquid limit. These include correlations for void ratio, compression index, permeability, K_O, undrained strength and critical state friction angle. Liquid limit is used as a correlating parameter for several reasons. From a practical point of view, measurements of liquid limit are very common and are routinely made in large numbers in geotechnical site investigations. The measurement is relatively inexpensive and simple to make, and does not require an intact sample. This ability to perform the measurement on highly disturbed sample material is a very significant advantage of the liquid limit, particularly in relation to deep or offshore investigations where obtaining good quality intact samples may be prohibitively expensive. From a technical point of view, liquid limit is a very robust indicator of soil composition and can be used as a proxy for such. A key feature of the limit is that it is a function of both the fraction and type of clay minerals present in a fine-grained soil, quantities which are known to have a large effect on a soil's engineering properties. The correlations developed in this work are based on a dataset of soils possessing liquid limits in the range of 25-100 % and tested over a stress range of 0.1-100 MPa. The correlations are not claimed to be applicable outside these ranges. In addition, the proposed strength correlations will likely underestimate the strength of natural sediments that possess a bonded microstructure such as that caused by cementation.

7.3 STRENGTH BEHAVIOR

Triaxial tests were carried out to examine the validity of Terzaghi's (1923) definition of effective stress at pore pressures much higher than those typically encountered in geotechnical engineering practice. While the Terzaghi definition of effective stress has been verified for practically all soil types at relatively low pore pressures, its applicability at the much higher in situ pore pressures relevant to this work is far less well understood. Bishop and Skinner (1977) have shown that the Terzaghi definition of effective stress controls the shearing behavior of granular soils at high pore pressures. However, no experiments were performed by Bishop and Skinner (1977) on clayey materials, and the nature of interparticle contacts are potentially quite different for granular and claycy soils. A procedure similar to that used by Bishop and Skinner (1977) was adopted in this work to examine the principle of effective stress for fine-grained materials. Based on the results of these tests, it can be concluded that the magnitude of pore pressure in itself has no detectable effect on the shearing behavior of fine-grained soils for pore pressures up to *at least* 10 MPa. Modification of the conventional Terzaghi definition of effective stress is therefore not believed to be necessary to describe the behavior of these materials at the stress levels encountered in this work. While the Terzaghi definition of effective stress is commonly used for fine-grained soils without question even at high stresses, this is the first time in which experimental verification of its applicability has been demonstrated.

The results of K_O-consolidated triaxial compression tests performed on eight resedimented fine-grained soils demonstrate conclusively that the common assumption of these soils exhibiting constant normalized properties is not valid when behavior is evaluated over a significant stress range. This finding generalizes the results of Abdulhadi (2009) and Jones (2010) who tested R. Boston Blue Clay and R. Ugnu Clay respectively at stresses up to 10 MPa. Most soils demonstrate consistent variations in both undrained strength ratio and critical state friction angle with stress level. The direction and rate at which these strength properties change with stress depend on the soil's composition, with high plasticity soils showing a more rapid reduction in normalized strength properties with increasing stress compared to low plasticity soils. Correlations have been developed which allow a reasonable estimate of the drained and undrained triaxial compressive strength of a fine-grained sediment to be obtained by knowing 3 pieces of information about the sediment: the preconsolidation stress, OCR (in the case of undrained strength) and liquid limit. In the case of critical state friction angle, only preconsolidation stress and liquid limit are essentially required, as friction angle does not vary significantly with overconsolidation for OCRs < 8. Previous correlations between strength properties and the Atterberg limits do not consider the effect of stress level on normalized properties, and this fact likely contributes to much of the scatter present in these correlations.

For all soils investigated, increasing consolidation stress results in a more ductile stress–strain response during undrained shearing as strain to failure increases and the amount of post-peak strain softening reduces. The increase in strain to failure associated with stress level occurs to the same extent at each OCR. Again, this finding generalizes the results of Abdulhadi (2009) and Jones (2010) who tested R. Boston Blue Clay and R. Ugnu Clay respectively.

Variations in strength properties as a function of stress level and soil type are closely linked to the value of K_O, with unique relationships existing between K_{ONC}, critical state friction angle and undrained strength ratio. These relationships are independent of soil composition. Higher values of K_{ONC} are associated with both lower critical state friction angles and lower undrained strengths. This finding is consistent with the result that higher plasticity soils display a more rapid increase in K_{ONC}, and a more rapid decrease in both strength ratio and friction angle, with increasing consolidation stress. The relationship between friction angle and K_{ONC} found in this work compares well with the popular correlation of Jâky (1948). In contrast to friction angle, which is merely correlated to K_{ONC}, evidence suggests that the pre-shear K_{ONC} may have a direct causal impact on the measured undrained strength ratio. It is therefore concluded that the maintenance of K_O conditions during virgin consolidation in the triaxial device is especially important, as even small deviations from this state may result in significant errors in the interpreted undrained strength. Since the majority of previous experimental work performed on soil has not involved K_O-consolidation prior to shearing, a unique relationship between undrained strength and K_O for all fine-grained soils has not previously been reported.

The strong inverse relationship between K_O and normalized undrained strength is in some ways counter-intuitive. For a given σ'_{vc}, a higher K_{ONC} corresponds to greater mean stress, which one might expect would produce a higher shear strength. On the other hand, one may instead consider K_O as being a measure of the horizontal stress necessary to prevent lateral straining of the soil due to the application of a given vertical stress. A higher K_O would therefore imply that a soil is relatively weaker, in that it requires a larger horizontal stress to maintain one-dimensional compression. Alternatively, a lower K_O implies that a soil offers greater resistance, in that it requires much less horizontal stress to support a given vertical stress. In other words, the ability of a soil to maintain a higher shear stress during one-dimensional consolidation corresponds with a higher strength during both drained and undrained shearing.

The relationship describing the variation in Young's modulus of RBBC with stress proposed by Santagata (1998) based on the results of tests performed below 2 MPa is found to apply equally well for all fine-grained soils. However, extrapolation of this relationship to stresses higher than about 10 MPa will likely result in a large overestimate of the Young's modulus of a NC soil. Based on the experimental results of this work, a modified relationship

(Equation 6-10) is proposed to describe the variation in Young's modulus of NC fine-grained soils at high stresses. Unlike the relationship of Santagata (1998) which is based on small strain measurements of E_{uMAX}, the author's proposed equation is based on measurements of E_u at ε_a = 0.01 %. In addition, in contrast to Santagata's relationship, Equation 6-10 does not include void ratio as an input parameter.

The anisotropic nature of soil means that its behavior is different depending on the orientation and relative magnitudes of the principal stresses. However, significantly less strength data are available for modes of shear other than triaxial compression. In terms of undrained strength, the results of limited DSS and TE test programs do not permit any general conclusions to be drawn regarding the undrained strength behavior of fine-grained soils in these modes of shear. For RBBC there is essentially no change in undrained strength ratio with stress level in DSS and TE modes of shear, while for Skibbereen Silt the undrained strength ratio increases consistently in DSS as it does in TC. A more consistent behavior is observed for friction angle. The critical state friction angle of RBBC decreases consistently with increasing stress level in TE and DSS, as it does in TC. The friction angle of Skibbereen Silt increases consistently with increasing stress level in DSS, as it does in TC. The increase in the critical state friction angle of Skibbereen Silt with increasing consolidation stress is quite atypical and the author is not aware of any other soil exhibiting this strength behavior.

Systematic variations in K_{ONC}, critical state friction angle, and undrained strength ratio with consolidation stress level reflect an overall change in the shape of a soil's yield surface. High plasticity soils display a large reduction in normalized undrained strength and friction angle and a large increase in K_{ONC} with increasing stress. This reflects a yield surface which becomes more elongated about the effective stress axis as consolidation stress increases. On the other hand, low plasticity soils display much less of a change in the shape of their yield surface, and may even have a yield surface which becomes increasingly anisotropic, i.e. less oriented about the effective stress axis. Apart from RBBC, however, many of these soils have only been tested in triaxial compression mode of shear, with the result that the evolution of much of the yield surface is only hypothesized and not well understood.

The underlying changes in soil micro-structure which are responsible for the variations in strength properties have not been determined. However, a reasonable hypothesis can be formed to explain these results (since variations in the strength of fine-grained soils have been found to be very similar whether one thinks in terms of friction angle or undrained strength ratio, for simplicity this discussion will focus on using friction angle as the sole measure of shear strength). A possible explanation for the observed results can be proposed based on the concept of an intrinsic friction angle (ψ) initially developed by Skempton (1960). As discussed in Chapter 2, intrinsic friction angle (not to be confused with φ'_{cs}) is the friction angle of the solid material forming soil or rock particles. At extremely high pressures, when the porosity of soil or rock approaches zero and the particles become fused together, it is intuitive to expect that the internal friction angle of the material would approach its intrinsic friction angle. Skempton (1960) quoted typical ψ values for rock minerals (e.g. a tangent ψ for quartz ~ 13.25°) and, although no experimental data were available for clay minerals, predicted that clay minerals should have much lower values of ψ. It could therefore be expected that at very high pressures the internal friction angle of a soil consisting primarily of quartz would be higher than the friction angle of a soil consisting primarily of clay minerals. The results of this work show that this is in fact the case (keep in mind that values of φ'_{cs} quoted in the author's results are expressed in terms of a secant angle, whereas ψ describes a tangent angle) For example, extrapolation of the trendlines shown in Figure 6-53 to higher stresses would predict much greater friction angles for Skibbereen Silt and R. Presumpscot Clay (7.5 % and 22.8 % clay minerals respectively) than for R. London Clay and R. GoM Eugene Island Clay (54.6 % and 53.9 % clay minerals respectively). If one considers the other extreme, at the lowest consolidation stresses investigated in this research, soils possess a high porosity and the intrinsic strength of individual soil particles has a negligible effect on the aggregate strength of a sample. Instead, strength behavior is likely governed more by the arrangement, fabric and shape of soil particles. Figure 6-53 illustrates that there is no obvious consistent trend in friction angle as a function of soil type at these very low stresses. In summary, it is hypothesized that the strength properties of fine-grained soils are governed by factors such as particle arrangement and fabric at very low consolidation stresses, and by the intrinsic strength of their constituent minerals in the limit of extremely high stresses. Intermediate stresses of relevance to engineering practice involve a very gradual transition between these two extreme behaviors.

Particle reorientation during one-dimensional compression cannot explain variations in the strength properties of fine-grained soils. As particles become more horizontally aligned with increasing vertical effective stress, they therefore become less favorably oriented with a potential failure plane in triaxial compression. Particle reorientation might therefore be expected to increase the normalized strength of a soil, especially for high plasticity soils which contain a larger portion of platy-shaped clay particles compared to more silty low plasticity soils. The opposite is found to be the case, however, as higher plasticity soils display the fastest reductions in normalized undrained strength and friction angle with increasing stress.

7.4 RECOMMENDATIONS FOR FUTURE WORK

Based on the results and conclusions of this work, the following are areas in which the author feels further research would be most beneficial and impactful:

- Most design applications in which shear strength properties need to be considered involve a combination of multiple modes of shearing. Of the soils included in this thesis, only R. Boston Blue Clay and Skibbereen Silt have been tested in modes other than TC. Additional DSS and TE test programs are needed to be performed on other soils in order to establish general trends in strength properties as a function of stress level and soil type for these modes of shear. Preferably these experimental programs would involve the soils included in this work, since the TC behavior of these soils is already reasonably well established.
- The research presented in this thesis has involved testing the consolidation and shear strength properties of soils at effective stresses up to σ'_{vc} = 100 MPa. In the field, these in situ stresses typically occur at several kilometers depth and at temperatures far higher than surface temperature. It is well known that the mechanical properties of soil and rock are significantly affected by temperature (particularly above 80°C - 100°C when the recrystallization of clay minerals such as smectite alters the microfabric of fine-grained soils). However, the author's experimental program has only involved laboratory testing at room temperature. It would be of great benefit to systematically evaluate the effects of temperature on consolidation and strength properties as a function of composition. This could be successfully achieved by a laboratory investigation involving a controlled temperature setting and the use of resedimented soil samples.
- The triaxial tests performed by the author using the high pressure triaxial system relied on external measurements of axial strain. As a result, the small strain behavior of the soils

could not be determined accurately at strains less than about 0.01 %, by which point soils may already have experienced a significant reduction in Young's modulus. Santagata (1998) measured small strain behavior at axial strains as low as 0.0001 %, though only for a single material (RBBC) and for σ'_p up to 2 MPa. It would be extremely useful to modify the high pressure triaxial cell developed in this work to accommodate internal strain measurement. This would allow an extension of the work of Santagata (1998) to stresses as high as 100 MPa. It would also be beneficial to perform these tests on several soils of different composition, so that a more general understanding of small strain behavior can be achieved, similar to what has been done in this research for strength behavior.

- At high in situ stresses and temperatures the mechanical behaviour of soils can become more influenced by time-dependent diagenetic processes such as cementation. Such processes cannot [currently] be mimicked in a laboratory setting. Despite the problems of high cost and sampling disturbance associated with obtaining deep samples, it would be beneficial to carry out more high quality laboratory testing of these intact materials and to examine the extent to which their measured behaviour can be predicted by testing of the corresponding resedimented material.
- Many correlations are presented in this thesis which relate the mechanical properties of fine-grained soils to liquid limit. The measurements of liquid limit made on the soils were carried out using distilled water, as is standard practice. However, many of the soils tested, in particular those from the Gulf of Mexico, exist at high in situ pore fluid salinities. Furthermore, much of this salt still exists in the soil when a liquid limit measurement is performed on the processed material. It is known that salt concentration can have a significant impact on both liquid limit (e.g. Green 1956) and mechanical properties (e.g. Horan 2012). However, it is not known if salt concentration will affect both liquid limit and mechanical properties in such a way that the proposed correlations will be significantly affected. If they are significantly affected, it is not known to what extinct, or if it is possible to account for pore fluid salinity in modified versions of the correlations. Available data from the author, Horan (2012) and Fahy (2014) suggest that, unless a soil has first been leached of any pre-existing natural salts, the effect of salt at concentrations typically encountered in nature does not have a dramatic impact on liquid limit or mechanical

properties. However, this evidence requires confirmation by gathering and analyzing additional data.

- In addition to the effect of pore fluid salt concentration on liquid limit, the impact of the chosen measurement technique for determining the limit also requires further investigation. The liquid limits of the soils investigated in the research were determined by either the Casagrande cup method (ASTM D4318) or the fall cone method (BS 1377). These two methods should give identical results, at least for $w_L < 100$ % (Head 1980). However, limited data from the author's work suggest that these two measurement techniques may produce significantly different liquid limits even at values below 100 %. Additional liquid limit measurements made using both methods are necessary to confirm or disprove this evidence. If it is the case that the two methods give significantly different results, this finding may have important consequences for geotechnical engineering practice where liquid limit measurements are routinely made using the two methods and many empirical correlations between liquid limit and engineering properties are in use.

REFERENCES

Abdulhadi, N.O. (2009). "An Experimental Investigation into the Stress-Dependent Mechanical Behavior of Cohesive Soil with Application to Wellbore Instability", Ph.D. Thesis, Massachusetts Institute of Technology

Abdulhadi, N.O., Germaine, J.T. & Whittle, A.J. (2012) "Stress-Dependent Behavior of Saturated Clay", *Canadian Geotechnical Journal*, 49 (8), 907-916

Adams, A. L. (2014). "Permeability Anisotropy and Resistivity Anisotropy of Mechanically Compressed Mudrocks", Ph.D. Thesis, Massachusetts Institute of Technology

Adams, A. L., Germaine, J.T., Flemings, P.B. & Day-Stirrat, R.J. (2013). "Stress induced Permeability Anisotropy of Resedimented Boston Blue Clay", *Water Resources Research* 49, pp. 6561–6571, doi:10.1002/wrcr.20470

Ahmed, I. (1990). "Investigation of Normalized Behaviour of Resedimented Boston Blue Clay using Geonor Direct Simple Shear", S.M. Thesis, Massachusetts Institute of Technology

Amorosi, A. & Rampello, S. (2007). "An Experimental Investigation into the Mechanical Behavior of a Structured Stiff Clay", *Géotechnique* 57 (2), pp. 153-166

Anderson, G.R. (1991). "Physical Mechanisms Controlling the Strength and Deformation Behavior of Frozen Sand", Sc.D. Thesis, Massachusetts Institute of Technology

ASTM D422 Standard Test Method for Particle-size Analysis of Soils, in *ASTM 04.08 Soil and Rock* (1), 2007

ASTM D2487 Standard Practice for Classification of Soils for Engineering Purposes (Unified Soil Classification System), in *ASTM 04.08 Soil and Rock* (1), Revision 11

ASTM D2974 Standard Test Methods for Moisture, Ash, and Organic Matter of Peat and Other Organic Soils, in *ASTM 04.08 Soil and Rock* (1), Revision 13

ASTM D4186 Standard Test Method for One-Dimensional Consolidation Properties of Saturated Cohesive Soils using Controlled-Strain Loading, in *ASTM 04.08 Soil and Rock* (1), Revision 12

ASTM D4318 Standard Test Methods for Liquid Limit, Plastic Limit, and Plasticity Index of Soils, in *ASTM 04.08 Soil and Rock* (1), Revision 12

Atterberg, A., 1911. Über die physikalische Bodenuntersuchung und über die Plastizität der Tone. Internationale Mitteilungen für Bodenkunde, 1, pp. 10-43

Bailey, W.A. (1961). "Effects of Salt on the Shear Strength of Boston Blue Clay", SB Thesis, Massachusetts Institute of Technology

Bellwald, P. (1990). "A Contribution to the Design of Tunnels in Argillaceous Rock", Ph.D. Thesis, Massachusetts Institute of Technology

Belviso, R., Federico, A. & Popescu, M. (2001). "K_O-Undrained Shear Strength Ratio of Normally Consolidated Clays from CIUC tests", *Soft Soil Engineering*, Zwets & Zeitlinger, pp. 575-579

Berman, D.R. (1993). "Characterization of the Engineering Properties of Boston Blue Clay at the MIT Campus", S.M. Thesis, Massachusetts Institute of Technology

Berre, T. (1985). "Suggested International Code of Soil Engineering Practice for Triaxial Compression Tests", Report No. 56103-30. Norwegian Geotechnical Institute

Berre, T. (1992). "Geotechnical Properties of Clay-Shales", Report No. 541082-3. Norwegian Geotechnical Institute

Betts, W.S. (2014) "Compression and Permeability Behavior of Gulf of Mexico Mudrocks, Resedimented and In-situ", M.S. Thesis, University of Texas at Austin

Biot, M.A. (1941). "General Theory of Three-Dimensional Consolidation", *Journal of Applied Physics* 12 (2), pp. 155-164

Bishop, A.W. (1973). "The Influence of an Undrained Change in Stress on the Pore Pressure in Porous Media of Low Compressibility" (Technical Note), *Géotechnique* 23 (3), pp. 435-442

Bishop, A.W. (1976). "The Influence of System Compressibility on the Observed Pore-Pressure Response to an Undrained Change in Stress in Saturated Rock" (Technical Note), *Géotechnique* 26, (2), pp. 435-442

Bishop, A.W. & Eldin, A.K.G. (1950). "Undrained Triaxial Tests on Saturated Sands and Their Significance in the General Theory of Shear Strength", *Géotechnique* 2 (1), pp. 13-32

Bishop, A.W. & Henkel, D.J. (1962). The Measurement of Soil Properties in the Triaxial Test, Edward Arnold Ltd., London

Bishop, A.W., Webb, D.L. & Lewin, P.I. (1965). "Undisturbed Samples of London Clay from the Ashford Common Shaft: Strength-Effective Stress Relationships", *Géotechnique* 15 (1), pp. 1 - 31

Bishop, A.W., Kumapley, N.K. & El-Ruwayih, A. (1975). "The Influence of Pore-Water Tension on the Strength of Clay", *Philosophical Transactions of the Royal Society of London*, 278, pp. 511-554

Bishop, A.W. & Skinner, A.E. (1977). "The Influence of High Pore-Water Pressure on the Strength of Cohesionless Soils", *Philosophical Transactions of the Royal Society of London*, 284, pp. 91-130

Bjerrum, L. (1973). "Problems of Soil Mechanics and Construction on Soft Clays", State-of-the-Art Report to Session IV, *8th International Conference on Soil Mechanics and Foundation Engineering*, Moscow, pp. 111-159

Bolton, M.D. (1991). A Guide to Soil Mechanics, MD & K Bolton

Brooker, E.W. & Ireland, H.O. (1965). "Earth Pressures at Rest related to Stress History", *Canadian Geotechnical Journal,* 2 (1), pp. 1–15

BS 1377 Methods of Test for Soils for Civil Engineering Purposes Part 2: Classification Tests, in *BSI (1990)*

Burland, J.B. (1990). "On the Compressibility and Shear Strength of Natural Soils", *Géotechnique* 40 (3), pp. 329-378

Butterfield, R. (1979). "A Natural Compression Law for Soils (an Advance on e-logp')", Technical Note, *Géotechnique* 29, (4), pp. 469 – 480

Cauble, D.F. (1996). "An Experimental Investigation of the Behavior of a Model Suction Caisson in a Cohesive Soil", Ph.D. Thesis, Massachusetts Institute of Technology

Casey, B. (2011). "The Significance of Specimen End Restraint in High Pressure Triaxial Testing of Cohesive Soil", S.M. Thesis, Massachusetts Institute of Technology

Casey, B. and Germaine, J.T. (2013). "The Stress Dependence of Shear Strength in Fine-Grained Soils and Correlations with Liquid Limit", *Journal of Geotechnical and Geoenvironmental Engineering*, 139 (10), 1709-1717. doi: 10.1061/(ASCE)GT.1943-5606.0000896

Casey, B., Germaine, J.T., Flemings, P.B., Reece, J.S., Gao, B., and Betts, W. (2013). "Liquid Limit as a Predictor of Mudrock Permeability", *Journal of Marine and Petroleum Geology*, 44, 256-263. http://dx.doi.org/10.1016/j.marpetgeo.2013.04.008

Calvello, M., Lasco, M., Vassallo, R. & Di Maio, C. (2005). "Compressibility and Strength of Active Clays: Influence of Pore Fluid Dielectric Constant", *Proceedings of International Conference on Problematic Soils*, Eastern Mediterranean University, May 2005, pp. 459-466

Carrier, W.D. (2003). "Goodbye, Hazen; Hello, Kozeny-Carman", Technical Note. *Journal of Geotechnical and Geoenvironmental Engineering*, ASCE, 129 (11), pp. 1054-1056

Cooling, L.F. & Skempton, A.W. (1942) "A Laboratory Study of London Clay", *Journal of the Institution of Civil Engineers* 17 (3), pp. 251-276

Daigle, H. & Dugan, B. (2011). "Permeability Anisotropy and Fabric Development: a Mechanistic Explanation", *Water Resources Research*, 47, W12517, doi:10.1029/2011WR011110

Day-Stirrat, R.J., Flemings, P.B., You, Y. & Aplin, A.C. (2012). "The Fabric of Consolidation in Gulf of Mexico Mudstones", *Marine Geology* 295-298, pp. 77–85. doi:10.1016/j.margeo.2011.12.003

De Groot, D.J. (1992). "The Multidirectional Direct Simple Shear Apparatus with Application to Design of Offshore Arctic structures", Sc.D. Thesis, Massachusetts Institute of Technology

Di Maio, C., Santoli, L. & Schiavone, P. (2004). "Volume Change Behaviour of Clays: the Influence of Mineral Composition, Pore Fluid Composition and Stress State. Mechanics of Materials 36, pp. 435–451, doi:10.1016/S0167-6636(03)00070-X

Expedition 308 Scientists (2006a). Expedition 308 Summary. *In* Flemings, P.B., Behrmann, J.H., John, C.M. and the Expedition 308 Scientists, *Proceeding of Integrated Ocean Drilling Program (IODP) 308*. College Station TX (IODP Management International, Inc.). doi:10.2204/iodp.proc.308.101.2006

Expedition 308 Scientists (2006b). Site U1322. *In* Flemings, P.B., Behrmann, J.H., John, C.M., and the Expedition 308 Scientists, *Proceedings of Integrated Ocean Drilling Program (IODP) 308*. College Station TX (IODP Management International, Inc.). doi:10.2204/iodp.proc.308.106.2006

Fahy, B.P. (2014). "The Influence of Salinity on the Mechanical Behavior of High Plasticity Soils", S.M. Thesis, Massachusetts Institute of Technology

Foott, R. & Ladd, C.C. (1981). "Undrained Settlement of Plastic and Organic Clays", *Journal of the Geotechnical Engineering Division*, ASCE, 107 (8), pp. 1079-1094

Gao, B. (2013). "Pore Pressure within Dipping Reservoirs in Overpressure Basins", M.S. Thesis, The University of Texas at Austin

Germaine, J.T. (1982). "Development of the Directional Shear Cell for Measuring Cross-Anisotropic Clay Properties", Sc.D. Thesis, Massachusetts Institute of Technology

Germaine, J.T. & Ladd, C.C. (1988). "Triaxial Testing of Saturated Cohesive Soils: State of the Art Paper", *Advanced Triaxial Testing of Soil and Rock*, ASTM STP 977, pp. 421 – 459

Germaine, J.T. & Germaine, A.V. (2009). Geotechnical Laboratory Measurements for Engineers, John Wiley and Sons

Green, (1956). "Effects of Pore Water Salt Concentration of Homoionic Clays", S.M. Thesis, Massachusetts Institute of Technology

Grennan, J.T. (2010). "Characterization of a Low Plasticity Silt", S.M. Thesis, Massachusetts Institute of Technology

Gutierrez, M., Nygard, R., Hoeg, K. & Berre, T. (2008). "Normalized Undrained Shear Strength of Clay Shales", *Engineering Geology* 99, pp. 31-39

Haley & Aldrich, Inc. (2002). Geotechnical Data Report, Vassar Street Student Housing (MIT), Cambridge, MA.

Hart, B.S., Flemings, P.B. & Deshpande, A. (1995). "Porosity and Pressure: Role of Compaction Disequilibrium in the Development of Geopressures in a Gulf Coast Pleistocene Basin", *Geology*, 23 (1), pp. 45 – 48

Hazen, A. (1892). "Some Physical Properties of Sands and Gravels, with Special Reference to their use in Filtration", 24th Annual Report, Massachusetts State Board of Health, Public Document No. 34, pp. 539–556

Head K.H. (1980). Manual of Soil Laboratory Testing, Volume 1: Soil Classification and Compaction Tests, Pentech Press

Hillier, S. (1999). "Use of an Air Brush to Spray Dry Samples for X-ray Powder Diffraction", *Clay Minerals* 34, pp. 127-135

Hillier, S. (2003). "Quantitative Analysis of Clay and Other Minerals in Sandstones by X-ray Powder Diffraction (XRPD)", *International Association of Sedimentologists Special Publication 34: Clays and Clay Cements in Sandstones*. Blackwell, Oxford, pp. 213-251

Horan, A.J. (2012). "The Mechanical Behavior of Normally Consolidated Soils as a Function of Pore Fluid Salinity", S.M. Thesis, Massachusetts Institute of Technology

Horseman, S.T., Winter, M.G., & Entwistle, D.C. (1993). "Triaxial Experiments on Boom Clay", *The Engineering Geology of Weak Rock*, Balkema, Rotterdam

House, R.D. (2012). "A Comparison of the Behavior of Intact and Resedimented Boston Blue Clay", M.Eng. Thesis, Massachusetts Institute of Technology

Jâky, J. (1944). "A nyugalmi nyomâs tényezöje (The coefficient of earth pressure at rest)", *Magyar Mérnok és Epitész Egylet Közlönye (Journal for Society of Hungarian Architects and Engineers)*, October, pp. 355–358.

Jâky, J. (1948). "Pressure in Silos." In *Proceedings of the 2nd International Conference on Soil Mechanics and Foundation Engineering*, Rotterdam, The Netherlands, 1, pp. 103–107.

John, C.M. & Adatte, T. (2009). Data report: X-ray Analyses of Bulk Sediment in IODP Holes U1320A and U1324B, northern Gulf of Mexico. *In* Flemings, P.B., Behrmann, J.H., John, C.M. and the Expedition 308 Scientists. *Proceedings of the Integrated Ocean Drilling Program (IODP) 308.* College Station TX (IODP Management International, Inc.). doi:10.2204/iodp.proc.308.214.2009

Jones, C.A. (2010). "Engineering Properties of Resedimented Ugnu Clay from the Alaskan North Slope", S.M. Thesis, Massachusetts Institute of Technology

Kenney, T.C. (1964). "Sea-Level Movements and the Geologic Histories of the Postglacial Marine Soils at Boston, Nicolet, Ottawa and Oslo", *Géotechnique* 14 (3), pp. 203-230

Kontopoulos N.S. (2012). "The Effect of Sample Disturbance on Preconsolidation Pressure for Normally Consolidated and Overconsolidated Clays", Ph.D. Thesis, Massachusetts Institute of Technology

Ladd, R.S. (1978). "Preparing Test Specimens using Undercompaction", *Geotechnical Testing Journal* 1 (1), pp. 16 – 23

Ladd, C.C. (1985). "Overview of Clay Behaviour", MIT Special Summer Course 1.605

Ladd, C.C. (1991). "Stability Evaluation during Staged Construction", 22nd Karl Terzahgi Lecture, *Journal of Geotechnical Engineering* 117 (4), pp. 540-615

Ladd, C.C. & Varallyay, J. (1965). "The Influence of Stress System on the Behavior of Saturated Clays during Undrained Shear", Research Report R65-11, Soils Publication No. 177, Department of Civil Engineering, Massachusetts Institute of Technology

Ladd, C.C. & Foott, R. (1974). "New Design Procedure for Stability of Soft Clay", *Journal of the Geotechnical Engineering Division*, ASCE, 100 (7), pp. 763-786

Ladd, C.C., Young, G.A., Kraemer, S.R. & Burke D.M. (1999). "Engineering properties of Boston Blue Clay from special testing program", Special Geotechnical Testing: Central Artery/Tunnel Project in Boston, Massachusetts. ASCE GSP 91, pp. 1-24

Lade, P.V. & de Boer, R. (1997). "The Concept of Effective Stress for Soil, Concrete and Rock", *Géotechnique* 47 (1), pp. 61-78

Lambe, T.W. & Whitman R.V. (1969). Soil Mechanics, John Wiley and Sons

Marsden, J.R., Holt, R.M., Nakken, S.J. & Raaen, A.M. (1992). "Mechanical and Petrophysical Characterization of Highly Stress Mudstones", *Proceedings of Eurock 92 Conference*, Balkema, Rotterdam, pp. 51-56

Mayne, P. W. & Kulhawy, F. H. (1982). "K_0 – OCR Relationships in Soil." *Journal of the Geotechnical Engineering Division*, ASCE, 108 (6), pp. 851-872

Mazzei, D.P.C. (2008). "Normalized Mechanical Properties of Resedimented Gulf of Mexico Clay from Integrated Ocean Drilling Program Expedition Leg 308", M.Eng. Thesis, Massachusetts Institute of Technology

Mesri, G. & Olson, R.E. (1970). "Shear Strength of Montmorillonite", *Géotechnique* 20 (3), pp. 261-270

Mesri, G. & Olson, R.E. (1971). "Mechanisms Controlling the Permeability of Clays", *Clays and Clay Minerals* 19, pp. 151-158

Mesri, G. & Hayat, T. M. (1993). "The Coefficient of Earth Pressure at Rest", *Canadian. Geotechnical Journal*, 30, pp. 647–666.

Moniz, S.R. (2009). "The Influence of Effective Consolidation Stress on the Normalized Extension Strength Properties of Resedimented Boston Blue Clay", M.Eng. Thesis, Massachusetts Institute of Technology

Nüesch, R. (1991). "Das mechanische Verhalten von Opalinuston", Sc.D. Thesis, Eidgenössischen Technischen Hochschule, Zürich

Neuzil, C.E. (1994). "How Permeable are Clays and Shales?" *Water Resources Research* 30 (2), pp. 145-150

O'Brien, N.R. (1971). "Fabric of Kaolinite and Illite floccules", *Clays and Clay Minerals* 19, pp. 353-359

Pandian, N.S., Nagaraj, T.S. & Raju, P.S.R.N. (1995). "Permeability and Compressibility Behavior of Bentonite Sand/Soil Mixes", *Geotechnical Testing Journal*, GTJODJ, 18 (1), pp. 86-93

Paterson, M.S. & Wong, T.F. (2005). Experimental Rock Deformation – The Brittle Field, Springer-Verlag, Berlin Heidelberg

Petley, D.N. (1999). "Failure Envelopes of Mudrocks at High Confining Pressures", Geological Society of London, Special Publications, 158, pp. 61-71

Petley, D.N., Jones, M.E., Stafford, C., Leddra, M.J. & Kageson-Loe, N.L. (1993). "Deformation and fabric changes in weak fine-grained rocks during high pressure consolidation and shear", *Geotechnical Engineering of Hard Soils-Soft Rocks*, Balkema, Rotterdam, pp. 737-743

Quigley, R.M. & Thompson, C.D. (1966). "The Fabric of Anisotropically Consolidated Sensitive Marine Clay", *Canadian Geotechnical Journal* 3 (2), pp. 61-73

Quirós, G.W., Little, R.L. & Garmon, S. (2000). "A Normalized Soil Parameter Procedure for Evaluating In-Situ Undrained Shear Strength", Offshore Technology Conference, Houston, Texas, May 2000

Reece, J. S., Flemings, P. B., Dugan, B., Long, H., & Germaine, J.T. (2012). "Permeability-Porosity Relationships of Shallow Mudstones in the Ursa Basin, northern Deepwater Gulf of Mexico", *Journal of Geophysical Research* 117, B12102, doi:10.1029/2012JB009438

Reynolds, R. & Germaine, J.T. (2007). "Benefits and Pitfalls of Multistage Embankment Construction", Seventh International Symposium on Field Measurements in Geomechanics, pp. 1-12. doi: 10.1061/40940(307)44

Roscoe, K.H. & Burland, J.B. (1968). "On the Generalized Stress-Strain Behaviour of 'Wet' Clay", in *Engineering Plasticity*, Cambridge University Press, pp. 535 – 609

Rubey, W.W. & Hubbert, M.K. (1959) "Role of Fluid pressure in Mechanics of Overthrust Faulting, Part 2. Overthrust Belt in Geosynclinal Area of Western Wyoming in Light of Fluid-pressure Hypothesis, *Geological Society of America Bulletin* 70, pp. 167 – 205

Sawyer, D. E., Jacoby, R., Flemings, P.B. & Germaine, J.T (2008). Data report: Particle Size Analysis of Sediments in the Ursa Basin, IODP Expedition 308 Sites U1324 and U1322, northern Gulf of Mexico. *In* Flemings, P.B., Behrmann, J.H., John, C.M. and the Expedition 308 Scientists. *Proceedings of the Integrated Ocean Drilling Program (IODP) 308*. College Station TX (IODP Management International, Inc.). doi:10.2204/iodp.proc.308.205.2008.

Santagata, M.C. (1994). "Investigation of Sample Disturbance in Soft Clays Using Triaxial Element Tests", S.M. Thesis, Massachusetts Institute of Technology

Santagata, M.C. (1998). "Factors Affecting the Initial Stiffness and Stiffness Degradation of Cohesive Soils", Ph.D. Thesis, Massachusetts Institute of Technology

Schmidt, B. (1966). "Discussion of 'Earth Pressures at Rest related to Stress History' by Brooker and Ireland (1965)", *Canadian Geotechnical Journal,* 3 (4), pp. 239–242

Schneider, J. (2011). "Compression and Permeability Behavior of Natural Mudstones", Ph.D. Thesis, The University of Texas at Austin

Schofield, A.N. & Wroth, C.P. (1968). Critical State Soil Mechanics, McGraw-Hill

Seah, T.H. (1990). "Anisotropy of Resedimented Boston Blue Clay", Sc.D. Thesis, Massachusetts Institute of Technology

Seed, H.B., Woodward, R.J. & Lundgren, R. (1964). "Fundamental Aspects of the Atterberg Limits", *Journal of the Soil Mechanics and Foundations Division,* ASCE 90 (SM6), pp. 75-105

Sheahan, T.C. (1991). "An Experimental Study of the Time-Dependent Undrained Shear Behaviour of Resedimented Clay Using Automated Stress-Path Triaxial Equipment", Sc.D. Thesis, Massachusetts Institute of Technology

Skempton, A.W. (1954). "The Pore Pressure Coefficients A and B", *Géotechnique* 4 (4), pp. 143-147

Skempton, A.W. (1957). "Discussion on Airport Paper No. 35: The planning and design of the new Hong Kong Airport", *Proceedings of the Institute of Civil Engineers,* 7 (2), pp. 305-325

Skempton, A.W. (1960). "Effective Stress in Soils, Concrete and Rocks", Conference on Pore Pressure and Suction in Soils, Butterworths, pp. 4-16

Skinner, A.E. (1969). "A Note on the Influence of Interparticle Friction on the Shearing Strength of a Random Assembly of Spherical Particles", *Géotechnique* 19 (1), pp. 150-157

Stokes, W.L. & Varnes, D.J. (1955). Glossary of Selected Geologic Terms, Colorado Scientific Society Proceedings 16, Denver, Colorado

Suklje, L. (1969). Rheological Aspects of Soil Mechanics, Wiley Interscience, New York, 123

Taylor, D.W. (1942). "Research on Consolidation of Clays", Serial 82, Massachusetts Institute of Technology

Taylor, R.N. & Coop, M.R. (1993). "Stress Path Testing of Boom Clay from Mol, Belgium", *The Engineering Geology of Weak Rock*, Balkema, Rotterdam, pp. 77-82

Terzaghi, K. (1923). "Die Berechnung der Durchlässigkeits-Ziffer des Tones aus dem Verlauf der hydrodynamischen Spannungserscheinungen", Sitzungber Akad. Wissen Wien Math-naturw Kl 132, pp. 105-124

Terzaghi, K.T. (1943). Theoretical Soil Mechanics, John Wiley and Sons, New York, NY

Terzaghi, K., Peck, R.B. & Mesri, G. (1996). Soil Mechanics in Engineering Practice, 3rd Edition, John Wiley and Sons Inc., New York

Van Olphen, H. (1963). An Introduction to Colloid Chemistry, John Wiley and Sons Inc., New York

Walbaum, M. (1988). "Procedure for Investigation of Sample Disturbance using the Direct Simple Shear Apparatus", S.M. Thesis, Massachusetts Institute of Technology

Whittle, A.J. & Kavvadas, M. (1994). "Formulation of the MIT-E3 Constitutive Model for Overconsolidated Clays", *Journal of the Geotechnical Engineering Division*, ASCE, 120 (1), pp. 173-198

William, E. (2007). "Engineering Performance of Bringelly Shale", Ph.D. Thesis, University of Sydney

Wissa, A.E.Z. (1969). "Pore Pressure Measurement in Saturated Stiff Soils", *Journal of Soil Mechanics and Foundations Division, ASCE* 95 (S.M.4), pp. 1063-1073

Wissa, A.E.Z., Christian, J.T., Davis, E.H. & Heiberg, S. (1971). "Consolidation at Constant Rate of Strain", *Journal of the Soil Mechanics and Foundations Division*, ASCE 97 (SM10), pp. 1393-1493

Yang, Y. & Aplin, A.C. (1998). "Influence of Lithology and Effective Stress on the Pore Size Distribution and Modelled Permeability of some Mudstones from the Norwegian Margin", *Marine and Petroleum Geology* 15, pp. 163-175

Yang, Y. & Aplin, A.C. (2010). "A Permeability-Porosity Relationship for Mudstones", *Marine and Petroleum Geology* 27, pp. 1692-1697. doi:10.1016/j.marpetgeo.2009.07.001

Yassir, N. A. (1989). "Mud Volcanoes and the Behavior of Overpressured Clays and Silts", Ph.D. Thesis, University College London, University College London